THE MEASUREMENT OF THE VELOCITIES OF PARTICLES IN AN AIR-SOLID FLOW

by

D.G.H. Andrews

Thesis submitted in partial fulfilment
of the requirements for the degree of
Doctor of Philosophy under the conditions
of the Council for National Academic Awards

School of Mechanical Engineering,
Thames Polytechnic.
London.

November 1979

THE MEASUREMENT OF THE VELOCITIES OF PARTICLES IN AN AIR-SOLID FLOW

D.G.H. Andrews

ABSTRACT

Theoretical investigations of two-phase flows have not so far produced a useful model since the interdependence of the many variables has been difficult to predict. Progress towards such a model is dependent on accurate experimental work on two-phase flows. Particle velocity is an especially important property, but most available techniques either disturb the flow or are slow or inaccurate.

The laser-Doppler velocity meter, LDV, was developed for measurements in single-phase flows, but it has been demonstrated by a few authors to be practical for particle veocity measurements in air-solid flows. The aim of the investigation was to find the range for which the LDV was suitable, and also to make useful measurements in a pipe conveying a dilute suspension of solids pneumatically.

Air and solid velocity distributions across the diameter of a vertically upward flowing air-solid suspension in a 50 mm diameter pipe were made using an LDV. The solids conveyed were spherical glass balls, mean diamter 455 μm, and sand, mean diameters 176 μm and 366 μm. The maximum ratio of solids to air mass flow rate was 2.5 and the maximum mean air velocity was 50 ms^{-1}. Significant slip between the phases was found. Some of the correlations postulated between the particle velocity and other flow properties, such as the pressure drop, were investigated.

Velocity measurements were also attempted with an LDV on plastic pellets, with effective diameters of 2 to 3 mm and varying degrees of success were achieved. The optical properties of the particles appears to be important when applying the laser-Doppler particle measuring technique to flows conveying particles of this size.

ACKNOWLEDGEMENTS

The author would particularly like to thank his supervisors, Dr. J.S. Mason and Dr. A. Birchenough, for the help and encouragement that they gave him in this work. Also the support of the School of Mechanical Engineering and Thames Polytechnic is gratefully acknowledged.

The School's technicians, under the supervision of Mr. W.S. Churchill, were very patient with the author, and constructed much of the apparatus used. Mr. Dymo D. also provided a useful piece of electronic equipment.

Finally, the author would like to thank Mrs. Ann Follis for completing the daunting task of typing this thesis.

Financial support was provided by the Science Research Council.

AUTHOR'S NOTE

All the work in this thesis is the sole and original work of the author, except where otherwise stated by acknowledgement or reference.

Some of the work in the thesis has been presented at a conference, details of which are given in Appendix IV.

TABLE OF CONTENTS

LIST OF TABLES

LIST OF FIGURES

CHAPTER 1

INTRODUCTION

1.1 Air-Solid Flows

Multiphase systems occur frequently, both in the natural and man-made world, and have therefore drawn much interest. A multiphase system consists of a fluid medium and one or more particulate components which can be either solid, liquid or gas. Examples of such multiphase systems in nature are, for instance, dust particles in suspension in the atmosphere, blood, silt conveyed in rivers, et cetera, and multi-phase systems of industrial interest include chemical reactors, pneumatic and hydraulic conveyors, dispersion of soot particles from chimneys, and many others. The systems investigated in this project were two-phase air-solid flows. There has been much work, both experimental and theoretical, on such flows during the last few years [Soo (1967), Boothroyd (1971), Birchenough (1975)].

However, air-solid flows are extremely complex and purely theoretical analysis of the flow is unlikely to be successful due to the very large numbers of variables involved in such flows. Many solutions of single phase fluid behaviour are of a semi-empirical nature, since the behaviour has not been explained theoretically. When solid particles are added to such a fluid the interactions between the particles, between the particles and the fluid, and between the particles and the boundaries of the fluid have to be taken into account. This does not mean that theoretical approaches to the problem cannot produce any useful results. If appropriate approximations are made to simplify the problem it should be possible to predict the behaviour of an air-solid flow in different situations. However, in order to test the validity of such approximations, and the accuracy of the predictions, it is necessary for

experimental techniques to be devised to measure the properties of the flow.

The aspect of air-solid flows investigated in this project is pneumatic conveying which is widely used for bulk solids transport throughout industry. Pneumatic transport involves the conveying of particulate solids through pipes by an air flow. The solids conveyed can vary widely in size, shape and chemical composition; for instance, pneumatic conveying has been used to convey grain, chemicals, plastic chips, foodstuffs, cement and many other materials. Since such systems are so widespread in industry a greater knowledge of the flow behaviour leading to improved plant designs would be greatly welcomed.

This investigation is mainly based on applying the laser-Doppler velocity meter to the measurement of particulate velocities in a pneumatic conveying duct. The particulate velocity is an important property of air-solid flows, but it is difficult to measure. The laser-Doppler velocity meter had been used by a few authors [Riethmuller and Ginoux (1973), Birchenough(1975)] for particle velocity measurements in air-solid flows and seems to offer many advantages over other techniques.

1.2 Pneumatic Conveying

Pneumatic conveying was the first aspect of air-solid flows to be widely used in industry, although many other uses have been developed, such as heterogeneous reactors and dust collectors. Initially, the major use of pneumatic conveying was in the transportation of grain [Segler (1951)], and was particularly utilised in emptying grain from large containers such as ships. For this a reduced pressure system is used and the grain is carried up by the air flow into a collecting nozzle. This system is still used, but many other applic-

ations for pneumatic conveying have been found. The range in pneumatic conveying systems at present in use is enormous, from the conveying of chemicals around a factory to the transportation of domestic rubbish over long distances.

Pneumatic transport has many advantages over other forms of bulk transport. Large quantities of solids can be moved without contact with human beings, which is often desirable when the solid is either poisonous or requires a high degree of hygiene. Dust from powders is often a health hazard which can be avoided by using pneumatic conveying. Since the system can be largely automated, large reductions in labour costs can be achieved. Hydraulic transport of solids is also common in industry and it is more energy efficient than pneumatic transport. However, many materials have to be kept dry and, therefore, pneumatic transport is more appropriate in these cases.

Pneumatic transport is often classified into dilute phase and dense phase conveying. In dilute phase conveying the majority of the volume of the pipe is occupied by the air and there is little variation in the solids concentration along the pipe. In dense phase conveying only a small proportion of the volume of the pipe is occupied by the air and the solids tend to collect together in dense slugs with air gaps between them. Dilute phase conveying relies on the suspension of particles in the air flow, whereas in dense phase conveying the particles are closely packed together and are forced down the pipe by the pressure drop along it. The transport velocities are higher and the pressure drop less in dilute phase systems as compared to those in dense phase systems. This is because in dilute phase flows large mass flow rates of air are required and the pressure drop is largely due to the air phase, the opposite being true for dense phase conveying. The value of the solids to air mass flow ratio at the transition from dilute to dense phase flow is dependent mainly on the properties of the solids

conveyed. Only dilute phase flows were investigated in this project.

The design of pneumatic conveying plants requires consideration of several points. Pneumatic conveying is more energy consuming than most other forms of bulk solids transport and therefore it is particularly important for the system to be running at the highest possible efficiency. The size of the blower or compressor should be no bigger than that required for the designed solids mass flow rate. However, in order to do this, the total pressure drop along the conveying line must be calculated. If the air mass flow rate produced by the compressor is too low for dilute phase flow, saltation in horizontal pipes and choking in vertical pipes can occur, which causes blocking of the pipe. Since the pressure drop along a pipe cannot be accurately predicted, present design practice often involves using a compressor much bigger than necessary to avoid blockages, which reduces the efficiency of the plant. Other factors to be taken into account include electrostatic charging of particles, particle degradation and bend wear. Electrostatic charging can increase the pressure drop, and also cause explosion from sparks. Inflammable materials such as sulphur cannot be transported pneumatically because of the risk of explosion. Particle degradation can be a problem, especially for solids such as foodstuffs, where the final size range is important. Bend wear is also important to avoid since holes in bends can cause expensive delays in the process and possibly release dangerous solids into the environment. The metal removed by the abrasive wear of the pneumatic conveying plant can contaminate the material conveyed [Mills (1977)].

1.3 Modelling of Flows

It has been established that there is a need for a model of air-solid flows in order that the behaviour of the flow can be predicted under any conditions, including dependence on the size of the conveying

duct, the mass flow rate of both phases, the type of solid, and the geometry of the conveying system. Single-phase flows have been modelled successfully under some conditions and velocity profiles predicted, but no satisfactory model has yet been produced for two-phase flows. This is mainly due to the large number of parameters of the flow.

Since theoretical modelling of the flow is extremely difficult, it is desirable that experimental work should be done so that more knowledge of the behaviour of air-solid flows can be obtained. However, accurate measurement of the properties of air-solid flows presents many problems, especially since the flow tends to be hostile to most forms of instrumentation. Therefore, there is a need for adapting measuring instruments to air-solid flow conditions. All possible properties of the flow should be measured so that useful comparison with the results published by other workers can be made.

1.4 Work Undertaken

The main aim of this investigation was to develop instrumentation for measuring the properties of two-phase flow and to apply it to measure the properties of several types of air-solid flows. In this work, the problems involved in the investigation of air-solid flows are examined and the previous work on such flows is reviewed. The work was mainly concerned with measuring particle velocity distributions, which are known to be an important factor in two-phase flows. Many problems and inaccuracies have been found in most methods of particle velocity measurement used previously. The laser-Doppler velocity meter was found to be the best solution to the problem (see Chapter 2).

The pneumatic conveying plant which was available for the project was slightly modified in order that some problems involved in its earlier use could be rectified. Also, a small pneumatic conveying plant was constructed in order that the performance of the laser-Doppler

velocity meter could be tested in a variety of flows. This is described in chapter 3. The meters measuring the mass flow rates of the air and the solids in both conveying plants were calibrated and the physical properties of the solids to be conveyed were measured. In the main conveying plant two types of solids were used, spherical glass ballotini and irregular sand particles. The ballotini were used because they had a small size range and were spherical, which reduced the number of variables in the flow. The sand had a large size range and was angular in shape, and so the difference in the flow using the sand as compared to that with the ballotini indicated the effect of the size range and particle shape. Large plastic chips were used in the small conveying rig so that the laser-Doppler velocity meter could be tested with much larger particles. (see chapters 4 and 11)

The laser-Doppler velocity meter was developed to measure the velocity of fluid in single-phase flows [Yeh and Cummins (1964)], using the Doppler shift of light frequency when scattered by very small particles moving with the fluid. (see chapter 5) A few authors [Reithmuller and Ginoux (1973), Birchenough (1975)] have used the laser-Doppler velocity meter for particle velocity measurements in air-solid flows. The instrument has many advantages over other forms of particle velocity measurement, such as the non-obstruction of the flow, and was therefore used in the project. There are, however, many difficulties involved with the use of the laser-Doppler velocity meter in air-solid flows and these are given in chapter 6.

Measurements were taken in the main conveying plant with the solids described above. These measurements included the particle velocity profiles and the pressure drop in the pipe (see chapters 7, 8, 9 and 10).

CHAPTER 2

PNEUMATIC CONVEYING

2.1 Introduction

In this chapter some of the theoretical analyses of two-phase air-solid flows published in the literature are reviewed. The majority of the published work has concerned the pressure drop along a pipe, which is of great importance in the design of pneumatic conveying systems. A few authors have analysed theoretically other parameters of the flow, such as solids velocity distribution, and the more relevant papers are briefly described here.

Also described in this chapter are some of the methods of particle velocity measurement which have been employed for both local and mean velocity measurement. The techniques are compared, giving the advantages and disadvantages of each. The reasons for adopting the laser-Doppler velocimeter, LDV, for this investigation are briefly stated.

2.2 Literature Survey

2.2.1 Pressure Drop Investigations into the behaviour of air-solid flows were initially concerned with grain elevators. Cramp and Priestley (1924) attempted to calculate the forces acting on each grain, taking account of the drag on the particle and the friction between the pipe wall and the particle. From this they obtained an expression giving an estimate of the pressure drop in the elevator. Cramp (1925) extended this method to the prediction of the pressure drop in a pneumatic transport system conveying other materials.

There has been much work published on the pressure drop encountered in an air-solid flow since then. Most of the work has been based on the assumption that the total pressure drop along a straight

length of pipe, Δp_T, can be split up into several non-interacting parts, i.e.

$$\Delta p_T = \Delta p_{a\alpha} + \Delta p_{ah} + \Delta p_{af} + \Delta p_{s\alpha} + \Delta p_{sh} + \Delta p_{sf} \qquad (2.1)$$

where $\Delta p_{a\alpha}$ is the pressure drop due to the acceleration of the air,

Δp_{ah} is the pressure drop due to the static head of air,

Δp_{af} is the pressure drop due to the friction between the pipe and the air,

$\Delta p_{s\alpha}$ is the pressure drop due to the acceleration of the particles,

Δp_{sh} is the pressure drop due to the static head of the particles,

and Δp_{sf} is the pressure drop due to the friction between the particles, and between the particles and the pipe wall.

A few of the papers will be surveyed below, in some cases giving the final expressions for the pressure drop. In order to simplify the problem, all the theoretical derivations required assumptions and the validity of some is rather dubious.

Voigt and White (1948) derived an equation for the pressure drop due to the friction between the air and the particles, and the pipe wall, Δp_f . They started with the Fanning equation for the pressure drop in a pipe due to the friction of a single phase fluid:-

$$\frac{\Delta p}{L} = \frac{4\rho \bar{v}^2 f}{2gD} \qquad (2.2)$$

where f is the friction factor. They assumed that this expression could be extended for use in air-solid flows using dimensional analysis and produced the expression :-

$$\frac{\Delta p_f}{\Delta p_{af}} = 1 + A \left(\frac{D}{d}\right)^2 \left(\frac{\rho_a}{\rho_s} \frac{L_s}{Re}\right)^k \qquad (2.3)$$

where A and k are functions of $\left[\frac{1}{3}(\rho_s - \rho_a)\ \rho_a\ gd^3/\mu\right]^{\frac{1}{2}}$, the actual values being found experimentally, and Re is the Reynolds number of the air in the pipe. Although the expression does not involve the particle

velocity, one of the assumptions made in the analysis was that the slip velocity ($\bar{v}_a - \bar{v}_s$) is proportional to the air velocity $\bar{v}_a$. In neither the present work nor other experimental investigations of the air velocity (e.g. Jokati and Tomita (1971) and Jodlowski(1976)) was this assumption found to be justified.

The pressure drop due to the acceleration of the particles, was investigated by Hariu and Molstad (1949). They calculated the upward acceleration, α, of each particle in an accelerating upward flowing mixture to be :-

$$\alpha = \frac{3\rho_a}{4\rho_s d} \times (\bar{v}_a - \bar{v}_s)^2 C_D - g - \frac{f_s \bar{v}_s}{D} \qquad (2.4)$$

where C_D is the drag coefficient of the particles and f_s is the friction factor of the solids. In this derivation they assumed that the particle-wall friction pressure drop could be represented by a modified Fanning equation [equation (2.2)] in which the variables of the fluid were substituted with those of the solid. The pressure drop due to the acceleration of the particles from zero velocity to $\bar{v}_s$ was found to be:-

$$\Delta p_{s\alpha} = \frac{\alpha G_s}{g\bar{v}_s} \qquad (2.5)$$

where G_s is the solids mass velocity. The modification of the Fanning equation to give the pressure drop due to the friction between the particles and the walls has been used by several authors [Stemerding (1962), and Rose and Duckworth (1969)] . It seems reasonable to assume that the pressure drop due to the friction of the solids, Δp_{sf} is a function of the solids velocity, but whether it is proportional to the square of the mean velocity, as implied by the modification of the Fanning equation, should be investigated.

Clark et al (1952) also used the drag of the particles on the air to derive an equation for the pressure drop due to the solids friction in a horizontal conveying line :-

$$\Delta p_{sf} = \frac{L_s L}{\bar{v}_s \pi R^2} \left(1 - \frac{\rho_\tau}{\rho_s}\right) \left(\frac{\rho_a}{\rho_\tau}\right) \left(\frac{\bar{v}_a - \bar{v}_s}{v_\tau}\right) \qquad (2.6)$$

where v_τ is the terminal velocity of the particles in a fluid density ρ_τ. This analysis assumes that the drag on each particle is not affected by the walls or other particles, which is reasonable in dilute flow since the particles are in close proximity to each other and to the pipe wall for only a very small proportion of the time. However, they also assumed that collisions of a particle with other particles and with the wall did not affect the drag. This seems unlikely since even in dilute flows, particle-wall collisions occur frequently, changing the momentum of the particles.

McCarthy and Olson (1968) derived an expression for the total pressure drop using a continuum approach. They equated the change in momentum of the mixture with the shear stress and pressure gradient. The final equation for the pressure drop involved both the solid and air velocity, so that measurement of these variables was needed in order to test this analysis.

Rose and Duckworth (1969) produced an expression for the total pressure drop due to the solids and air in fully developed flow by considering the forces acting on a small section of the mixture in the pipe. Assuming that the solids velocity and shear stress in fully developed flow is constant, the total pressure drop was found to be :-

$$\Delta\rho_T = g\, L \sin\theta \quad \rho_a + \frac{G_s}{\bar{v}_s} \left(1 - \frac{\rho_a}{\rho_s}\right) + \frac{4L}{D} \tau_w \qquad (2.7)$$

where θ is the angle of inclination of the flow to the horizontal. The dependence of the variables in equation (2.7) on the properties of the conveyed material and the conveying system was further analysed using dimensional analysis, and a semi-empirical formula for the pressure drop using their experimental results was given. Dimensional analysis was also used by Boothroyd (1966) in a similar way to produce a

semi-empirical expression using experimental results. In both these cases the mean velocity was incorporated in the final expression.

Yang (1977) also used a modified Fanning equation for pressure drop due to the particle-wall friction. He produced an equation for the solids friction factor which was a function of a modified Reynolds number, and obtained the coefficients in this equation by correlating the results of other authors. This approach to the particle friction pressure drop implies that the relation to the particle velocity is not simply a square law.

At very low solids to air mass flow rate ratios, the phenomenon of drag reduction has been reported by many authors. This is the reduction of the pressure drop to less than that of the single phase fluid. When this occurs the use of equation (2.1) for the analysis of the total pressure drop becomes unsatisfactory because it suggests that the pressure drop due to the air phase is unchanged by the presence of particles. If this was so then when drag reduction occurred the frictional pressure drop due to the solids would have to be negative. This problem was overcome [Pfeffer and Kane (1974)] by combining the frictional losses of the two phases together :-

$$\Delta p_f = \Delta p_{af} + \Delta p_{sf} \qquad (2.8)$$

The total frictional pressure drop, Δp_f, is always positive, and can be found, with the reservations given above, from the modified Fanning equation :-

$$-\frac{\Delta p_f}{L} = \frac{4\,\bar{v}_a^{\,2}}{2D}\, f_m \qquad (2.9)$$

There have been many other papers describing theoretical or semi-empirical derivations of the pressure drop in air-solid flows [e.g. Jones et al (1967), Jokati and Tomita (1971) and Jodlowski (1976)]. The expressions given by these and other authors were analysed and

compared by Modi et al (1978). In most cases they found that the correlations in each paper usually predicted well the experimental results given in that paper, but usually disagreed with the experimental results given in other work. This probably indicates that the assumptions made in the analyses were not valid in all cases, and not all the parameters influencing the flow were taken into account. Richarson and McLeman (1969) found that the pressure drop could vary by as much as 100% between runs, and attributed this to the electrostatic charging of the particles. None of the correlations mentioned here take account of the electrostatic charge.

2.2.2Properties other than Pressure Drop There has been comparatively little work published on a theoretical solution of the properties of air-solid flows other than the pressure drop, although these are also of importance in the design of pneumatic conveying systems. The distribution of properties such as the particle velocity across the flow is very difficult to predict, but some approximate solutions have been found.

Soo (1962) and (1969) calculated the velocity and concentration distribution across a pipe of small particles for low solid to gas mass flow rate ratios. He suggested that the vleocity profile was described approximately by the expression :-

$$\frac{v_p - v_{pw}}{v_{pc} - v_{pw}} = \left(\frac{x}{R}\right)^{1/m} \qquad (2.10)$$

where m is a constant found by experiment. However, the results of Birchenough (1975) did not fit this expression at all well. Further experimental and theoretical work is needed to produce a valid expression for the particle velocity distribution.

Chan (1976) examined the forces acting on an air-solid mixture and produced a computer program to solve the equations of motion. He showed that a large number of computer drawn graphs giving the particle

velocity, electric-potential, particle density, mass flux, and diffusivity distributions in horizontal pipe flows with varying flow constants. However, as with all theoretical analyses, many assumptions had to be made, for instance that the flow was incompressible, and that all the particles had the same electric charge. Much experimental work is needed to measure the distribution of the properties so that they can be compared with the results predicted by the computer program. In this way it can be found if the assumptions were reasonable.

2.3 Particle Velocity Measurement

In the last section several theoretical analyses, many of them requiring a knowledge of the particle velocity, of the behaviour of two-phase flows were described. Several methods have been employed in the measurement of particle velocity, some of which will be described in this section. The methods can be divided into those measuring the mean particle velocity across the pipe, and those which measure the local particle velocity in a small volume, so that the particle velocity profile across the pipe can be found by moving the measuring volume along a diameter.

One of the first methods of measuring the average particle velocity was the isolation method [Segler (1951), Mehta et al (1957)]. A section of the pipe was isolated by two slide valves acting simultaneously and weighing the solids contained in that section. This gave the dispersed phase density of the particles, ρ_m, and using the mass flow rate of the solids, $\dot{m}_s$, the mean particle velocity $\bar{v}_s$, can be calculated as:-

$$\bar{v}_s = \frac{\dot{m}_s}{\rho_m . 2\pi R^2} \qquad (2.12)$$

However, there are several problems involved with this method. It is not a very accurate method since the isolation of the pipe cannot be

completed instantaneously. The plant has to be shut down after each measurement, unless a bypass system is provided, and it is a very tedious procedure.

A common method of mean particle velocity measurement involves the use of cross-correlation of the signals from two transducers set at a distance apart from each other along the flow. The time delay between similar signals from each transducer gives the velocity between them. Richardson and McLeman (1960) injected a pulse of air into the flow and, using two transducers to measure the electrostatic field at the outside of the pipe, the time for the pulse to pass from one transducer to the other was measured. However, the injection of an air pulse must have greatly disturbed the flow, and also the velocity of the air pulse was not necessarily equal to that of the particles. A more accurate method was used by Ottjes et al (1976), utilising two sensors measuring the flow of electrical charge through the pipe, and using an electronic cross-correlator to find the time delay between similar signals and the degree of correlation of those signals. This method causes no flow disturbance, but relies on a flat particle velocity correlation over long lengths of pipe, which indicated that the profile was flat.

There are several optical methods of particle velocity measurement, but unlike those methods described above the solids-to-air mass flow rate ratio is limited to a small value in order that the light can penetrate the flow. Photographic methods have been used for both mean and local velocity measurements. Jokati and Tomita (1971) and Jodlowski (1976) took high speed cine films of the flow and, by examining the film frame by frame, the mean particle velocity was obtained by averaging the velocity of each particle. McCarthy & Olson (1968) took double flash photographs using a very narrow depth of field camera. The distance each particle moved between flashes was measured, together with the time delay between flashes, giving the

velocity of the particles. Since the particles were only in focus over a very small distance, the velocity distribution was obtained.

In order to make local particle velocity measurements, some authors used a probe inserted into the flow. Soo et al (1964) used a fibre optic probe which recorded the local particle number density by pulses as the light beam between two fibre optics was interrupted by the particles. The local mass flux was recorded by an electrostatic ball probe. They assumed that the charge per unit mass on the particles was constant, and the charge on the particles was measured using the contact charging effect. From this, using an equation of the form of equation (2.12), the local velocity was calculated. The spatial resolution of this method was not good, since the probe was over 3mm in diameter, and also accuracy was limited because the charge per unit mass has been shown to vary considerably [Chan (1976)]. Peskin and Dwyer (1964) used an electrostatic probe similar to that used by Soo et al to measure the mass flux. From this they calculated the velocity of the particles. However, in order to do this the particle velocity at the centre of the pipe was assumed to be equal to the air velocity at the centre of the pipe. This assumption was found to be incorrect, both in the present work and by other authors.

Eichhorn et al (1964) employed an aerofoil shaped probe with a slot cut in the leading edge. Two optical fibres were embedded in the probe and light was shone down them. The light reaching the other end of the fibre was measured and, as particles went through the slot, they interrupted the beams. The time for one particle to pass from one fibre to the other was measured to give the local particle vleocity. Intrusive velocity measurement probes like this, however, have an unknown and possibly large effect on the particle velocities. Also, the probes tend to become quickly eroded by the abrasive flow and have to be replaced frequently.

Non-intrusive cross-correlation techniques for measuring local particle velocities have been used. Reibold et al (1970) and Venselaar et al (1978) passed two parallel laser beams through the flow and observed the signals arriving from one point on each beam using two photomultipliers. Again, an electronic cross-correlator was used to obtain the time delay of a particle passing between the beams. This method has been used successfully, but Lehmann (1975) found that the instrument was only suitable for measuring velocities below about 25 ms^{-1}. In order that the particles have a significant probability of passing through both beams the beams have to be quite close together, and at high velocities; the time resolution of most available correlators is not sufficient to measure the time delay accurately.

The laser-Doppler velocimeter , LDV, has been used for particle velocity measurements in two-phase flows by several authors [e.g. Boutier and Philbert (1972), Rinkevichyus (1969), and Riethmuller and Ginoux (1973) and Birchenough (1975)] . This method is also non-intrusive and can provide instantaneous measurement of the local particle velocity. There are no limitations on the velocity which this instrument can measure and the measuring volume can be made very small, in both cases it is superior to the laser cross-correlation technique. For these reasons the LDV was chosen for the particle velocity measurements undertaken in this project. The problems and principles of the laser-Doppler velocity meter are described in chapters 5 and 6.

2.4 Conclusions

In this chapter various theoretical derivations of the behaviour of the air-solid flows have been described, but it can be seen that there is little agreement either in the theoretical or experimental work. This indicates that there is a need for more accurate experimental investigations into the behaviour of the flows. The particle

velocity is an important factor in the flow but it is difficult to measure without causing significant disturbances to the flow. Some of the methods used in measuring the particle velocity were described and it was shown that many of them are inaccurate. The laser-Doppler velocity meter seems to offer a useful technique for such measurements and was therefore used in this project.

CHAPTER 3

PNEUMATIC CONVEYING PLANTS

3.1 Large Plant, Design Requirements

The main pneumatic conveying rig was designed to produce a vertical dilute phase air-solid flow in a vertical pipe. In order that the flow properties were not specified to the conveying system, the air-solid flow had to be fully developed at the measuring point. Also, the air and solid mass flow rates were required to be constant and the swirl in the flow kept to a minimum.

The system was designed to give a range of air and solids mass flow rates, with a simple and accurate method of measuring each, in order that the flow properties could be studied under a variety of known conditions. Since the measuring procedure was time-consuming, properties of the flow had to remain steady for periods of up to about 90 minutes.

The diameter of the vertical test pipe was chosen as 50 mm, since this was small enough to be practical in the restricted space available and large enough to be of industrial significance. The pipe needed to be transparent and resistant to abrasion, so that laser-Doppler velocity measurements could be made through the wall.

3,2 Original Large Conveying Plant

The pneumatic conveying plant used in the project had been designed and used in previous work by Birchenough (1975). It is shown in figures 3.1 and 3.2, excluding the modifications described in the next section.

The air was supplied by a Roots positive displacement blower which delivered a maximum of 9.4×10^{-2} $m^3 s^{-1}$ of air at 1.9×10^5 Nm^{-2} absolute.

The air was oil-free to prevent contamination of the solid. The blower was driven by a 15 KW electric motor having an operating speed of 2860 r.p.m.. A valve through which air could be vented to atmosphere provided variation of the air mass flow rate.

The air from the blower was cooled in a heat exchanger mounted above the blower. Cooling of the air was necessary since light plastic pipes were used for the air supply line. The variation of the flow rate of the cooling water provided some degree of control of the temperature of the air. The blower and heat exchanger were supported on anti-vibration pads in a sound-proofed room.

The air left the blower room in a 75 mm diameter P.V.C. pipe. An orifice plate meter, designed to B.S. 1042 and with sufficient up and downstream straight pipe, was situated halfway along the horizontal section. This provided metering of the air mass flow rate and it was calibrated as described in section (4.2).

After being reduced in diameter to 25 mm in order to increase the air velocity, the air line was connected to the mixing chamber which is described in section (3.3). The solids were conveyed to the mixing chamber by a screw feeder and were mixed with the air. The air-solids mixture left the mixing chamber via a 50 mm diameter mild steel pipe, which brought the flow down to floor level and included a section of rubber tubing to reduce the transmission of vibrations. The short length of pipe at floor level included a section which could be removed and replaced with a venturi contraction to reduce the pressure so that sub-micron titanium dioxide particles could be injected into the flow for air velocity measurements - see section (7.2).

The air-solid mixture then passed up the vertical test pipe, which was a 3 metre length of Q.V.F. glass pipe with a diameter, measured at either end, of 49.84 mm. The pipe was firmly anchored to and supported by, a triangular frame of square steel tubing. The glass

pipe had pressure tappings at intervals along its length, each carefully drilled so that the inside of the glass was not chipped. Above the glass pipe was a metre length of perspex pipe, 51.71 mm in diameter, in which Pitot-static measurements could be made - see section (4.2). The flow then passed into the collecting/storage hopper

This hopper, 4.5 m^3 capacity, acted as both a cyclone separator and a store for the solids. The air passed out through a filter above the hopper and was vented to the atmosphere via a duct. The storage hopper was pivoted on two points and rested on an hydraulic load cell at the third point. This load cell was found to be an inaccurate measure of the mass of the solids in the hopper - see section (4.3).

The solids in the storage hopper were discharged into the feed hopper underneath by means of a 150 mm diameter butterfly valve. A valve-controlled pressure balance pipe was provided to equalise the pressure in the two hoppers before opening the butterfly valve. The feed hopper had a 1 m^3 capacity, and the solids from the hopper fed into the mixing chamber by means of a screw feeder. The flow of the soldis out of the hopper could be assisted by a Simon's bin activator. The screw feeder consisted of a 47 mm screw driven by an electric motor via a Carter hydraulic gear unit which controlled the rate of rotation of the screw. The particles from the feed hopper fell into a trough, which could be vibrated to assist the flow, and were then transported by the screw and discharged into the mixing chamber. The method of calibrating the mass flow rate through the screw feeder is described in section (4.3).

The platform from which measurements were taken was completely separate from the rest of the pneumatic conveying plant and rested on rubber pads to reduce vibration. The height of the platform was such that the velocity measurements were taken about 2.5 metres from the bottom of the test pipe.

3.3 Modification of the Large Plant

Some problems had been encountered previously in the performance of the mixing chamber. Two arrangements had been tried, neither of which were ideal. In the first, shown in figure 3.3a, air entered the bottom of the chamber vertically through a 25 mm diameter pipe and, after mixing with the solids entering through the side, left through the top of the chamber by a 50 mm diameter pipe. This arrangement produced a good mixing of the two phases of the flow, but, due to the abrasive nature of the flow, the extension shaft of the screw feeder which passed through the chamber was rapidly worn through. In the second arrangement, shown in figure 3.3b, the air again entered the chamber through a 25 mm pipe, but the air-solid mixture left through a horizontal pipe below the screw feeder port. This arrangement was found to stop the erosion of the extension shaft of the screw feeder and it also reduced the number of bends needed after the chamber. However, in this arrangement the solids gain substantial downward momentum before reaching the air flow and thus require a large amount of energy to be entrained into the flow. It was found that this system became blocked at higher values of solids to air mass flow rate ratios.

The arrangement of the mixing chamber used in this project is shown in figure 3.3c. The air entered the bottom of the chamber by a 50 mm diameter pipe and left by a 50 mm diameter pipe at the side, above the screw feeder port. The entrance pipe was situated to one side of the chamber so that the extension pipe was not subjected to the direct flow as it was in the first arrangement. Since the exit port was above the screw feeder port, the solids needed less energy to become entrained into the flow than in the second arrangement. The use of a 50 mm diam. entrance pipe reduced the back pressure from the mixing chamber and did not reduce the mixing of the phases. In use it was found that this arrangement did not block even at the highest possible solids mass flow

rate, and the extension shaft of the screw feeder did not fail even after many hours use.

It was noticed that the flow in the glass pipe had been given a slight swirl by the preceeding bends. An attempt to remove this swirl was made by replacing the bend at the bottom of the vertical section with a steel box, shown in figure (3.4). It was found that, although the box appeared to reduce the swirl, it also produced a very large pressure drop and caused blockages. The former bend was replaced and the small degree of induced swirl tolerated.

Another problem was encountered in calibration of the orifice plate meter. It was possible to measure the air mass flow rate either by a Pitot-static traverse in the perspex pipe above the glass pipe, or by a laser-Doppler traverse in the glass pipe (section (7.3). However, these measurements could only be made in the absence of solids in the flow. Pressure pulsations were caused by the solids and, with the rig in its original configuration, it was not possible to discover if these pressure pulsations affected the calibration of the orifice plate meter. This problem was overcome by replacing the vertical section of the 75 mm diameter P.V.C. air supply pipe with a 50 mm diameter perspex tube having the facility for making Pitot-static traverses. The measurements were taken at about 2.5 m from the start of the pipe to allow the flow to become fully developed. The calibration of the orifice plate meter is described in section (4.2). The plant is shown with its modifications in figures (3.5) and (3.5a).

3.4 Small Pneumatic Conveying Plant

The large conveying plant was used to investigate the properties of the air-solid flow and, from the results obtained, it was decided to investigate the performance of the laser-Doppler velocity meter in a variety of situations. A pneumatic conveying plant was designed to convey a selection of solids in a continuous circuit so that small quantities of

of the solids could be used.

The plant is shown in figure 3.6. Air was supplied by a Roots reciprocating blower driven by an electric motor. After passing through an air reservoir to reduce any pressure pulsations, the air entered a venturi feeder (see figure 3.7), into which the solids were entrained by the flow. The pressure in the venturi feeder was controlled by the distance between the nozzle and the exit pipe, and also by the air mass flow rate from the blower. The air mass flow rate could be reduced by opening an outlet valve situated between the blower and the reservoir. The solids entered the feeder from a hopper above it, the mass flow rate being controlled by a gate valve.

The air-solid mixture left the venturi feeder by a 50 mm diameter steel pipe and passed into a horizontal, 40 mm square steel pipe. After about 2 metres of horizontal flow, the air-solid mixture then passed round a square section bend into a vertical square-section pipe about 2.5 metres long. The pipe reverted to the round section and the flow was returned to a point above the feed hopper.

After entering a funnel covered with filter cloth, the flow passed down a metre length of perspex pipe, 51.88 mm in diameter (measured). The bottom of the perspex pipe could be closed by means of a butterfly valve. The solids then entered the feed hopper, which was also covered with a filter cloth. It was found that the filter cloth produced so much back pressure that the venturi feeder mal-functioned. This problem was overcome by connecting an air release pipe between the hopper and the collecting hopper of the large plant, using the filter in the large plant to remove any fines contained in the air flow.

The air mass flow rate was measured by taking an air velocity profile with a Pitot-static tube in the pipe between the reservoir and the venturi feeder. The solid mass flow rate was measured by closing the butterfly valve in the perspex pipe above the hopper and measuring

the time needed to fill the pipe between two levels. Since the bulk density of the solids was measured (see section 4.4), and the volume between the two levels in the pipe was known, the solids mass flow rate could be calculated. Although neither the air not the solids mass flow rate measurements were very accurate, they provided an estimate of each with sufficient accuracy for what was required. The properties of the LDV, rather than those of the flow, were being investigated.

The square section pipe was employed so that the removal of transparent windows was simplified: Flat glass windows were set into the pipe near the end of both the horizontal and vertical sections, to enable laser-Doppler velocity measurements to be made. The use of removable windows meant that they could be replaced or cleaned, thus reducing the attenuation of the light by the window. Flat windows were chosen for their ease of manufacture and their lack of refraction problems which can be encountered with round glass pipes.

The piping of the small conveying rig was fixed to the framework of the large rig, with the blower underneath. This meant that the vertical square-section pipe passed through the platform and so the laser-Doppler equipment could be placed on the platform for measurements to be taken in the square pipe.

① Air Blower Assembly

② Heat Exchanger

③ Outlet Valve

④ Soundproof Room

⑤ Air Delivery Pipe

⑥ Orifice Plate

⑦ Hoppers, Screw Feeder, and Filter Unit

⑧ Air Outlet Duct

⑨ Test Section

⑩ Platform

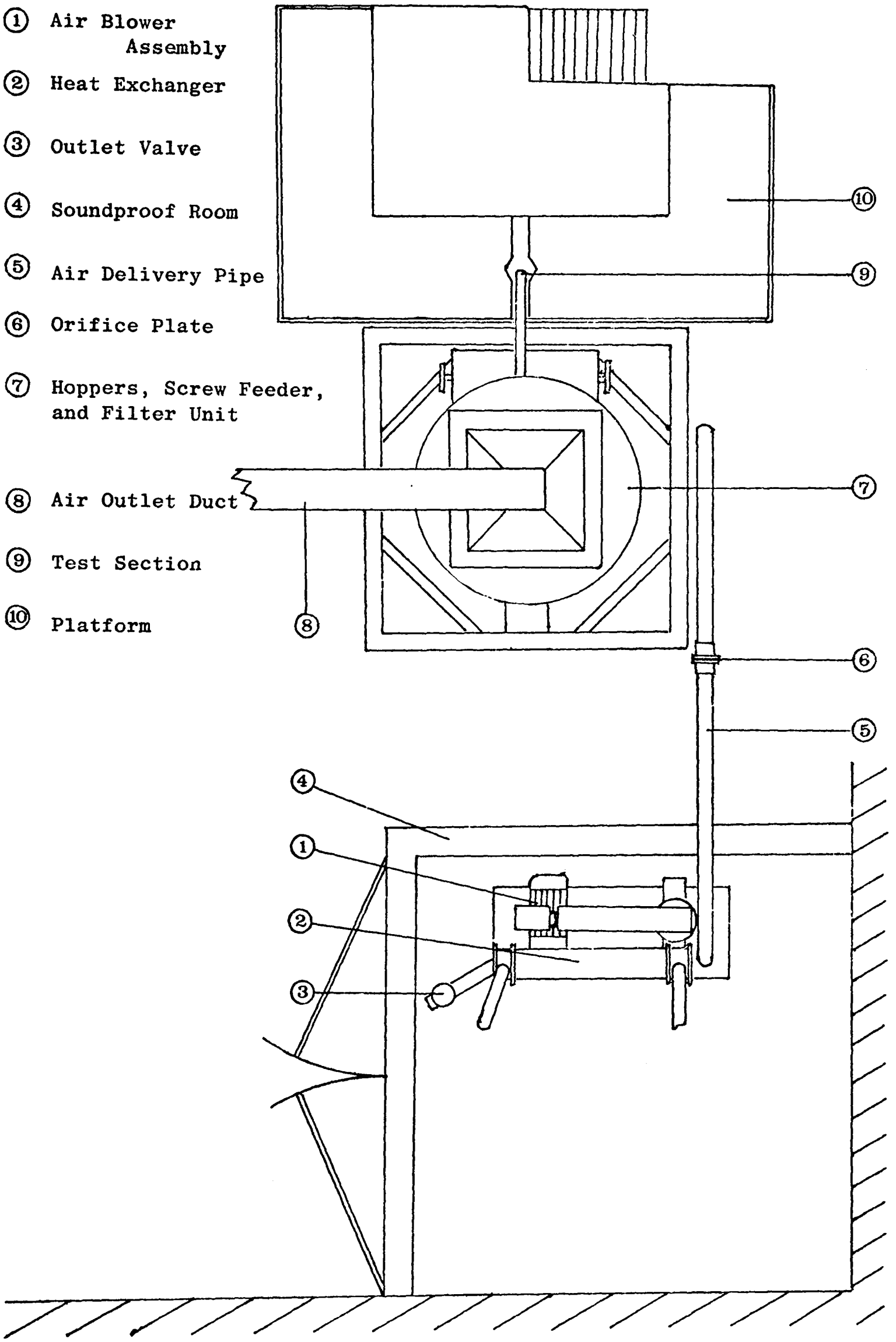

LARGE PLANT, PLAN VIEW

Figure (3.1)

① Air Outlet Duct
② Filter Unit
③ Collecting/Storage Hopper
④ Load Cell
⑤ Orifice Plate
⑥ Pressure Balance Pipe
⑦ Butterfly Valve
⑧ Access Port
⑨ Bin Activator
⑩ Screw Feeder Unit
⑪ Replaceable Section
⑫ Rubber Tubing
⑬ Mixing Chamber
⑭ Glass Test Section
⑮ Perspex Section
⑯ Platform

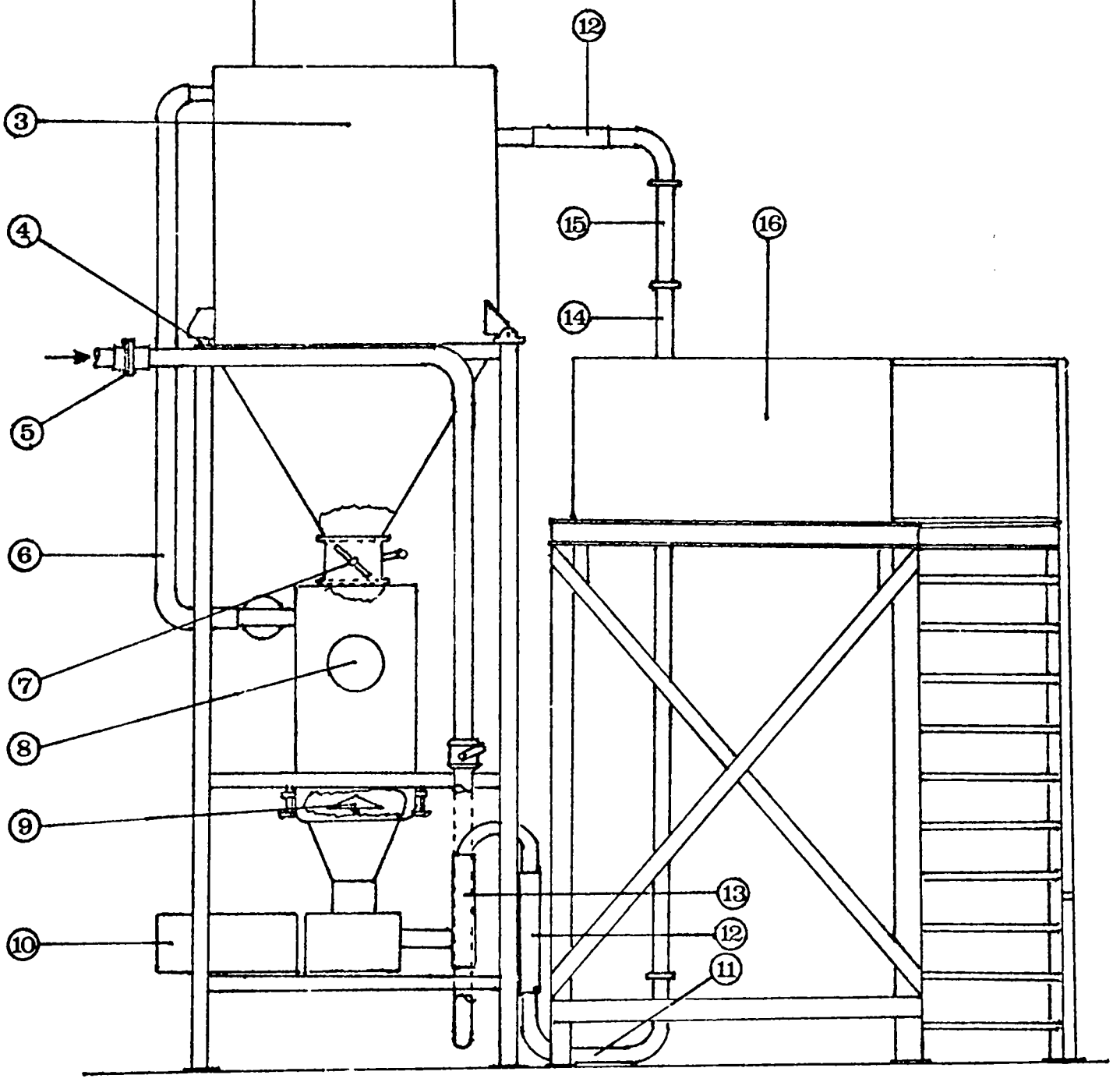

LARGE PLANT, ELEVATION (UNMODIFIED)

Figure (3.2)

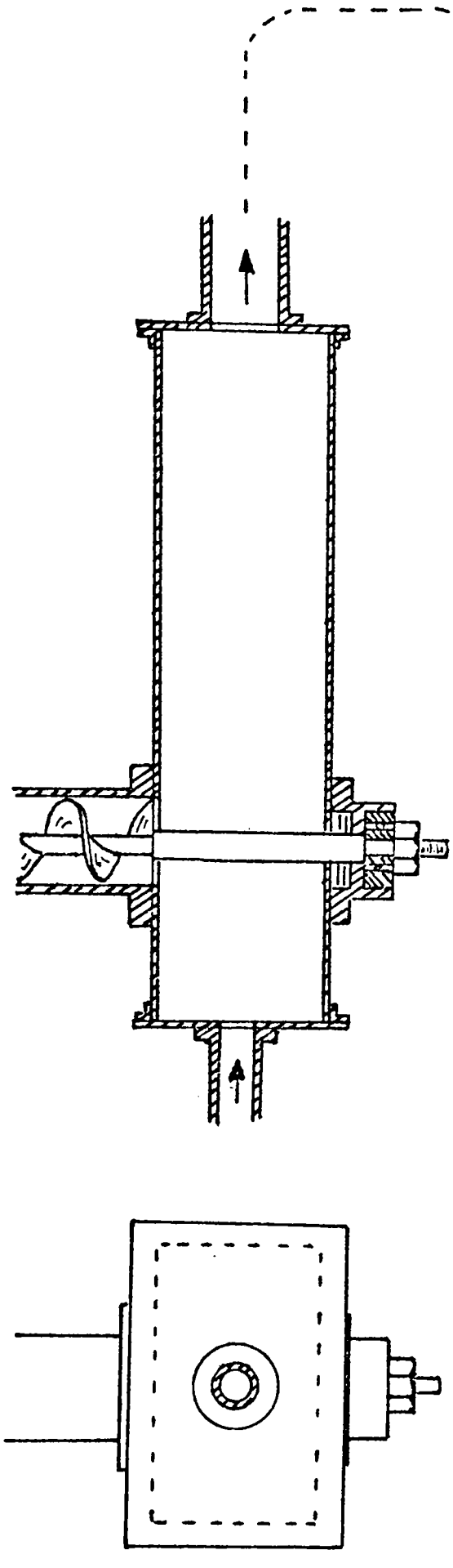

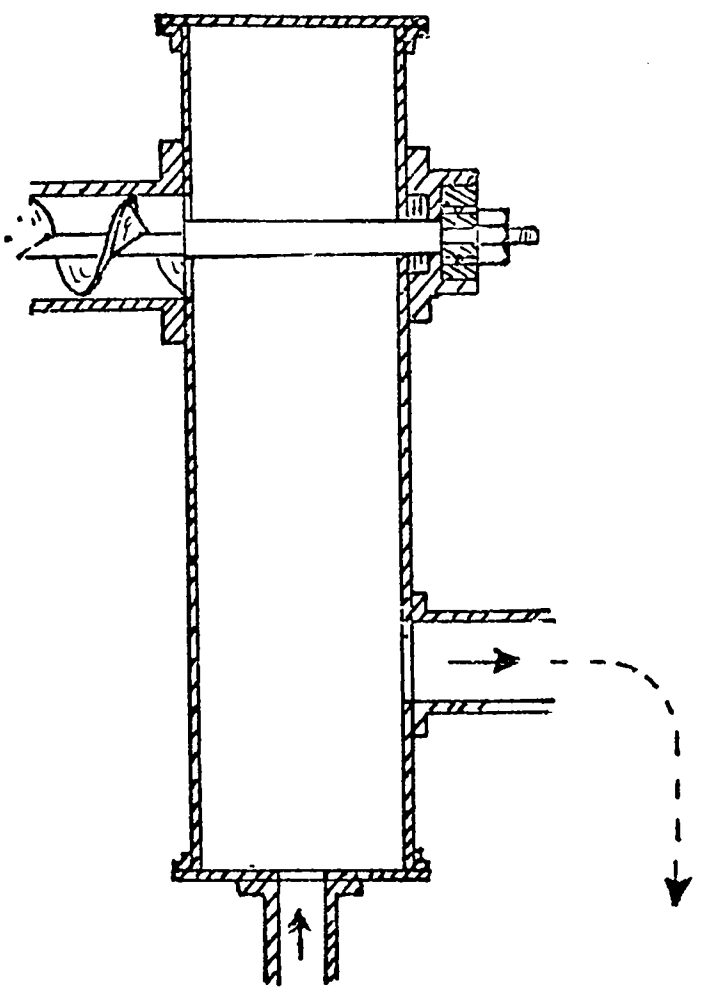

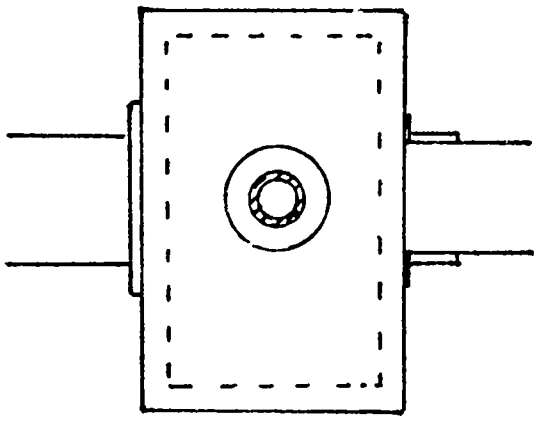

MIXING CHAMBER, INITIAL ARRANGEMENTS

Figure (3.3a)

Figure (3.3b)

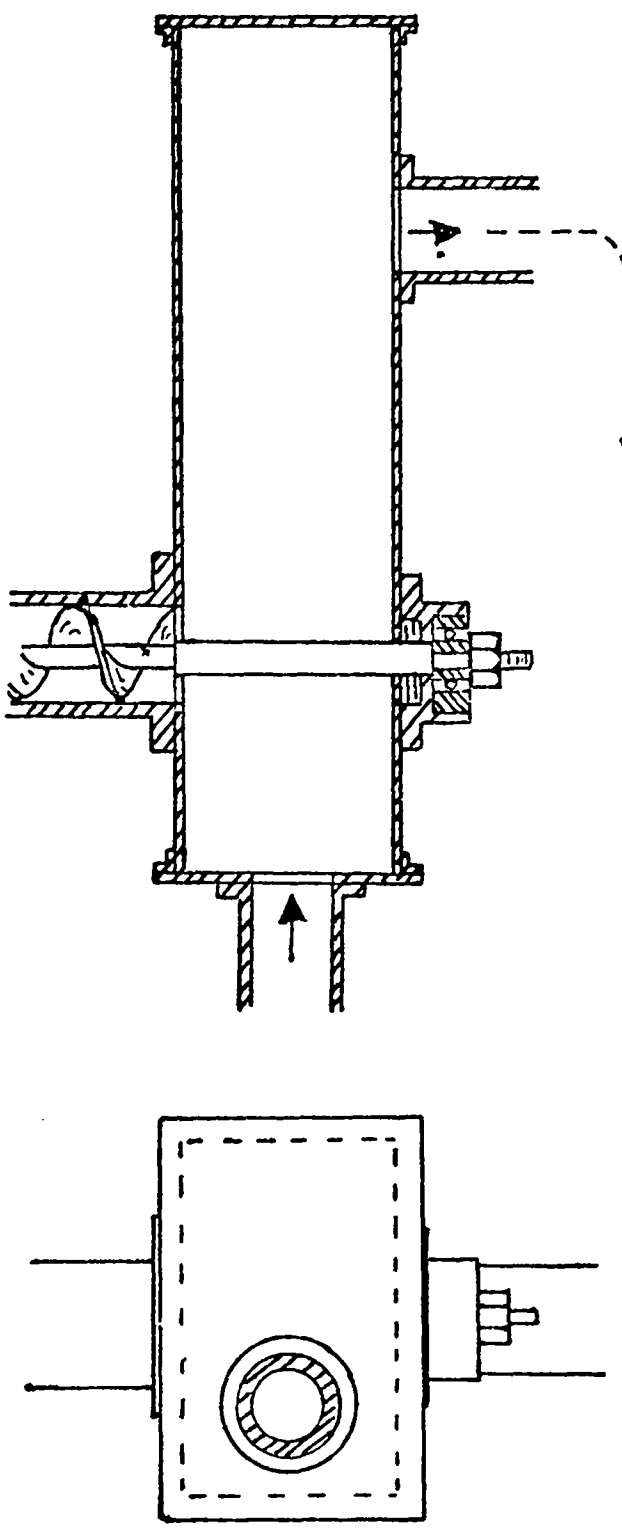

MIXING CHAMBER, FINAL ARRANGEMENT

Figure (3.3c)

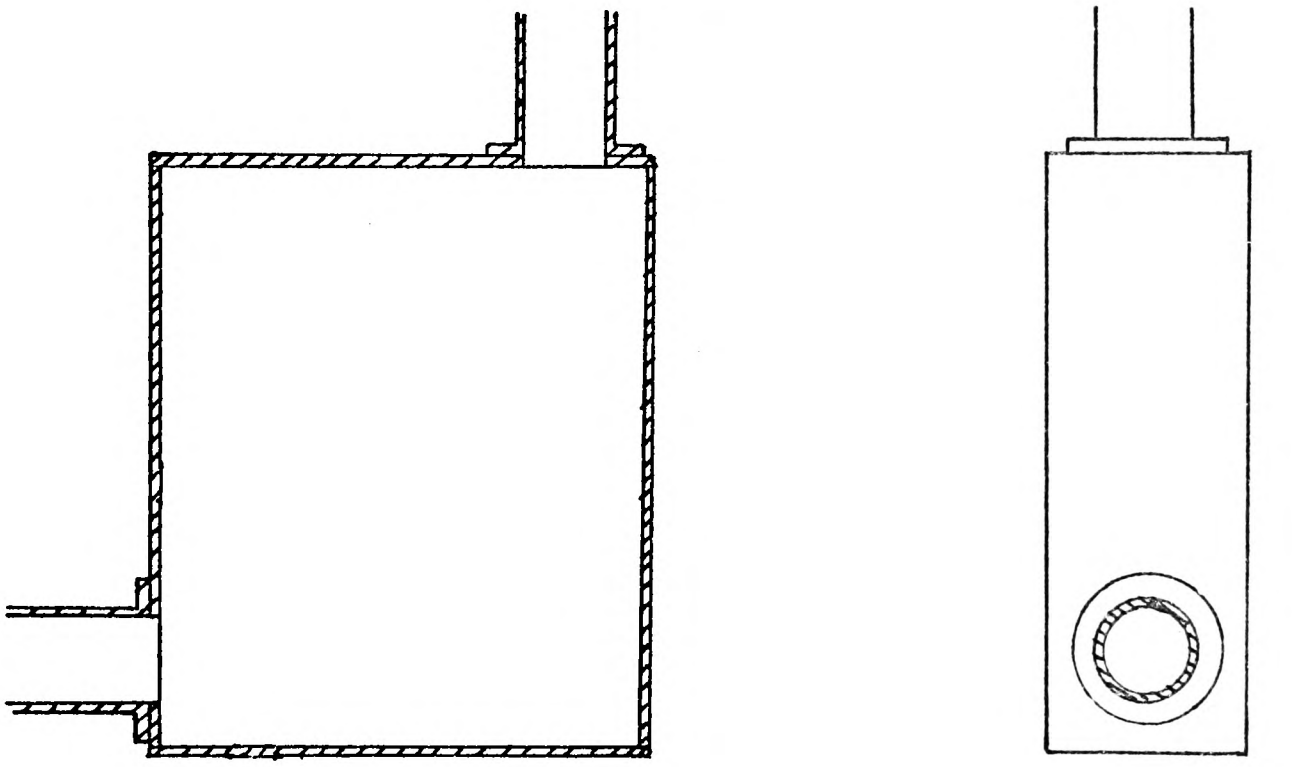

BOX BEND TO REDUCE SWIRLING FLOW

Figure (3.4)

① Air Outlet Duct
② Filter Unit
③ Collecting/Storage Hopper
④ Load Cell
⑤ Orifice Plate
⑥ Pressure Balance Pipe
⑦ Butterfly Valve
⑧ Access Port
⑨ Bin Activator
⑩ Screw Feeder Unit
⑪ Replaceable Section
⑫ Rubber Tubing
⑬ Mixing Chamber
⑭ New Perspex Pipe
⑮ Glass Test Section
⑯ Perspex Section
⑰ Platform

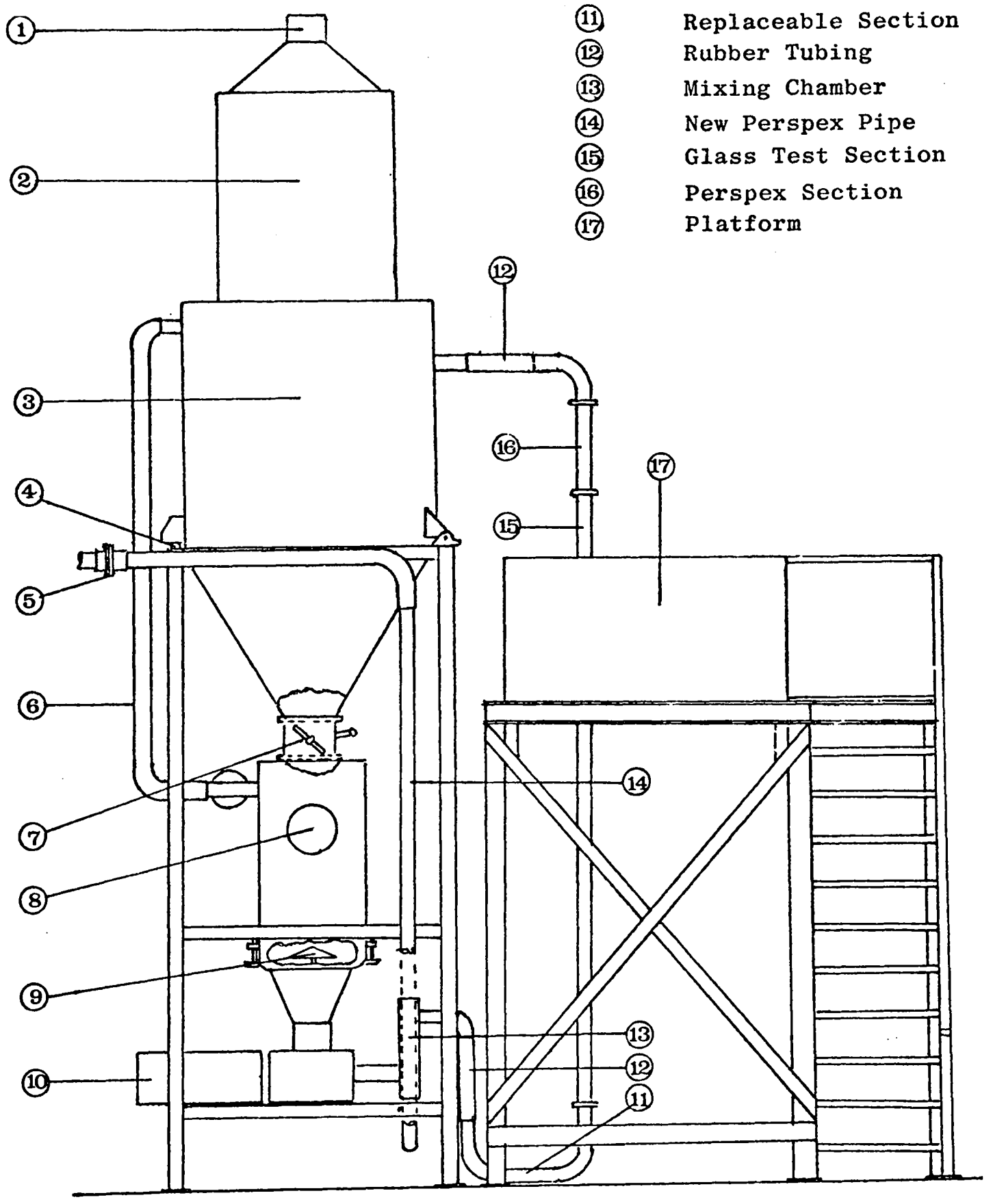

MODIFIED LARGE CONVEYING PLANT

Figure (3.5)

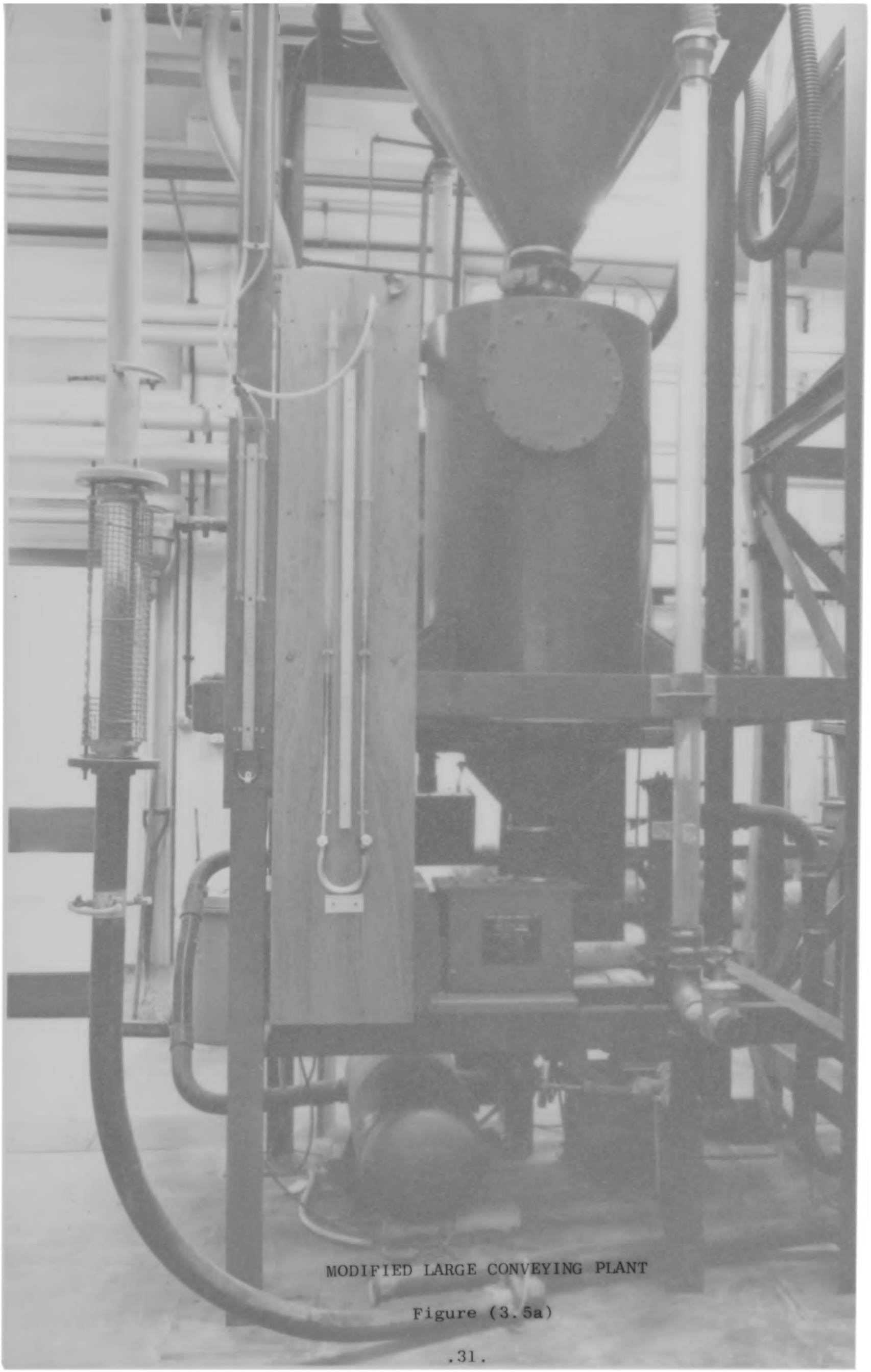

MODIFIED LARGE CONVEYING PLANT

Figure (3.5a)

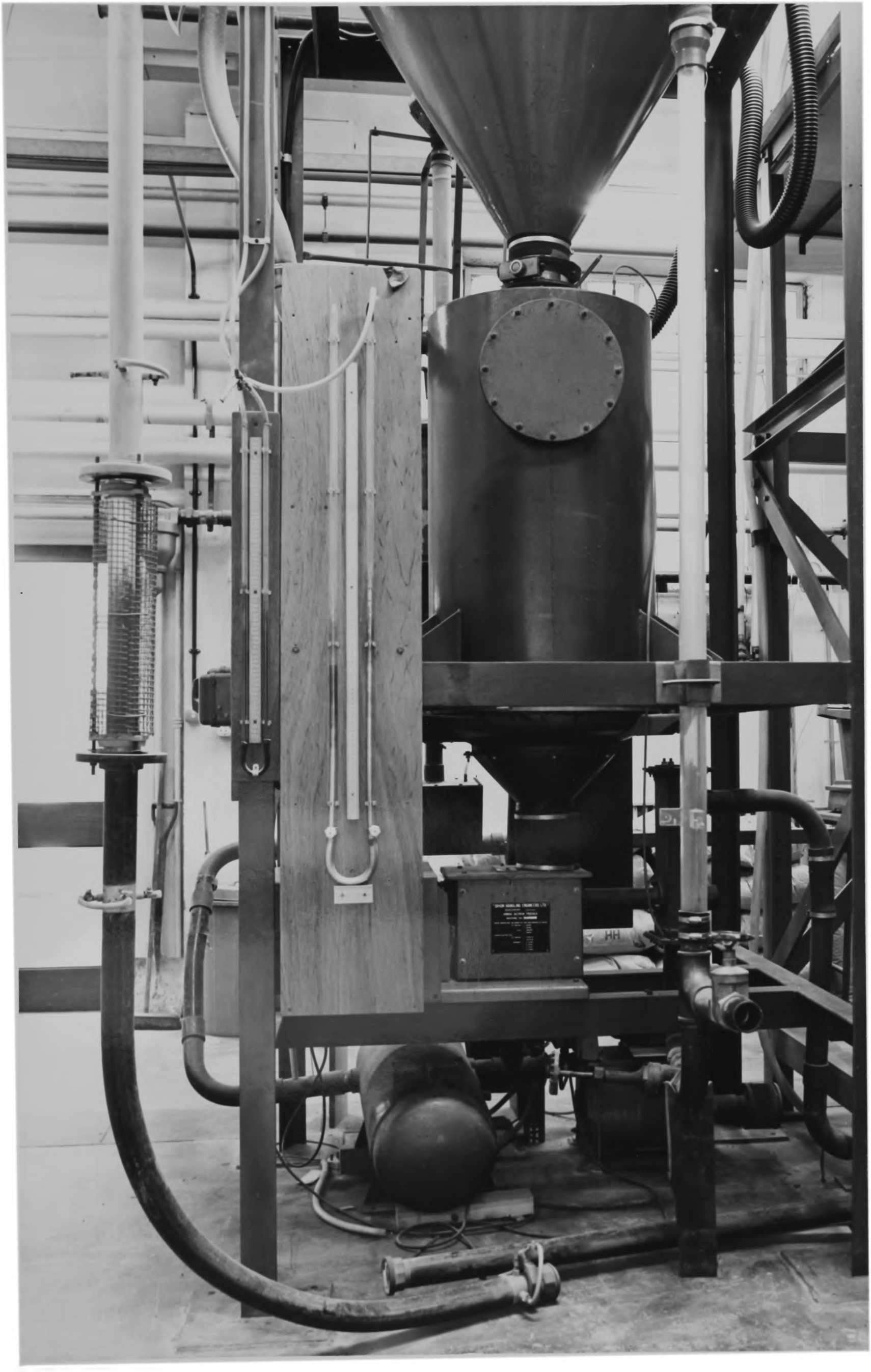

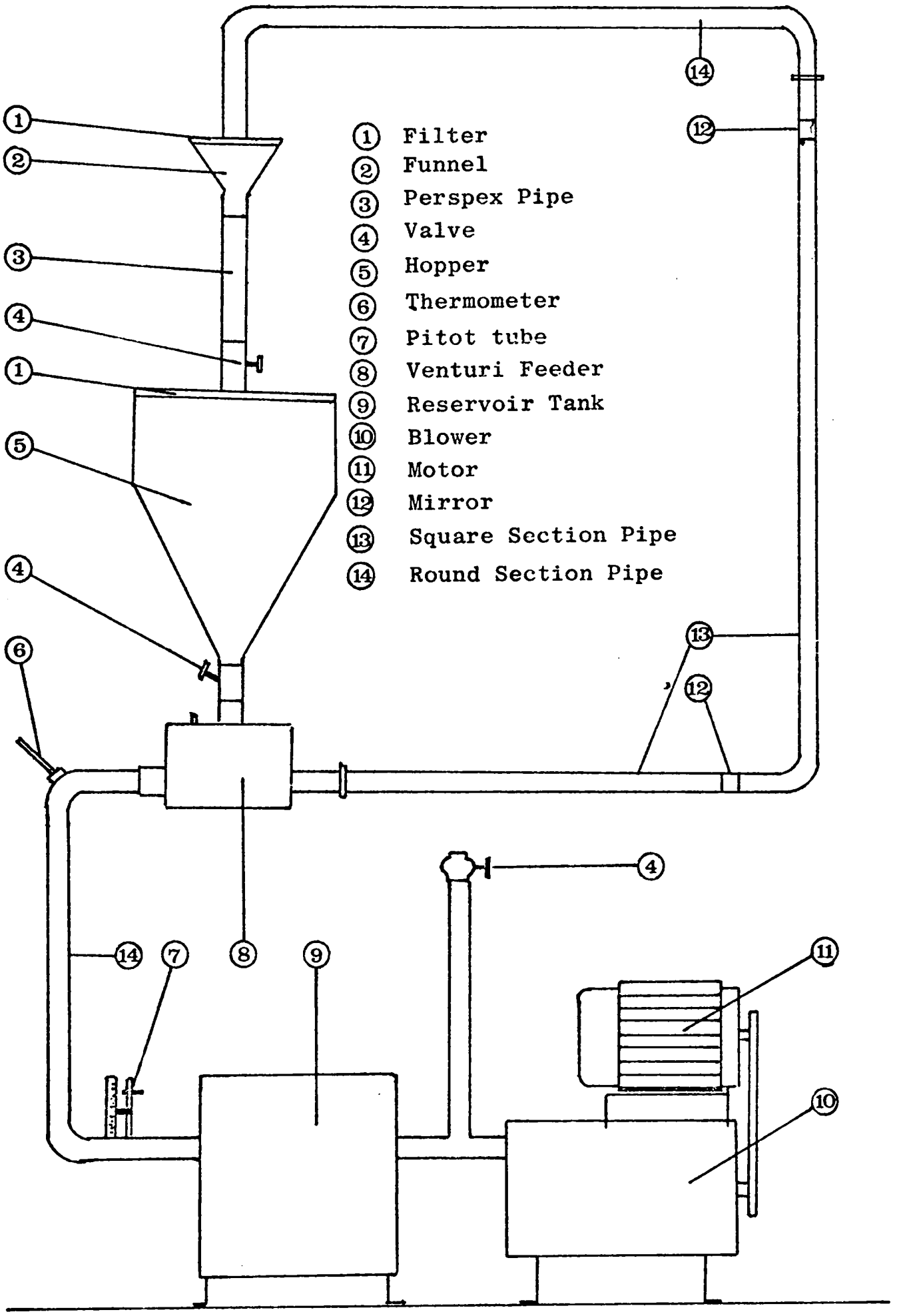

SMALL CONVEYING PLANT

Figure (3.6)

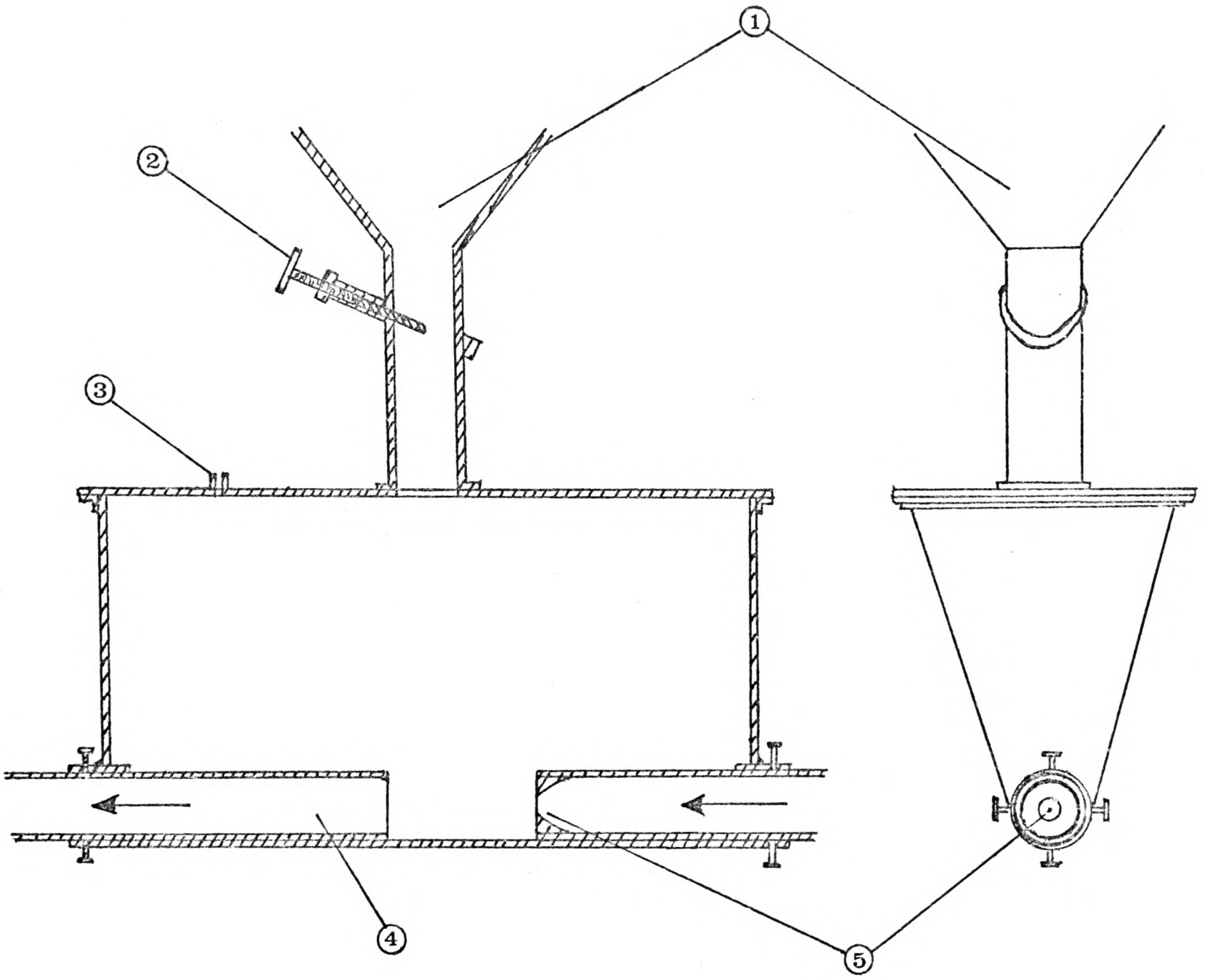

① Hopper
② Solids Feed Valve
③ Pressure Tapping
④ Outlet Pipe
⑤ Contraction

VENTURI FEEDER

Figure (3.7)

CHAPTER 4

CALIBRATION AND MATERIALS

4.1 Introduction

Since the properties of the two-phase flow in the large pneumatic conveying plant were being studied, it was necessary to be able to measure accurately the air and the solid mass flow rates. The air mass flow rate was measured with an orifice plate meter which was designed to conform with B.S. 1042. Although the Standard provides the calculation needed for obtaining the air mass flow rate without calibration, the air flow through the orifice contained pulsations, especially when solids were added to the flow, and calibration was necessary to discover whether the Standard was still valid. The solid was delivered into the flow by a screw feeder having variable speed control, and calibration gave the relation between the speed of rotation of the screw and the mass flow rate for the solid. Calibration was necessary for each type of solid used.

The properties of the particles used in the project were measured so that it was possible to compare the results obtained with each type of particle, and also it was possible to compare the results with those measured by other workers.

4.2 Calibration of the Orifice Meter

The orifice plate is shown in figure (4.1). It was set between two flanges in the P.V.C. pipeline in the position shown in figure (3.5). Static pressure tappings were set at positions 'D' and 'D/2' as described in BS 1042. The pressure drop across the orifice plate was measured with a water-filled U-tube manometer and the upstream pressure was measured with a mercury-filled U-tube manometer. The temperature of the

air was recorded by a thermocouple protruding into the flow after the heat exchanger, and the atmospheric pressure was measured with a mercury barometer.

Initially calibration was carried out in the absence of solids in the flow. The air mass flow rate was measured with a Pitot-static tube in the perspex pipe above the glass test pipe (see figure (3.5)). The Pitot-static pressure was measured with an oil-filled inclined manometer, and was measured at 2 mm intervals along orthogonal diameters of the pipe. For each calibration test the air temperature was allowed to settle before the measurements of pressure drop across the orifice plate, upstream pressure at the orifice plate, Pitot-static pressure profile and static pressure at the test point were taken.

The air mass flow rate was calculated from the Pitot-static traverse using the method described in Ower and Pankhurst (1977). Bernoulli's equation :

$$p_o = p\left[1+\frac{\gamma-1}{2}\ M^2\right]^{\frac{\gamma}{\gamma-1}} \qquad (4.1)$$

gives the relation between the Pitot pressure, p_o, the static pressure, p, and the Mach number, M. The ratio of the specific heat at constant pressure to that at constant volume, γ, is equal to 1.4 for air, and equation (4.1) can be expanded as a polynomial to give :-

$$p_o = p + \tfrac{1}{2}\rho v^2\left[1 - \frac{M^2}{4} - \frac{M^4}{64} - \ldots\right] \qquad (4.2)$$

However, since the maximum velocity expected in the test pipe was about 60 ms^{-1}, the maximum value of M will be about 0.2, and so the third and subsequent terms can be ignored as negligible, giving:-

$$p_o - p = \tfrac{1}{2}\rho v^2 \qquad (4.3)$$

The density, ρ, of the air at the test point can be found from the static pressure, so that, using equation (4.3), the velocity profile of the air across the pipe can be calculated from the variation of the

Pitot-static pressure, $(p_o - p)$, across the pipe.

Some examples of the velocity profile are shown in figure (4.2). There was little deviation of the measured velocity profile from the standard power law velocity profile (Ower and Pankhurst (1977)).

The air mass flow rate can be calculated from the air velocity profile as follows. The air mass flow rate through an annulus with radius r, and very small width δr, is $\delta \dot{m}_a$, such that :-

$$\delta \dot{m}_a = 2\pi r.\ \delta r.v(r) \qquad (4.4)$$

where v(r) is the air velocity at radius r. The total air mass flow rate, $\dot{m}_a$, through the pipe, radius a, is therefore :-

$$\dot{m}_a = 2\pi \int_o^a v(r).r.dr \qquad (4.5)$$

The volumetric flow rate is given by :-

$$\dot{V}_a = \frac{\dot{m}_a}{\rho} \qquad (4.6)$$

and the average velocity by :-

$$\bar{v} = \dot{V}_a / \pi r^2 \qquad (4.7)$$

The air mass flow rate was calculated from each Pitot-static profile using the computer program given in Appendix I. The value obtained was compared with that calculated using BS 1042 and the results are given in table (4.1).

There was good agreement between the two methods of measuring the air mass flow rate. The tendency of the values obtained from the Pitot-static profiles to be less than those from BS 1042 was probably caused by air leaking back up the screw feeder into the feed hopper. Although these results suggested that a reasonably accurate measure of the air mass flow rate could be obtained using BS 1042, it was noticed that when

solids were added to the flow in the mixing chamber pressure pulsations occurred in the U-tube manometer measuring the pressure drop across the orifice plate. In order that the effect of these pulsations on the calibration of the orifice plate meter could be quantified, it was necessary to modify the pipework of the rig so that a Pitot-static traverse could be taken upstream of the mixing chamber. These changes are described in section (3.3), and the position of the traverse is shown in figure (3.5). The method of taking and processing the results was the same as described previously, and the results obtained are given in table (4.2). There was even closer agreement between the Pitot traverse results and those from BS 1042 than before. This implied that the pulsations were not sufficient to invalidate the use of the Standard to calculate the air mass flow rate through the orifice plate, and so the air mass flow rate was calculated using BS 1042 throughout this investigation. The closer agreement of the measurements upstream of the mixing chamber with BS 1042 as compared to those downstream of the mixing chamber can be explained by the loss of some air through the screw feeder.

4.3 Calibration of the Screw Feeder

The solid mass flow rate was adjusted by a dial on the Carter gears which controlled the speed of rotation of the screw feeder. The rotational speed of the screw was measured and found to be directly proportional to the setting on the dial. Calibration of the screw feeder was necessary in order to find the relationship between the setting on the dial and the solid mass flow rate for each type of solid used.

Initially the solid mass flow rate was measured with no air flow, by removing the bottom from the mixing chamber and collecting and weighing the solids delivered in a set time. It was found that the

solid mass flow rate was directly proportional to the setting on the dial, with a different constant of proportionality for each solid. Tests were made to measure the effect of the bin activator and the trough vibrator, and neither was found to change measurably the mass flow rate (see figure 4.3).

However, even though a small air line between the mixing chamber and the feed hopper helped to reduce the pressure difference across the solids in the feeder, it was thought that the air flow might cause significant back pressure against the flow of solids. Therefore, the solid mass flow rate was measured with varying rates of air flow. The procedure for measuring the solid mass flow rate was as follows: With the pressure difference across the orifice plate and the screw feeder dial set at the desired values, the system was allowed to run for a short time in order to reach equilibrium with the butterfly valve between the two hoppers open. The butterfly valve was then closed and the system run for a set time before being shut down. The solids in the collecting hopper were than removed via a chute out of the inspection hatch in the feed hopper (see figure (3.5)). The solids were then weighed and returned to the feed hopper.

This procedure was followed for each type of solid for a series of different air and solid mass flow rates. The results are shown in figures (4.4) and (4.5). It was found that the mass flow rate of solids was proportional to the setting on the dial for each mass flow rate of air, but the constant of proportionality, k, varied with the air mass flow rate. The variation of k with the pressure difference across the orifice plate is shown in figures (4.6) and (4.7), with the curve of the best polynomial fit using the method of least squares. The relation between the setting on the dial, ℓ , and the solid mass flow rate, $\dot{m}_s$, was given by the equation :-

$$\dot{m}_s = k\ (\ell + 2.47)\ \text{Kgs}^{-1} \qquad (4.8)$$

The load cell under one of the supports of the collecting hopper was also calibrated. Standard weights were placed centrally on top of the filter above the hopper and the readings on the load cell were noted. Also, during the calibration of the screw feeder the reading of the load cell was noted before the solid in the hopper was weighed. The results are shown in figure (4.8). The large degree of scatter in the results was partly due to the inaccuracy of the load cell and partly due to the fact that the load cell was situated at only one of the three support points, and the piling of the solid at different points in the hopper caused a variation in the load measured. A more accurate method of weighing the solid in the collecting hopper would involve the positioning of a load cell at each supporting point.

4.4 Properties of the Solids

It was important to know the properties of the solids that affected the behaviour of the flow in order that comparison could be made between flows transporting different types of particles, and also so that comparison could be made with work published by other authors. The particle properties of interest for the project were the mean particle size and the range in sizes, the particle shape, and the particle density. Since the size and shape of the particles changed after several circuits in the plant, the properties were measured before and after conveying. The properties which were measured, as described in the following sections, are given in table (4.3).

Care was needed to ensure that the measurements were taken on a representative sample of the solids. In most cases the system shown in figure (4.9) was employed. The total volume of solid could be separated into two portions, with each portion containing solid from all parts

of the original volume. The process was then repeated on one of the two halves, one of which was halved again and so on until a small sample was obtained. This process ensured that a sample was obtained which was representative of all parts of the original volume. In the case of samples taken from the solid in the large conveying rig after it had completed several circuits, the bottom of the screw feeder was removed and the sample collected as the solid was delivered by the screw feeder. It was hoped that the solid was sufficiently mixed in the feed hopper for this to be a reasonably representative sample.

Two types of solid were used in the large conveying plant, ballotini, which were nearly spherical and had a small size distribution, and sand, which was angular with a large size distribution. Titanium oxide particles, which were submicron in diameter, were also conveyed in this rig in order to produce light scattering for LDV air velocity profiles to be measured (see section 7.2). In the small plant two different sorts of plastic chips, both roughly cylindrical in shape, were used.

4.5 Particle Size Analysis

The size range of the ballotini was too small for sieve analysis to be used to measure the size distribution. The method used for size analysis was measurement of individual particles under a microscope. Since the particles were nearly spherical, it was possible to measure their diameters directly using a scale in the eyepiece of the microscope. Where the particles were obviously elongated, the average of the long and short diameters was taken. About 1000 particles were measured and the size distribution is shown in figure (4.10a). In order to reduce the effect of the distribution in particle size on the flow, the ballotini was sieved to between the diameters 450 μm and 500μm. The size distribution was remeasured and the result is shown in figure (4.10b).

The size distribution of the sand, type 52/100, was much wider than that of the ballotini and it was possible to use sieve analysis to obtain the size distribution. The size distribution is shown in figure (4.11). A batch of sand was also sieved to between 300 μm and 355 μm before conveying in the large plant. The size distribution of this sand was measured using the microscope as described above. However, since the grains were very irregular in shape the linear cross-section was measured in two orthogonal directions and the mean taken (Fig. 4.12).

The spread in sizes of the sieved sand [figure (4.11)] does not appear to be very much less than that of unsieved sand [figure (4.12)] and the maximum size of the particles appears to be greater. There is also little difference in the standard deviation of the two types of unused sand given in table (4.3). However, this was probably largely caused by the difference in the size measuring tachniques applied to these two samples, since the equivalent diameter obtained from sieving is likely to be different from that obtained by microscope analysis. The sieved sand could be assumed to have a much smaller spread in sizes since it was obtained from one sieve, giving a nominal diameter range of 300 - 355 μm, i.e. much less than the size range of the sieved sand.

The mean diameter of both the ballotini and the sand was found to decrease after it had been circulated around the plant. The glass ballotini was crushed by the screw feeder and fines were produced, as can be seen in figure (4.13), which shows the size distribution after passing once through the screw feeder. The size distribution after many circuits is shown in figure (4.14). The corner of the sand grains became rounded after repeated circuits as described in section 4.6, and the resulting distribution is shown in figures (4.15) and (4.16).

The titanium dioxide was collected on a prepared grid as it issued from the pressure tapping at the top if the test section. As titanium dioxide was too small for measurement on an optical microscope, several

electron micrographs (figure (4.17)) were taken in the School of Biology. From these the size distribution shown in figure (4.18) was obtained.

The plastic chips used in the pneumatic conveying rig were too large to be analysed for their size distribution with the sieves available. Individual chips were weighed on an accurate balance and using the specific gravity, measured as described in the next section, the distribution of the volume of the particles could be calculated. From this, the distribution of the diameters of spheres of equivalent volumes were found (see figures (4.19) and (4.20)).

4.6 Particle Density and Shape

The specific gravity of the solids was measured using a specific gravity bottle by measuring the weight of water displaced by a known weight of solids. The bulk density of each solid was measured by weighing a known volume of solids poured into a measuring cylinder. The bulk density was also measured after the solids had been conveyed. The results of these measurements are given in table (4.3).

A rough measure of the particle shape was obtained using the method suggested by Riley (1977). About 4×10^3 mm^3 of the solid was weighed, poured into a measuring cylinder and then covered with water. After mixing, the solid was allowed to settle out for about 30 minutes, and the height, h_s, of the solid column was accurately measured. The measuring cylinder was then dropped 100 times from a height of 10 mm and the height, h_t, measured. The plot (figure (4.18)) of the ratio of the change in height to the original height $((h_s - h_t)/h_s)$ against the change in height $(h_s - h_t)$ shows the variation of shape of the different particles. The solids have to be sieved to a small size distribution before these measurements can be taken since the compacting of the solids is dependent both on the size and shape of the particles.

CALIBRATION OF THE ORIFICE PLATE DOWNSTREAM OF THE MIXING CHAMBER, WITH NO SOLIDS IN FLOW

Run	Air Mass Flow Rate		
	B.S.1042 ($\times 10^2 kgs^{-1}$)	Pitot-static ($\times 10^2 kgs^{-1}$)	Difference (%)
1	2.48	2.46	-1.2
2	3.48	3.48	0.0
3	4.39	4.36	-0.7
4	4.82	4.82	0.0
5	5.41	5.53	2.2
6	6.04	6.12	1.3
7	6.52	6.50	-0.3
8	6.97	6.85	-1.7
9	7.14	7.04	-1.4
10	7.65	7.68	0.4
11	7.91	7.85	-0.8
12	8.50	8.26	-2.8
13	9.66	9.45	-2.2
14	9.91	9.77	-1.4
15	10.12	9.94	-1.8
16	10.44	10.30	-1.3
17	10.72	10.45	-2.5

TABLE (4.1)

CALIBRATION OF ORIFICE PLATE UPSTREAM OF THE MIXING CHAMBER, WITH SOLIDS IN THE FLOW

Run	Screwfeeder Setting	Air Mass Flow Rate			Solid mass loading ratio
		B.S. 1042 ($\times 10^2 kgs^{-1}$)	Pitot-static ($\times 10^2 kgs^{-1}$)	Difference (%)	
P2	2	8.66	8.64	-0.2	0.76
P3	4	8.48	8.38	-1.2	1.06
P4	6	8.16	8.14	-0.2	1.66
P11	0	5.08	5.07	-0.2	0
P12	2	4.85	4.86	0.2	0.94
P13	4	4.83	4.86	0.6	1.92
P14	6	4.57	4.59	0.4	2.90
P21	0	12.40	12.34	-0.5	0
P22	2	12.06	12.05	-0.1	0.35
P23	4	12.80	12.73	-0.5	0.66
P24	6	12.80	12.71	-0.7	1.00
P25	8	12.70	12.08	-5.3	1.34

TABLE (4.2)

PROPERTIES OF SOLIDS

Solid	Sieve Range μm	Numerical Average Diameter μm	Standard Deviation μm	Weight Average Diameter μm	Standard Deviation μm	Density Kg m^{-3}	Poured Bulk Density Kg m^{-3}	Particle shape $(h_s-h_t)/h_t$
Ballotini								
unused	-	456.4	24.9	479.1	35.9	2898	1680	-
unused	425-500	461.8	24.2	462.3	25.0	2898	1690	0.074
once through screw feeder	425-500	440.9	34.2	448.2	29.4	2898	1730	-
used	425-500	297.5	171.0	450.2	43.6	2898	1700	-
Sand 52/100								
unused	-	176.3	37.7	260.6	68.7	2600	1480	-
unused	300-355	366.2	56.1	385.8	49.7	2600	1470	0.189
used	-	61.5	53.0	188.8	71.7	2600	1450	-
used	300-355	105.6	78.1	227.5	69.7	2600	1488	-
Black Plastic Pellets								
unused	-	3278	304	3290	294	993.5	61.2	-
Transparent Plastic Pellets								
unused	-	2304	357	3290	724	890.3	430	-
Titanium Oxide	-	0.267	0.111	0.385	0.103	4200	-	-

Table 4.3

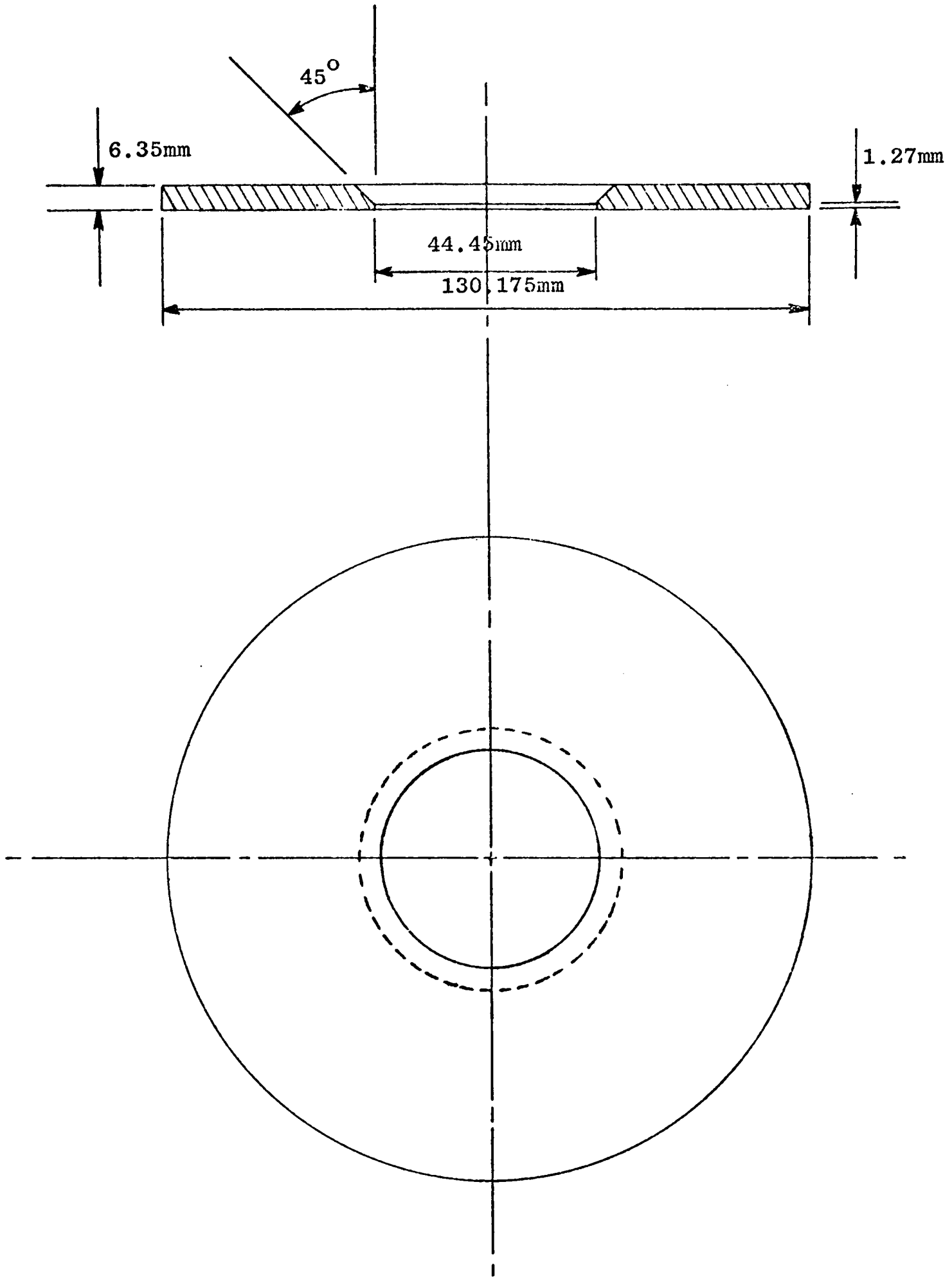

ORIFICE PLATE

Figure (4.1)

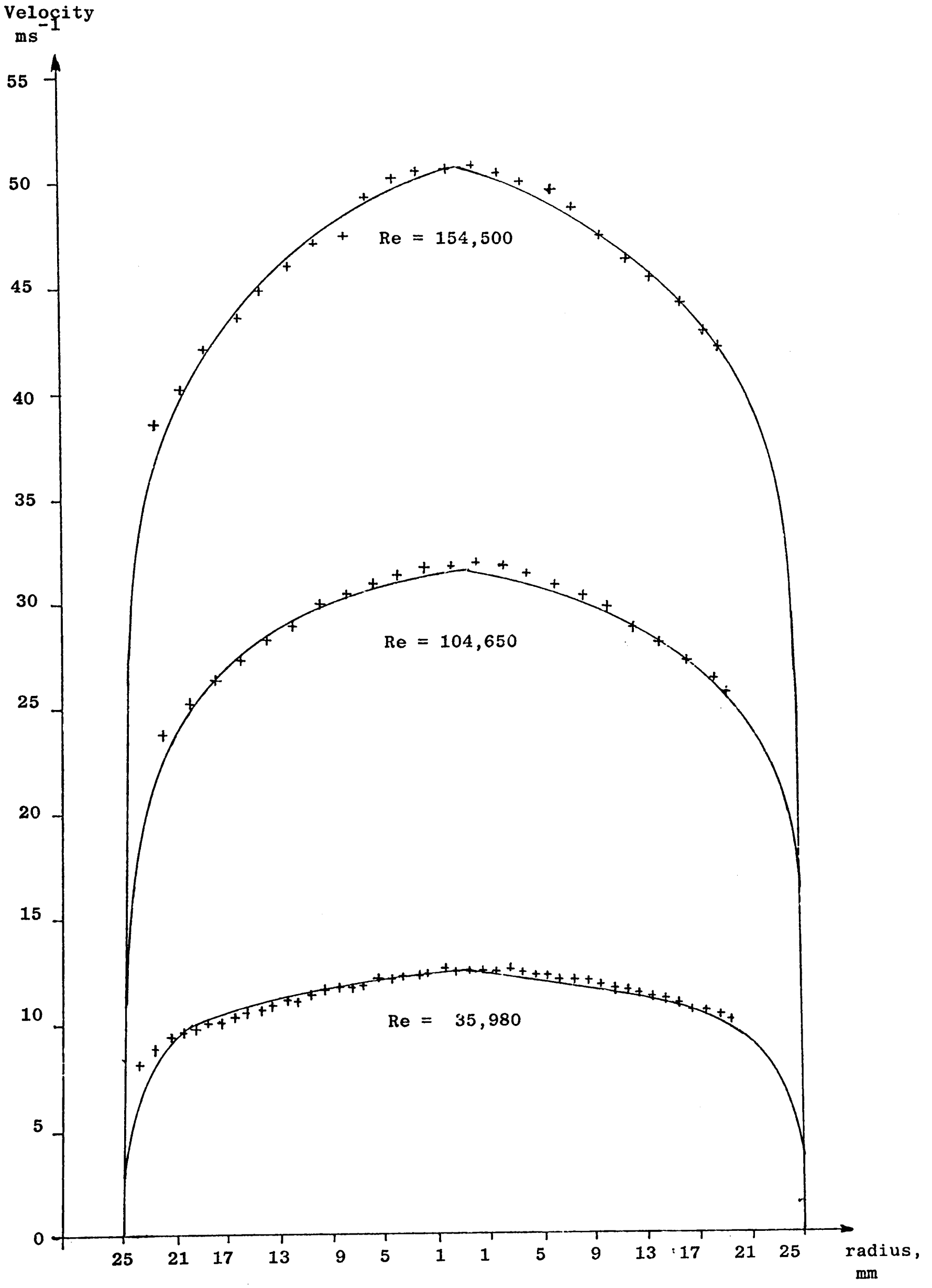

AIR VELOCITY PROFILES

Figure (4.2)

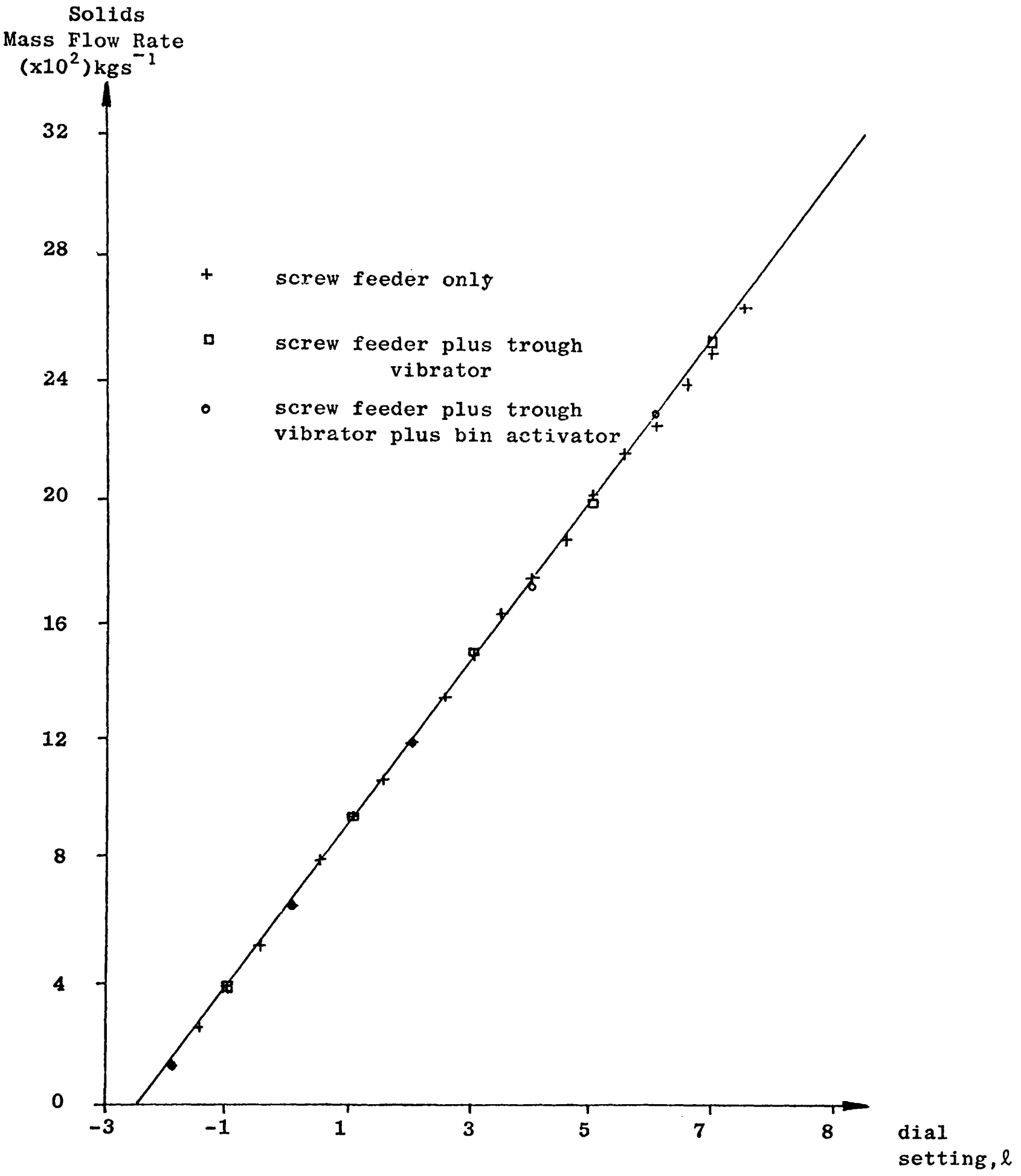

CALIBRATION OF SCREW FEEDER WITH BALLOTINI,
WITH NO AIR FLOW

Figure (4.3)

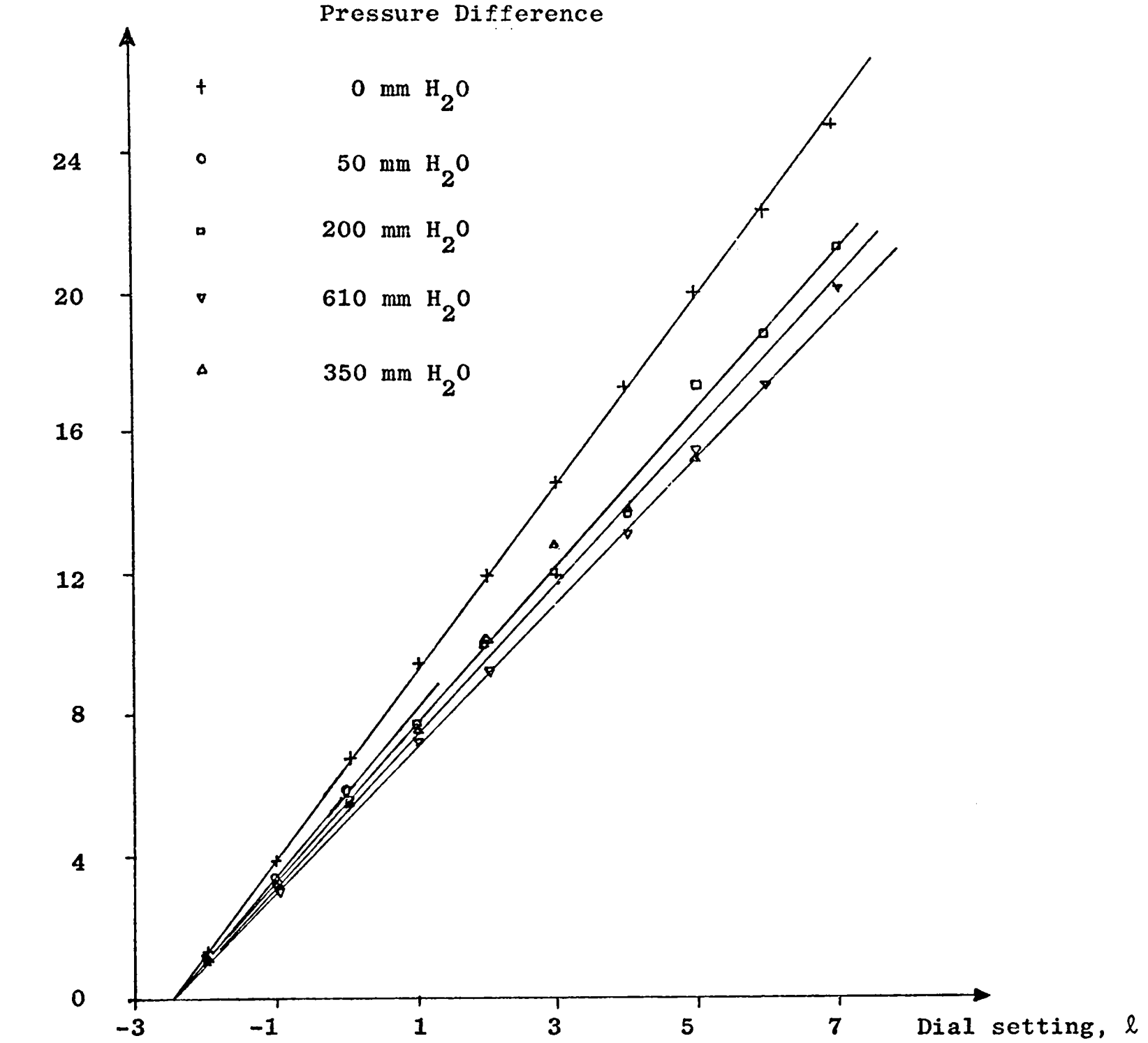

CALIBRATION OF SCREW FEEDER WITH BALLOTINI

Figure (4.4)

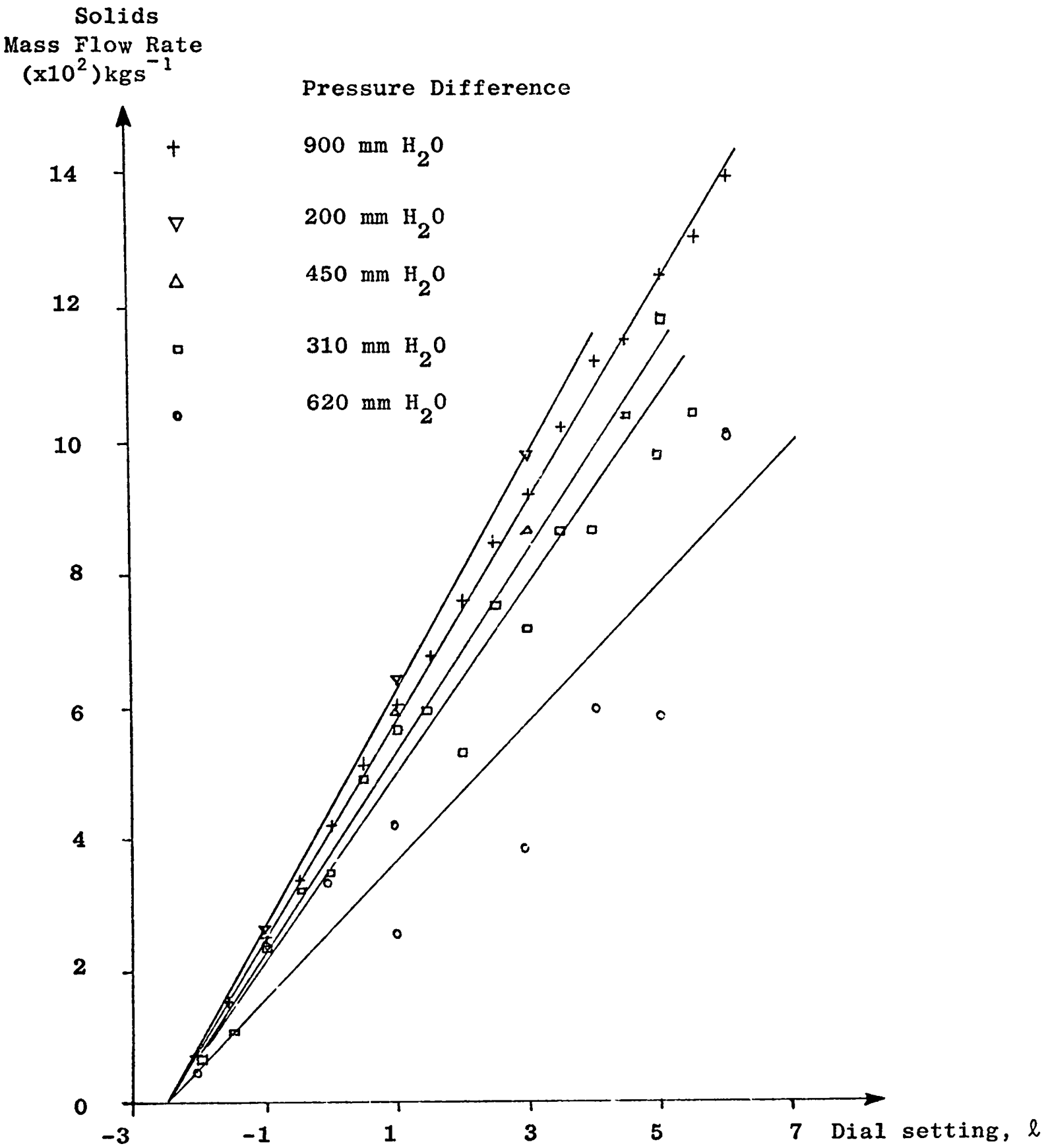

CALIBRATION OF SCREW FEEDER WITH SAND

Figure (4.5)

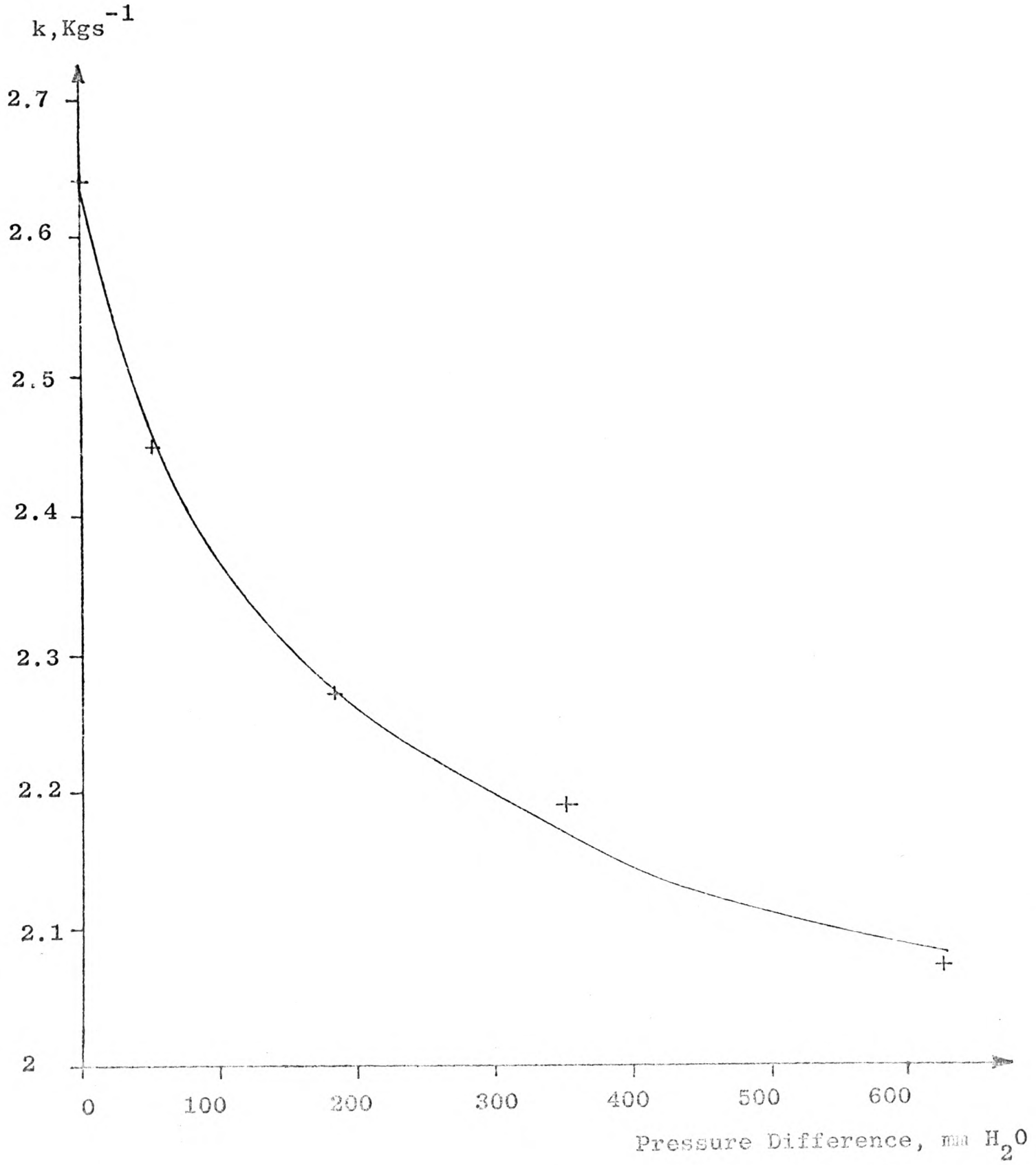

CALIBRATION CURVE OF SCREW FEEDER, BALLOTINI

Figure (4.6)

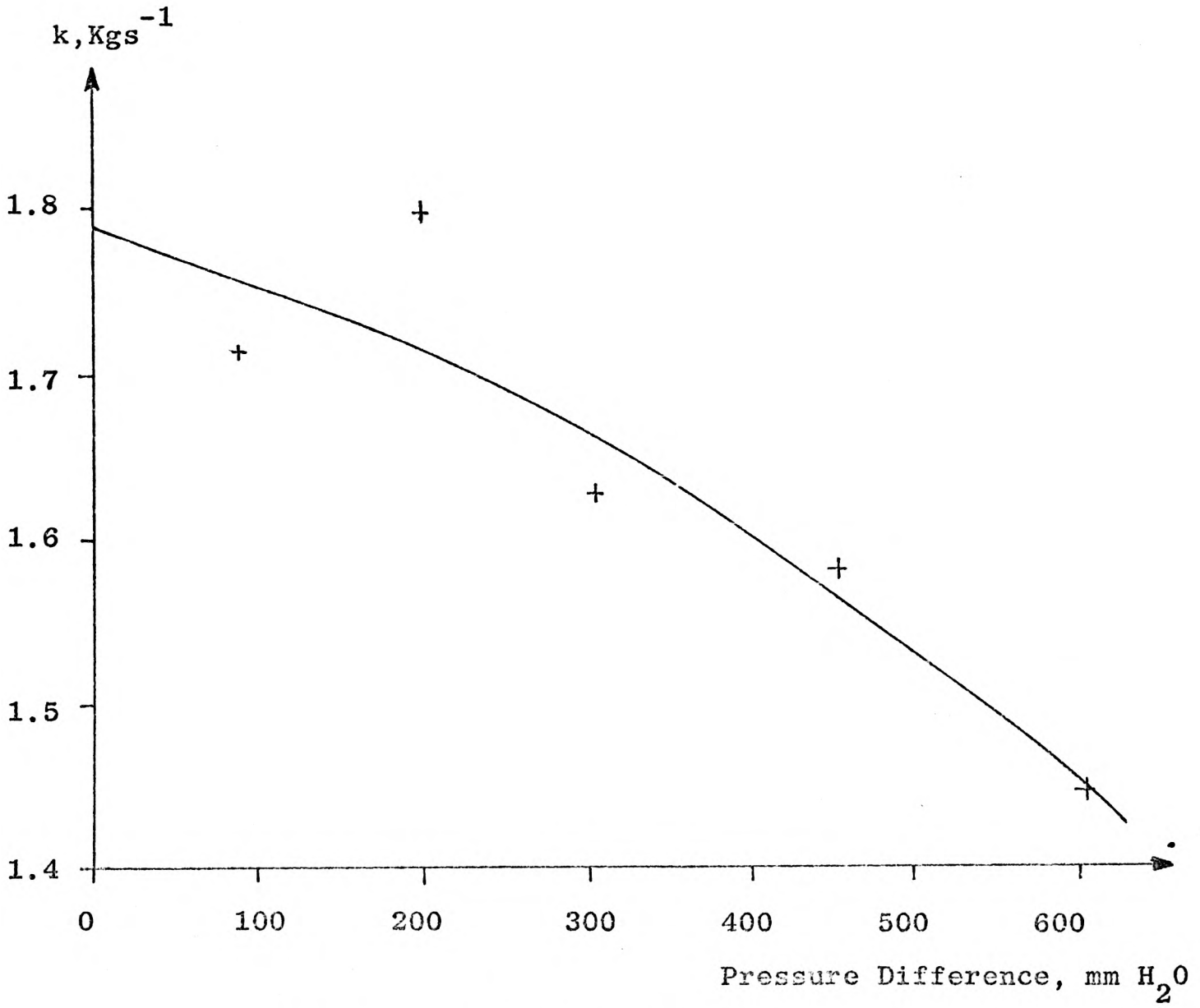

CALIBRATION CURVE OF SCREW FEEDER, SAND

Figure (4.7)

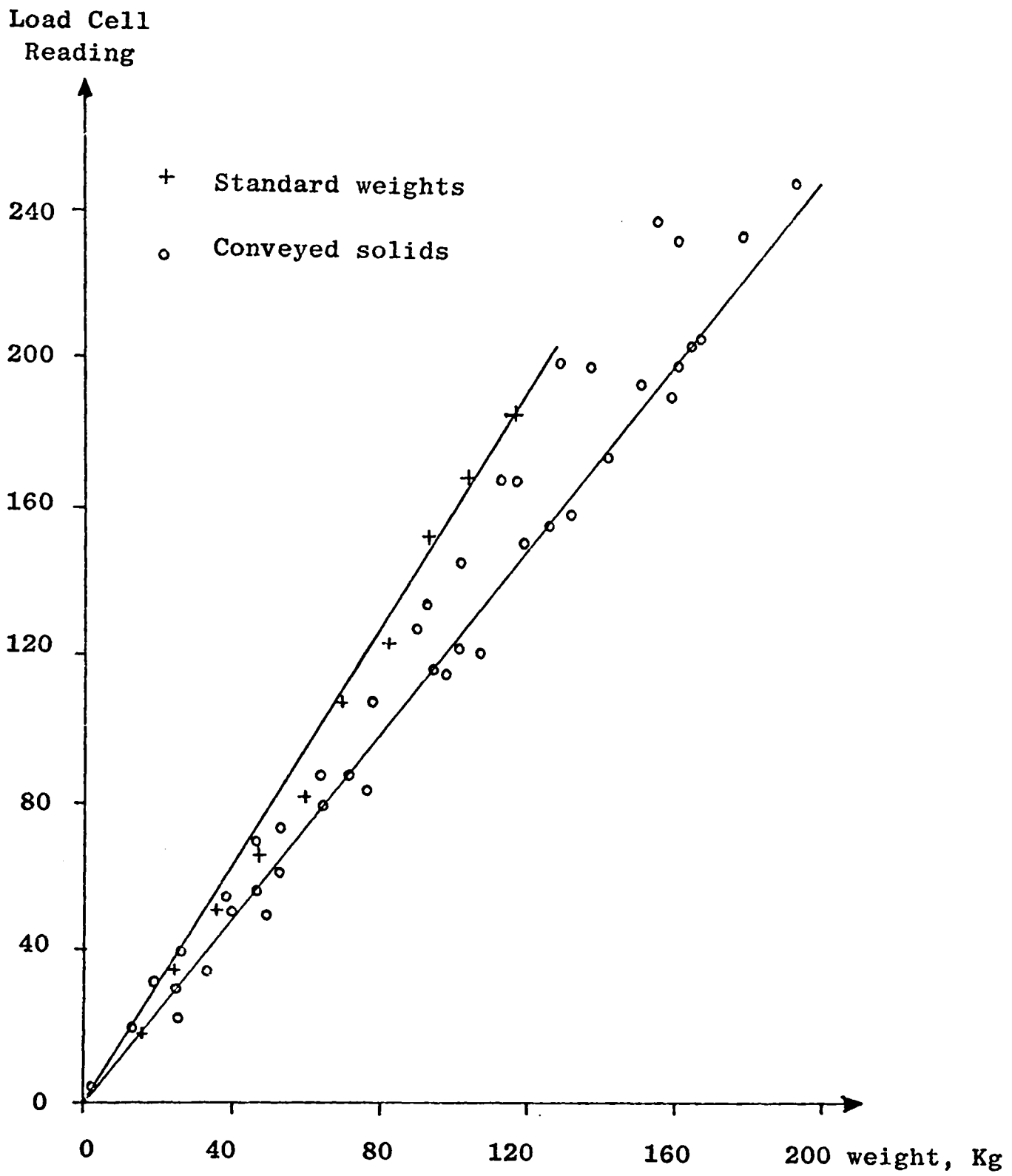

CALIBRATION OF LOAD CELL

(Figure (4.8)

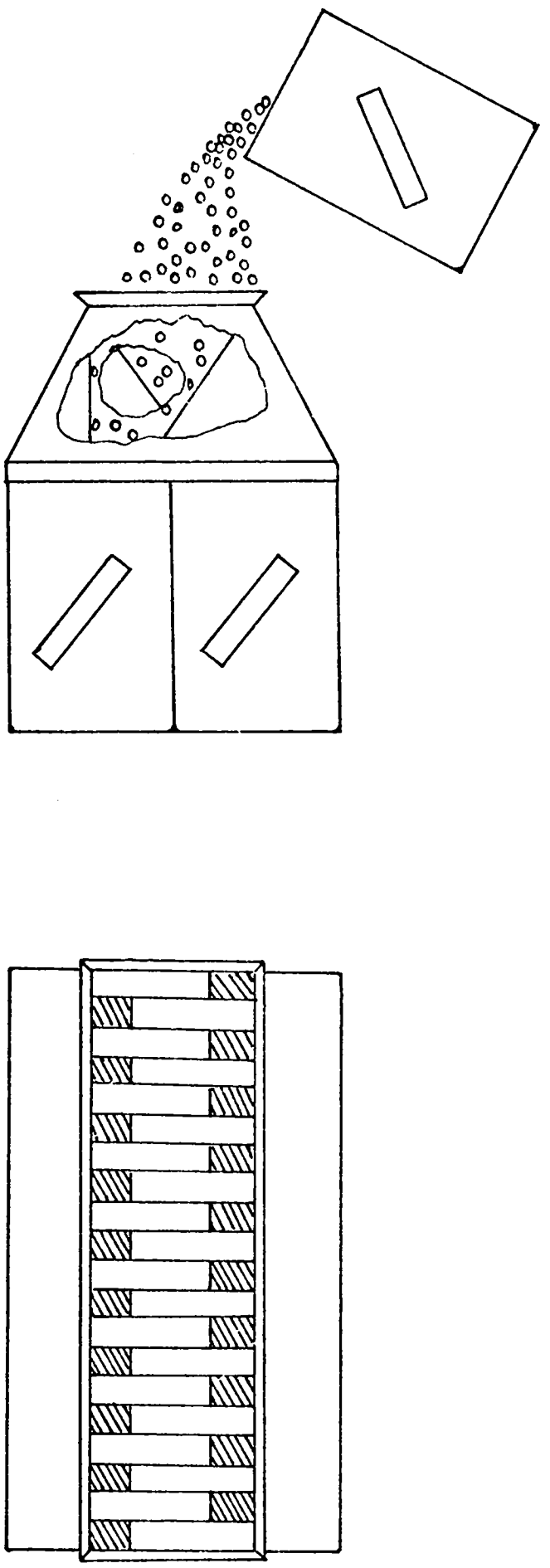

RIFFLER FOR SELECTING SOLID SAMPLE

Figure (4.9)

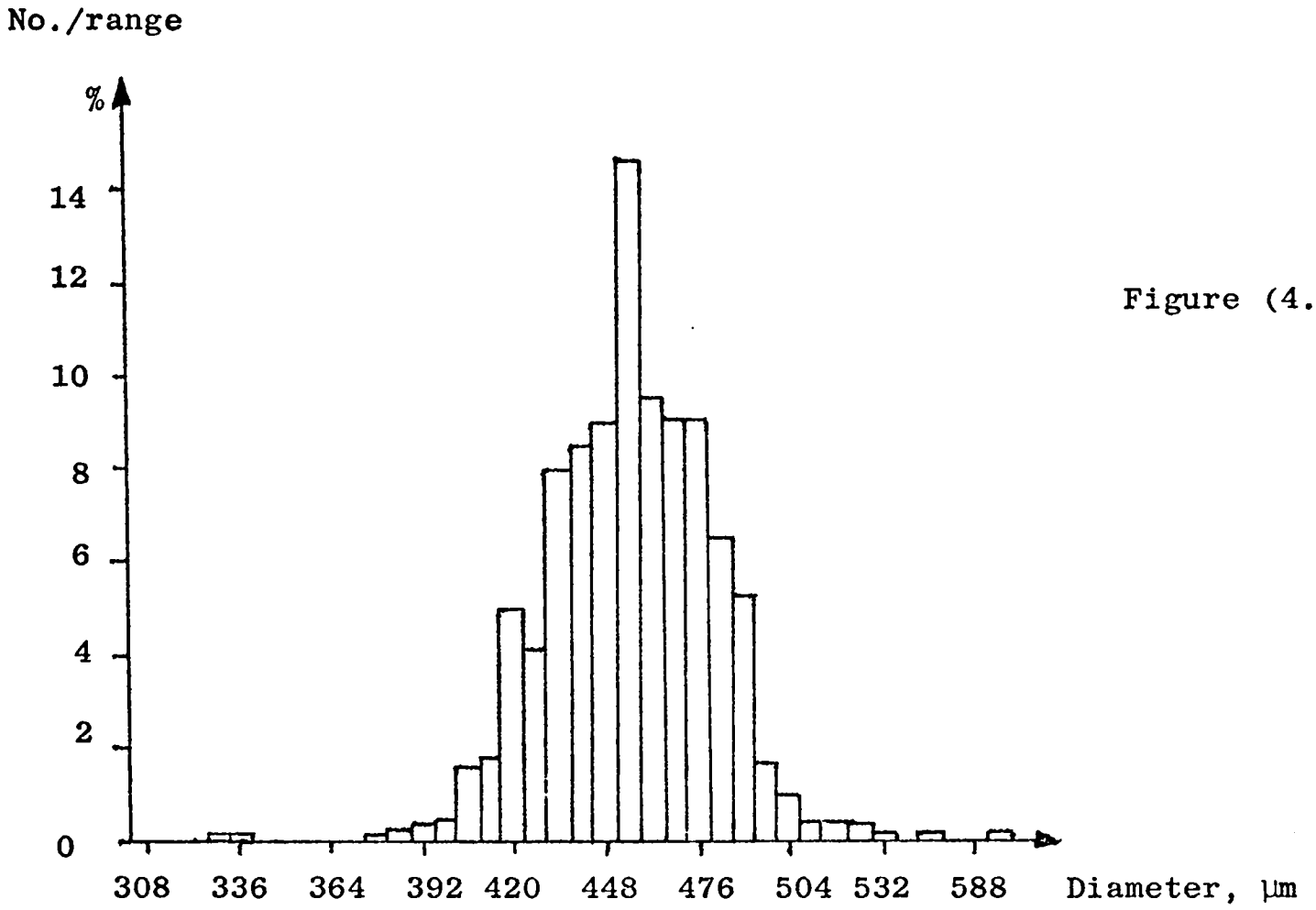

Figure (4.10a)

SIZE ANALYSIS OF BALLOTINI, UNUSED, UNSIEVED

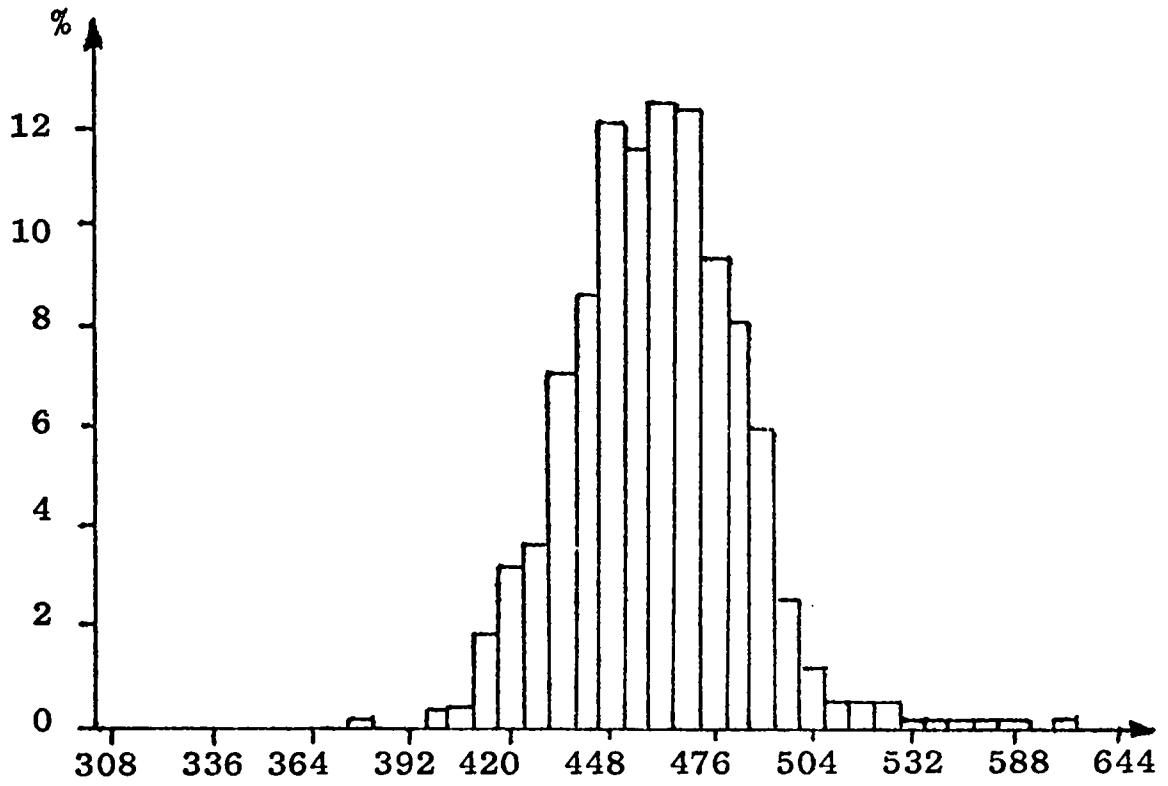

Figure (4.10b)

SIZE ANALYSIS OF BALLOTINI, UNUSED, SIEVED 450 - 500 µm

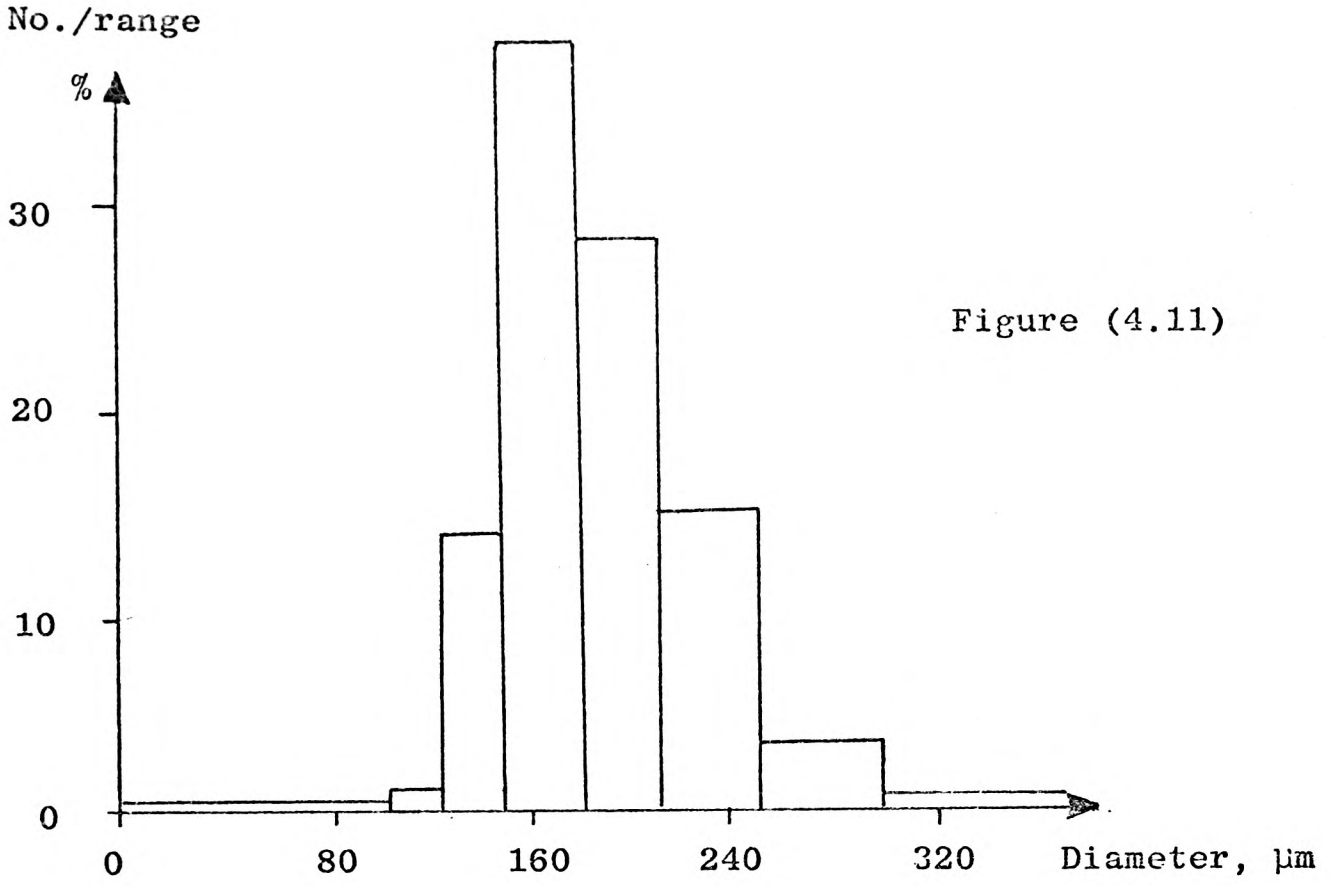

Figure (4.11)

SIZE ANALYSIS OF UNUSED, UNSIEVED SAND

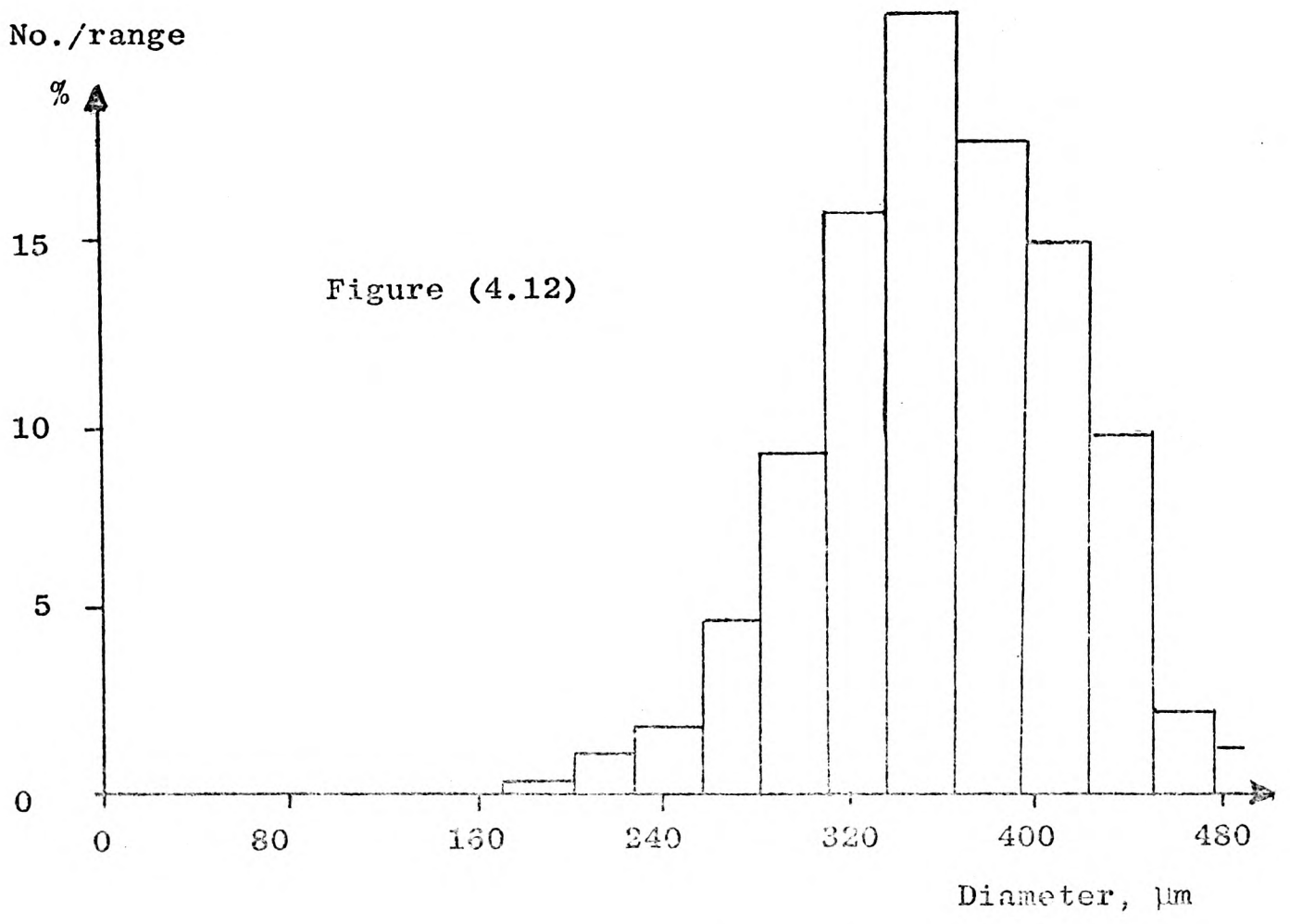

Figure (4.12)

SIZE ANALYSIS OF UNUSED SAND, SIEVED 300 - 355 µm

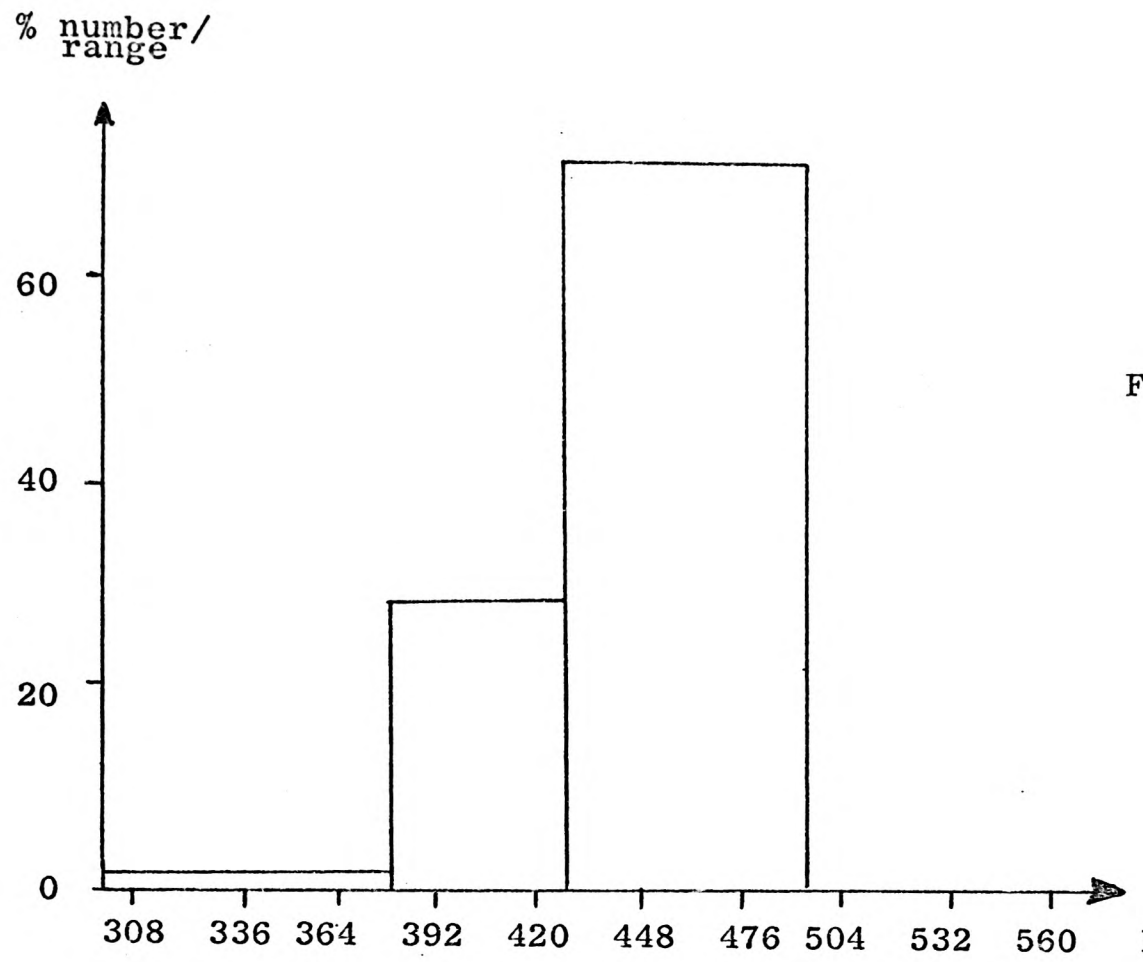

Figure (4.13)

SIZE ANALYSIS OF BALLOTINI WHICH PASSED ONCE THROUGH SCREW FEEDER

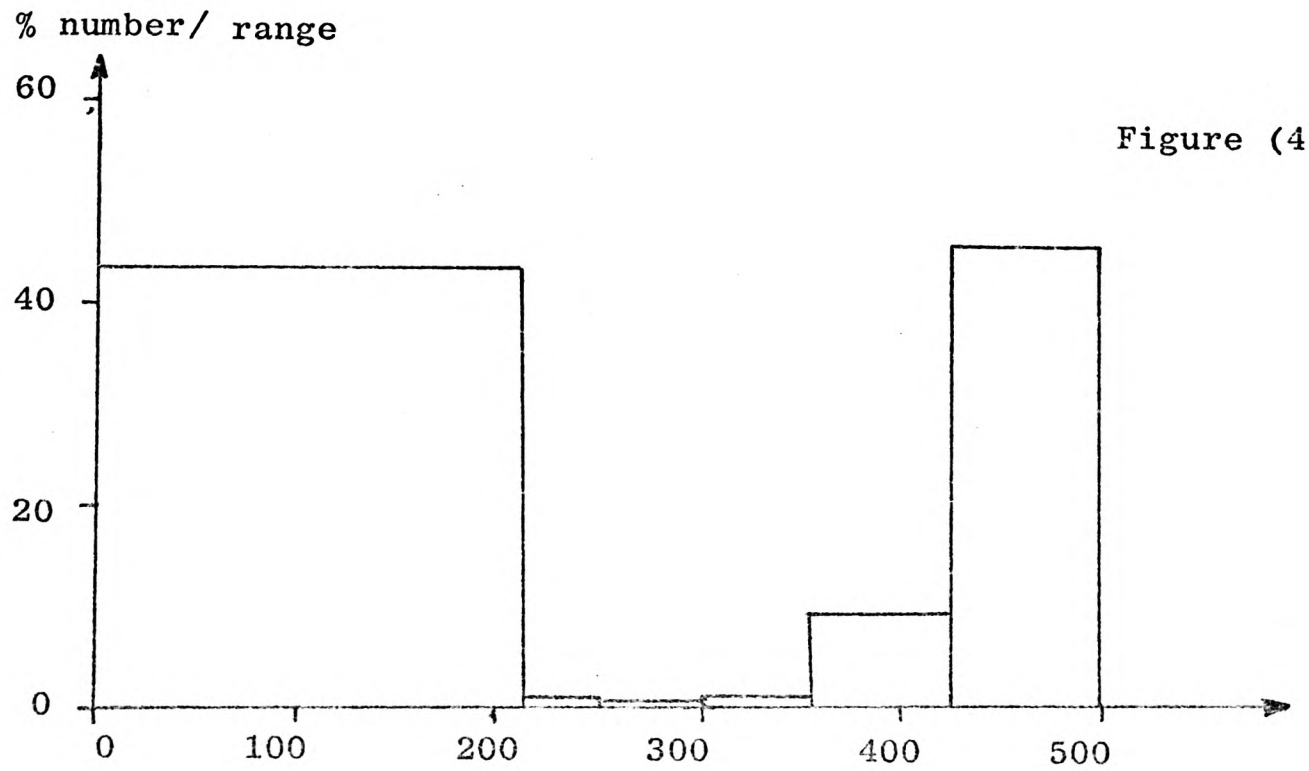

Figure (4.14)

SIZE ANALYSIS OF BALLOTINI AFTER MANY RUNS

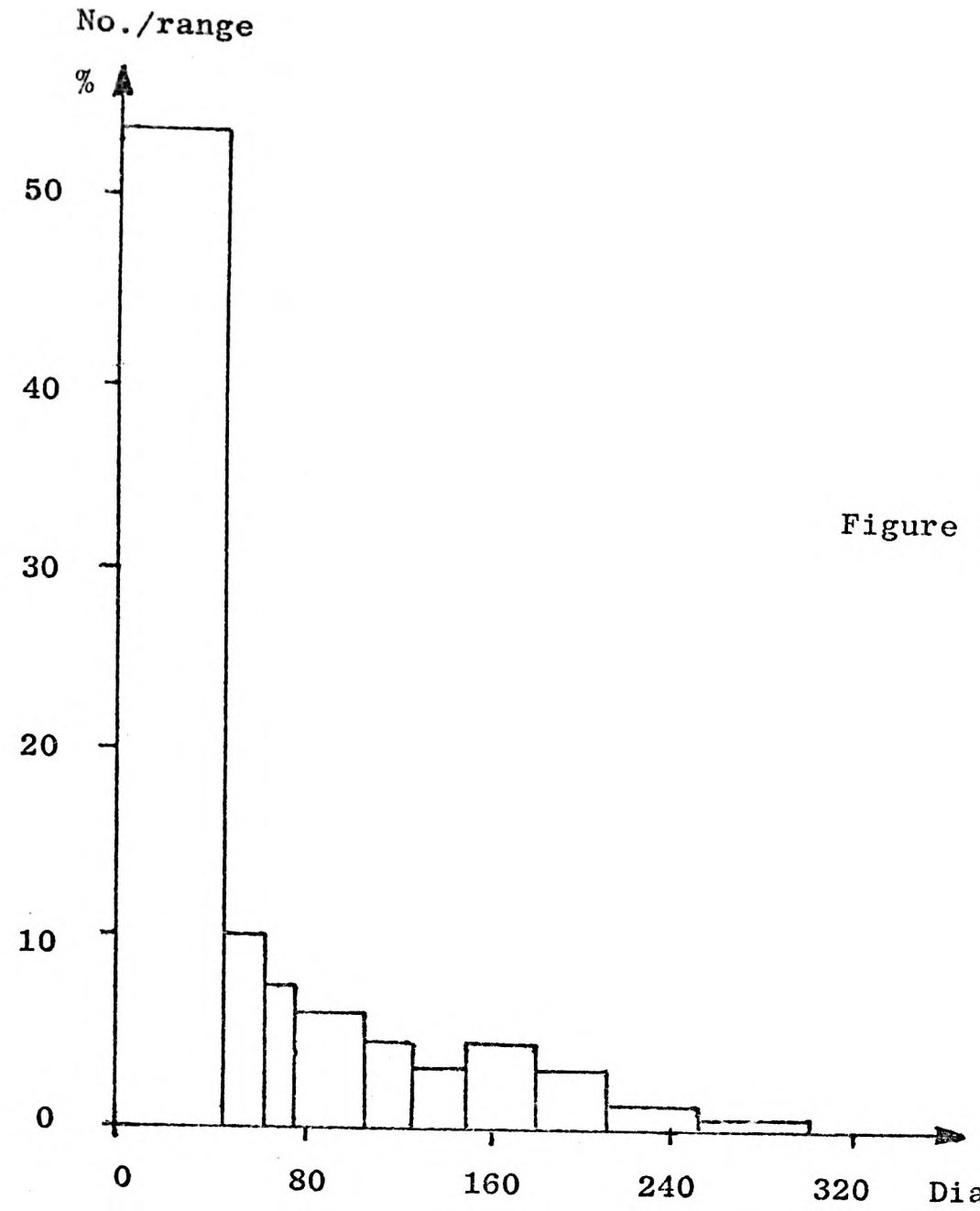

Figure (4.15)

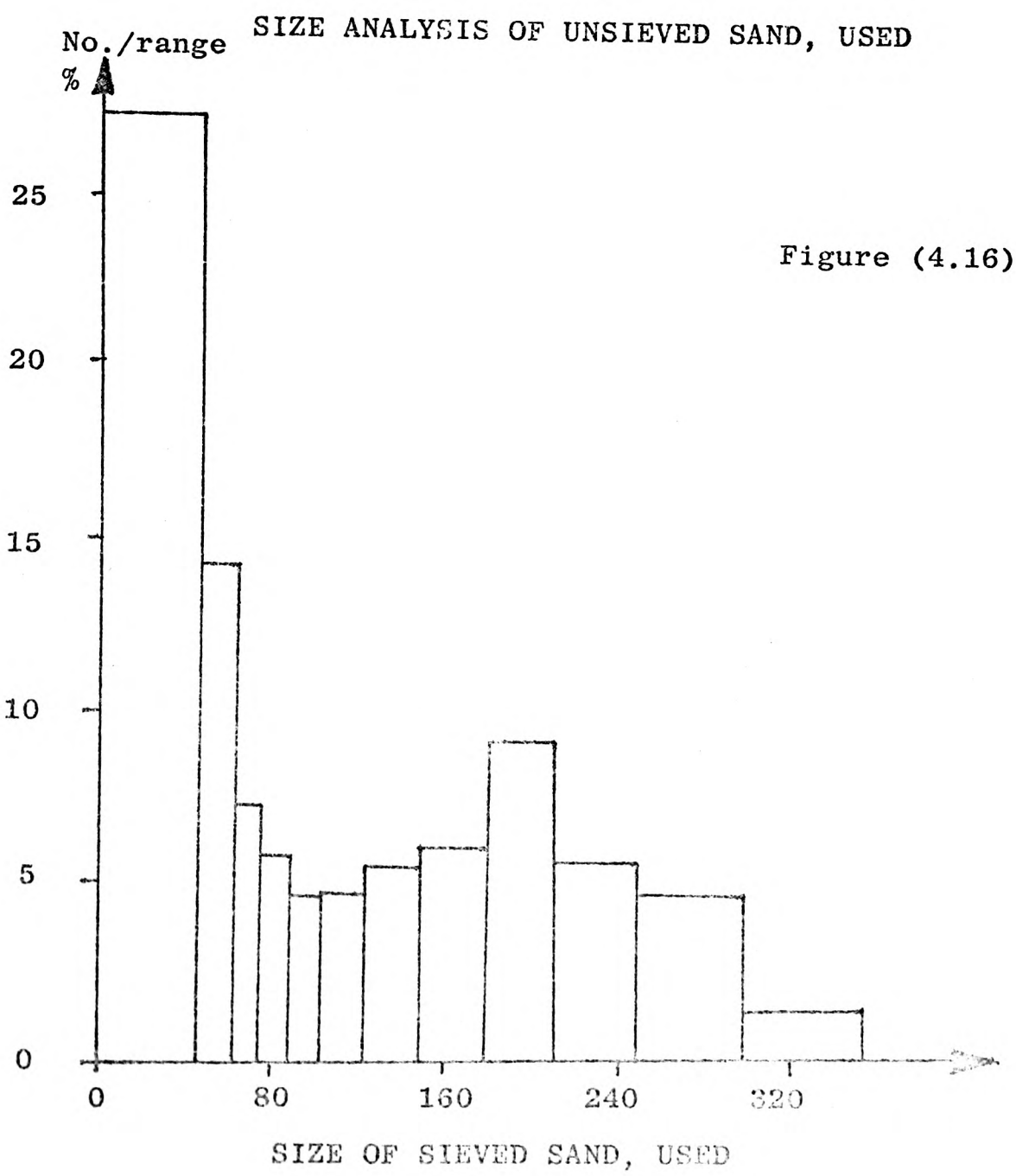

Figure (4.16)

MICROGRAPH OF TITANIUM OXIDE

Figure (4.17)

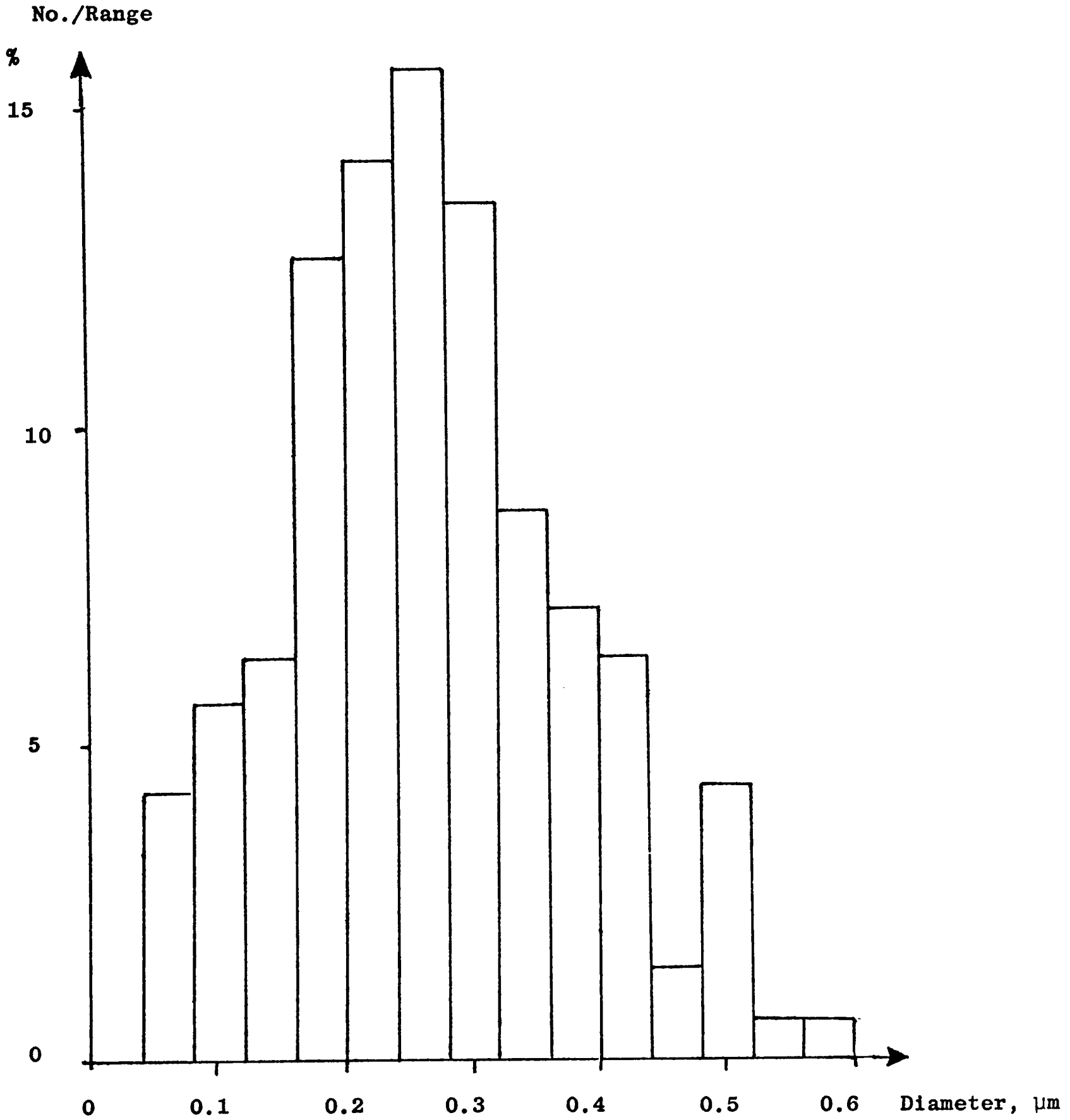

SIZE ANALYSIS OF TITANIUM OXIDE

Figure (4.18)

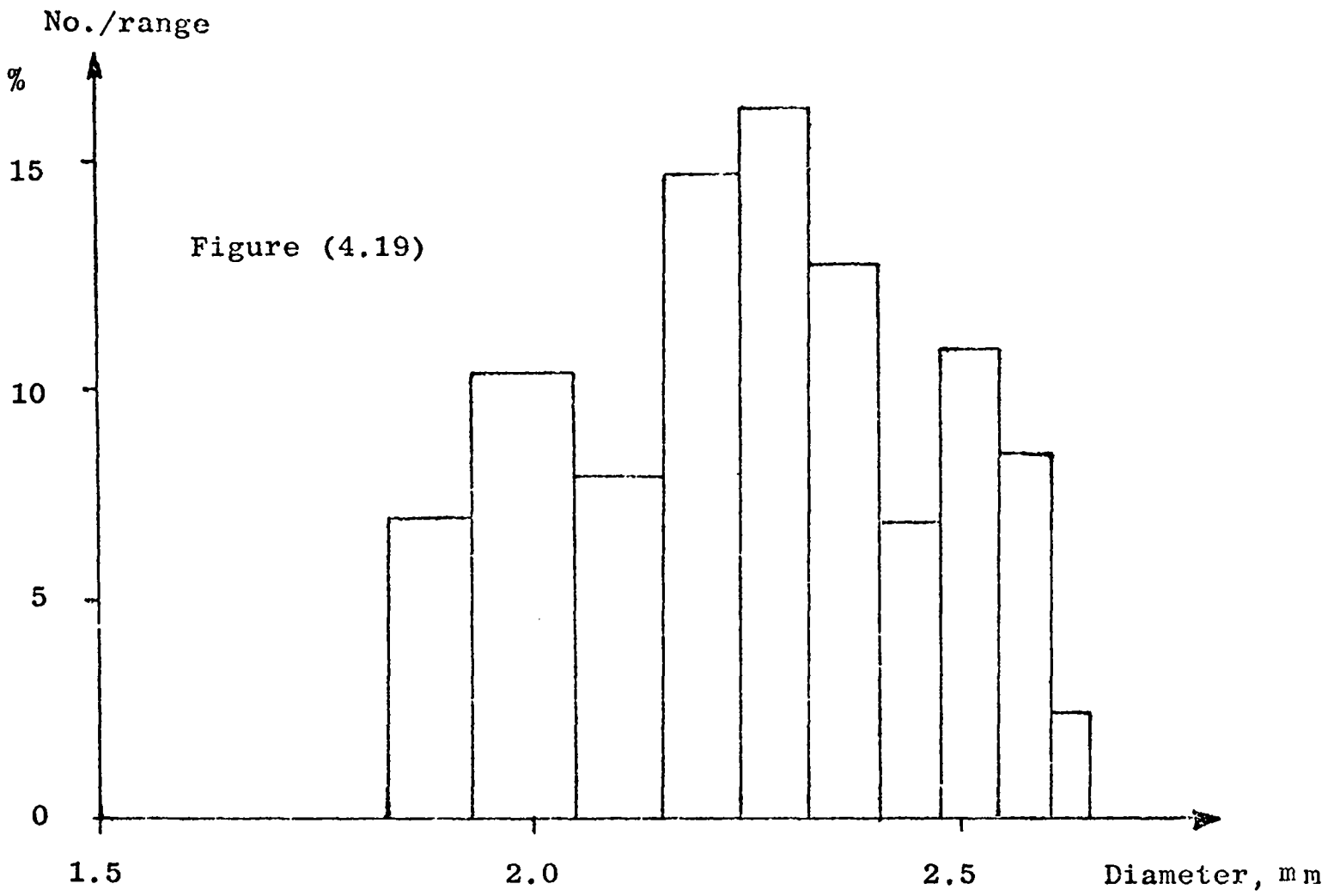

Figure (4.19)

SIZE ANALYSIS OF BLACK PLASTIC PELLETS

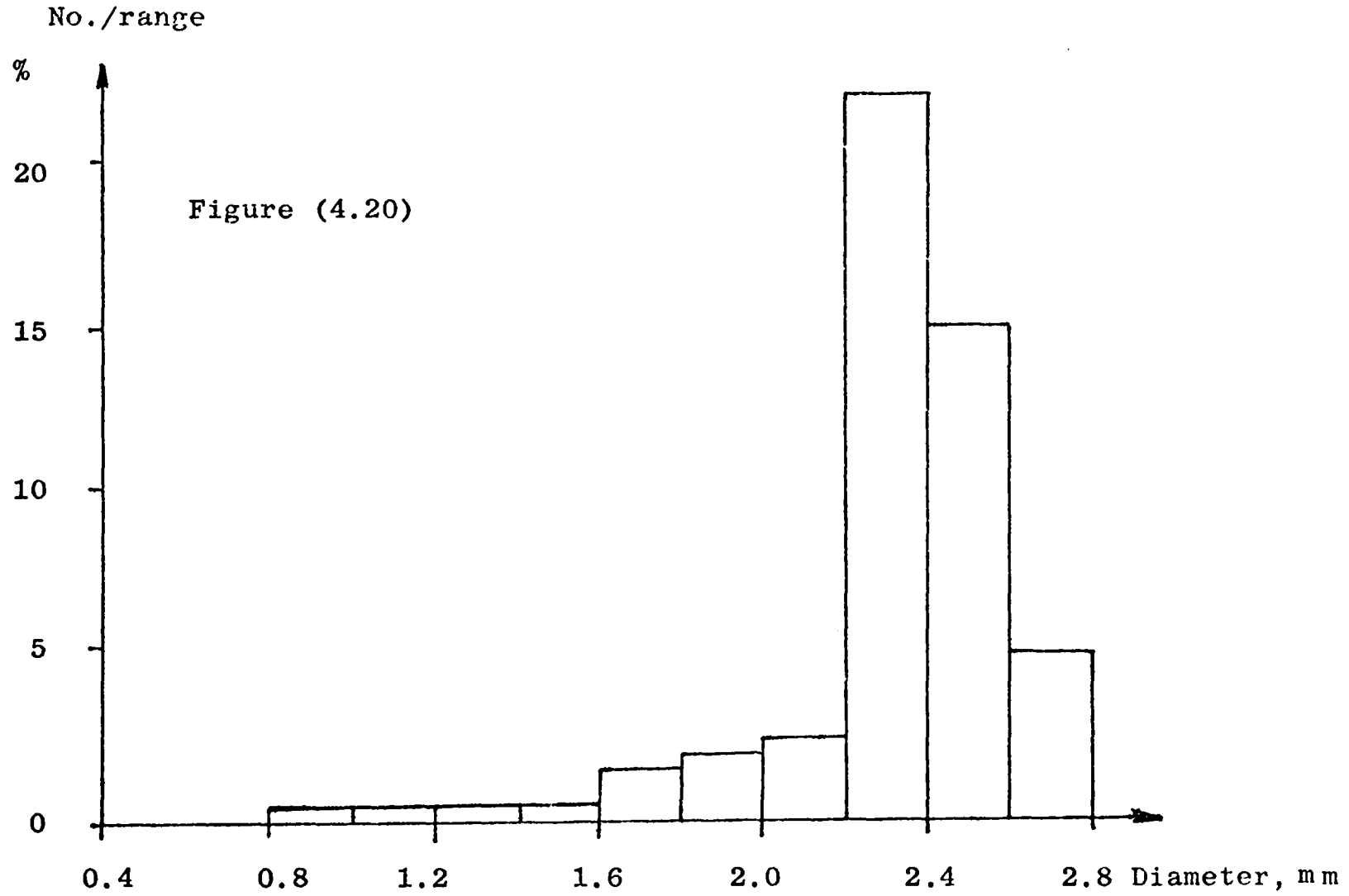

Figure (4.20)

SIZE ANALYSIS OF TRANSPARENT PLASTIC PELLETS

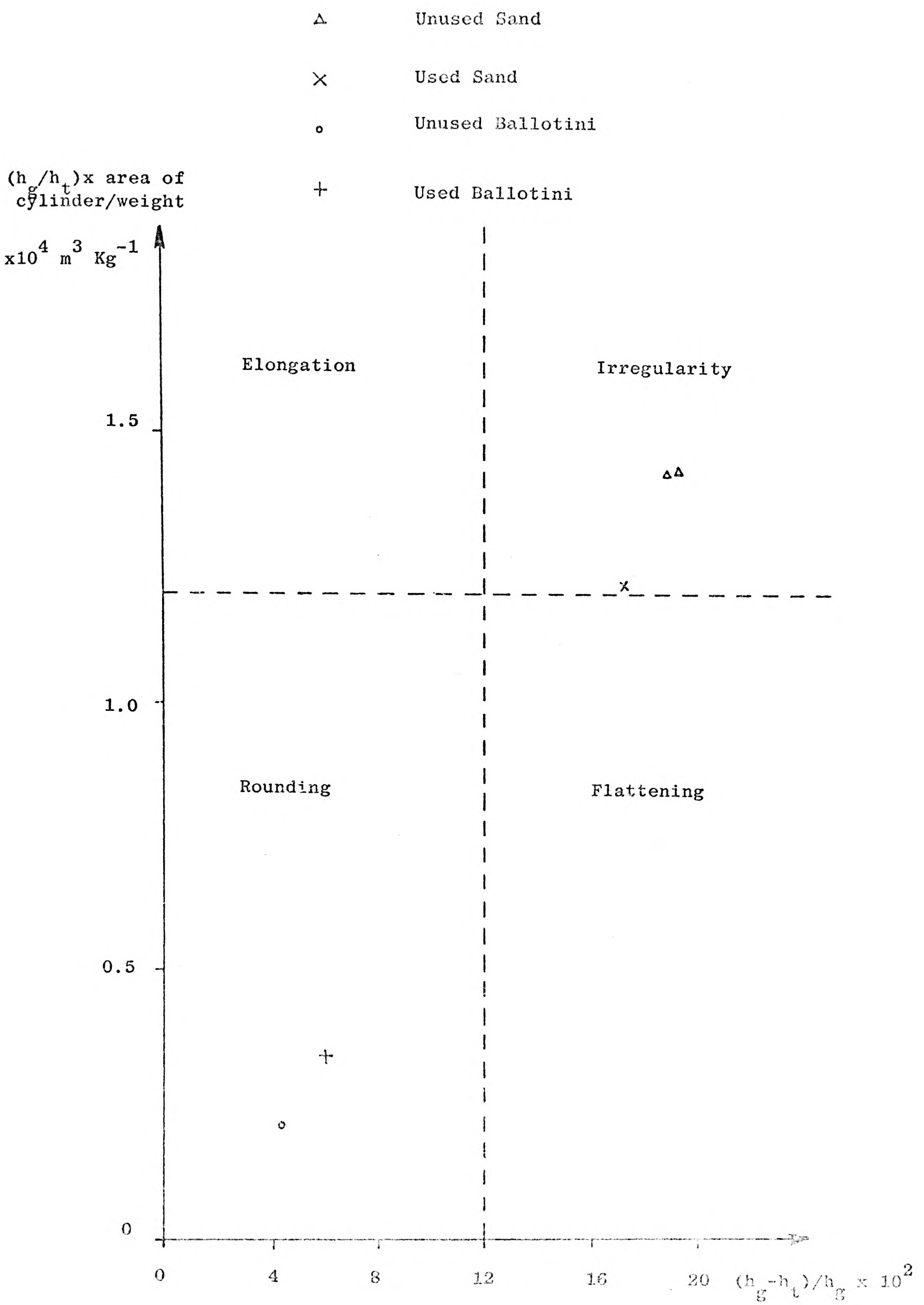

PARTICLE SHAPE

Figure (4.31)

CHAPTER 5

LASER DOPPLER VELOCITY METER

5.1 Introduction

This chapter describes the principles involved in the laser-Doppler velocity meter (LDV) and gives a brief history of its development. The various possible systems are discussed and some of the parameters influencing the signal quality, such as the measuring volume size are investigated.

5.2 Principles of Operation

The basis of the LDV is the Doppler effect, which is the change in frequency of a wave when measured by a receiver which is moving relative to the transmitter. Using the Special Theory of Relativity, the frequency shift is calculated below.

The transmitter is at the origin of the co-ordinate system Σ, which is moving at velocity V along a x-axis of the co-ordinate system Σ', (figure 5.1). If light, frequency ν is emitted by the transmitter when the origins of the two co-ordinate systems coincide, then in system Σ, at point $\underline{r}$, the wave can be represented by :-

$$\psi = \frac{A}{r} \cos 2\pi i\nu \left(t-\frac{r}{C}\right)$$

$$= \frac{A}{r} \cos 2\pi i\nu \left(t - \frac{x \cos \theta_1 + y \sin \theta_1}{C}\right) \qquad (5.1)$$

and in system Σ' it can be represented by :-

$$\psi' = \frac{A'}{r'} \cos 2\pi\, i\, \nu' \left(t - \frac{x' \cos \theta_1' + y' \sin \theta_1'}{C}\right) \qquad (5.2)$$

Substituting the Lorentz transformations :

$$x = \beta(x' + Vt') \qquad t = \beta\,(t' + \frac{Vx'}{C^2})$$

$$y = y' \qquad \beta = 1/\sqrt{\ }\ (1 - \frac{V^2}{C^2})$$

$$z = z'$$

into equation (5.1) gives :

$$\psi = \frac{A}{r} \cos 2\pi\nu i \left[\beta\ t'(1 - \frac{V}{C} \cos\theta_1) - \frac{\beta V x'}{C}\ (\cos\theta_1 - \frac{V}{C}) - \frac{\beta y}{C} \sin\theta_1\right] \qquad (5.3)$$

Since the phase of the light wave is the same when measured in either co-ordinate system, the co-ordinates of t', x', and y' will be identical in equations (5.2) and (5.3).

Thus:-

$$\nu\ \beta\ (1 - \frac{V}{C} \cos\theta_1) = \nu' \qquad (5.4)$$

which defines the frequency, ν', of the light when measured in co-ordinate system Σ'.

If the wave is reflected by a surface at rest in co-ordinate system Σ', the frequency, ν', of the reflected wave in that co-ordinate system will be defined by equation (5.4). However, when measured in co-ordinate system Σ the frequency, ν_r, of the reflected wave can be found by a second application of equation (5.4), to give:

$$\nu_r = \nu' \Big/ \beta\ (1 - \frac{V}{C} \cos\theta_2)$$

$$= \nu\ \frac{(1 - V \cos\theta_1/C)}{(1 - V \cos\theta_2/C)} \qquad (5.5)$$

(figure 5.2).

This means that the velocity of a surface, or a particle, can be determined by measuring the change in frequency when scattered by the object. However, for velocities producing a frequency shift of less than about 50 MHz, direct measurement of the frequency difference is impossible, since the difference is extremely small compared to the original frequency. In cases where the velocity is sufficient to produce a very large frequency shift, such as particles moving in a supersonic air flow, it is possible to employ direct frequency measuring methods such as the Fabry-Perot interferometer (James et al (1968)). A method which overcomes this problem for lower velocities uses the optical heterodyning of the scattered light with the original unscattered light, giving a resultant beat frequency which is equal to the frequency shift :-

$$\nu_D = \nu - \nu_r$$

$$= \nu - \nu \frac{(1 - V \cos \theta_1/C)}{(1 - V \cos \theta_i/C)}$$

$$= \frac{\nu V(\cos \theta_1 - \cos \theta_2)}{C(1 - V \cos \theta_2/C)} \qquad (5.6)$$

If the light is scattered by angle 2θ, and the velocity, V, is at angle ϕ to the x-axis (figure 5.3), then :-

$$\cos \theta_1 = \cos (\phi + \theta - 90)$$

$$= \sin \phi \cos \theta + \sin \theta \cos \phi) \qquad (5.7)$$

$$\cos \theta_2 = \cos (90 + \theta - \phi)$$

$$= - \sin \theta \cos\phi + \cos\theta \sin\phi \qquad (5.8)$$

giving :-

$$\nu_D = - \frac{2V \nu \sin \theta \cos\phi}{C(1 - V \sin \theta_1/C)}$$

$$= \frac{2v_z \sin\theta}{\lambda} \qquad \text{since } V << C \qquad (5.9)$$

where $v_z = V \cos\phi$, the velocity in the z-direction. This method of mixing the scattered beam with the unscattered or reference beam is known as the reference beam mode.

Alternatively, light from two mutually coherent beams can be scattered by the object and then mixed, (figure (5.4)). The frequencies of the light scattered from the two beams can be found by applying equation (5.5) to give:-

$$\nu_{r_1} = \nu \frac{(1 - V \cos \theta_1/C)}{(1 - V \cos \theta_3/C)} \tag{5.10}$$

$$\nu_{r_2} = \nu \frac{(1 - V \cos \theta_2/C)}{(1 - V \cos \theta_3/C)} \tag{5.11}$$

and the difference between these frequencies is the beat frequency:-

$$\nu_D = \nu_{r_1} - \nu_{r_2} = \nu \frac{V(\cos\theta_2 - \cos \theta_1)}{C\ (1 - V \cos \theta_3/C)} \tag{5.12}$$

$$= 2\nu \frac{v_z \sin \theta}{C(1 - V \cos\theta'/C)} \tag{5.13}$$

using equations (5.7) and (5.8) for θ_1 and θ_2. The receiver need not be in the same plane as the two crossing beams, and the angle θ' is the angle between the x-axis and the receiver.

For V << C, equation (5.13) becomes

$$\nu_D = \frac{2\ v_z \sin\theta}{\lambda} \tag{5.14}$$

The Doppler frequency ν_D, defined by equation (5.14) is indepentent of the collecting angle θ' and is the same as that for reference beam mode, defined by equation (5.9). The reference beam mode is a special case of the dual-Doppler mode in which angle θ' in equation (5.13) is equal to θ, and the receiver is in the same plane as the two crossing beams.

5.3 Fringe Model

Another explanation of the principle of operation of the instrument is the fringe model. This model assumes that interference fringes are formed when two monochromatic beams intersect. The fringes are, in fact, only formed on a surface which intersects the crossover region, and do not exist by themselves. This means that the results obtained

using this model do not take into account the scattering properties of the particle, i.e. isotropic scattering is assumed. However, the model does give a useful, simple derivation of the 'Doppler' signal frequency, and gives correct results in most situations.

The amplitudes of two crossover monochromatic light beams are:-

$$\xi_1 = A_1 \exp \quad i\{2\pi\nu\ (t - \frac{r_1}{c}) + \phi_1\} \qquad (5.15)$$

$$\xi_2 = A_2 \exp \quad i\{2\pi\nu\ (t - \frac{r_2}{c}) + \phi_2\} \qquad (5.16)$$

assuming the beams to consist of plane waves. The phase of the waves is given by phase angles ϕ_1 and ϕ_2 and the distances from the sources are r_1 and r_2.

The intensity of light at the beam intersection falling on a screen normal to the optical axis is

$$I = \frac{1}{2T} \int_o^T (\xi_1 + \xi_2 + \xi_1^* + \xi_2^*)^2 \, dt$$

$$= \xi_1 \xi_1^* + \xi_2 \xi_2^* + \xi_1 \xi_2^* + \xi_2 \xi_1^* \qquad (5.17)$$

for $T >> \frac{1}{\nu}$

Substituting the amplitudes defined in equations (5.15) and (5.16) gives :-

$$I = A_1^2 + A_2^2 + 2A_1A_2 \cos\left[\frac{2\pi}{\lambda}(r_1 - r_2) + (\phi_1 - \phi_2)\right] \qquad (5.18)$$

This function oscillates with a period such that $(r_1 - r_2)$ is an integal number of wavelengths. For mutually coherent beams the phase differenc $(\phi_1 - \phi_2)$ is constant.

If the two beams cross at angle 2θ, then using the co-ordinate system shown in figure (5.5) :-

$$r_1 = x\cos\theta - z\sin\theta \qquad (5.19)$$

$$r_2 = x\cos\theta + z\sin\theta \qquad (5.20)$$

Therefore the intensity function repeats when:-

$2 Z_N \sin \Theta = N\lambda$ $\qquad$ N = integer

and the distance δ between the maximums is:-

$$\delta = \frac{\lambda}{2 \sin \theta} \tag{5.21}$$

(Durst, Melling and Whitelaw (1975)).

Thus there will be a series of light and dark fringes on the screen with separation δ between each maximum light intensity in the z-direction. As a particle passes through the crossover region, the intensity of the light scattered by the particle will oscillate with a frequency ν_F such that :-

$$\nu_F = \frac{v_z}{\delta} = \frac{2v_z \sin\theta}{\lambda} = \nu_D \tag{5.22}$$

where v_z is the velocity of the particle in the z-direction. Therefore, since $\nu_D = \nu_F$, the fringe model gives the same result as the Doppler shift model. The light and dark fringes can be regarded as the respective adding and subtracting of the two sets of plane waves. Since the model assumes isotropic scattering by the particle, any parameters other than the velocity deduced from the signal, such as the particle size, will be inaccurate using this model.

5.4 Frequency Shifting

If the frequency of the two light beams used in the LDV are not exactly equal, the difference frequency is added to or subtracted from the Doppler frequency. This gives the instrument directional sensitivity, which it does not have when both beams have the same frequency. With a frequency difference between the two beams, velocity variations about zero can be measured, and the frequency of the signal can be raised or lowered to bring it within the range of the signal analyser.

Applying the Doppler shift analysis, if the frequencies of the two beams are ν_1 and ν_2, then equations (5.10) and (5.11) for the scattered frequencies, become :-

$$\nu_{r_1} = \nu_1\left[\frac{1 - (V\cos\theta_1)/C}{1 - (V\cos\theta_3)/C}\right] \tag{5.23}$$

$$\nu_{r_2} = \nu_1\left[\frac{1 - (V\cos\theta_2)/C}{1 - (V\cos\theta_3)/C}\right] \tag{5.24}$$

giving a beat frequency at the receiver of

$$\begin{aligned}\nu_m &= \nu_{r_1} - \nu_{r_2} \\ &= \frac{(\nu_1 - \nu_2)}{[1-(V\cos\theta_3)/C]} + \frac{V}{C}\,\frac{(\nu_1\cos\theta_1 - \nu_2\cos\theta_2)}{[1 - (V\cos\theta_3)/C]} \\ &= \nu_s + \frac{V}{C}(\nu_1\cos\theta_1 - \nu_2\cos\theta_3)\end{aligned} \tag{5.25}$$

where $\nu_s = \nu_1 - \nu_2$ and $C >> V$

As in figure (5.3), the velocity V is at angle ϕ to the z-axis, thus identities (5.7) and (5.8) can be used in equation (5.25) to give:-

$$\nu_m = \nu_s - \frac{V}{C}\cdot(\nu_1+\nu_2)\sin\theta\cos\phi + (\nu_1-\nu_2)\cos\theta\sin\phi \tag{5.26}$$

The velocity components in the z and x-directions are respectively v_z and v_x, such that :-

$$v_z = V\cos\phi \tag{5.27}$$

$$v_x = V\sin\phi \tag{5.28}$$

and $\nu = \dfrac{\nu_1 + \nu_2}{2}$, the average incident frequency.

Thus:

$$\nu_m = \nu_s - \frac{2v_z}{C}\cdot\nu\sin\theta - \frac{v_x}{C}\cdot\nu_s\cos\theta \tag{5.29}$$

$$= \nu_s - \frac{2v_z}{C}\cdot\nu\sin\theta \quad , \quad \text{since} \quad v_x << C \tag{5.30}$$

and the total frequency shift is independent of the velocity in the x-direction, and consists of the sum or difference, depending on the direction of the flow, of the frequency difference between the incident

beams, and the Doppler frequency defined in equation (5.13).

In the fringe model, equation (5.18) becomes modified to:-

$$I = A_1^2 + A_2^2 + 2A_1A_2 \left[2\pi\{\nu_s t + (\frac{r_1}{\lambda_1} - \frac{r_2}{\lambda_2})\} + (\phi_1 - \phi_2) \right] \qquad (5.31)$$

which repeats when:-

$$\nu_s t + (\frac{r_1}{\lambda_1} - \frac{r_2}{\lambda_2})$$

is an integer.

Thus, using identities (5.19) and (5.20), the intensity has a repetitive pattern, with points of equal magnitude when :-

$$\nu_s t + (\frac{x\cos\theta - z\sin\theta}{\lambda_1} - \frac{x\cos\theta + z\sin\theta}{\lambda_2})_N = N \qquad (5.32)$$

So, equation (5.31) describes a series of moving fringes, which are inclined at an angle Ω to the x;axis, and are parallel with the y-axis. The separation between the fringes in the z- and x-directions are, respectively δ_z and δ_x, such that :-

$$\delta_z = \frac{C}{2\nu\sin\theta} \qquad (5.33)$$

$$\delta_x = \frac{C}{\nu_s\cos\theta} \qquad (5.34)$$

Therefore, the angle of the fringes to the x-axis is given by :-

$$\Omega = \tan^{-1}\frac{\delta_z}{\delta_x} = \tan^{-1}\frac{\nu_s}{2\nu} \qquad (5.35)$$

and the separation between the fringes is

$$\delta = \delta_x \sin\Omega \qquad (5.36)$$

A stationary object in the fringe pattern will receive an intensity variation of frequency from equation (5.31), and the frequency of intensity variation ν_m falling on an object moving through the fringes with velocity V at angle ϕ to the z-axis is :-

$$\nu_m = \nu_s - \frac{V\sin(\phi - \Omega)}{\delta} \qquad (5.37)$$

$$\nu_m = \nu_s - \frac{V\sin\phi}{\delta_x} - \frac{V\cos\phi}{\delta_z} \qquad (5.38)$$

$$= \nu_s - \frac{v_x}{C}\,\nu_s\cos\phi - \frac{2v_z}{C}\,\nu\sin\theta$$

$$= \nu_s - \frac{2v_z}{C}\,\nu\sin\theta, \quad \text{since} \quad v_x << C \qquad (5.39)$$

which is identical to the result obtained from the Doppler shift model (equation (5.30)).

5.5 Historical Review

The first use of the Doppler frequency shift of laser light to measure velocity was described by Yeh and Cummins (1964). They used a reference beam method, mixing light scattered by natural particles in flowing water with a beam which passed around the flow to produce a Doppler signal from which the particle velocity could be calculated, using equation (5.9). The reference beam mode has since been widely used and developed. Using an arrangement, such as that shown in figure (5.7), with one beam passing through the flow, the light scattered by particles present in the flow is remixed with the reference beam. This method was used by Welch and Tomme (1967), Lewis, et. al. (1968), and Iten and Mastner (1971) in turbulent water flows, and by Forman, George and Lewis (1965), and Huffaker, Fuller and Lawrence (1969) in turbulent air flows with added tracer particles. An alternative arrangement of the reference beam mode is shown in figure (5.6). In this, two laser beams cross in the flow and light is collected in the direction of one of the beams, the collected light including light scattered from the other beam. Goldstein and Hagan (1967), Pike et.al. (1968), and George and Lumley (1971) used this method to measure the velocity and turbulence of water flows from the frequency and frequency spread of the Doppler signal obtained.

The dual-Doppler mode of the LDV, in which two crossing beams are scattered by the particles, and the light from each is collected in one direction was first suggested by Rudd (1969a) Due to its many advantages, this mode has become the most commonly used system. Rudd (1969b) also suggested that the signals could be regarded as coming from the change in scattered light intensity as the particles passed through a series of interference fringes. This model gives a simple and useful derivation of the relation between the received frequency and the velocity of the particle, but it has been pointed out by several authors (Pike (1975), Farmer (1973)) that since there are no non-linear processes occurring in the probe volume, no actual fringes are formed, except on the surface of the particle.

There have been several developments of the dual-Doppler mode. An integrated optical unit to simplify alignment of the instrument was proposed by Mayo (1970) and by Durst and Whitelaw (1971). Several such integrated units are now commercially available. Systems have also been developed for measuring two or three components of the velocity [Grant and Orloff (1973), Brayton, Kalb and Crosswy (1973), and Oldengarm (1975)] . Frequency shifting of one or both beams was employed by Mazumder (1970), Ohrsuka (1971) and Durão and Whitelaw (1975) using Bragg cells, and by Oldengarm et al (1973) using a rotating radial diffraction grating. Smyth (1978) describes a system using two skewed radial diffraction gratings which are sandwiched together and rotated. This produces a fan of beams in three dimensions of different frequencies. By selecting certain beams, two or three component measurements can be made with directional sensitivity.

5.6 Optical Systems

5.6.1 Light Sources The light source chosen for a velocity meter using the principle described in section (5.2) must be very monochromatic,

so the frequency shift is greater than the line width. Although some conventional light sources satisfy this criterion, lasers are particularly suitable since their extremely small line widths reduce ambiguity.

Temporal coherence of the light beam is also important, since the clarity of the interference fringes depends on the phase correlation of the two beams. The coherence length of the light source is the distance over which the phase coherence of the beam is lost and, if the difference between the path lengths of the two crossing beams is greater than the coherence length, the fringes are not formed [Forman (1967)]. Conventional light sources are incoherent and require nearly zero path length difference for interference fringes. The coherence length of lasers depends mainly on the number of axial modes and their frequency separation, since these interfere with the basic transverse mode (TEM_{oo}) and introduce phase incoherence, but small path length differences using laser beams only slightly reduce the clarity of the fringes.

Other advantages of the laser light are its spatial coherence and high intensity. The spatial coherence of the light allows it to be focussed on a very small area and the high intensity of the light means that more light is scattered by the particles. The power of the laser required depends on the situation for which it is being used. The effect of particle size will be discussed in chapter 6. Since a minimum of scattered light intensity is needed, in situations where only a small fraction of the light is scattered by the particles, for example particles moving at high velocity, low concentration of particles, or long distance LDV, a higher power laser is needed than that required in less extreme situations.

5.6.2 Transmitting Optics In order to produce clear fringes, the transmitter of the system must produce two or more light beams which are mutually coherent. There are several types of beam splitter which can be used to produce the multiple beams, such as semi-reflecting mirrors, prisms diffraction gratings and acousto-optic cells. In most systems the two beams cross in the flow at their waists and some examples of suitable optical arrangements are shown in figure (5.8). Systems such as that used by Yeh and Cummins (1964) in which the reference beam does not pass through the flow, are very difficult to align. It is necessary to reduce the intensity of the reference beam in order not to damage the photosensitive surface of the photo-detector, since it is focussed directly onto this surface. The reference beam should have nearly the same intensity as the scattered light so that the signal visibility is not too small. The intensity can be reduced by placing a neutral density filter in the path of the reference beam.

Frequency shifting in the transmitting optics can be achieved by several methods, including the use of acousto-optic, electro-optic cells or mechanical methods.

An acousto-optic or Bragg cell uses the Bragg diffraction of light by atoms or molecules which are vibrating with a sound wave to impart a Doppler shift to the light. The cell can be made from a solid crystal or a liquid, and the series of diffraction beams have different frequencies. By selecting appropriate beams, the system can be used as a beam splitter. Typically, frequency changes of about 40 MHz are produced and, if smaller changes are required, it is possible to use two Bragg cells, either in series on one beam or in parallel on two beams, so that the final frequency difference between the two beams is equal to the difference between the two driver frequencies.

Electro-optic cells employ a varying electric field to raise or lower the frequency of the incident light. This can be achieved by

applying a rotating electric field to a circularly polarised light beam [Drain and Moss (1972)].

The most common mechanical method of frequency shifting is the radial rotating diffraction grating. It consists of a disc on which a radial diffraction grating has been etched or bleached. If a light beam passes through the grating a fan of beams is produced, all in the plane tangential to the grating. If the grating is rotated about its centre, each of the beams has a different frequency due to the Doppler shift. As with the Bragg cell, the grating can also be used as a beam splitter, the two first order beams are usually chosen. The frequency difference between these two beams can be up to 3 MHz. The line widths of the beams is increased by variations in the speed of the motor driving the disc.

Other mechanical methods of frequency shifting are possible, such as the rotating scattering plate [Hiller and Meier (1972)] and the rotating cylindrical reflection grating [Mazumder (1970)] .

5.6.3 Receiving Optics In most systems light from the scattering volume is focussed onto a surface in which there is a pinhole, and the light which passes through the pinhole falls onto the photosensitive device which converts the light received into an electrical signal. The pinhole reduced the effective volume from which light can be accepted, excluding extraneous light.

Figure (5.9) illustrates one arrangement of the reference beam mode, where the reference beam, together with light scattered from the other beam, is focussed onto the pinhole. Thus in the reference beam mode, the collecting optics are always aligned along the axis of the reference beam. A variable sized aperture (iris stop) is often used before focussing further in order to reduce extraneous light.

The dual-Doppler or fringe mode can have the receiving optics accepting light from any angle. Commonly the receiver is placed on or near the axis of the instrument, collecting light scattered in either the forward or backward direction. The forward scatter mode is shown in figure (5.10a) and the backward scatter mode in figure (5.10b).

The photosensitive device is usually either a photodiode or a photomultiplier. Photodiodes are very much cheaper and are more robust than photomultipliers. Also, photodiodes do not require the high voltage source needed by photomultipliers. However, photomultipliers are much more sensitive than photodiodes and produce less shot noise. In situations where there is a large amount of light scattered, photodiodes are often adequate but, in more difficult situations, a photomultiplier is necessary. When photon correlation is used for the signal processing, a special form of photomultiplier is used, which gives a separate electron burst as each photon arrives at the photosensitive surface.

5.6.4 Signal Processing The form of the signal produced by the photosensitive device as a particle crosses the measuring volume is represented in figure (5.11). It consists of a low frequency pedestal whose size and shape depend on various parameters, such as which part of the measuring volume is traversed, and the size and shape of the particle [Durst, Melling and Whitelaw (1976), Ungut et al (1978)]. The pedestal signal is modulated by the high frequency Doppler signal. The pedestal frequency is produced by the average light intensity variations experienced by the particle as it crosses the measuring volume.

The simplest method of extracting the Doppler frequency from the signal is to freeze the signal from one particle on a storage oscilloscope and counting the number of cycles in a set time. However, in order to get a reasonable statistical sample, large numbers of particle velocities

should be taken at each point [Yanta and Smith (1969)]. Also, if the time required to take the measurements is long, the conditions of the flow may change during the experiment.

The first method used for measuring the Doppler frequency was spectrum analysis [Yeh and Cummins (1964), Mazumder and Wankum (1969)]. Spectrum analysers usually consist of a narrow band filter which is' swept across the frequency range of interest and the output from the filter is plotted against the frequency on an X-Y plotter. The velocity and turbulence of the flow can be obtained from the frequency and width of the peak. However, the spectrum analyser does not make full use of the information available in the signal, since signals are only used when the filter has the same frequency as the signal.

Frequency trackers produce a voltage which is proportional to the Doppler frequency. Various tracking filters have been developed, for example Fridman et.al.(1968) and Deighton and Saylel (1971). After filtering out the pedestal frequency, the Doppler frequency is mixed with the frequency produced by a voltage controlled oscillator (VCO) to give an intermediate frequency. Using a frequency locked loop, the intermediate frequency is kept constant and the voltage controlling the VCO is proportional to the Doppler frequency. For the tracker to be able to follow the velocity variations of the flow, a nearly continuous signal is required. The turbulence intensity is proportional to the root-mean-square of the output voltage.

The period counter has been used to analyse the LDV signal by Brayton, Kalb and Crosswy (1973), Hobson, Lalor and Weston (1973) and by many others. This instrument times a fixed number of Doppler cycles to give the Doppler frequency after the pedestal signal has been removed by filtering. Thus the velocity of each particle is measured and the period counter is particularly suitable for measuring the

frequency of non-continuous signals. However, if there is more than one particle in the measuring volume simultaneously, the counter can give an erroneuous result due to the phase difference between the signal from each particle. In order to avoid such errors, the period counter has circuits which reject such double signals, but this means that in flows with large numbers of scattering particles the LDV produces signals unsuitable for processing with the period counter.

Another signal analyser that has been used on LDV signals is the photon-correlator. This was described by Pike (1972). As a particle passes through the fringes a series of bursts of photons are scattered and, on arriving at the photomultiplier, they are converted into electron bursts. The correlation function produced by these bursts can be used to calculate the velocity and turbulence of the flow. Very low light levels are needed for photon-correlation and it is possible to use the light scattered by molecules for processing.

Recently a form of spectrum analyser which makes use of all the signals has been developed by Baker and Wigley (1975). This is the filter bank and the output of all the narrow band filters which cover the frequency range of interest is measured, so that the total frequency distribution can be found.

5.7 Factors Affecting Signal Quality

5.7.1 Measuring Volume The measuring volume of the LDV is the volume from which signals are accepted and is defined mainly by the receiving optics, whilst the probe volume or crossover region is that region where the light intensity drops to e^{-2} of the maximum intensity. In order that the wave fronts are planer in this region and the 'fringes' are undistorted, the beams should cross at their waists. This ensures that the Doppler frequency produced by the particle is the same in all

parts of the probe volume, provided that the velocity is constant.

If the radius of the unfocussed beam is σ , and the focal length of lens is f_1, the beam radius at the waist will be

$$r_o = \frac{4f_1 \lambda}{\pi \sigma} \tag{5.40}$$

[Brayton and Goethert (1971)].

As the particle passes through the intersection region it will be subject to the electric field from the two beams, defined by :-

$$\xi_1 (x_1, y_1, z_1) = B_o \exp\left[-\frac{z_1^2 + y_1^2}{r_o^2} + ikx_1\right] \tag{5.41}$$

$$\xi_2 (x_2, y_2, z_2) = B_o \exp\left[-\frac{z_2^2 + y_2^2}{r_o^2} + ikx_2\right] \tag{5.42}$$

[Durrani and Greated (1977)].

(x_1, y_1, z_1) and (x_2, y_2, z_2) represent the co-ordinates of the particle in terms of the axes of the two beams. They are related by the equations:-

$$\begin{aligned} z_1 &= z\cos\theta + x\sin\theta & z_2 &= z\cos\theta - x\sin\theta \\ x_1 &= x\cos\theta - z\sin\theta & x_2 &= x\cos\theta + z\sin\theta \\ y_1 &= y_2 = y \end{aligned} \tag{5.43}$$

in terms of the common co-ordinate system (x,y,z) [see figure (5.12)].

The average light intensity falling on the particle at point (x,y,z) is defined by equation (5.17). Averaging out the oscillating terms $\xi_1 \xi_2^*$ and $\xi_2 \xi_1^*$, the intensity variation in the probe volume becomes :-

$$\begin{aligned} I &= \xi_1 \xi_2^* + \xi_2 \xi_2^* \\ &= 2B_o^2 \exp\left[-\frac{2}{r_o^2}(z^2\cos^2\theta + y^2 + x^2\sin^2\theta)\right] \end{aligned} \tag{5.44}$$

This drops to e^{-2} of its maximum value if the particle lies on the surface of the ellipsoid :-

$$z^2\cos^2\theta + y^2 + x^2\sin^2\theta = r_o^2 \tag{5.45}$$

Thus the dimensions of the probe volume defined as the volume enclosed by the surface on which a particle is exposed to a light intensity e^{-2} of the maximum light intensity, are :-

$$\sigma_z = \frac{2r_o}{\cos\theta} \qquad (5.46)$$

$$\sigma_y = 2r_o \qquad (5.47)$$

$$\sigma_x = \frac{2r_o}{\sin\theta} \qquad (5.48)$$

[see figure (5.13)] .

The number of fringes, N_F, in the e^{-2} probe volume can be determined as follows :-

$$N_F = \frac{\sigma_z}{\delta} = \frac{4r_o \tan\theta}{\lambda} = \frac{16f_1}{\pi\sigma} \tan\theta \qquad (5.49)$$

The size of the measuring volume, that is, the volume from which signals with amplitude greater than e^{-2} of the maximum signal amplitude are received by the photodetector, depends on both the size of the probe volume and on the collecting optics. In the system illustrated in figure (5.14), light from the probe volume is focussed on the pinhole by a combination of the two lenses. The centre of the probe volume is at the focal point of lens (1) and the pinhole is at the focus of lens (2). If the pinhole has a diameter d_{ph}, the diameter of the measuring volume from which light will reach the photodetector is d_v, such that :-

$$d_v = \frac{f_1}{f_2} \quad d_{ph} \qquad (5.50)$$

[Using equation (5.40)] .

The pinhole diameter, d_{ph}, is chosen so that the light reaching the photosensitive surface originates only from the probe volume or part of that volume. This reduces the noise due to extraneous light reaching the photodetector. It also reduces the possibility of erroneous signals that can be produced by the mixing of light scattered by two particles simultaneously crossing the two beams outside the

probe volume [Durst and Venkatesh (1975)].

The effective dimensions of the measuring volume, ΔX, ΔY, ΔZ, may be smaller than the probe volume dimensions σ_x, σ_y, σ_z, if the cylinder diameter d_v cuts the probe volume.

5.7.2 Frequency Broadening Effects The heterodyne frequency received by the photodetector is subject to several broadening effects. The most significant of these effects are:-turbulence broadening, velocity gradient broadening, and finite transit time broadening.

Turbulence broadening is caused by variations in the velocities of the particles from which the signals originate due to turbulence of the conveying fluid. The frequency spread $d\nu_D$ is defined by the equation :-

$$\frac{d\nu_D}{\nu_D} = \frac{dV}{V} \qquad (5.51)$$

where dV is the turbulence bandwidth of the fluid.

Velocity gradient broadening is produced by a gradient in the velocity of the fluid and therefore the scattering particles across the measuring volume. The frequency spread due to this effect is $d\nu_G$ such that :-

$$\frac{d\nu_G}{\nu_D} = \frac{1}{\sqrt{2}V} \left[\Delta Y \left(\frac{\partial V}{\partial y}\right)_z + \Delta Z \left(\frac{\partial V}{\partial z}\right)_y \right] \qquad (5.52)$$

[Humphrey, Melling and Whitelaw (1975)].

Thus, for the least velocity gradient broadening, the area of the measuring volume in the x-y plane should be as small as possible.

The finite time broadening is the effect of the finite length of the Doppler signal from each particle. The frequency spread, $d\nu_T$ produced by this effect is given by:-

$$\frac{d\nu_T}{\nu_D} = \frac{\lambda}{4\sqrt{2}\ \pi\ \sigma_x\ \sin\theta} \qquad (5.53)$$

In this case, for least signal broadening, the measuring volume should have the greatest possible x-dimension.

Other broadening effects on the signal before it reaches the photodetector are small compared to these three. However, the instrument with which the signal is analysed increases the frequency spread of the signal. The bandwidth, $d\nu_I$, of this effect depends on the properties of the instrument.

The total broadening, $d\nu$, of the signal, provided all the factors have Gaussian form, is given by

$$\left(\frac{d\nu}{\nu_D}\right)^2 = \frac{1}{\nu_D^2}\ (d\nu_D^2 + d\nu_T^2 + d\nu_G^2 + d\nu_I^2\ ) \qquad (5.54)$$

5.7.3 Signal to Noise Ratio (SNR) There are many sources of noise in the signal of the LDV, all of which tend to obscure the useful signal. The SNR should be as large as possible for the greatest accuracy of frequency measurement, although correlation techniques can be used to extract the signal from a very low signal to noise ratio.

Noise is produced by background illumination of the photodetector, shot noise produced in the photodetector, and noise in the circuits of the signal analyser. The laser also produces noise. A reasonably complete expression for the SNR in the LDV for small particles is derived by Buchave (1973)

$$SNR = \frac{2\ \frac{\eta\varepsilon^2}{h\nu}\ P_1 P_2}{2K\ \Delta f\ (P_1 + P_2 + P_B + \frac{h\nu}{\eta e}\ i_D) + \frac{4h\nu kT\Delta f}{G^2 e^2 \eta R_L}} \qquad (5.55)$$

This expression indicates that the SNR is inversely proportional to the bandwidth of the filter in the signal processor, but the bandwidth cannot be reduced without reducing the frequency range accepted by the instrument.

5.8 Discussion

This chapter describes the laser-Doppler velocity meter in general and explains the principle of operation of the instrument. The LDV has been mainly developed as an instrument for velocity measurements in single-phase flows, using light scattered by small seeding particles. Difficulties are encountered when using this instrument for two-phase flow velocity measurements and these are described in Chapter 6.

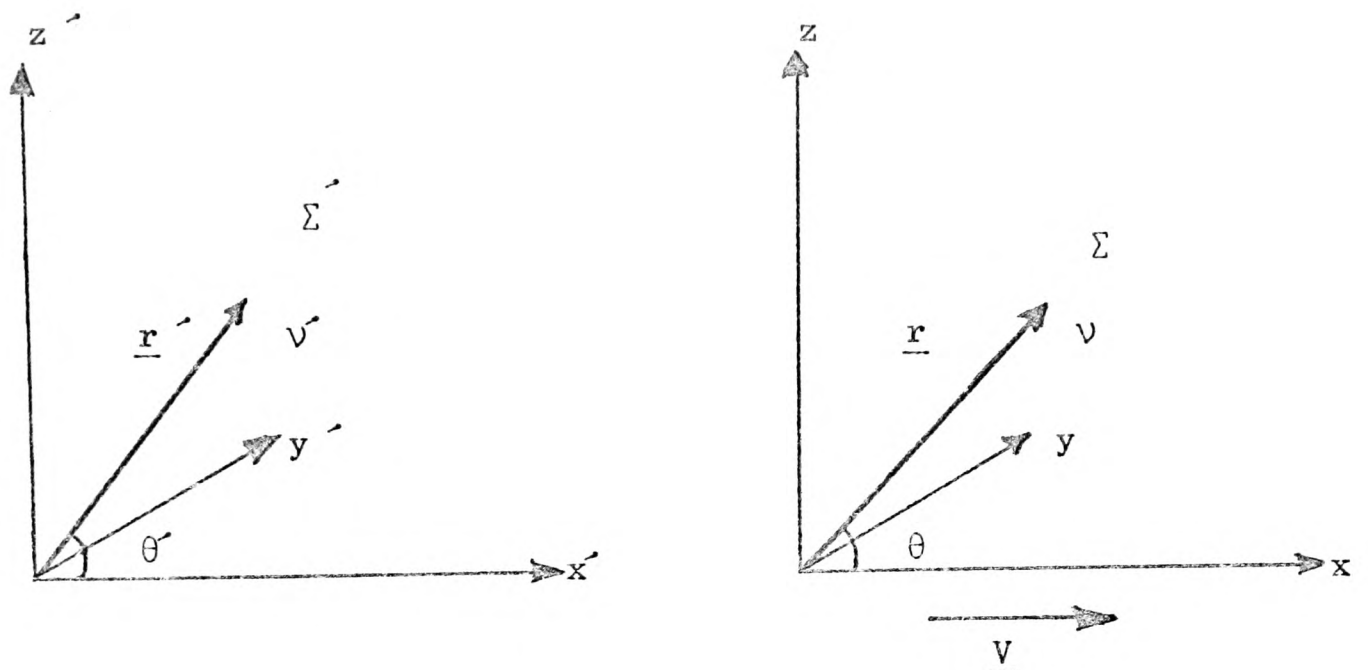

TWO CO-ORDINATE SYSTEMS IN
UNIFORM TRANSLATION

Figure (5.1)

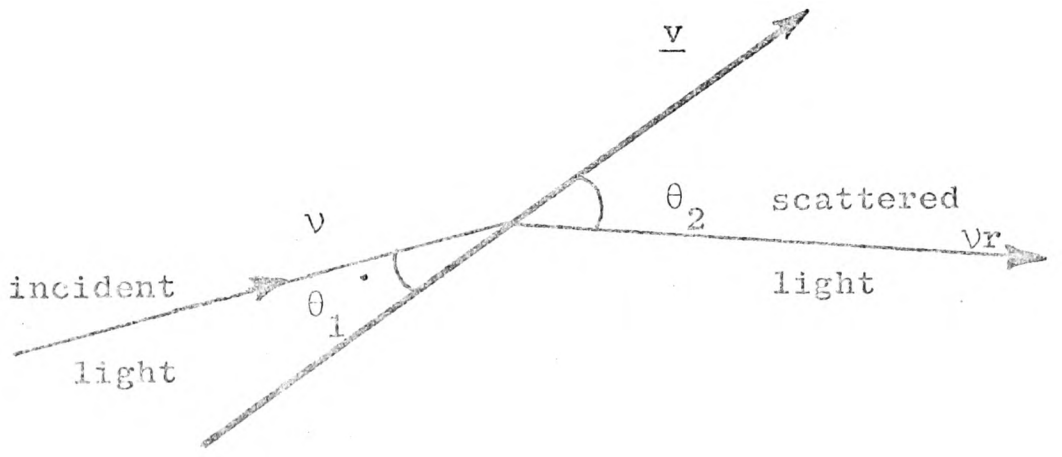

DOPPLER FREQUENCY SHIFT OF LIGHT SCATTERED
BY MOVING OBJECT

Figure (5.2)

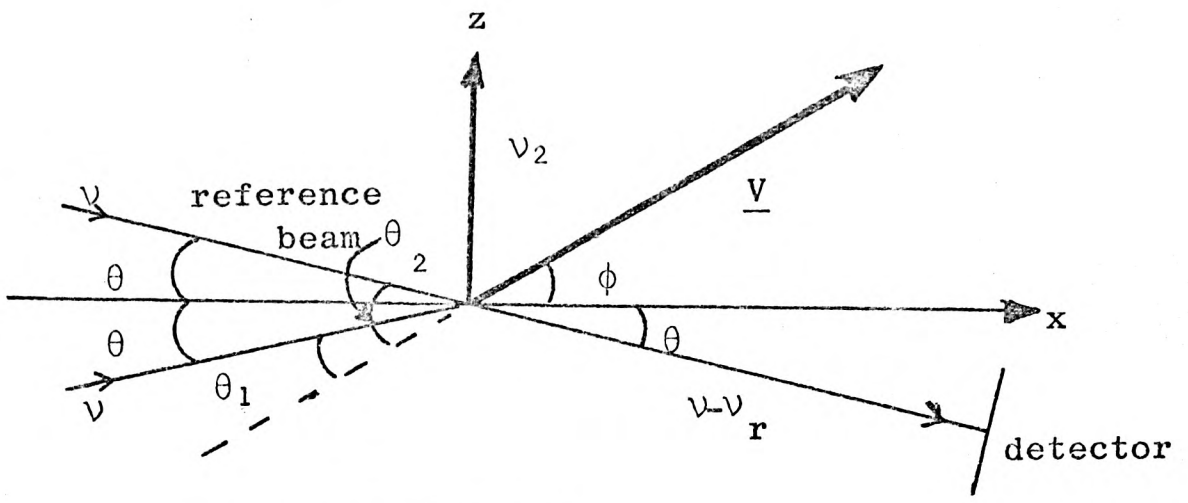

REFERENCE BEAM MODE
Figure (5.3)

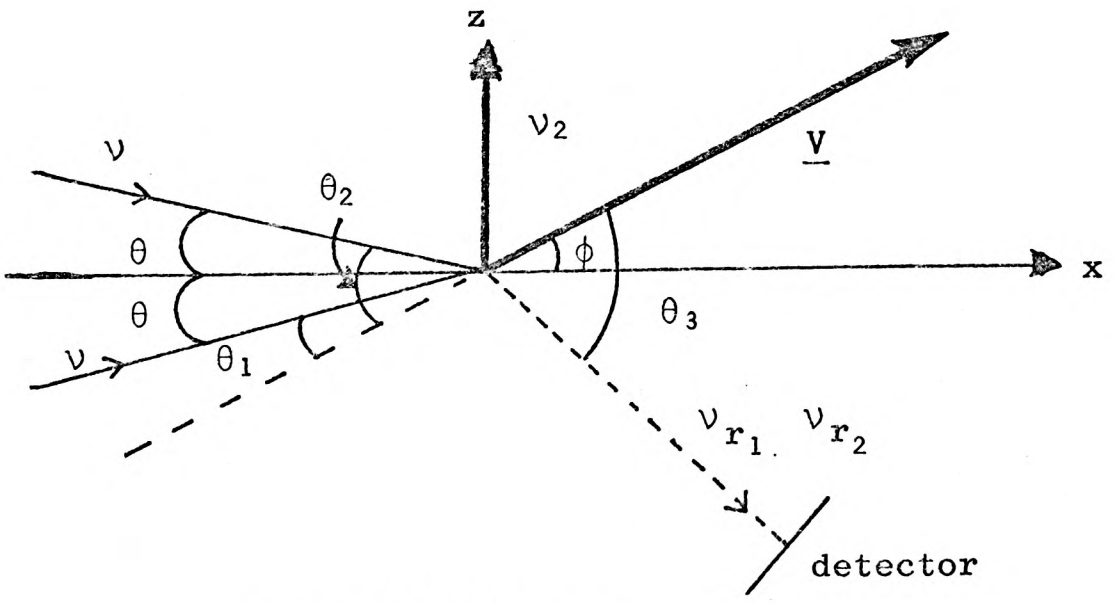

DUAL-DOPPLER MODE
Figure (5.4)

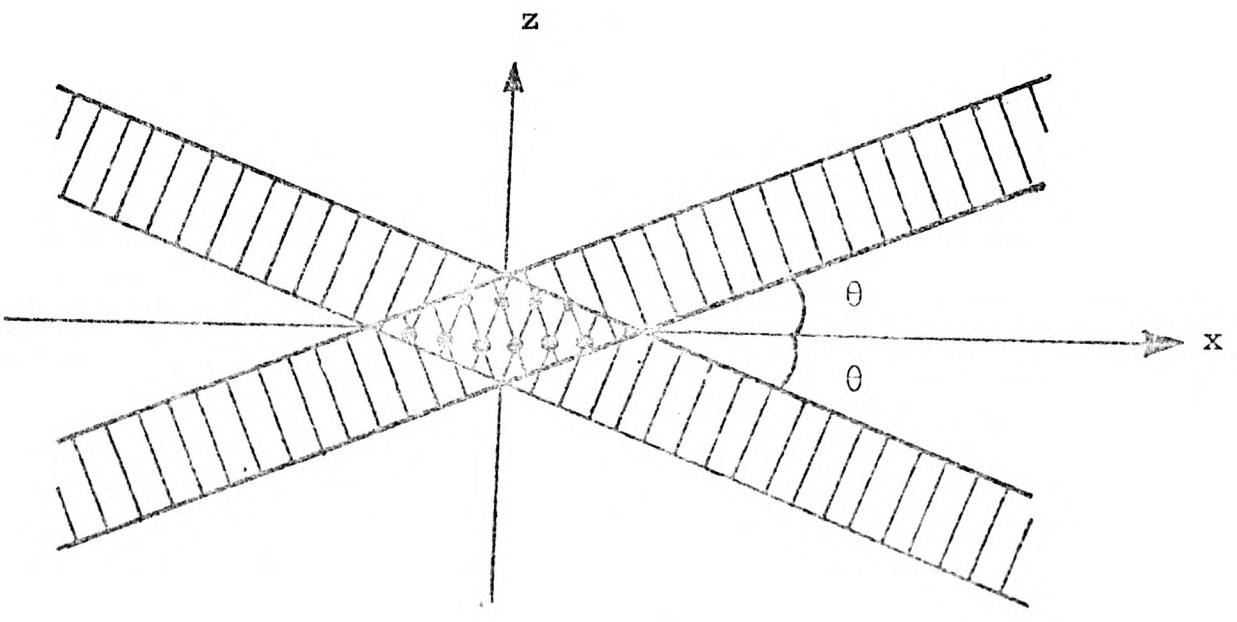

FRINGE MODEL
Figure (5.5)

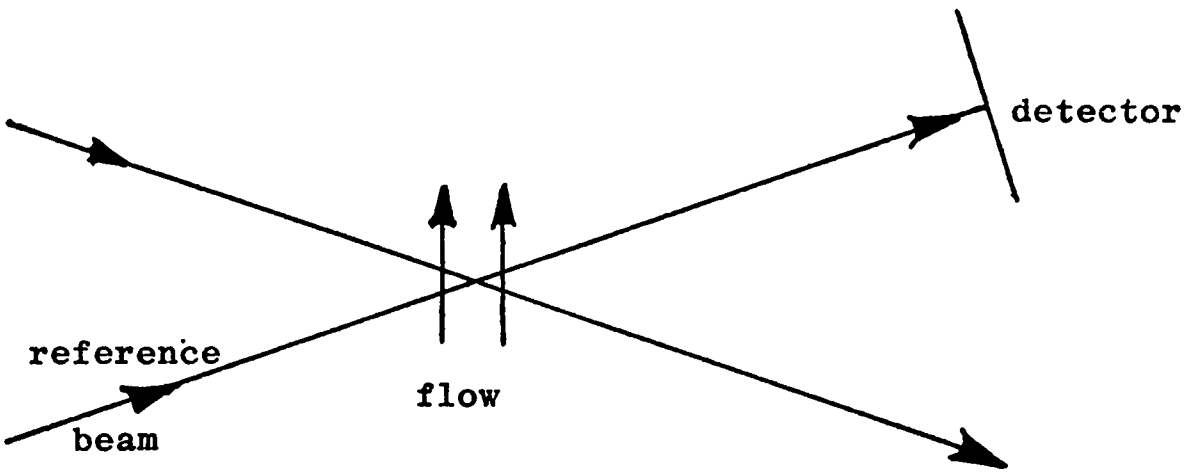

REFERENCE BEAM MODE, WITH CROSSING BEAMS

Figure (5.6)

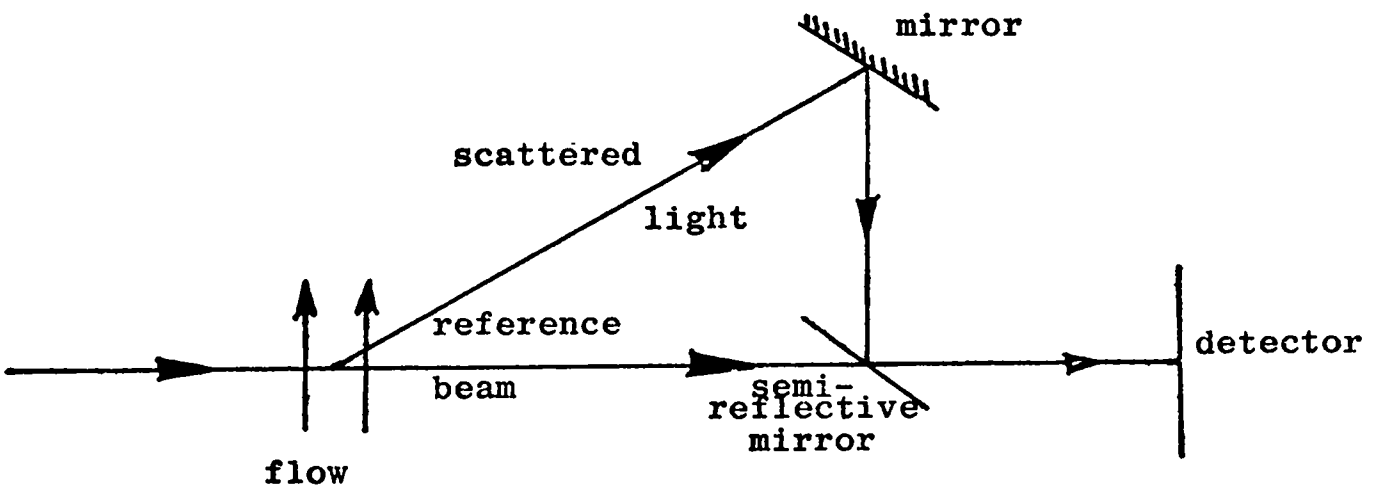

REFERENCE BEAM MODE, WITH SINGLE BEAM

Figure (5.7)

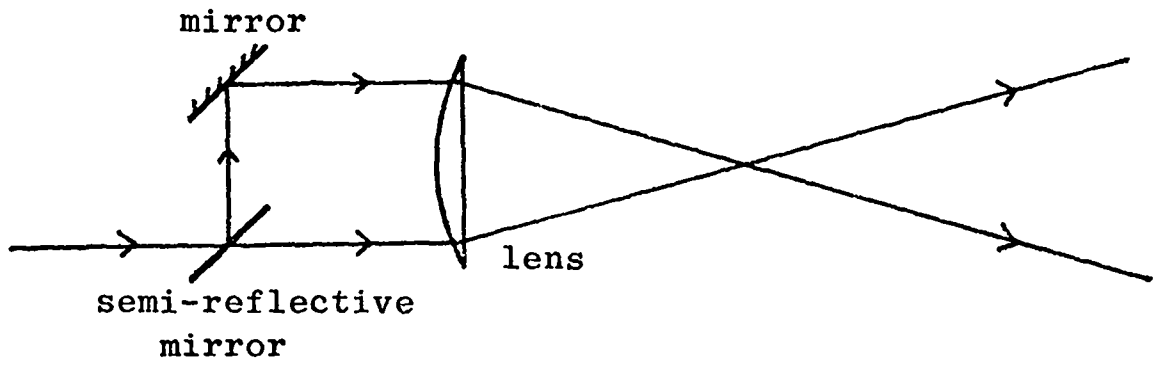

(a) SEMI-REFLECTIVE BEAM SPLITTER WITH SINGLE LENS

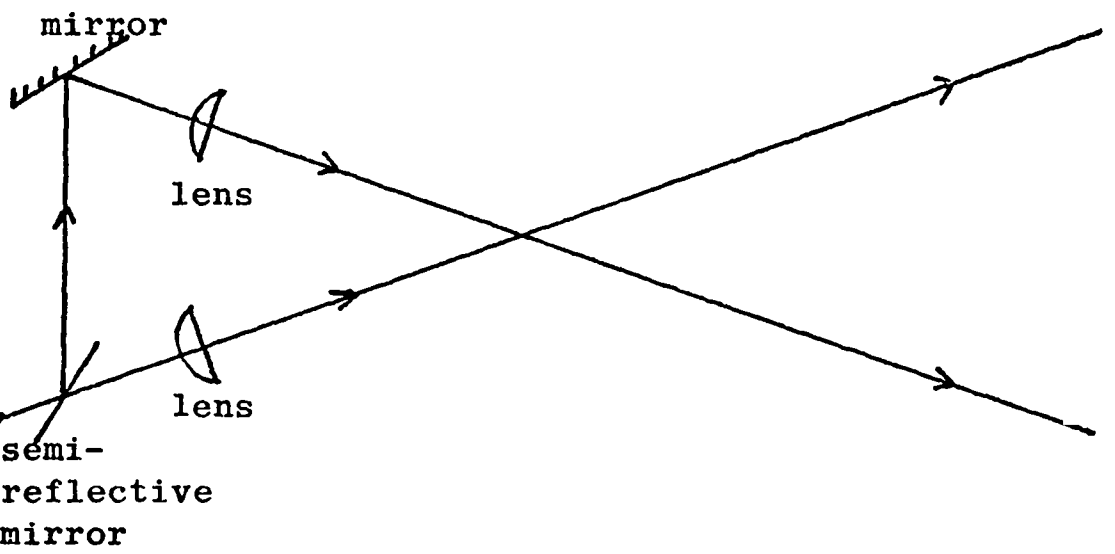

(b) SEMI-REFLECTIVE BEAM SPLITTER WITH TWO SEPARATE LENSES

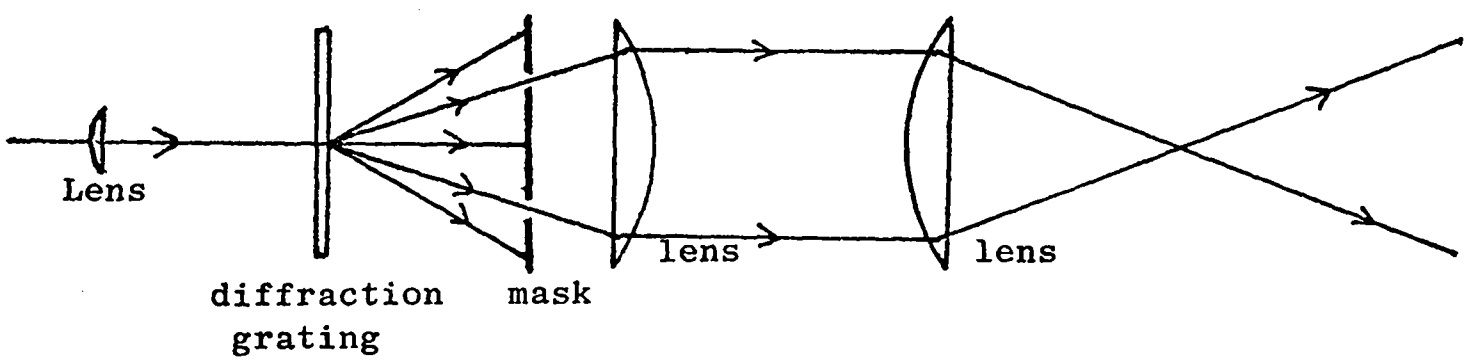

(c) DIFFRACTION GRATING AS A BEAM SPLITTER

TRANSMITTING OPTICS

Figure (5.8)

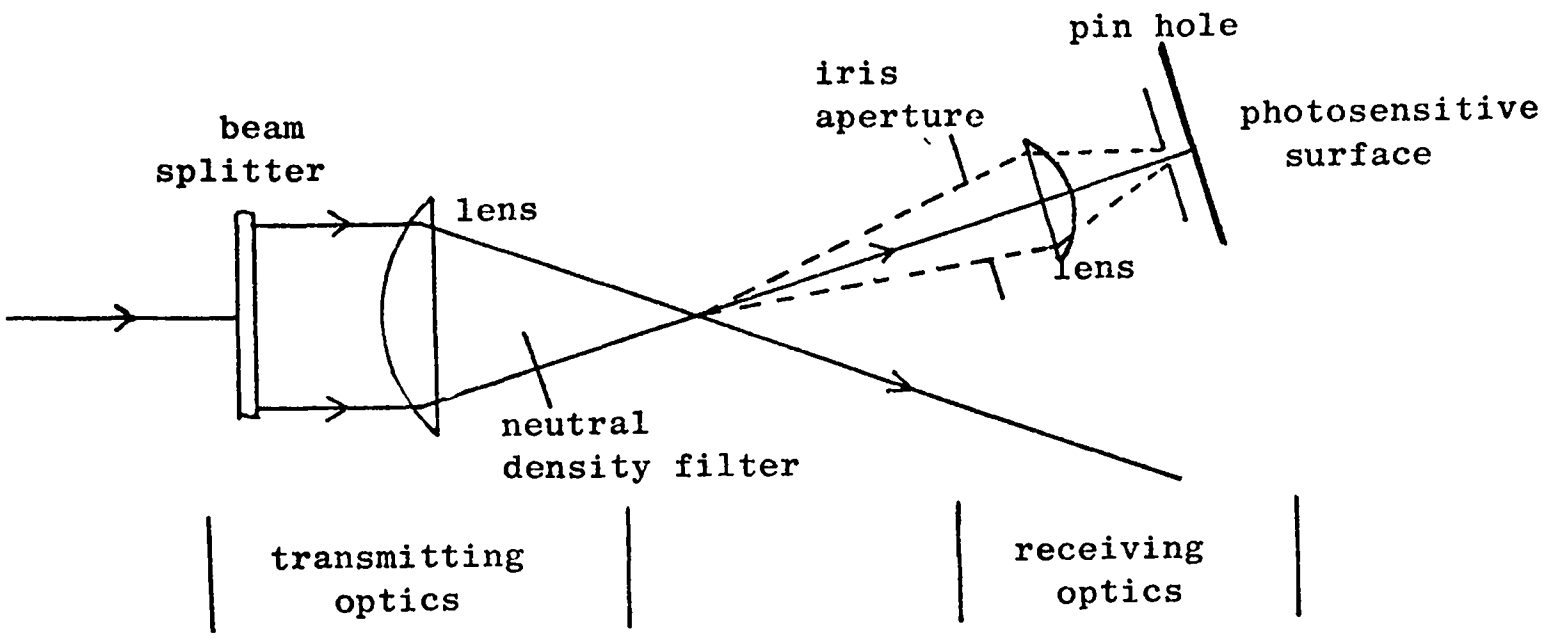

REFERENCE BEAM MODE
Figure (5.9)

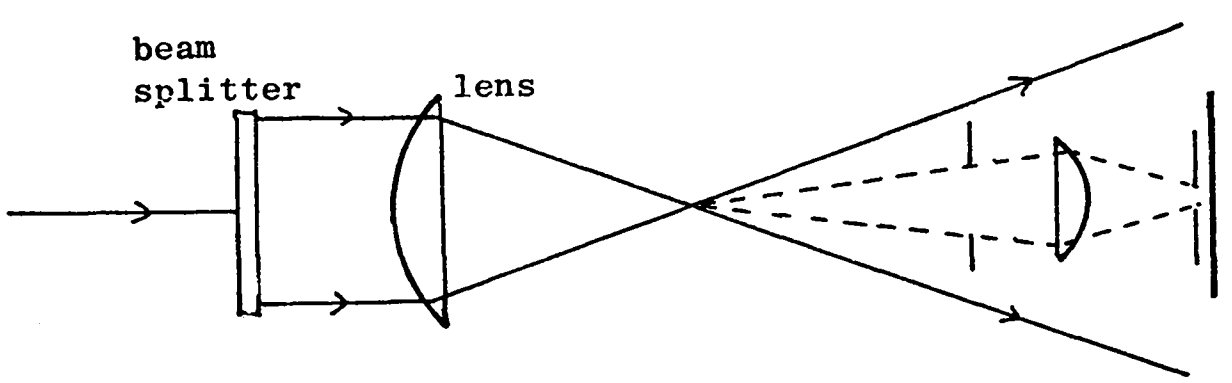

(a) Forward Scatter

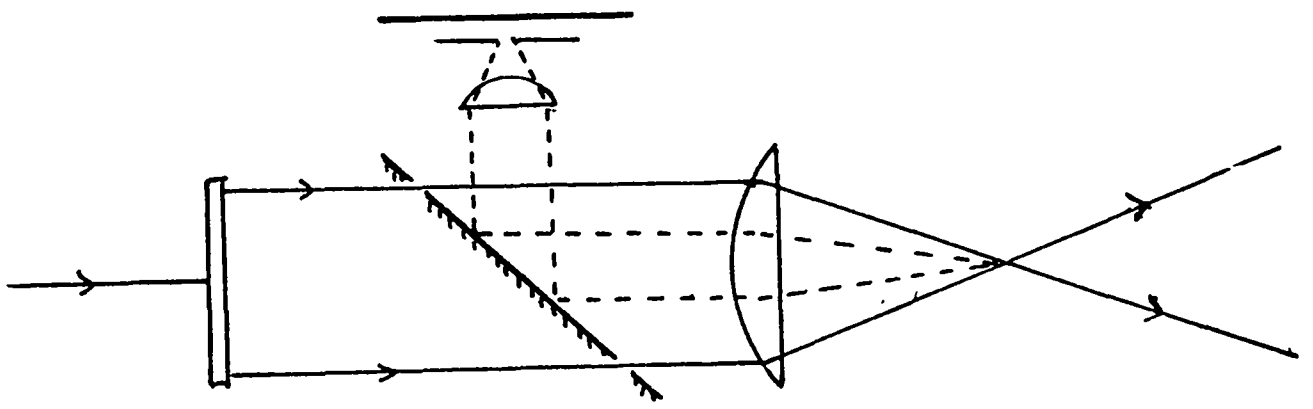

(b) Back Scatter

DUAL-DOPPLER MODE

Figure (5.10)

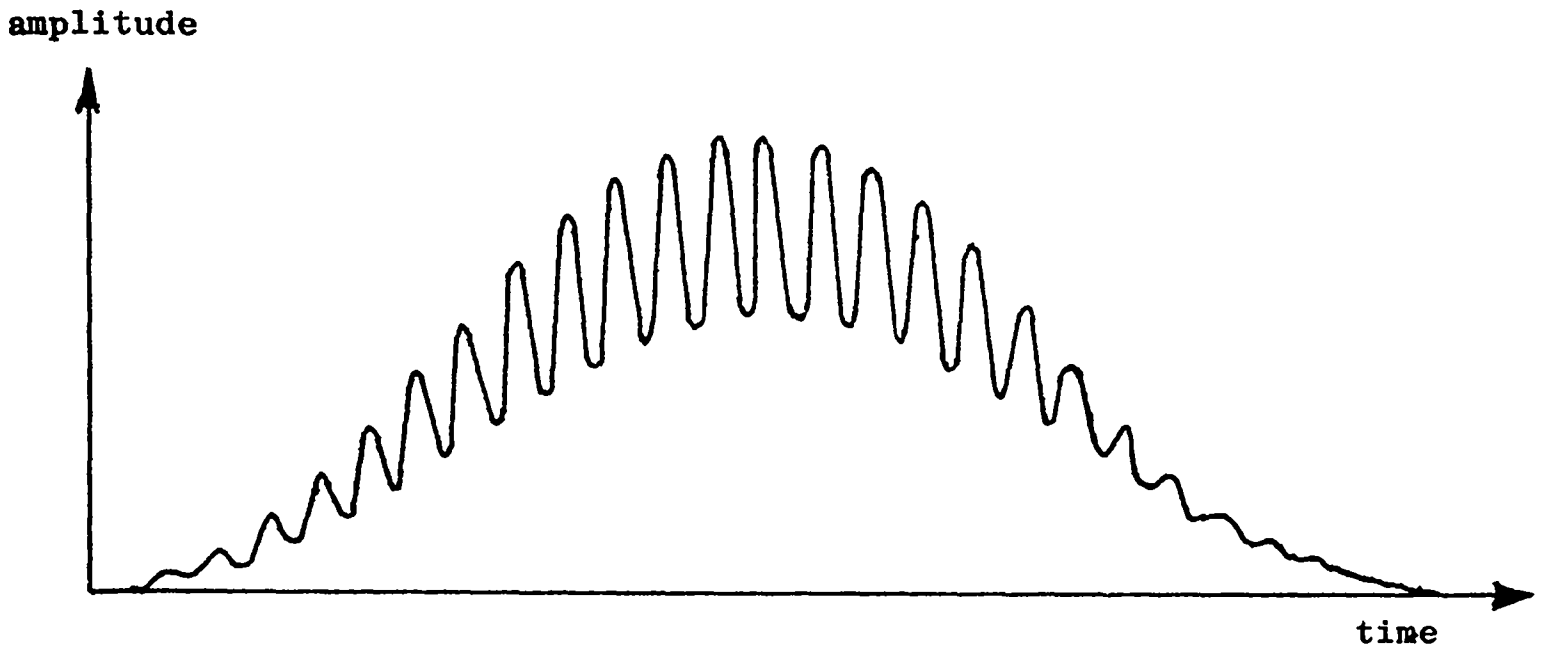

EXAMPLE OF LDV SIGNAL
Figure (5.11)

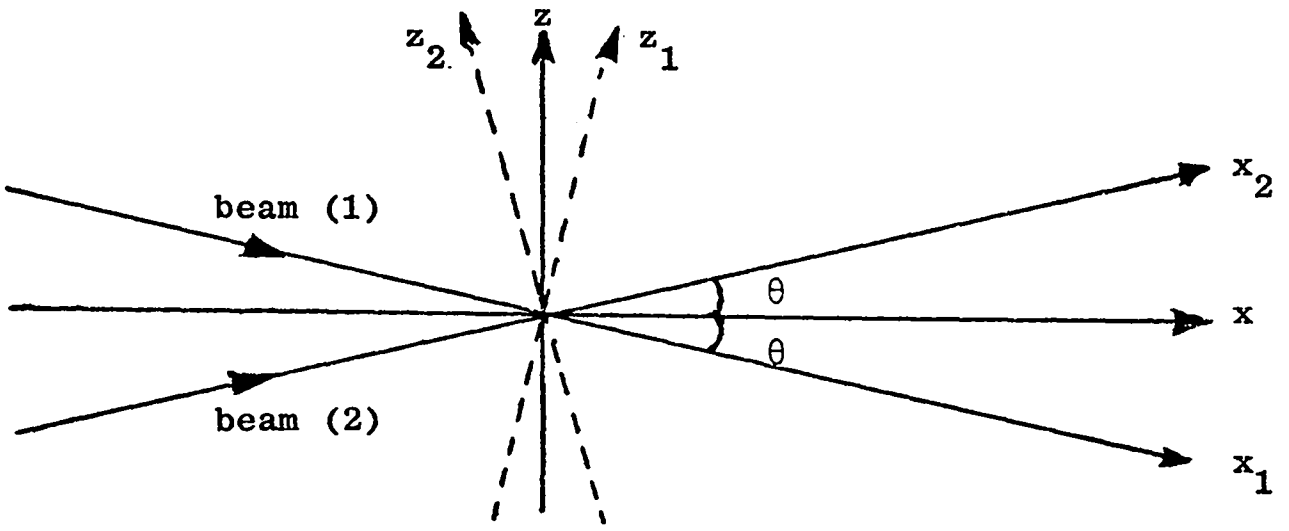

CO-ORDINATE SYSTEM FOR PROBE VOLUME
Figure (5.12)

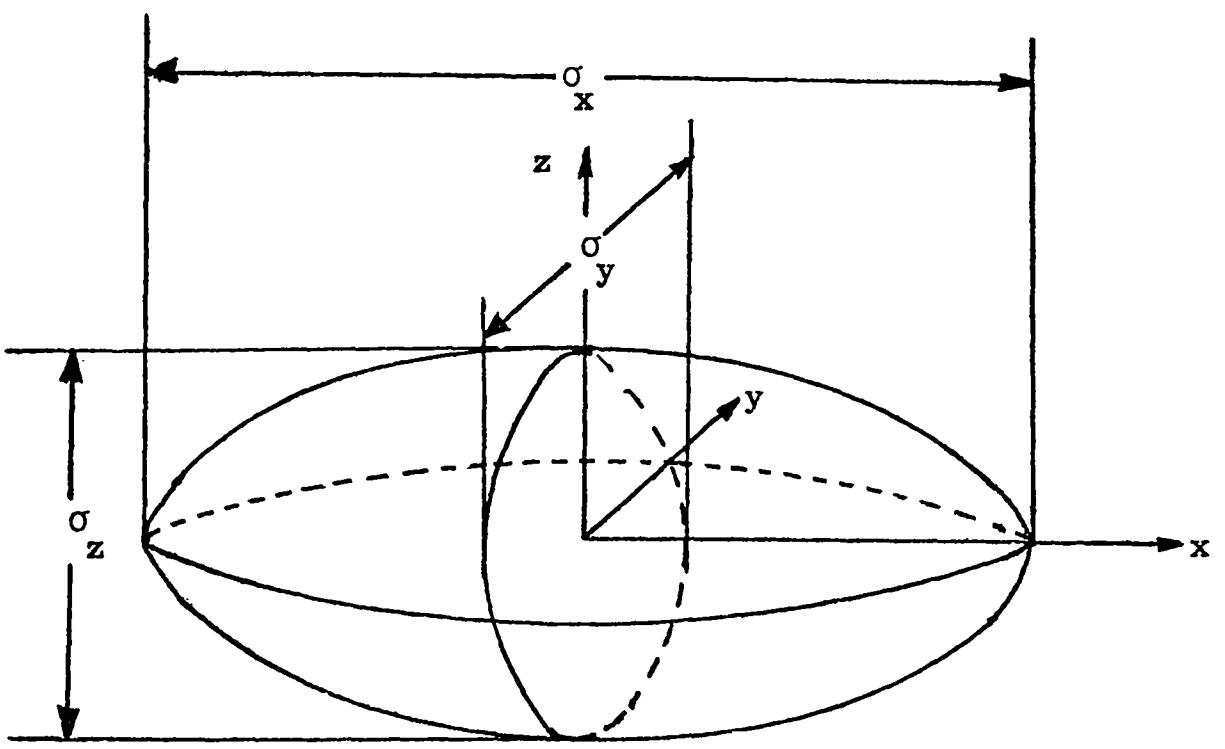

PROBE VOLUME
Figure (5.13)

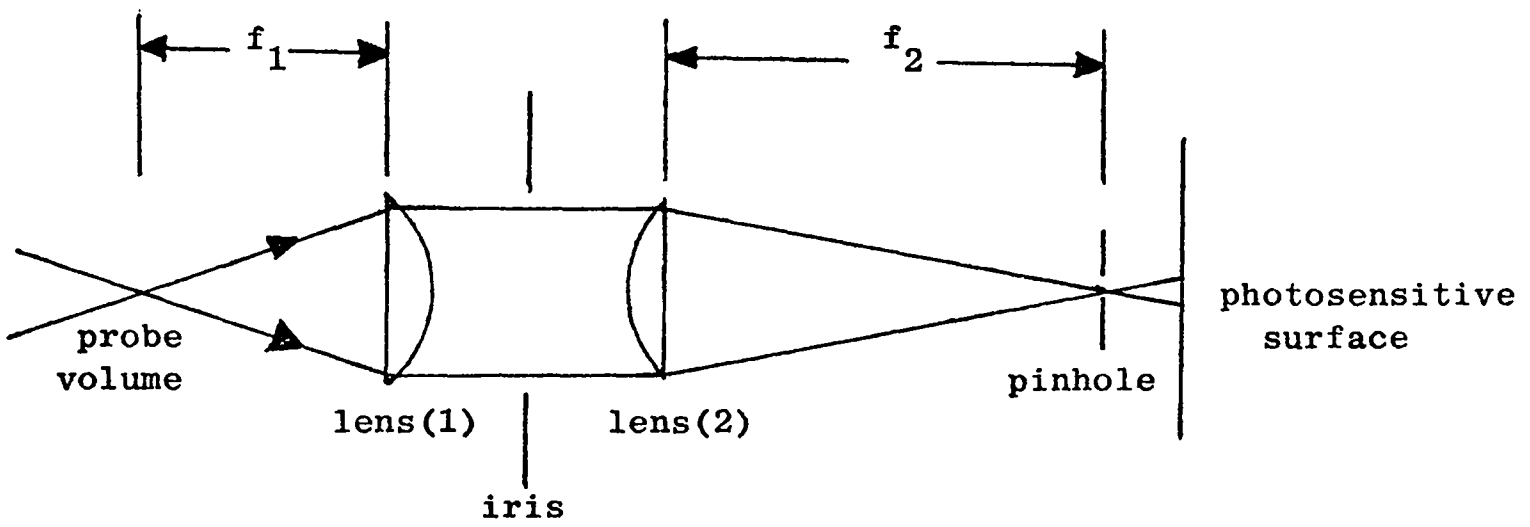

RECEIVING OPTICS

Figure (5.14)

CHAPTER 6

LASER-DOPPLER VELOCIMETRY FOR TWO-PHASE FLOW

6.1 Historical Review

Relatively little has been published on the use of the laser-Doppler velocity meter for measuring particle velocities in two-phase flows. The vast majority of work done using an LDV has been to measure the fluid velocity in single phase flow. This is done by measuring the velocity of particles small enough to follow the eddies in the conveying fluid, but large enough to give a useful signal amplitude. Several papers have been published on the size of particles needed for such measurements [Melling (1971), Mazumder and Kirsch (1975)] . The particles can be either natural contaminants of the fluid or they may be added. They are usually about 1 μm in diameter or less. Since these particles are very small and do not occupy a significant volume of the fluid, they do not significantly affect the behaviour of the fluid in most cases. However, in two-phase flows the particles are usually considerably larger and there are often differences between the velocity and turbulence of the particles and those of the flow.

In bubbly water flow, Davies (1973), used an LDV for measuring the velocity of the bubbles in upward vertical flow. The size of the bubbles is not mentioned in this reference. The frequency of the signal from individual particles was measured from the trace on a storage oscilloscope. The velocity of the bubbles was measured using the dual-Doppler in back-scatter mode, whilst the water velocity was measured using forward scatter in the reference beam mode and utilising the natural particles in the flow. Velocities of the order of 20 ms^{-1} were recorded.

Carlson (1973) employed an LDV for the investigation of particle velocities in an air-solid flow. He measured the velocities and number density of glass particles 44 μm and 214 μm in diameter in a flow with mean gas velocity of 30 ms^{-1} in a 3" square duct. Forward scatter dual-Doppler mode was used and a form of frequency tracker employed. Most of this thesis was on the theory of the LDV and only a few results were given.

Farmer (1973) attempted to measure the particle size, velocity and number density in an air-solid flow. He calculated the dependence of the shape of the signal on the size of the particle using the fringe theory. Thus, from the Doppler frequency, the number of impulses and the shape of the LDV signal, the velocity, number density and size of the particles could be obtained. However, the use of the fringe theory in obtaining the particle size from the Doppler signal has been shown to be incorrect (see section 6.3). More recent work [Farmer (1978)] has corrected this.

Barker, Reithmuller and Ginoux (1972) used an LDV for measuring the velocity of glass spheres from 100 μm to 500 μm in diameter in an air-solid flow from a nozzle. Dual-Doppler forward scatter mode was used and the Doppler frequency was measured from a storage oscilloscope. Reithmuller and Ginoux (1973) employed an LDV to measure the velocities of similar particles in a 42 μm diameter glass tube at velocities from 2 ms^{-1} to 100 ms^{-1}. The measurements were taken in a horizontal pipe with solids to air mass flow rate ratios of up to 15. In this case the signal processor was a period counter. These measurements demonstrated the suitability of the LDV for such a flow, but little detail is given.

Lehmann (1975) used both a dual beam, time of flight correlation velocity meter and a laser-Doppler velocity meter to measure the velocity of particles in a wet steam flow and an air solid flow containing glass

ballotini. He used several methods of analysis for the LDV signal, including frequency measurement from the trace on a storage oscilliscope, period counting, and an optical method using a Fabry-Pérot etalon for high velocity flows. Velocities of up to 100 ms^{-1} were measured. The LDV was found to be more suitable for the two-phase flow measurements than the correlation method.

Birchenough (1975) took measurements of alumina particles , 20 μm in diameter in an upward air-solid flow in a 50 mm diameter vertical pipe using an LDV. The flow was produced in the large pneumatic conveying plant described in section (3.2), and the dual-Doppler forward scatter mode was used. Signal analysis was by the DISA tracking filter described later in this chapter. Velocities of up to 60 ms^{-1} were measured in flows having solid to air flow rate ratios of up to 1.5. Average velocities of all the particles in the pipe were obtained by using a measuring volume length along the optical axis of the LDV, much greater than the pipe diameter. Using back scatter from the edge of the flow, measurements were taken in flows with solids to air mass flow rate ratios of up to 4.5.

The problems of taking LDV measurements in two-phase flows were analysed theoretically by Durst and Zaré (1975). The mechanisms of light scattering by large particles were investigated and the velocity of both an air jet and a steel ball 20 mm in diameter suspended in the flow and swinging, were measured simultaneously using an LDV. Also the velocity of air bubbles in glycerine was measured. They showed also that the alignment of the receiver is particularly important when measuring the velocity of large particles. More recent work by Durst (1978) includes measurement of particle velocity profiles in air-solid flows.

6.2 Scattering Mechanisms

The behaviour of light scattered by particles and molecules with diameters less than about one tenth of the wavelength of the incident light is described by the Rayleigh scattering theory. However, the particles used for light scattering in laser Doppler measurements are usually much larger than this. The particles used for light scattering in single-phase flows are normally of the order of one wavelength in diameter. For these particles the scattering mechanisms can be described by the Mié scattering theory [van de Hulst (1957), Kerker (1969)] . Mié scattering theory also applies to the larger particles used in pneumatic conveying, but for very large particles, several thousand wavelengths in diameter, the scattering is described by classical optics.

The Mié scattering theory is very complex and will not be examined in detail here. However, some aspects of the theory are important in laser velocimetry. The total intensity of light scattered by particles increases with particle diameter. The angular distribution of the reflected light intensity and polarisation varies with the particle size. For a sphere, with diameter of the same order of magnitude as the incident light wavelength, the light is mainly scattered in the forward direction, with very little in the backwards direction (intensity in backwards direction is circa 0.5% of the forwards intensity). For larger spheres, the angular distribution shows a large number of maxima and minima, with the angle of the forward scattered lobe increased and the light scattered in the backwards direction is decreased in proportion [Born and Wolfe (1964)] . This indicates that for small seeding particles in single-phase flow, the optical arrangements of the LDV should collect the light scattered either directly forwards or directly backwards, for maximum light intensity. For large particles, light can be collected from most directions, except directly backwards.

6.3 Signal Visibility

Figure (6.1) shows a typical signal from a single particle passing through the measuring volume. It is made up of a high frequency Doppler signal and a low frequency pedestal. The signal visibility or quality, η, is defined as half the ratio of the amplitude of these two parts. It is given by the equation :

$$\eta = \frac{I_1 - I_2}{I_1 + I_2} \qquad (6.1)$$

where I_1 is the intensity of light scattered at the centre of the measuring volume and I_2 is the intensity of the following minimum. A reasonably large visibility is required for the Doppler frequency to be extracted.

Simple fringe theory predicts that, as the size of the particle increases, the visibility of the signal will oscillate between zero and a maximum, the size of the maxima rapidly decreasing [see figure (6.2)]. This is because the large particles occupy more fringes and therefore scatter more light, increasing the pedestal signal, whilst the Doppler signal is unchanged. This theory predicts that the visibility for the particles used in this work would be negligible. However, as stated in section (5.3), the fringe theory does not take into account the scattering processes and, using the Mié theory of scattering from the two beams, the variation of the visibility with particle size can be calculated and this is shown in figure (6.3) [Durst et al (1976), Adrian and Orloff (1977)] . The results of Birchenough (1975) agreed well with the calculated results and show that a useful visibility is obtained from larger particles.

The particles used in the present work were much larger than those used in the last two references. The signal visibility obtained from these particles was much less than that obtained from smaller particles.

Webb (1976) investigated the angular variation of the signal visibility for particles ranging from 43 μm to 235 μm in diameter. He found that the visibility varied from near zero along the forward scatter optical axis, to a maximum at about 45^{o} through a series of lobes. These measurements were for stationary glass spheres, however, and Durão and Whitelaw (1979) showed that the signal visibility decreases with increasing velocity.

In the present work, visibilities of circa 0.2 were obtained for the ballotini and sand particles, and circa 0.5 for the large plastic chips. The larger visibility for the plastic chips was obtained using backscatter where surface scattering probably predominated, whilst the signal from the smaller particles, in the forward direction, was mainly due to edge effects.

6.5 Signal to Noise Ratio

The expression for the signal to noise ratio (SNR) given in equation (5.55) is independent of particle size. However, several factors encountered in two-phase flow measurement tend to decrease the SNR.

The light power of the two incident beams P_1 and P_2 is reduced due to scattering by the particles in the flow. Some of this scattered light reaches the photomultiplier, which increases P_B. This effect is very much greater in two-phase flows since the scattering cross-section of the particles is much greater. The pipe walls in two-phase flows tend to become frosted due to abrasion by the particles, and again P_1 and P_2 are decreased and P_B increased. From equation (5.55), decreasing P_1 and P_2 and increasing P_B increases the SNR.

Lehmann (1975) found that the SNR decreased rapidly with increasing particle size. The signal to noise ratio encountered in the project was small, but it was not measured.

6.6 Signal Processing

Due to the poor quality of the signal obtained from two-phase flow measurements for the reasons described above, the signal processing was very difficult. The various possible methods of signal analysis are described in section (5.6), but not all of these methods are suitable for use in two-phase flow measurements.

Measurement of frequency from a storage oscilloscope, although time-consuming and inaccurate, is the most common form of signal analysis used in two-phase flow measurements. This method was used in a large part of the present work. The other methods available were often found unsuitable for analysing the signal and alternative, more suitable methods, were unavailable due to the high cost of the instruments.

Tracking filters were available, but they require a fairly continuous signal. The signal produced from the two-phase flow is very intermittent, as can be shown as follows:

If the solid to air mass loading ratio is L, then the mass of solids in unit volume of air, density ρ_a is $L\rho_a$. Since the average weight of one particle, diameter d_s and density ρ_s is $\rho_s \pi d_s^3/6$, the number of particles in unit volume of air is $6L\rho_a/\rho_s \pi d_s^3$. Therefore, the average volume of empty air around each particle is $\rho_s \pi d_s^3/6L\rho_a$, and the average distance between particles is $d_s(\rho_s/L\rho_a)^{1/3}$. Ballotini, for example, produced a maximum value of L of about 2 in the large conveying plant. Using the values of the other parameters of the ballotini from table (4.3), the minimum distance between the particles was about 5mm. This meant that the signal, even at the highest solids to air mass loading ratio, was very intermittant.

The dimensions of the measuring volume [see section (5.7.1)] in the flow was about 50 μm, which was much smaller than the average particle diameter of about 500 μm. Thus the length of the individual signals was

dependent on the particle diameter. From this the maximum ratio of the length of signal from each particle to the average time between signals was 1:10. Interruptions of the beams by particles crossing them decreased this ratio. Figure (6.4) gives a typical signal obtained during the present study.

The frequency of the signal from successive particles crossing the measuring volume can differ greatly, due to turbulence. Tracking filters have great difficulty in following such a signal, since an extremely large slew rate is required.

Facility for spectrum analysis was available. Although it was possible in some cases to obtain the mean and distribution of the frequency using spectrum analysis, the intermittancy and noise in the signal made this method unpractical. Recording a velocity distribution took a long time and the noise in the signal made interpretation difficult.

Although no period counter was available for use throughout the project, one frequency reading was taken with a TS1 Counter System 1990 in the ballotini-air flow. It was found that the instrument was much more suitable for analysing the signal from such a flow than the tracking filter. This suitability is due to the measuring of individual signals, so that the intermittency of the signal is an advantage rather than a disadvantage. However, there are problems associated with the period counter. The signal has to have a good signal to noise ratio in the input signal, which can be achieved by narrow band filtering, but the filtering reduces the range of frequencies accepted by the instrument.

6.6 Laser Velocimetry Equipment

6.6.1 Light Source A Spectra-Physics helium-neon laser was used in the project. It operated in the TEM_{oo} mode, producing a beam of

wavelength 632.8 nm and with a beam diameter of 0.65 mm at the e^{-2} points . The beam was 5 mW power, with a divergence at the e^{-2} points of 0.17 milliradians.

6.6.2 Transmitting Optics Two sets of transmitting optics were available, one was a DISA 551 100 unit and the other involved the use of a radial diffraction grating supplied by Cambridge Consultants. The DISA unit is shown in figure (6.5). The laser beam was split by a biprism into two equally intense beams. The reflected beam was brought parallel with the transmitted beam by a surface mirror which could be moved to vary the separation between the two beams. Fine adjustment to the alignment of the beams was provided by two glass wedges in the transmitted beam, set with their tapers normal to each other. Rotation of the wedges allowed perfect intersection of the beams after focussing. The beams were brought to a focus using a single lens, three of which were provided with the unit, having focal lengths of 130mm, 300 mm and 600mm.

The second set of transmitting optics are shown in figure (6.6). The mode of operation of such a system is described in section (5.6.2). The bleached diffraction grating had 18,000 lines and the two first order beams had a combined intensity of about 60% of the incident intensity. A frequency difference between the two beams could be achieved by rotating the diffraction grating [see section (5.3)] using a constant speed motor, manufactured by Electro Craft Corp. The frequency difference could be adjusted from 0 to 2 MHz. The beam separation and the angle of the crossover 2θ were set by the choice of the two lenses L_2 and L_3, which were the lenses provided with the DISA unit.

6.6.3 Receiving Optics The receiving optics are shown in figure (6.7). The two units available were DISA 55L 10, and DISA 55L 12, which were identical except that the DISA 55L 12 had a shutter to

protect the photosensitive surface when the system was aligned.

Three lenses of focal lengths 200mm, 333mm and 600mm were provided to be used either singly or in combination as the collecting lens, L_1. The second lens, L_2, focal length 105mm, focussed the light onto the pinhole surface. The iris aperture could be used to reduce the light falling on the photosensitive surface and, if direct forward scatter dual-Doppler mode is used, the iris aperture could be used to block the unscattered laser beams. A variety of pinhole diameters was available which enabled the size of the measuring volume to be altered. The photomultiplier was EMI type 9658B, with a cathode voltage range from 500V to 1.4 KV, and a maximum anode current of 1mA. The cathode voltage was supplied by a DISA 55L 15 high voltage supply unit, providing 250V to 2KV.

6.6.4 Optical Arrangements Both the dual-Doppler and reference beam modes were investigated and it was found that the dual-Doppler mode tended to give better signals. It was also easier to arrange and less sensitive to disturbances. Therefore the dual-Doppler mode was used throughout the project. Forward scatter was used, except in the case of the plastic chips, when backscatter was used due to the high level of backward scattered light. The receiving optics were set at between 0^{o} and 45^{o} to the optical axis.

The optical components could be fixed onto an optical bench, as shown in figure (6.8), where the probe volume could be moved by moving the carriage on which the transmitting optics were fixed. Alternatively the optical components could be fixed to a board which could be moved by a screw, keeping all the components accurately aligned [see figure (11.1)].

6.6.5 Signal Processing Two tracking filters were available, the DISA 55L20 and the Cambridge Consultants CC02. A detailed description of the operation of these units is given in the DISA and Cambridge

Consultants Instruction Manuals. The principle of the DISA unit is as follows:

> The signal from the photomultiplier is filtered and then mixed with the output of a voltage controlled oscillator (VCO). The intermediate frequency produced is kept constant by a feedback loop which adjusts the voltage supplied to the VCO. This voltage is proportional to the Doppler frequency and it is the output of the instrument.

The Cambridge Consultants unit works in a similar way. However, as well as the output voltage which is proportional to the Doppler frequency, there is a direct digital reading of the Doppler frequency. This is provided by a frequency counter which measures the frequency allowed through a filter controlled by the output voltage. Spectrum analysis is also provided by applying a saw-tooth voltage to this filter and measuring the root mean square of the output.

An additional circuit [see figure (6.9)] was designed and built which removed low amplitude signals with an adjustable threshhold level. Since the larger particles scattered more light, this circuit allowed the removal of signals from small fines in the flow.

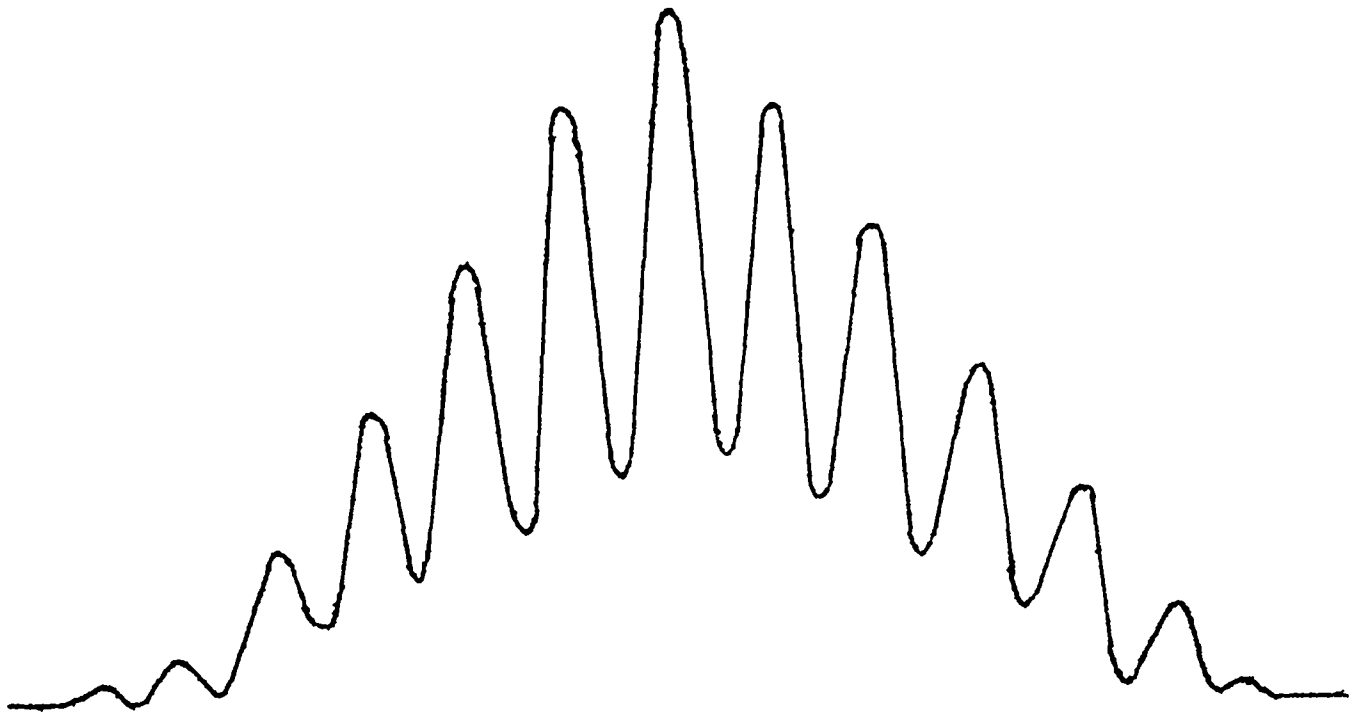

(a) Complete Signal

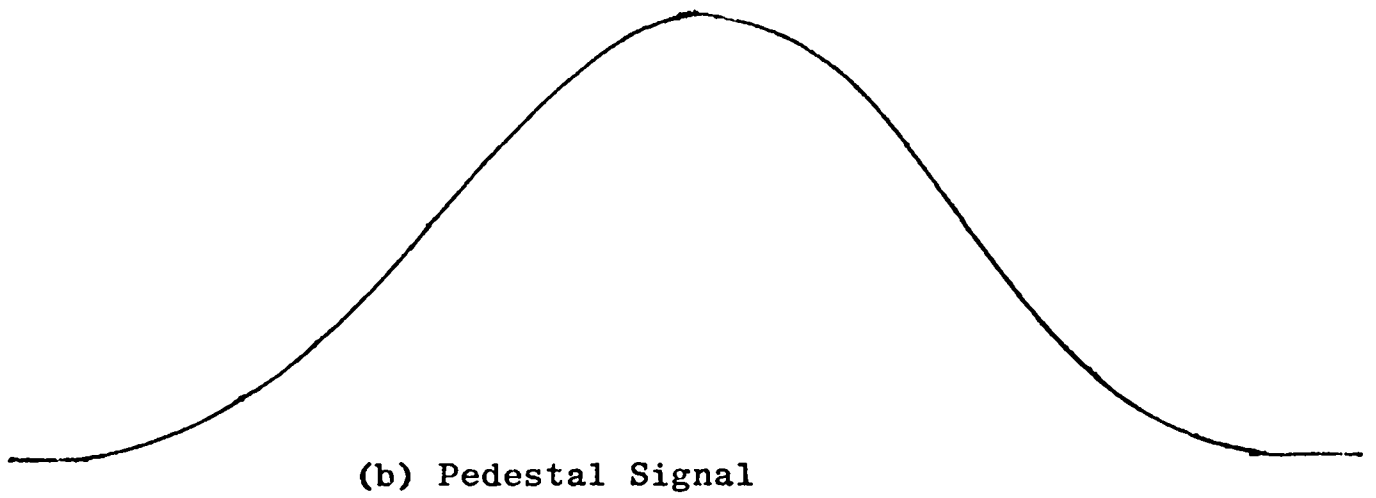

(b) Pedestal Signal

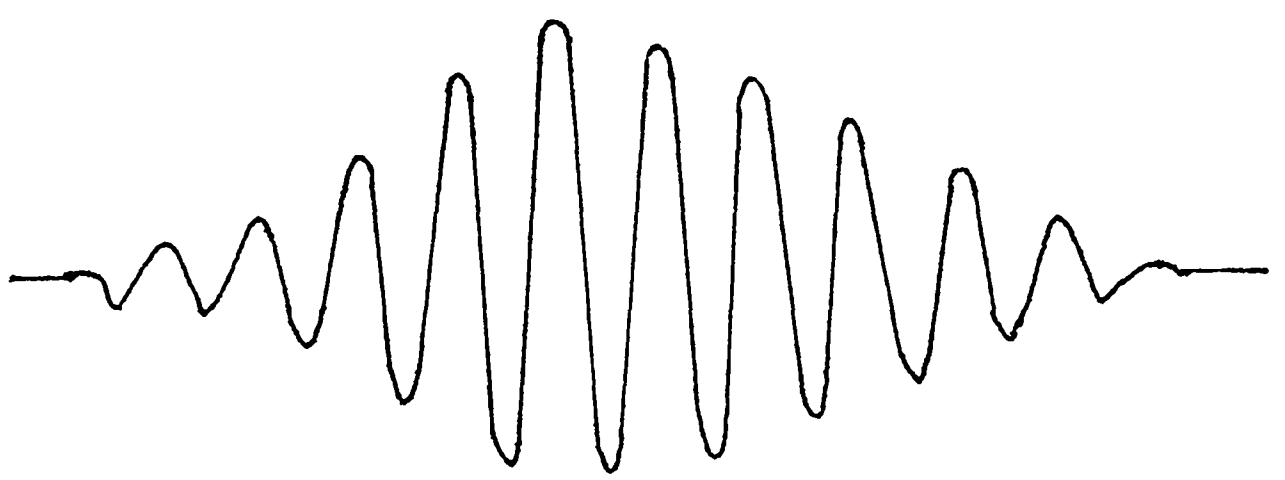

(c) Doppler Signal

TYPICAL LDV SIGNAL

Figure (6.1)

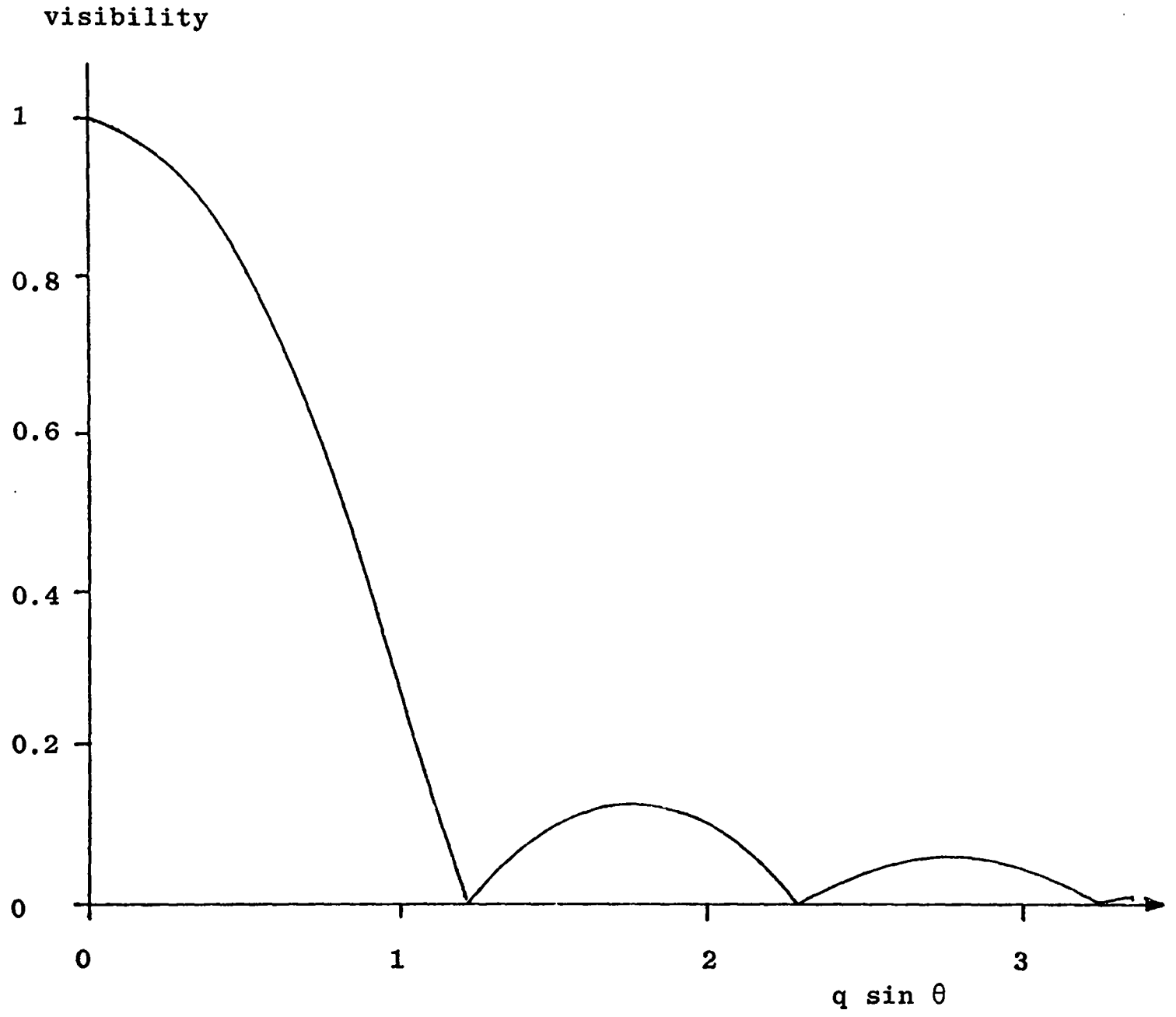

VARIATION OF VISIBILITY WITH PARTICLE SIZE USING FRINGE MODEL

Figure (6.2)

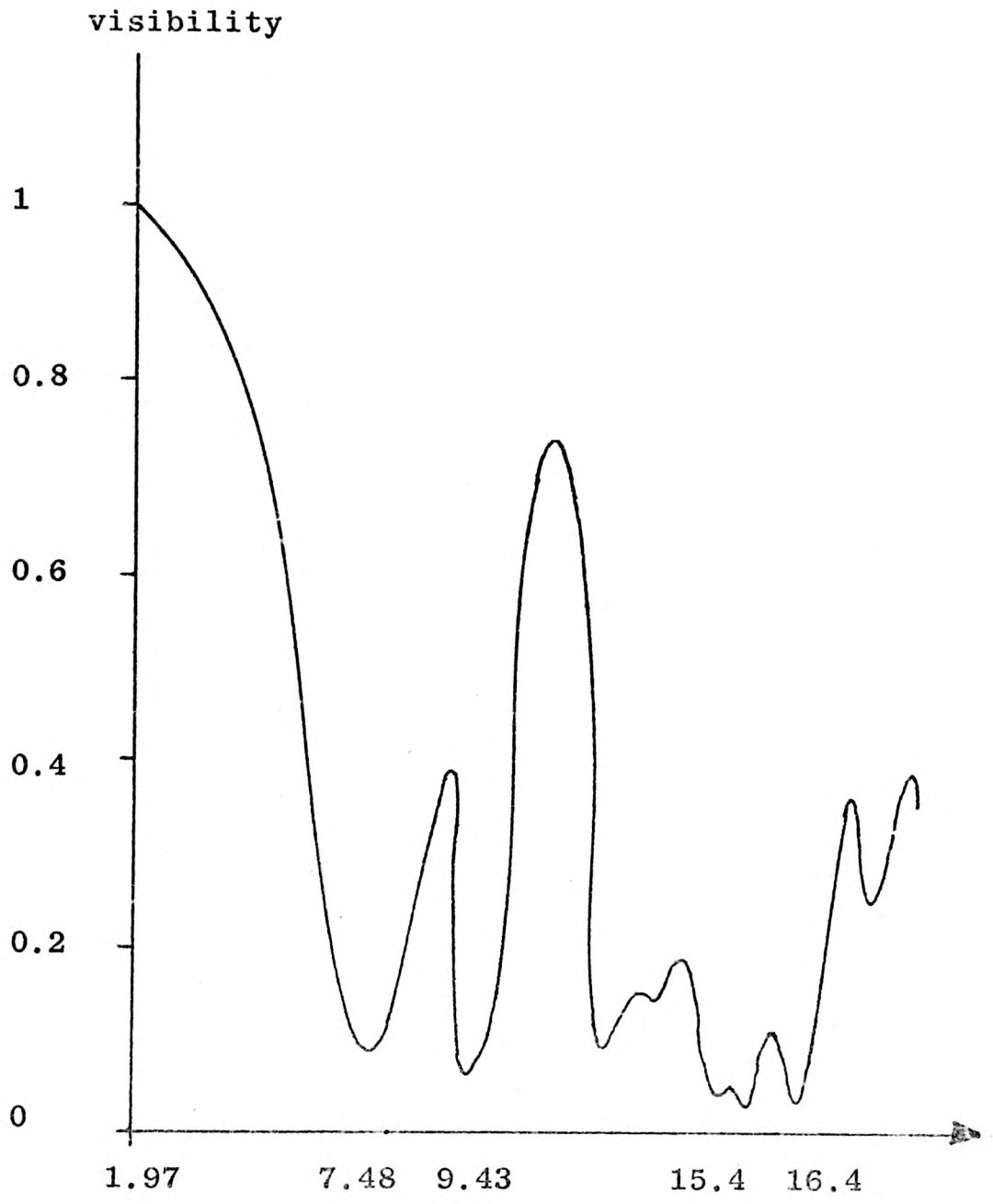

EFFECT OF PARTICLE SIZE ON VISIBILITY USING MIÉ THEORY

(Durst, Melling & Whitelaw (1976))

Figure (6.3)

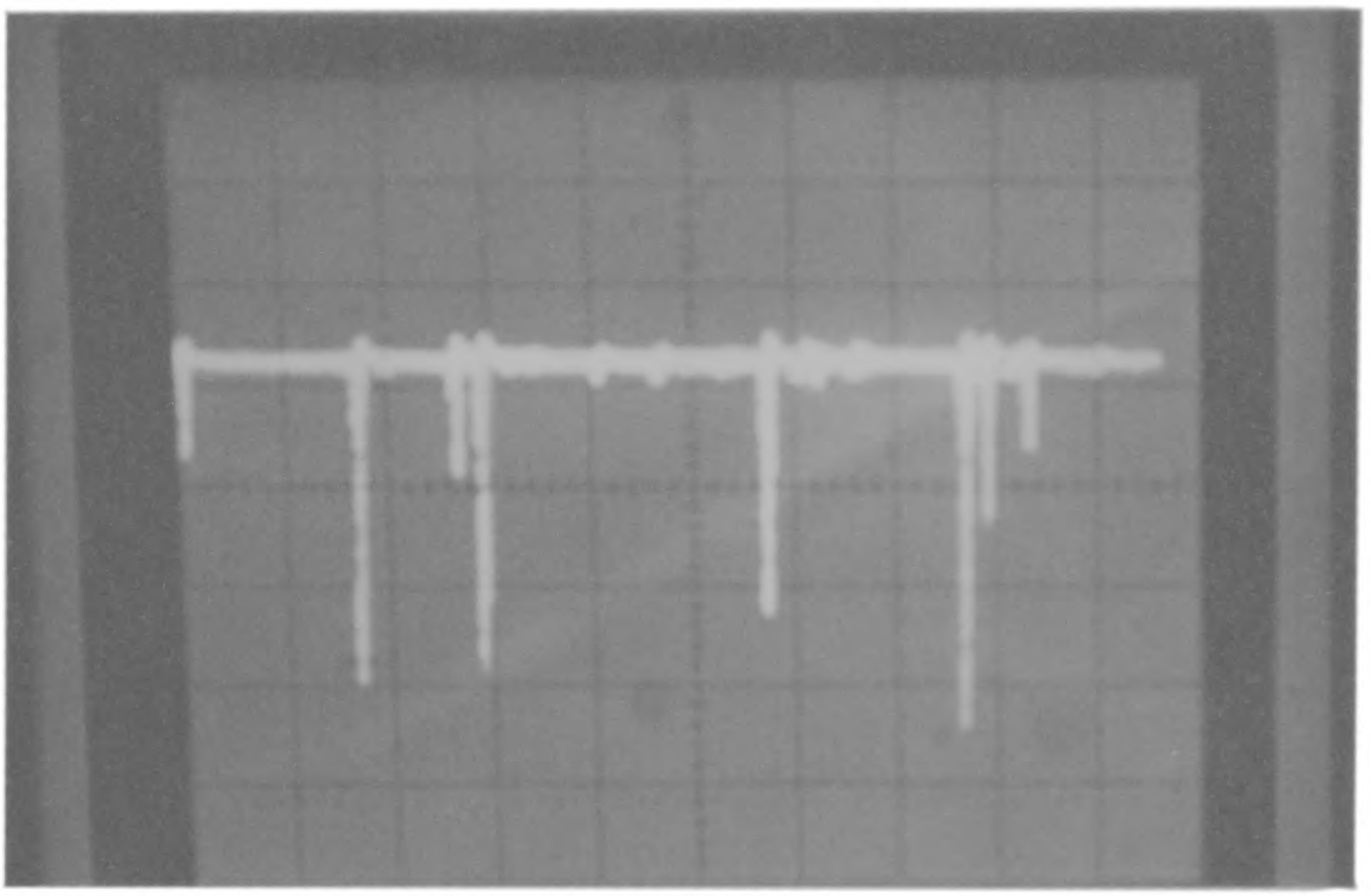

TYPICAL SIGNAL

Figure (6.4)

① Surface Mirror

② Biprism

③ Glass Wedges

④ Conveying Lens

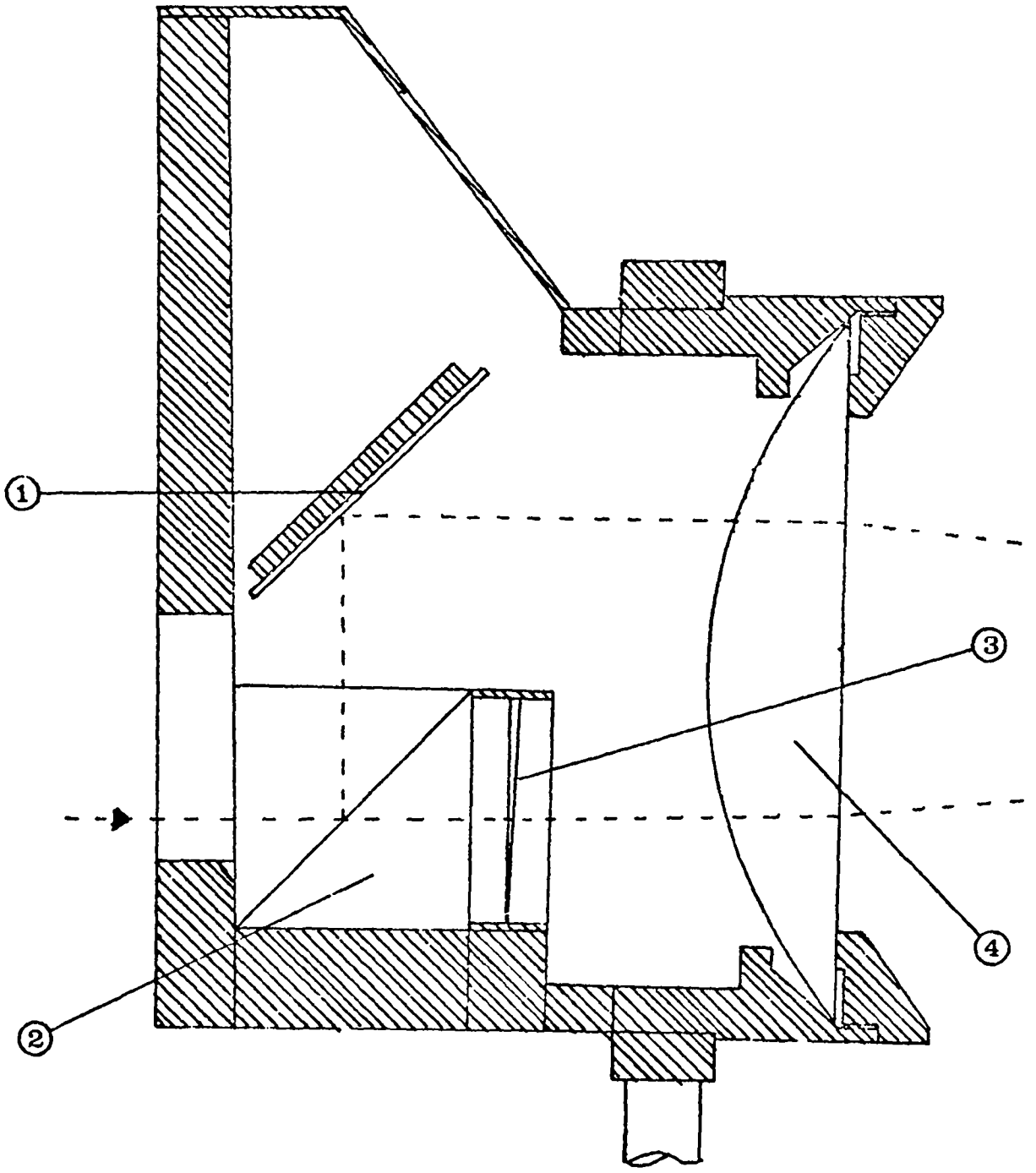

DISA 55L 100 TRANSMITTING OPTICS

Figure (6.5)

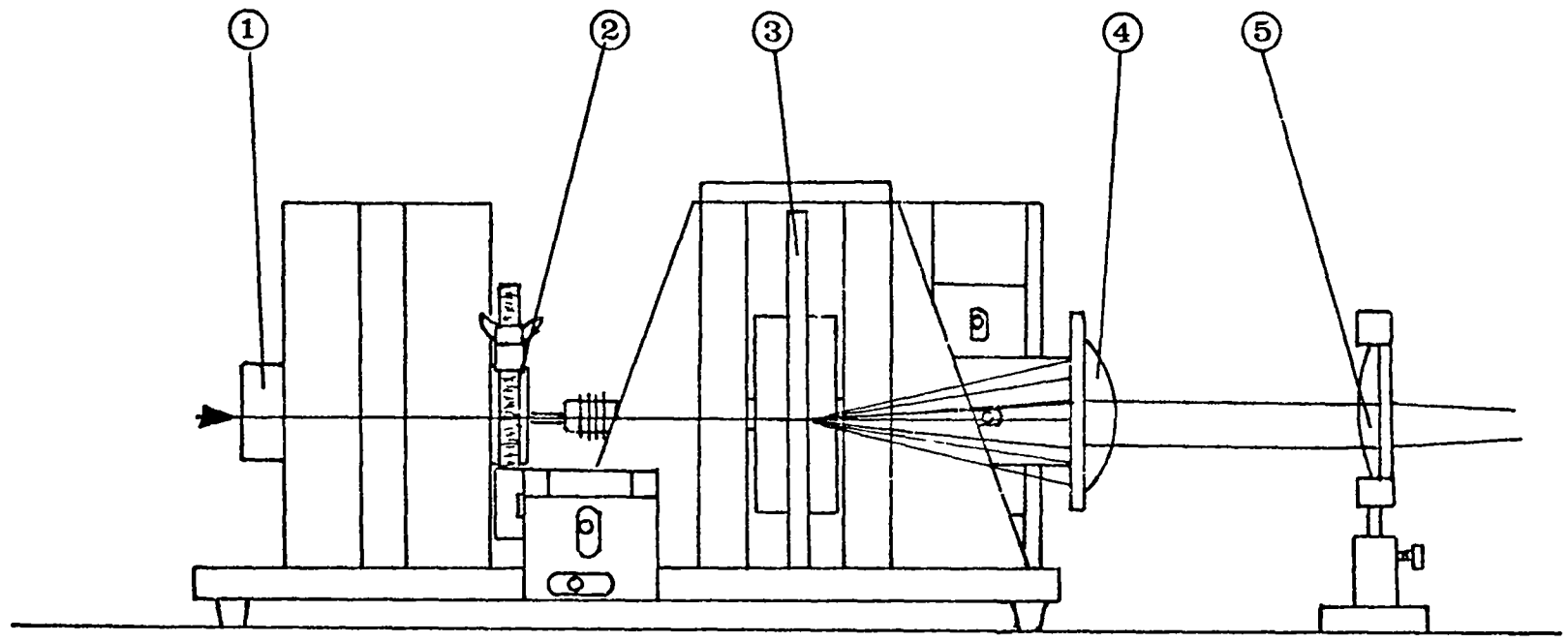

① Motor

② Lens, L_1

③ Radial Diffraction Grating

④ Lens, L_2 and Mask

⑤ Converging Lens, L_3

TRANSMITTING OPTICS WITH RADIAL DIFFRACTION GRATING

Figure (6.6)

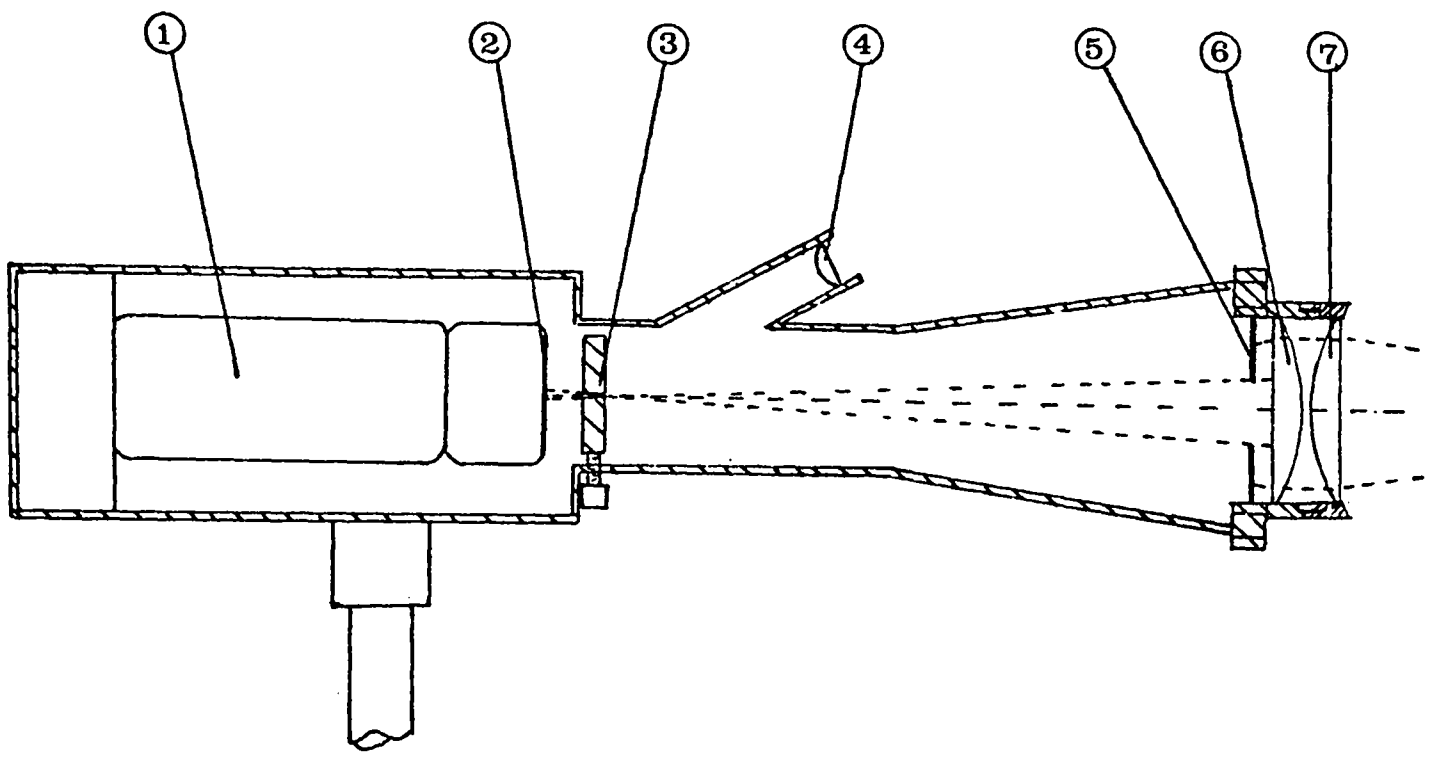

① Photomultiplier Tube

② Photosensitive Surface

③ Pinhole

④ View Finder

⑤ Iris Aperture

⑥ Lens, L_2

⑦ Collecting Lens, L_1

DISA 55L 10 RECEIVING OPTICS

Figure (6.7)

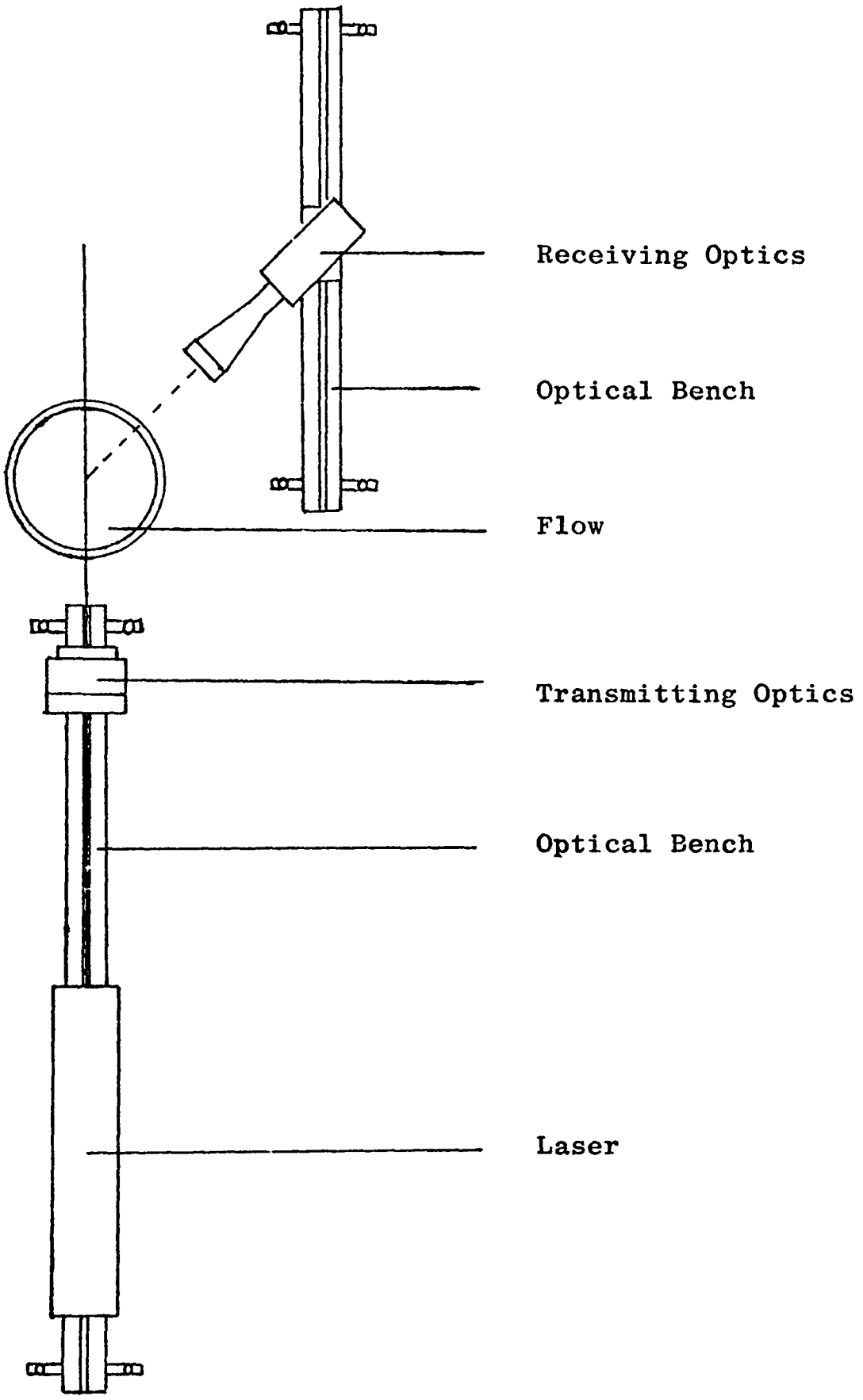

OPTICAL BENCH

Figure (6.8)

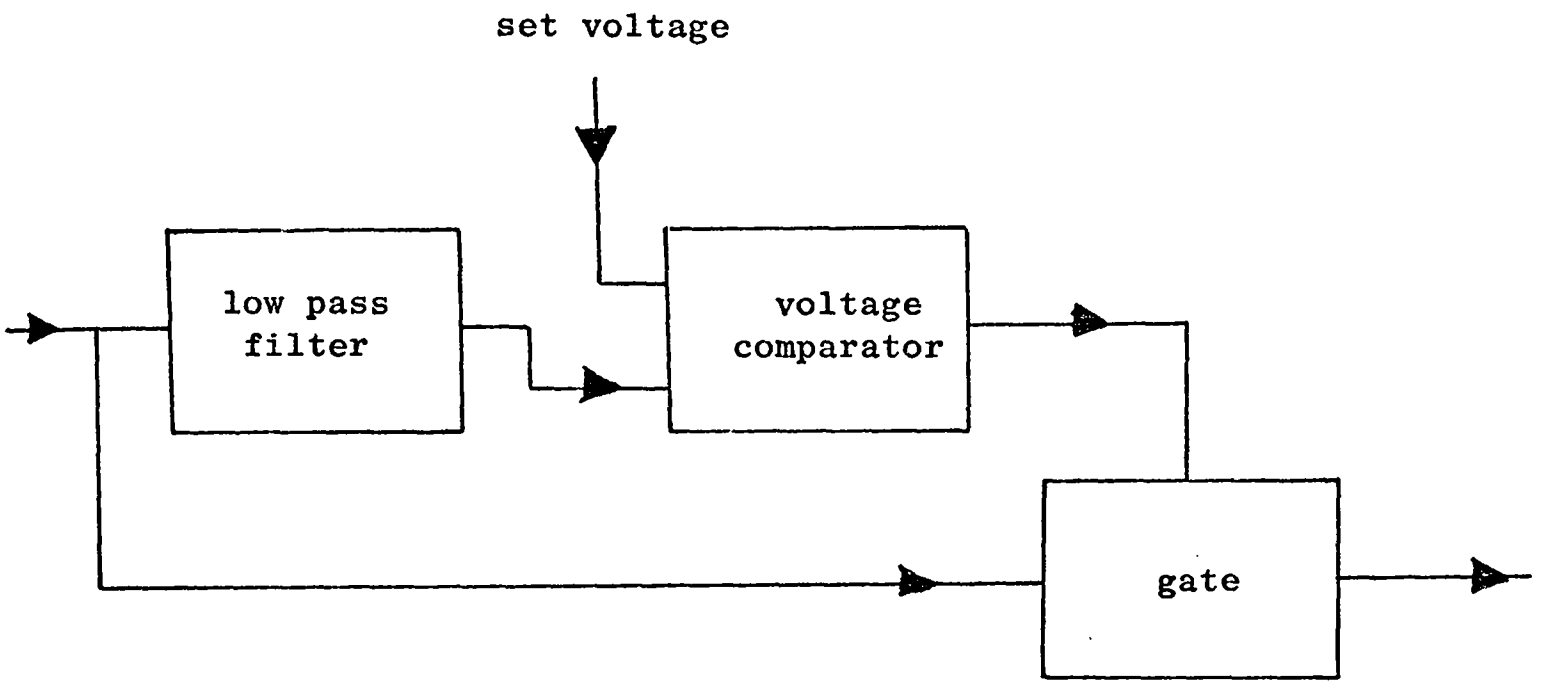

BLOCK DIAGRAM OF SIGNAL AMPLITUDE GATE

Figure (6.9)

CHAPTER 7

AIR VELOCITY MEASUREMENTS IN LARGE RIG

7.1 Introduction

The properties of the single-phase air flow were investigated in order that the effect of the solids on the flow could be found. The air-velocity profile was important because, when the solids velocities were measured (see Chapters 8 and 9), the velocity profiles of the air and the solids could be compared.

The air velocity profile was measured in the perspex tube above the glass test section using a Pitot-static tube. (This is described in section (4.2)). In this chapter air velocity measurements taken with the laser-Doppler velocimeter, LDV, are described. The air was seeded with submicron particles for light scattering, since the natural contaminants were too small and rare. The results from the LDV were compared both with the air velocity profile obtained previously and with the standard air velocity profile. Turbulence intensity measurements were also taken.

7.2 Seeding Arrangements

As described in section (6.1), LDV measurements in single-phase flows require trace particles in the fluid which are small enough to follow the turbulent flow with negligible slip, but large enough to scatter a significant intensity of light. Normal laboratory air does contain particles, but these are usually too small and diffuse for most LDV measurements. Photon correlation techniques [Pike (1974)] have been used in LDV measurements on non-artificially seeded air, but with other forms of signal analysis this is not possible.

In the work by Birchenough (1975), atomised paraffin oil was first used for seeding particles in the large rig, but it was found that the oil was deposited in a film on the glass pipe, which adversely affected the optics of the system and the LDV ceased to function. An alternative arrangement of injecting titanium oxide particles with submicron diameters into the flow, was used with more success. This system was used in the present project.

The apparatus is shown in figure (7.1). It is based on the design of Melling and Whitelaw (1973). Air is dried by passing it through a chamber containing silica gel, which can be dried by a heating element incorporated into this chamber. The air then enters the fluidising chamber. It is diffused through a foam filled cone and then passes through the titanium oxide powder, thereby fluidising it. Some of the particles become entrained in the air flow and pass out of the chamber with the air. The air-particle mixture then enters a venturi section in the large pneumatic conveying plant, in place of the horizontal section shown in figure (3.5). This reduced the pressure in the pipe in order that sufficient air flow through the fluidiser was achieved. The air supply to the fluidiser was normally taken from a tapping on the perspex pipe. This meant that no air was added to the flow after the air mass flow rate was recorded by the orifice plate meter. However, at low air mass flow rates the pressure drop across the fluidiser did not produce adequate particles in the flow and, to overcome this, a pressurised CO_2 bottle was used to supply the fluidising gas at these mass flow rates. The additional gas mass flow rate was measured by a rotameter included in the supply line.

7.3 Laser-Doppler Velocimeter Arrangement

The DISA transmitting and receiving optics were used in the forward-scatter, dual-Doppler mode, shown in figure (5.10a). This mode was chosen

since the majority of the light is scattered in the forward direction for submicron scattering particles. Light was collected at an angle of 30^{o} to the optical axis of the instrument in order to reduce the length of the measuring volume and hence the velocity gradient broadening of the signal [see section (5.7.2)], whilst still receiving sufficient light intensity. The frequency was measured using the DISA tracking unit.

The air velocity was calculated using equation (5.14) from the Doppler frequency. The broadening of the signal was found from the equation:-

$$\frac{\delta\nu}{\nu} = \frac{\xi_{rms}}{\bar{\xi}} \qquad (7.1)$$

where $\bar{\xi}$ is the mean output of the tracker and ξ_{rms} is the root-mean square, r.m.s., of that voltage. The r.m.s. voltage was measured with a DISA 55D35 RMS voltmeter. The turbulence intensity was found from the total broadening of the signal and by using equations (5.52), (5.53) and (5.54) to correct for the broadening effects of the velocity gradient and the finite transit time of a particle passing through the measuring volume.

7.4 Results and Discussion

7.4.1 Air-Velocity Profiles The standard air velocity profiles were calculated from the expression:

$$\frac{v_r}{v_c} = (1 - \frac{r}{a})^{1/m} \qquad (7.2)$$

where v_r is the velocity at radius r and v_c is the air velocity at the axis of the pipe. This equation is given in Ower and Pankhurst (1977). The value of m was calculated from the Reynolds number of the flow, Re, using the table given in the last reference. The measured and standard air velocity profiles were calculated from the results using the computer program given in appendix A.I.

Some of the measured air velocity profiles together with the standard profiles are given in figures (7.2) and (7.3). At low Reynolds numbers the fit between the measured and standard profiles is good, but the fit becomes worse as the Reynolds number is increased. This shows particularly in the standard deviation of the measured profile from the standard profile in table (7.1). The reason for the deterioration of the fit with increasing Reynolds number may be that the flow is still accelerating at the higher Reynolds numbers. However, the air velocity profiles measured with the Pitot-static traverses given in figure (4.2) show little deviation from the standard air velocity profiles. This indicates that the titanium oxide particles were not following the air velocity exactly. This was possibly due to the entraining of agglomerates of titanium oxide into the flow at the higher mass flow rates through the fluidiser. However, the deviations from the standard air velocity profiles were small and therefore the flow was assumed to be fully developed.

7.4.2 Air Mass Flow Rate The air mass flow rate was calculated from the air velocity profiles using equation (4.5). The results of the calculations are given in table (7.1) and compared with the total air mass flow rate through the pipe. This is measured using the orifice plate meter with B.S.1042, and also the additional gas entering the fluidising unit measured with a rotameter. Most of the results show quite good agreement but, in some cases, there was a significant difference between the mass flow rate given by the orifice plate meter and that calculated from the air velocity profile. This is especially true at low air mass flow rates, which may mean that the rotameter gave an inaccurate reading of the additional gas mass flow rate. However, since the profile was measured only across one diameter, and the Pitot-static traverses showed some asymmetry in the flow, then this is likely to be the dominant cause of any differences in the results.

7.4.3 Air Turbulence Intensity The axial turbulence intensity, $\delta v/v$, of the air in a circular pipe is given by Ower and Pankhurst (1977) calculated from the results of Laufer (1954). The Reynolds number in the case of Laufer's work was 50,000, which is at the lower end of the range measured here. Some of the results are shown in figures (7.4) and (7.5). Although there is some scatter in the results, they all follow the published axial air velocity profile quite well. There is no obvious trend in the turbulence profile with increasing Reynolds number.

Run No.	Reynolds No.	Deviation from Std. velocity ms^{-1}	Air Mass Flow Rate		
			Orifice Meter Kgs^{-1}	Profile Kgs^{-1}	Difference
1	30,167	0.82	$3.00x10^{-2}$	$2.84x10^{-2}$	5%
2	46,218	0.94	$4.65x10^{-2}$	$4.31x10^{-2}$	7%
3	40,791	0.82	$3.44x10^{-2}$	$3.57x10^{-2}$	3%
4	51,520	1.41	$4.46x10^{-2}$	$4.71x10^{-2}$	5%
5	60,933	0.87	$5.49x10^{-2}$	$5.52x10^{-2}$	1%
6	72,710	1.21	$6.91x10^{-2}$	$7.07x10^{-2}$	1%
8	84,448	1.56	$7.93x10^{-2}$	$8.03x10^{-2}$	1%
10	90,184	2.04	$8.27x10^{-2}$	$8.12x10^{-2}$	2%
13	89,708	2.89	$8.64x10^{-2}$	$8.21x10^{-2}$	5%
14	74,948	3.41	$8.73x10^{-2}$	$8.90x10^{-2}$	2%
15	108,644	2.29	$9.65x10^{-2}$	$9.91x10^{-2}$	3%
16	105,922	2.89	$10.29x10^{-2}$	$10.03x10^{-2}$	3%
17	115,454	4.21	$10.71x10^{-2}$	$10.77x10^{-2}$	1%

TABLE 7.1

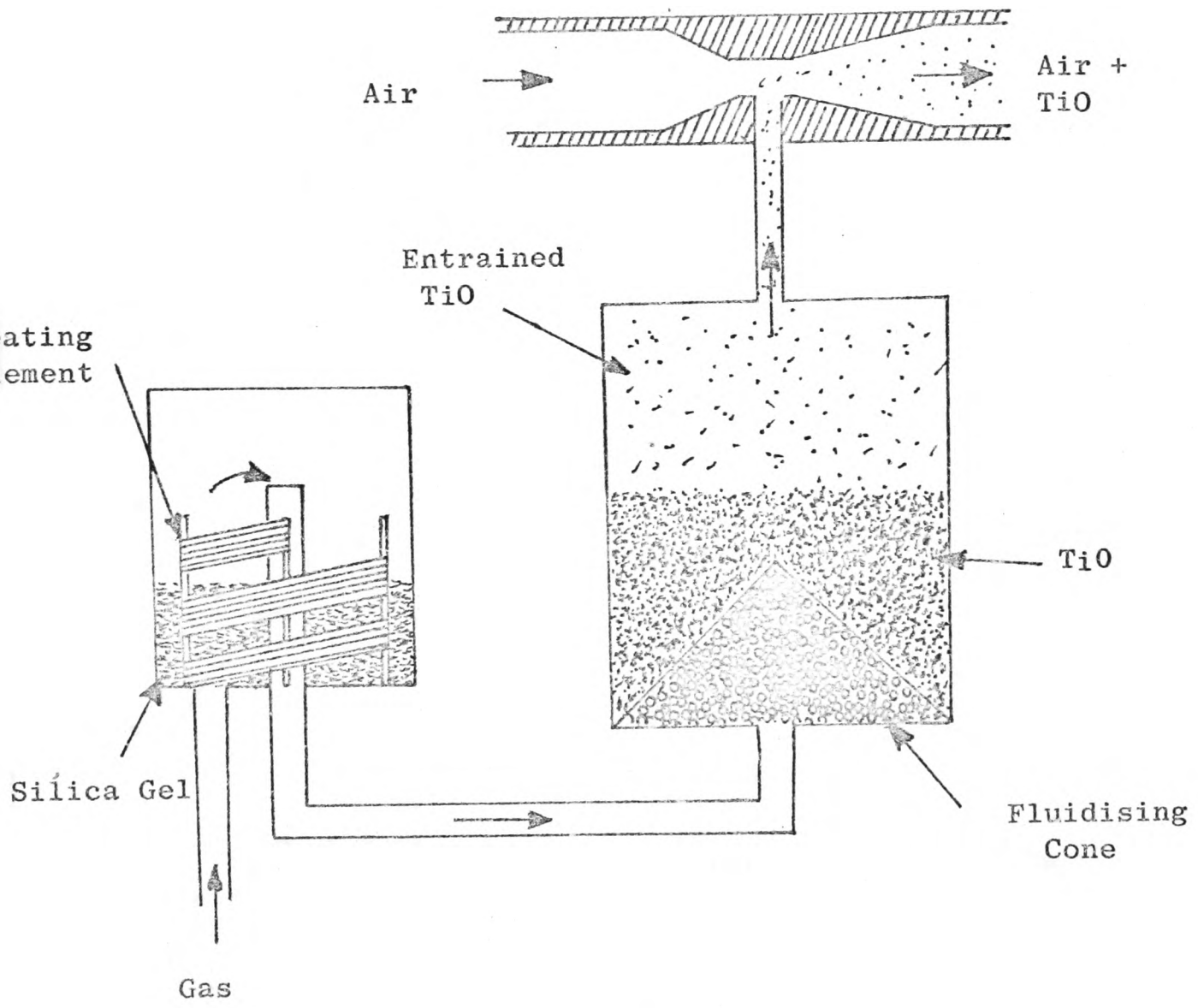

TITANIUM OXIDE SEEDING UNIT

Figure (7.1)

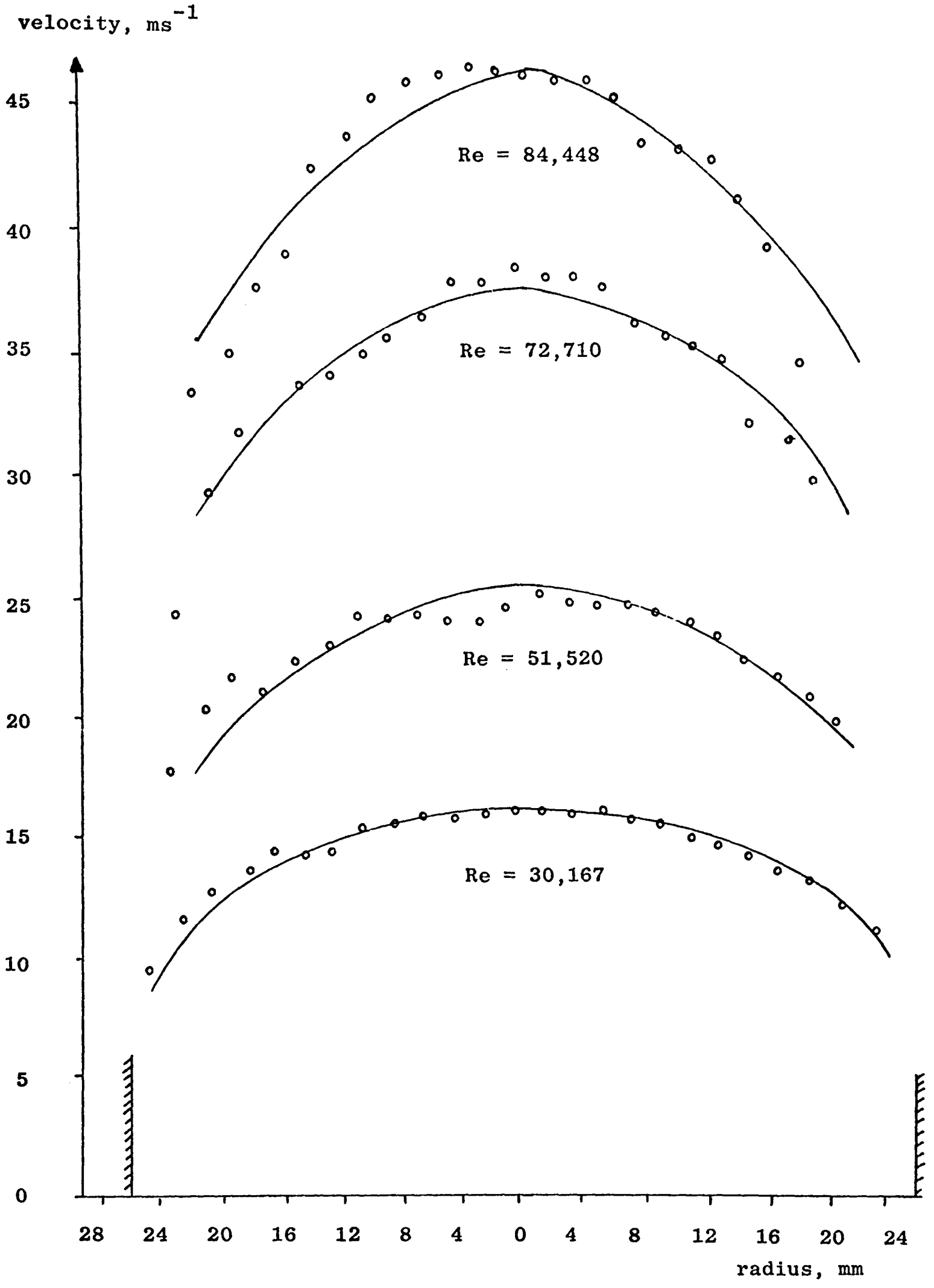

CLEAN AIR VELOCITY PROFILES (from LDV)

Figure (7.2)

CLEAN AIR VELOCITY PROFILES (from LDV)

Figure (7.3)

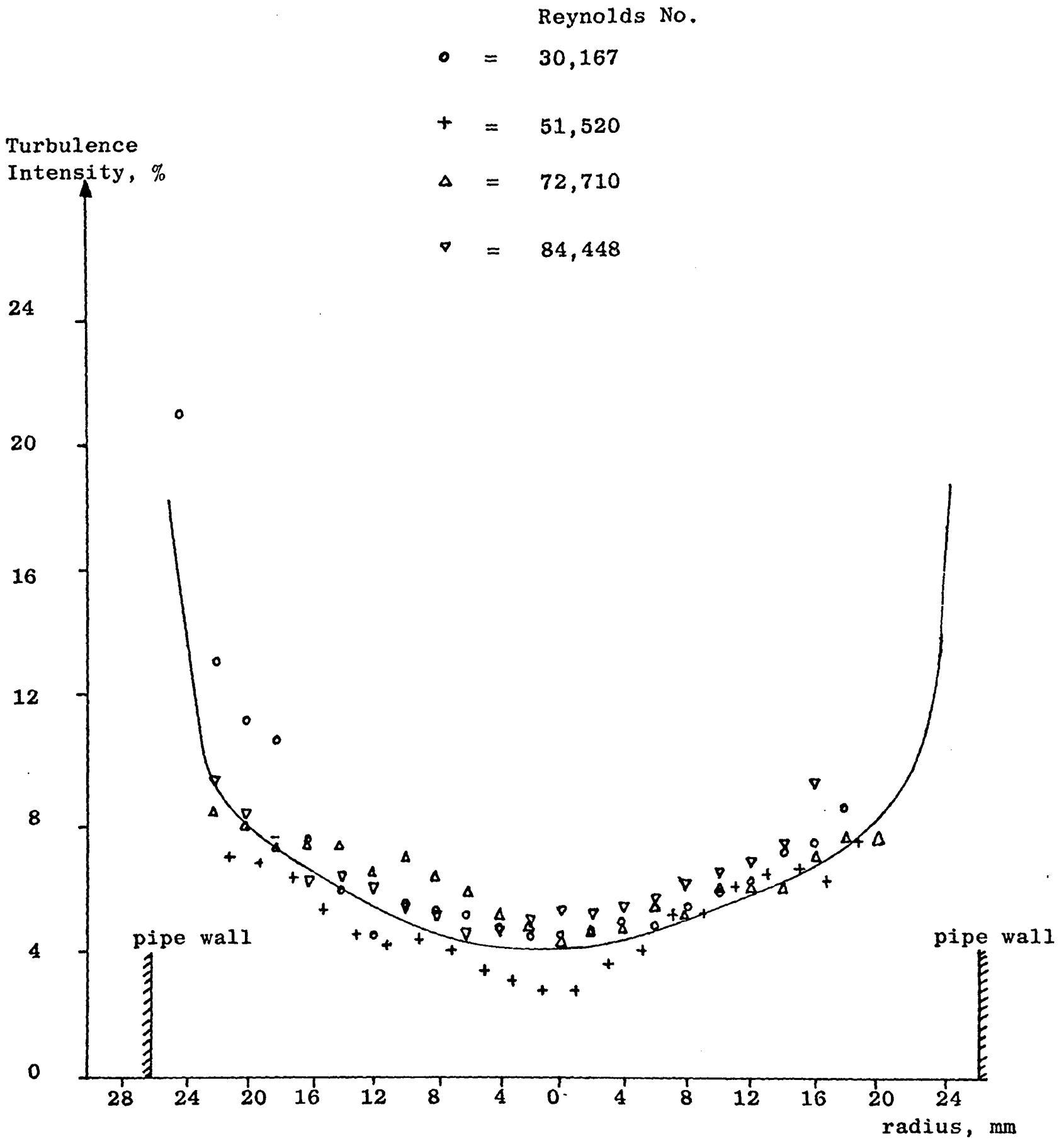

TURBULENCE INTENSITY OF CLEAN AIR

Figure (7.4)

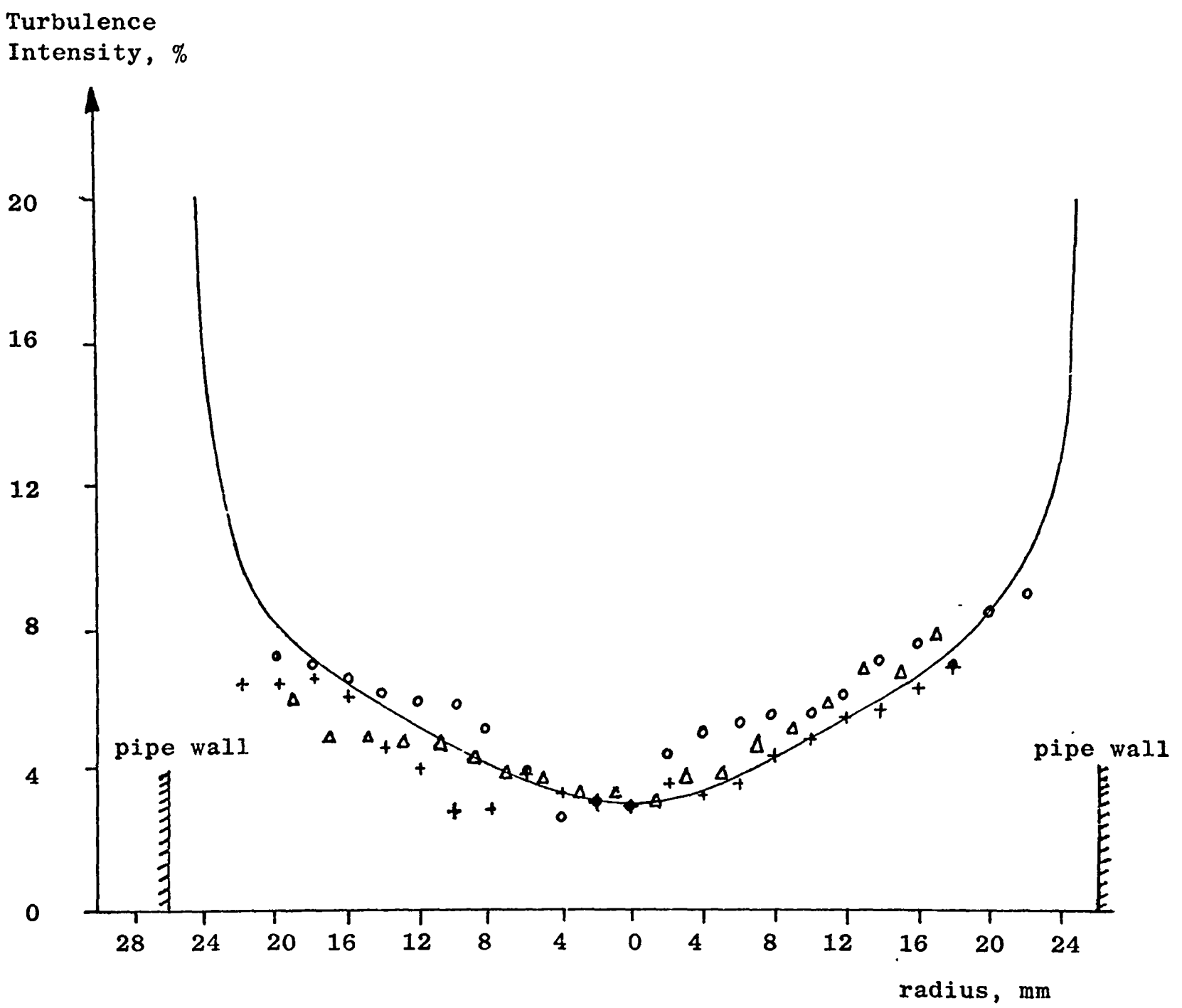

TURBULENCE INTENSITY OF CLEAN AIR

Figure (7.5)

CHAPTER 8

MEASUREMENTS ON AN AIR-BALLOTINI FLOW

8.1 Introduction

This chapter describes the experimental investigation of a flowing suspension of ballotini particles, mean diameter 455 μm, in air in the vertical test pipe of the main conveying plant. The measurements were taken in flows with solids to air mass flow rate ratios, or solids loading ratios, of up to 2.3 and with average air velocities at the measuring point in the range 10 ms^{-1} to 50 ms^{-1}. The average air velocity was calculated from the air mass flow rate measured with the orifice plate meter and the static pressure in the pipe at the measuring point.

The following properties of the flow were measured:

Particle velocity profiles
Particle turbulence intensity profiles
Air velocity profiles
Particle number density profiles
Pressure drop in pipe.

The results obtained from the air-ballotini flow are compared with those taken in the air-sand flow in chapter 10. The physical properties of the glass ballotini are given in chapter 4, which also describes the calibration of the orifice plate meter and the screw feeder for the mass flow rate of the ballotini.

8.2 Particle Velocity Measurements

8.2.1. Instrumentation The DISA optics were used in the laser-Doppler velocity meter system employed for the particle velocity measurements. The instrument was arranged in the dual-Doppler mode, using forward scatter. Reference beam mode was tested, but the signal produced was inferior to that from the dual-Doppler mode, and it was more difficult to set up. The receiving optics were set at 30^{o} to the optical axis of the instrument. This angle was chosen because the spatial resolution improves and velocity gradient broadening decreases with increasing angle, but above 30^{o} insufficient light was received

for signal analysis. Backscatter mode was also tried, i.e. with a collection angle of 180^{o} to the optical axis, but no useful signals were received with this arrangement. The angle of the crossover of the beams was 2^{o}.

Great difficulty was encountered in analysing the signal. At low air velocities, below about 20 ms^{-1}, the signal was found to be sufficiently good for the Cambridge Consultants tracking filter to follow the signal. However, for higher air velocities at the test section, neither the DISA nor the Cambridge Consultants tracker was capable of tracking the signal. For this reason, at the higher mean air velocities the signals were displayed on the screen of a storage oscilloscope and the frequency was measured directly from the trace. This method is described in more detail in Chapter 6. In an attempt to ensure that the conditions of the flow remained constant during the measurements, the frequency at each point was averaged from only five particles at each measuring point. This meant that the accuracy of these measurements was less than those made using the tracking filter.

8.2.2 Results and Discussion Some of the particle velocity profiles are shown in figures (8.1) to (8.4). These show the mean axial velocity, v_{pr}, at each point calculated from the Doppler frequency, ν_D, using equation (5.14). The results from each half of the traverse were averaged in order to decrease the scatter. Since the air velocity profile was found to be nearly symmetrical, it was felt that this averaging was justified. The velocity profiles in figure (8.1) were obtained using the Cambridge Consultants tracker, whilst those in figures (8.2), (8.3), and (8.4) were obtained from the average period of the Doppler signal measured from the oscilloscope trace.

It was difficult to keep the average air velocity constant for a series of particle velocity profiles, since the pressure drop in the pipe was increased by adding particles, which reduced the volumetric flow rate at the measuring point for the same air mass flow rate. The variation in the average air velocity increased the spread in the results. However, a large number of particle velocity profiles were measured, and there are enough with sufficiently similar average air velocities for the effect of the solids loading ratio on the flow to be found. Figure (8.5) shows particle velocity profiles at the same solids loading ratio but different velocities.

The velocity close to the pipe wall could not be measured, since inconsistent readings were obtained in this region. This was partly due to the high turbulence intensity found near the wall, especially at high velocities when in most cases no clear signal could be received from closer than 10 mm from the wall. Also, near the wall part of the measuring volume is in the wall, which, as well as reducing the number of particles producing signals, also gives spurious signals from wall vibrations.

Figure (8.1) shows a large degree of scatter in the points, with no smooth variation of the velocity with radius. The degree of scatter is greater in figures (8.2) and (8.5) because each mean local particle velocity was measured from only five particles. In both cases the scatter could be reduced by taking the measurements over a longer period and thus averaging over a larger number of particles. However, this would have increased the length of time needed to measure the profile, and the duration of each run was limited by the quantity of solids in the hopper.

The particle velocity profiles were all fairly flat with little variation either with the mean air velocity or with the solids loading ratio. This can be seen more clearly in figures (8.6) to (8.11), which are smoothed plots of the ratio of the local particle velocity, v_{pr}, to the centre particle velocity, v_{pc}, against the ratio of the radial position, r, to the total radius of the pipe, a. In nearly all cases the profile becomes more flat with increasing solids to air mass flow rate ratios, which was expected since there is greater interparticulate interaction at the higher solids loading ratios. At a solids to air mass loading ratio of 0.5, the particle velocity profile was found to become flatter with decreasing average air velocities, but at a solids loading ratio of 1.2, the trend was found to be in the opposite direction. These particle velocity profiles will be analysed in greater detail and compared with those measured in the air-sand flow and with the results of other authors in Chapter 10.

8.3 Turbulence Intensity Measurements

8.3.1 Introduction The axial particle turbulence intensity is defined as the ratio of the root-mean-square value of the axial particle velocity variation to the mean axial particle velocity. It is necessary to measure the velocity of a large number of particles in order to obtain

reasonable accuracy in the turbulence intensity [Yanta and Smith (1973) (see chapter 5)]. For this reason, since the velocity of only five particles was measured for the higher velocity flows, the turbulence intensity of the particles was not found in these cases. For velocities measured with the tracking filter the r.m.s. variation of the output voltage about the mean was measured using a DISA 55D35 RMS Voltmeter, and the mean output voltage was measured using a DISA 55D31 Digital Voltmeter. Since there were particles in the probe volume for only a small proportion of the time (~2%), the output voltage was at a constant level for most of the time. This meant that the root-mean-square of the output voltage as recorded by the r.m.s. meter was likely to be biased and the recorded value of the turbulence intensity was probably less than the actual value of the particle turbulence intensity, even when the signal was integrated over a long period. The error produced in the turbulence intensity from this effect was dependent on the properties of the meter and was probably small compared to the scatter in the results. The spread in particle sizes, especially due to the fines in the flow after repreated runs, might have increased the measured particle turbulence intensity, since the slip velocity of the particles is a function of the particle diameter. However, although the number of small particles in the flow increased dramatically with use, as shown in chapter 4, the small particles gave signals which were small compared to those from the unbroken ballotini and were unlikely to have contributed to the output voltage of the tracker. The weight distribution of the particle diameter, given in table (4.3), is probably more significant than the numerical distribution for the output of the tracking filter, and this showed only a small variation after use.

8.3.2 Results and Discussions Some of the measured particle turbulence intensity profiles are shown in figure (8.12) and compared with the measured turbulence intensity profiles of the free air. The velocity gradient broadening calculated using equation (5.52) was very small and the finite transit time broadening given by equation (5.53) was negligible, whilst the degree of scatter in the results was large. For this reason no correction for broadening was applied to the measurements of turbulence intensity.

The turbulence profiles shown in figure (8.12) indicate that the particle turbulence has less variation across the pipe than the free air. The central turbulence intensity increased with the solids loading ratio, and at solids loading ratios above about 1, the central turbulence intensity was greater than the measured central turbulence intensity of the free air. The flatter turbulence profiles were expected since the particles had greater momentum than the conveying air and were larger that the eddies in the air, and local air turbulence would have only a small effect on particles passing through it. The increase in the turbulence intensity and in the variation in the turbulence across the pipe with increasing solids loading ratio is probably due to the increase in particle-particle and particle-wall collisions, thus increasing the variation in particle velocities, especially near the pipe wall. The turbulence intensity profile is further analysed in chapter 10.

8.4 Air Velocity Measurements

8.4.1 Introduction Local air velocity measurements in an air-solid flow present many difficulties due to the abrasive nature of the flow. Kolanski et al (1976) used a hot film anemometer to measure the air velocity in the presence of solids, with solids loading ratios up to 1.9 and air velocities up to about 15 ms^{-1}. However, they do not mention any problems encountered due to the abrasion of the particles, nor how they

overcame them. Kramer and Depew (1972) used a Pitot tube for local air velocity measurements and employed a wall tapping for the static pressure. Specially made steel Pitot tubes were used at low air velocities and glass covered Pitot tubes at higher velocities in order to withstand the abrasion. Flows with mean air velocities from 3 to 60 ms^{-1} and with solids loading ratios from 0 to 5 were measured. Durst (1978) used an LDV to measure the local velocities of both phases simultaneously in an air solid flow. He used very sophisticated electronics to separate the signal of the large conveyed particles and the submicron seeding particles, making use of the difference in amplitude and frequency of the signal from each. A computer was used to analyse the frequency and the variation in frequency of the two signals. However, no mention is made of the range of velocities or solids loading ratios in the flow being tested.

It was hoped to use a technique similar to that of Durst in the present investigation. Unfortunately, the optics and electronics available were inadequate for this method and the attempt was abandoned. Instead, the air velocity in the presence of particles was measured by a Pitot-static tube. The measurements were taken in the perspex tube just above the test section, using a commercially manufactured steel Pitot-static tube. The Pitot pressure was taken from the Pitot-static tube and the static pressure was taken from an adjacent wall tapping. Kramer and Depew (1972) reported a 3% error incurred from the use of a wall static tapping due to the radial variation of the static pressure. In the experiments described here, no measurable difference was found between the static pressure at the wall and that recorded by the steel tappings on the Pitot-static tube, but as the small holes for the static pressure on the Pitot-static tube tended to become blocked easily, the wall tapping was used for the measurements. The difference between the Pitot and static pressures was found using an inclined paraffin filled

manometer and the air velocity was calculated using equation (4.3). At velocities below about 30 ms^{-1} and solids loading ratios below about 1.7 it was found that the Pitot tube remained unblocked long enough for a complete velocity profile to be measured, but above these values the Pitot tube became blocked too quickly for measurements to be practical. The air velocity was measured across the same diameter as the solids velocity.

8.4.2 Results and Discussion Figures (8.13) to (8.16) show some of the air velocity profiles measured, together with the solids velocity profile measured in the glass test section during the same run and the free air velocity profile for the same air volumetric flow rate measured by Pitot-static tube as described in chapter 4. It can be seen that the solids have little effect on the air velocity profiles, except for a slight flattening near the pipe wall. These results are in good agreement with those given by Kolansky et al (1976) and Durst (1978), who also found a slight flattening of the air phase velocity profile. Doig and Roper (1967) found significant flattening of the air profile at solids loading ratios above about 3.

The air phase velocity profile showed no significant change with increasing solids loading ratio in the range of values tested and the deviation from the free air velocity profile is small. This is shown in figure (8.17), which is a plot of the logarithm of the velocity against the logarithm of the radius. The results measured are compared with the standard velocity profile given in the equation:

$$\frac{v_r}{v_c} = (1 - \frac{r}{a})^{1/m} \qquad (8.1)$$

with the value of the constant, m, taken from Ower and Pankhurst (1977) for the measured value of Reynolds number. Since there is such a small deviation from the free air velocity profile, assumptions that the air flow is unaffected by the presence of particles by authors such as

Chan (1976) are reasonable at low solids to air mass flow rate ratios, provided that any deviations from the free air velocity profile in the region near the pipe wall which was not investigated are too small to affect the flow greatly.

8.5 Solids Number Density

8.5.1 Measurement Technique A possible means of measuring the distribution of the particle number density in the pipe was provided by counting the number of light pulses received by the photomultiplier in a set time, provided the particles have a low enough number density for the possibility of the particles passing through the measuring volume simultaneously to be negligibly small. Since each light pulse is produced by a particle in the measuring volume, the number of pulses per second gives a measure of the number of particles crossing the area of the measuring volume per second. This technique has been utilised by several authors [Farmer (1978), Reithmuller and Ginoux (1975)], and in the present project such a method was investigated.

The number of pulses received by the photomultiplier was recorded on a counter/timer, Advance Instruments TC13. The minimum amplitude of the pulses which were counted was set by the threshold level of the counter. This meant that only particles scattering sufficient light would be counted. These particles had to be above a minimum size and pass through light beams with sufficiently high intensity. Thus, by choosing an appropriate threshold level, the fines in the flow could be excluded from the count, together with particles not passing through the central region of the measuring volume. Because the area of the region of the measuring volume defined in this way is not known, the exact number density cannot be measured, but by measuring the number of pulses across the pipe, the relative distribution of the particle number density can be found. The total number of particles in the flow can be

calculated from the mass flow rate of the solid and the average particle size, and from this the actual particle number density profile can be found.

Unfortunately, there is a complication involved with this method caused by the variation in the light intensity in the measuring volume as it is traversed across the pipe. The particles scatter light in the two beams, and the intensity of the beams decreases as it crosses the flow. If the threshold was kept at a constant level the volume in the flow from which signals from particles are counted would effectively decrease as the pipe traversed, assuming that secondary scattering of the light pulses is rate. The decrease in light intensity is exponential in form, (Beers Law), provided that the particles are evenly distributed [Mettler and Stevenson (1976)], and the exponential variation in the number of pulses counted had to be removed for the calculation of the particle number distribution.

8.5.2 Results and Discussion Some of the uncorrected results of the number of pulses counted across the pipe are given in figure (8.18), which shows evidence of the exponential variation across the pipe. The results were corrected by multiplying by the factor e^{fx}, where f is a constant and x is the distance from the pipe wall nearest the laser. The value of f was found by trial and error, the correct value producing a reasonably symmetrical distribution, which was expected. The resulting profiles are shown in figure (8.19). These show that at low solids loading ratios the particle number density is fairly constant across the pipe, but at higher solids loading ratios a peak in the particle number density develops at the centre of the pipe. Soo et al (1964) also found that the particle number density profile became less flat with increasing solids loading ratio in a suspension of 50 μm diameter glass particles in air in a 5 inch diameter vertical pipe. However, Kramer and Depew (1972) found that the number density profiles became flatter with

increasing solids loading ratio. They used 62 μm diameter glass particles in a 1 inch diameter pipe. This disagreement in the results is probably due to the great sensitivity of the particle distribution on the conditions in the flow, especially the electrostatic charge on the particles, which can vary greatly with the conveyed materials, with the material from which the conveying plant is made, and also with the air humidity. For this reason a large variation in the results of different researchers is likely.

The very large degree of scatter in the results was principally caused by the changing of the alignment of the optics during a traverse. Since the forward scatter mode of the LDV was employed, the receiving optics had to be aligned on the probe volume by 'eye' for each measuring point. Variation in the alignment changes the part of the probe volume from which signals are received. With the apparatus available exact repeatability of the alignment could not be achieved, so that the accuracy of the measured number density profile was poor. Therefore, the particle number density profile was not measured in the subsequent parts of this investigation.

8.6 Pressure Drop Measurements

8.6.1 Introduction The importance of the pressure drop in a pneumatic conveying plant was described in chapter 2. It was hoped to correlate the results of all the measurements on the two-phase flow and find the dependence of all the properties of the flow, particularly the pressure drop, on each other.

The pressure drop in an air-solid flow has been measured by many authors with a great variety of results, even for similar flows. Accurate measurement of pressure drop is very difficult since the pressure does not remain steady at each point. Since the pressure drop tends to vary

rapidly and erratically, care has to be taken that any damping of the fluctuations does not bias the mean pressure. For this reason the pressure line connecting the pressure tapping to the transducer should be kept as short as possible, and the resonance peaks of the transducer should be outside the frequency range of the fluctuations. Another problem encountered in such readings is blockage of the pressure tappings by the solid particles and the tappings have to be kept clear during the pressure measurements. As with all static pressure measurements, the edges of the tappings must be smooth and unchipped or the accuracy of the readings is greatly reduced.

Difficulties are encountered when measuring the pressure from several tappings since all the pressures vary independently. Mason and Smith (1973) photographed a bank of manometers which were registering the pressure at a series of tappings. This method produced a record of all the pressures simultaneously, but the mean pressure at each tapping was not found. Duckworth and Chan (1972) describe a pressure transducer which they used for pressure measurements in air-solid flows. The transducer could be placed near the tapping and they produced an electrical signal which could be averaged electronically.

In this investigation the pressure was measured using a manometer bank. The height of the water in each tube was found electrically by measuring the capacitance between two wires in the tube. The height was shown on a digital display. The instrument gave the instantaneous pressure at each tapping and, by recording a number of readings, the mean pressure could be calculated. There were twelve tappings in the test pipe.

8.6.2 Results and Discussion During each experimental run the change in pressure up the pipe was measured. Some of the results are

shown in figure (8.20), in which the pressure drop in the pipe above the first tapping, which was about 1 m from the start of the vertical pipe, are plotted against the height above that tapping. The first non-linear part of the graph is due to the acceleration of the particles and the air. The pressure drop due to the acceleration of the particles was derived theoretically by Hariu and Molstad (1949) and is given in equation (2.5), which is non-linear. The pressure drop becomes quite linear at about one metre above the first tapping. This indicates that at the measuring point, about 2.5 metres above the first tapping, the flow was probably fully developed. At high solids loading ratios and high velocities the pressure fluctuated violently and it was difficult to obtain a straight line.

Figure (8.21) is a graph of the pressure gradient in the linear region against the solids loading ratio. The pressure gradient increases with the solids loading ratio and, at higher velocities, the pressure gradient decreases much more rapidly. This indicates that the solids can be conveyed more economically at lower air velocities since the pressure drop is very much less. These results will be compared with those obtained for sand (see chapter 9) and with the published results of other authors in chapter 10.

8.7 Conclusions

In this chapter the measurement of a variety of properties of an air flow conveying glass ballotini in suspension has been described. Difficulties encountered in the measurements meant that the experiments tended to be rather time consuming and the accuracy of the results was limited. However, useful results were obtained and, in chapter 10, these will be compared with the results for the air-sand flow in the next chapter.

The laser-Doppler velocity meter was shown to be a useful instrument for measuring both the particle velocity and particle turbulence in the air-ballotini flow, but greater speed and accuracy in the measurements could have been achieved with more appropriate electronic processing.

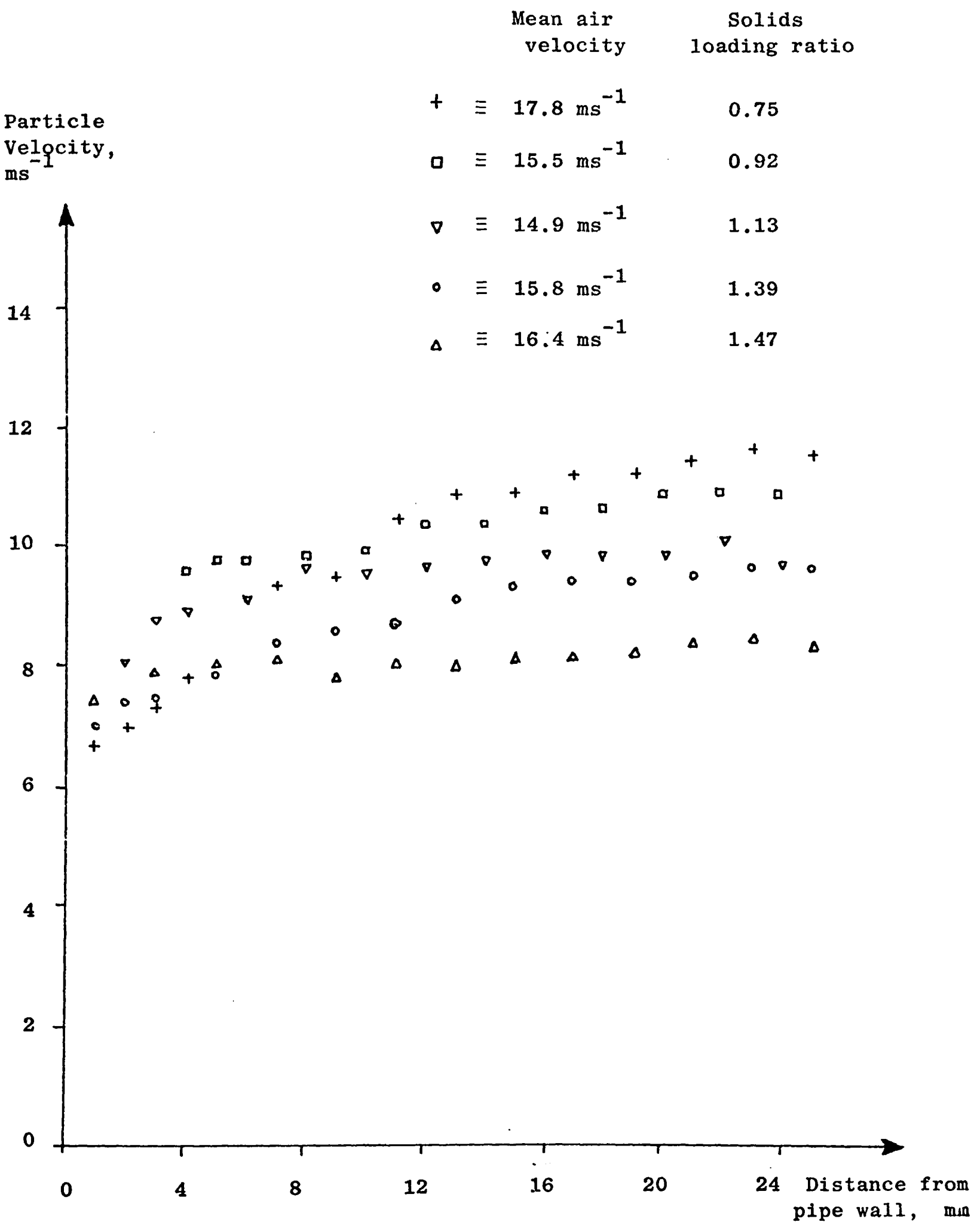

PARTICEL VELOCITY PROFILES
Runs 1

Figure (8.1)

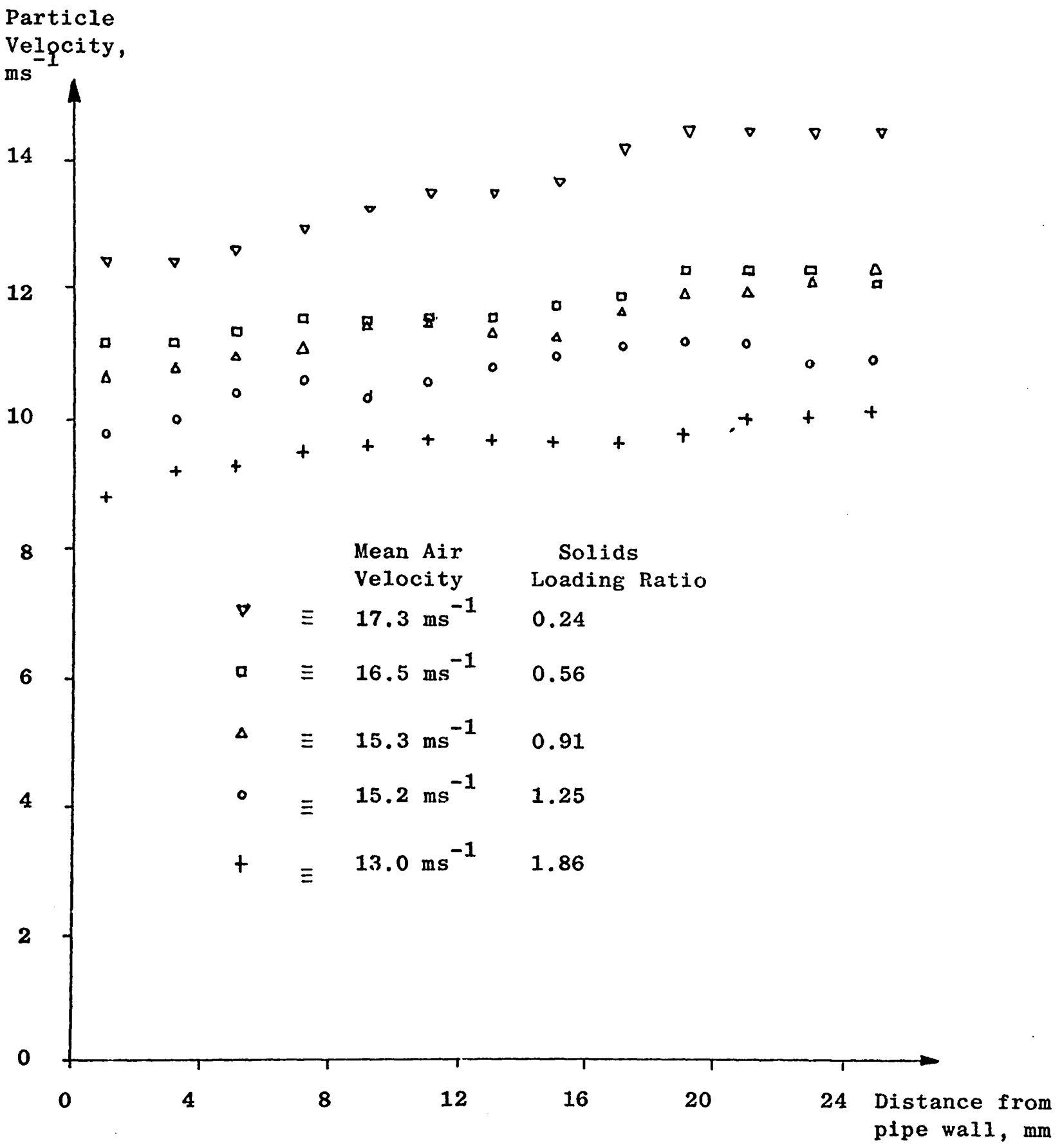

PARTICLE VELOCITY PROFILES, Runs 2

Figure (8.2)

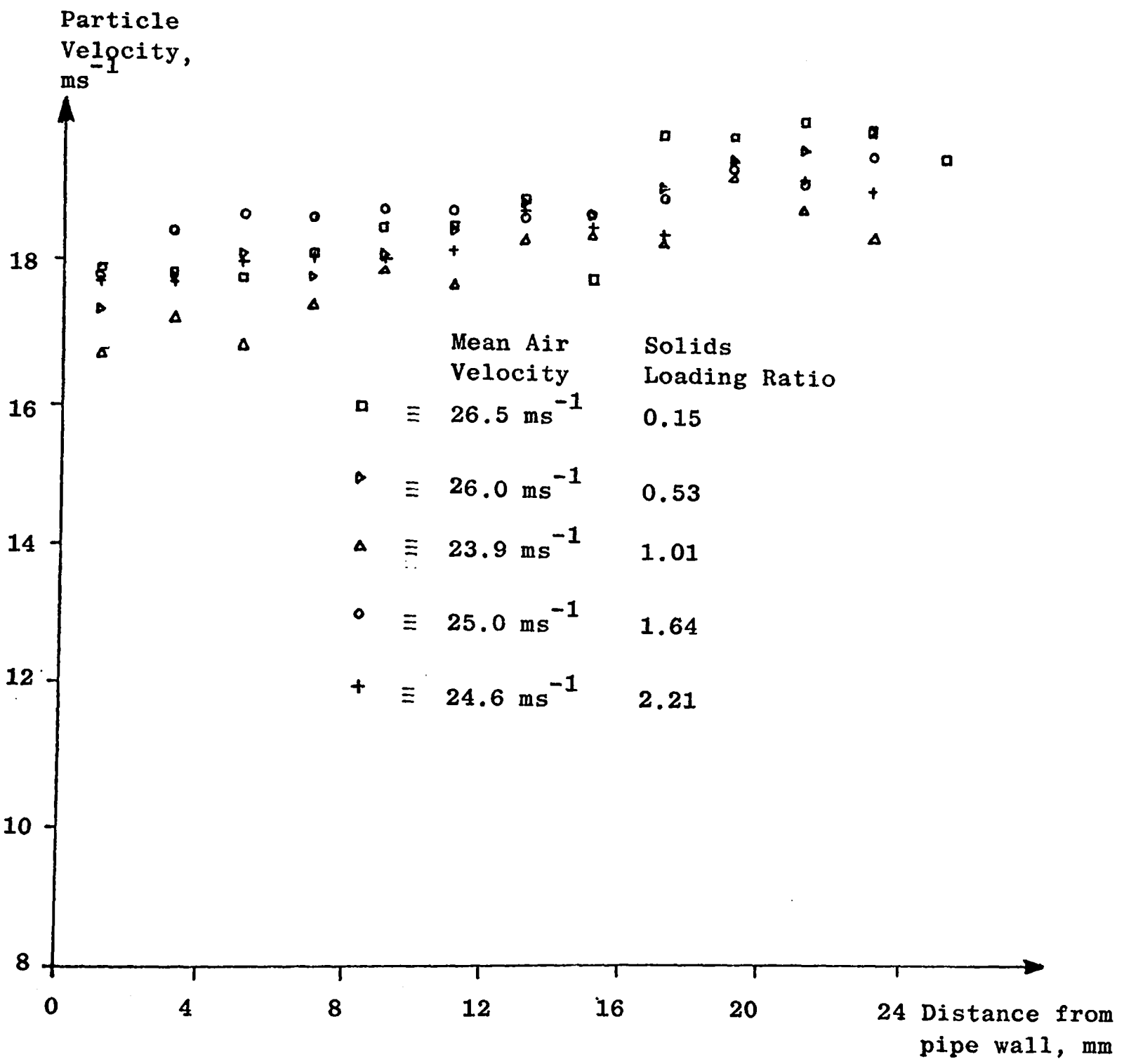

PARTICLE VELOCITY PROFILES, Runs 3

Figure (8.3)

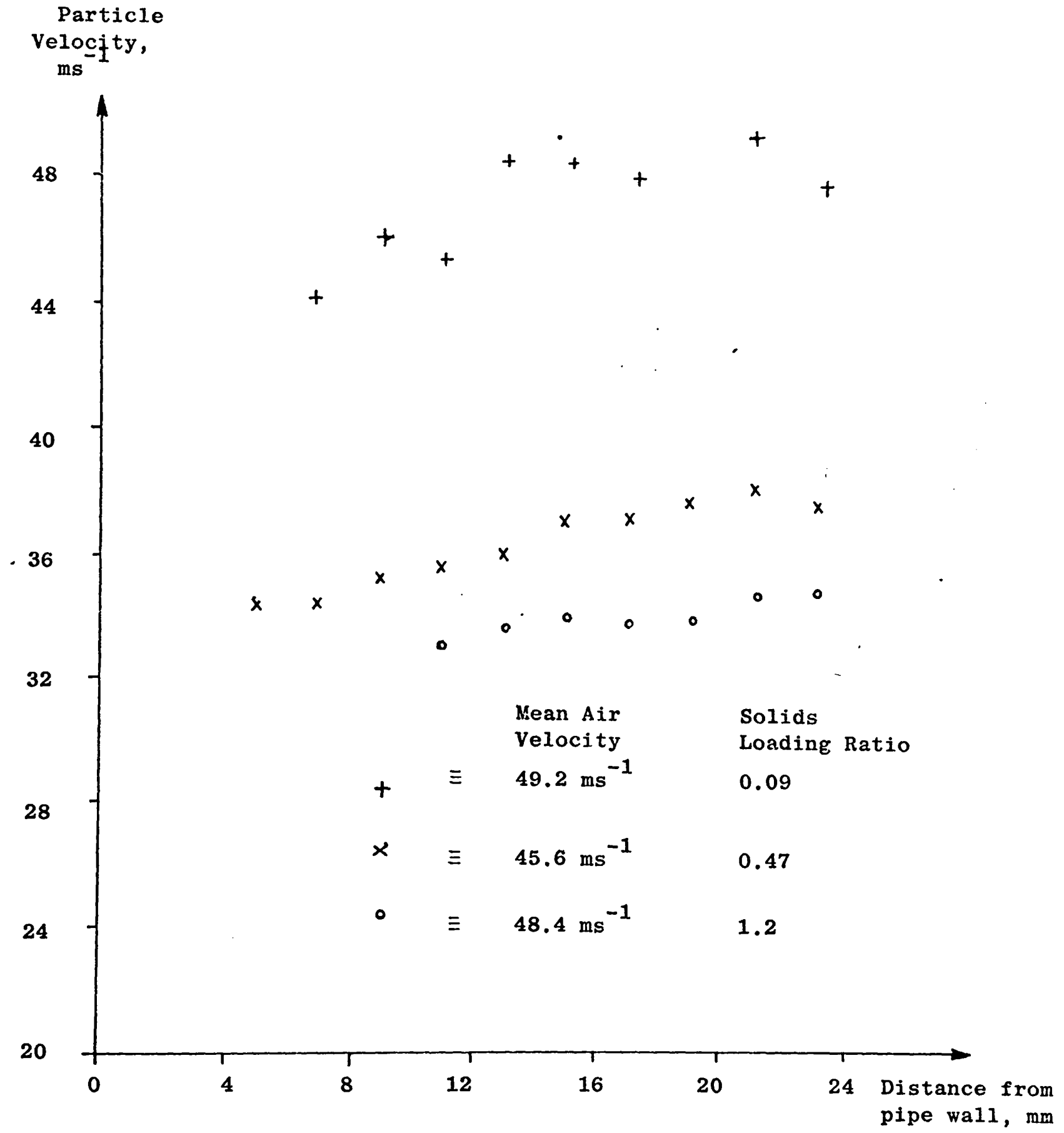

PARTICLE VELOCITY PROFILES, Runs 4

Figure (8.4)

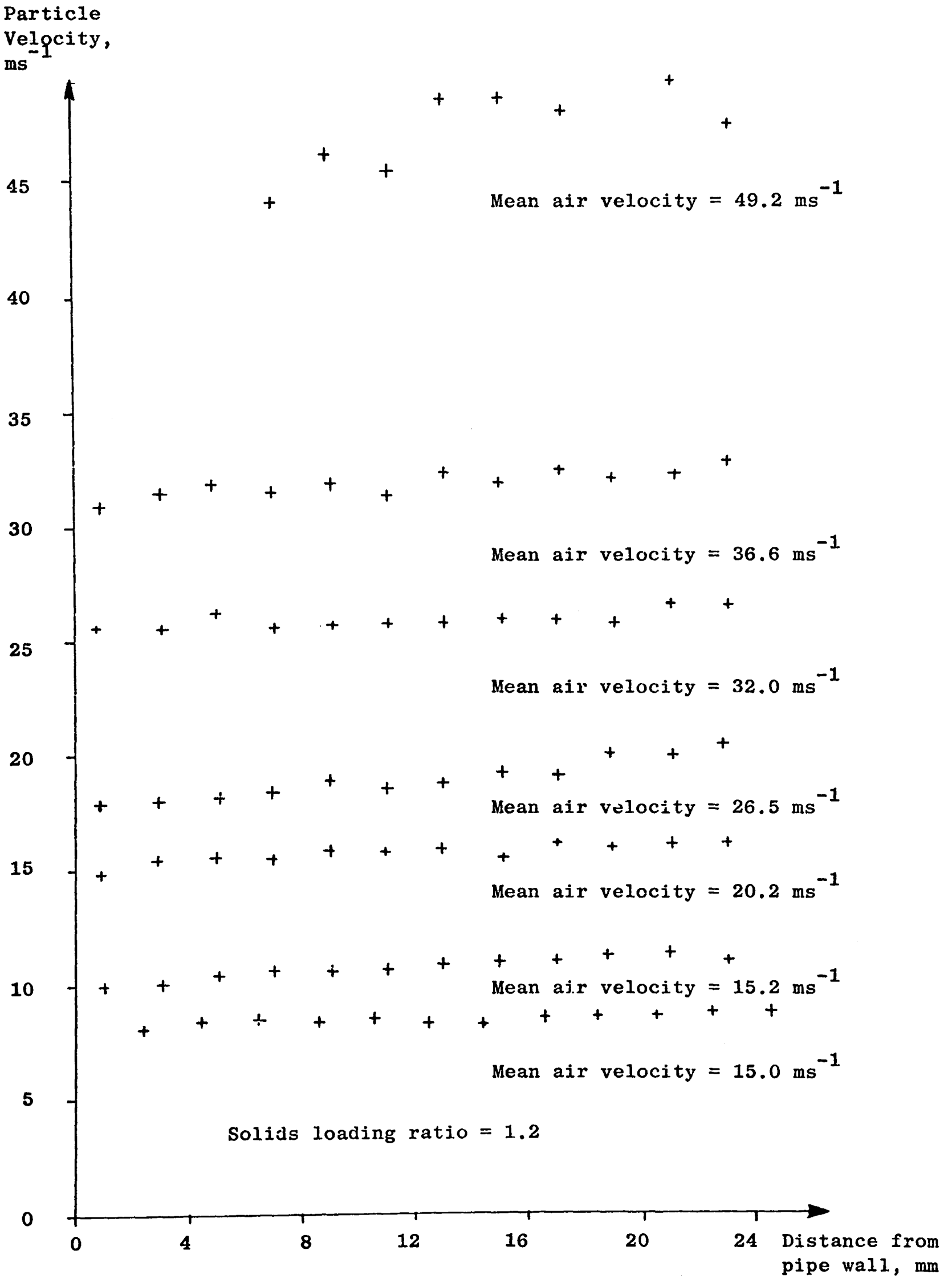

Runs B, VELOCITY PROFILES AT CONSTANT SOLIDS LOADING RATIO

Figure (8.5)

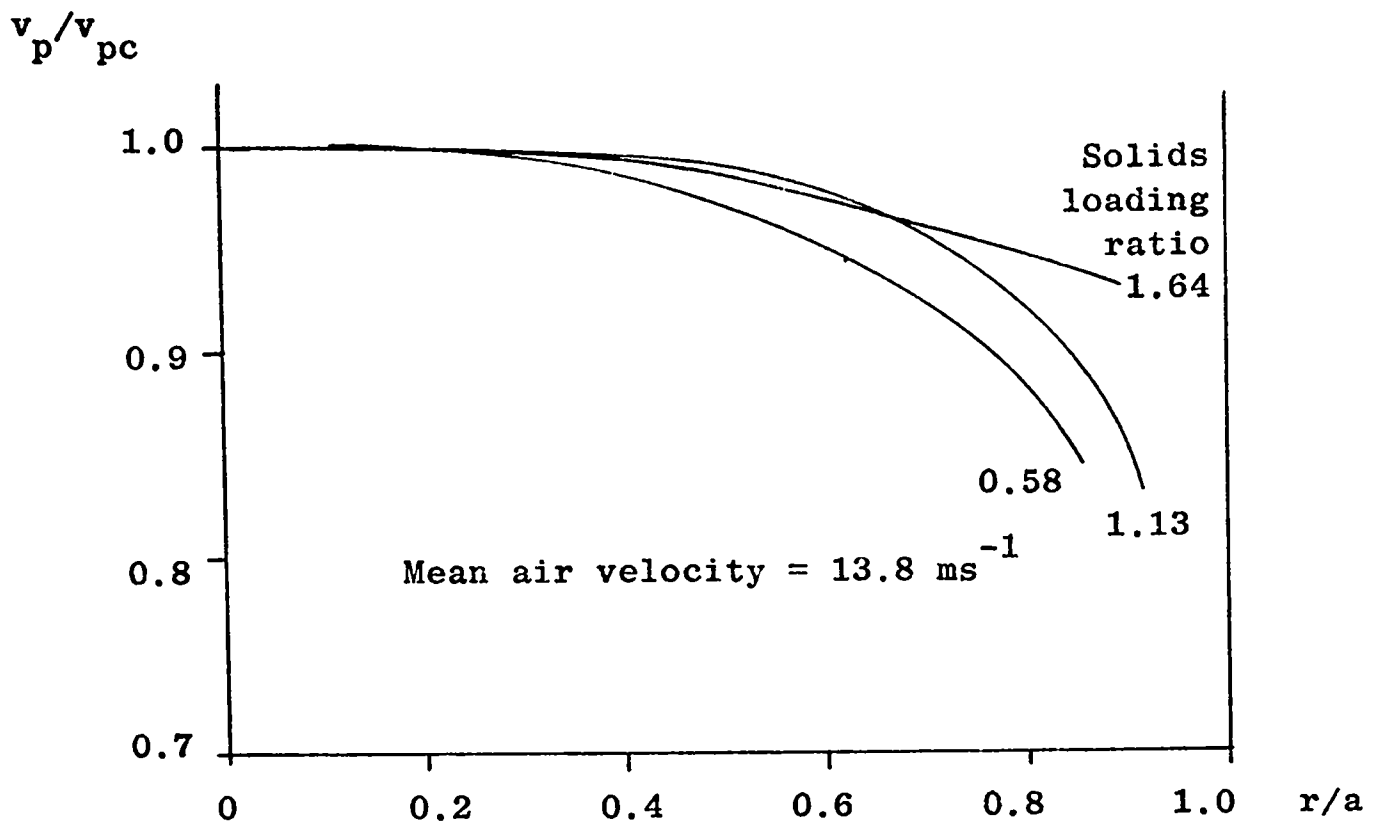

PARTICLE VELOCITY PROFILES AT CONSTANT AIR VELOCITY

Figure (8.6)

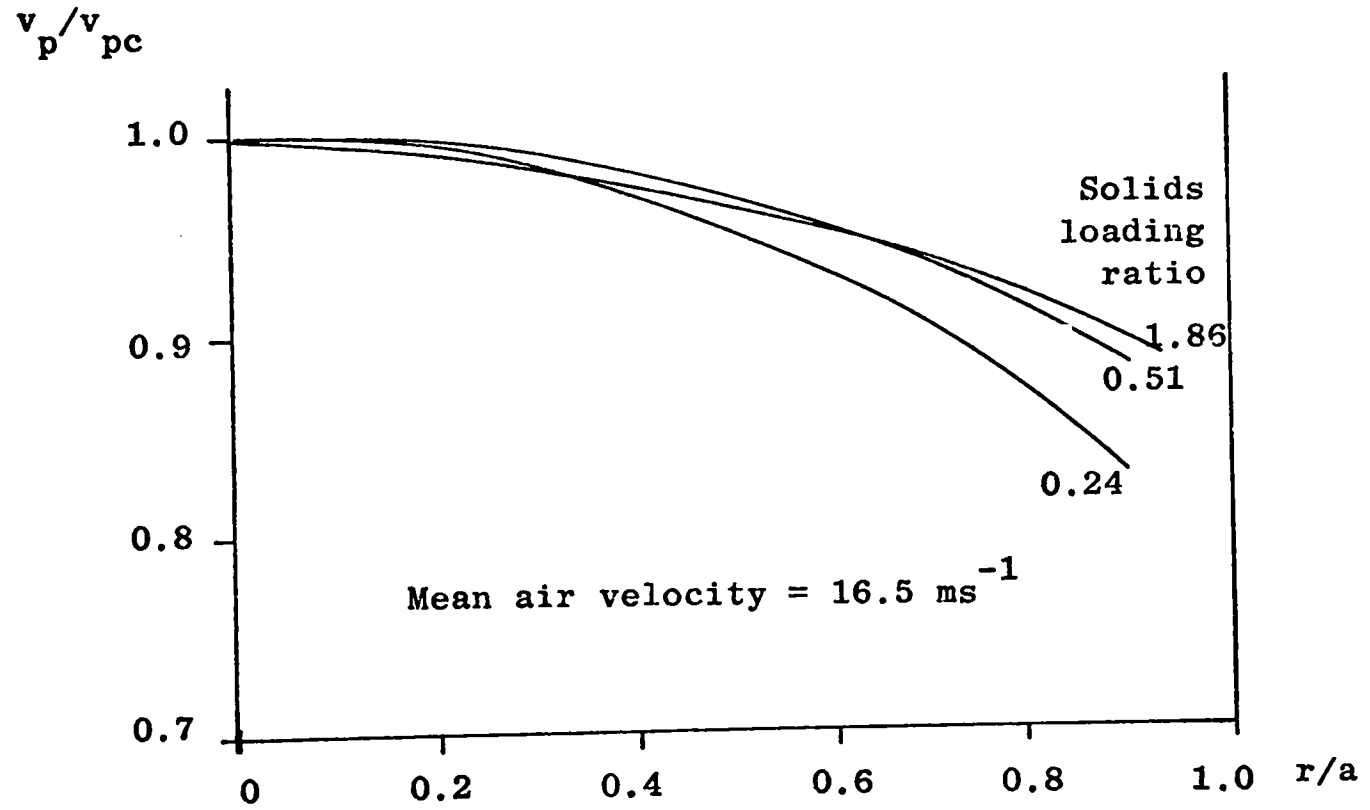

PARTICLE VELOCITY PROFILES AT CONSTANT AIR VELOCITY

Figure (8.7)

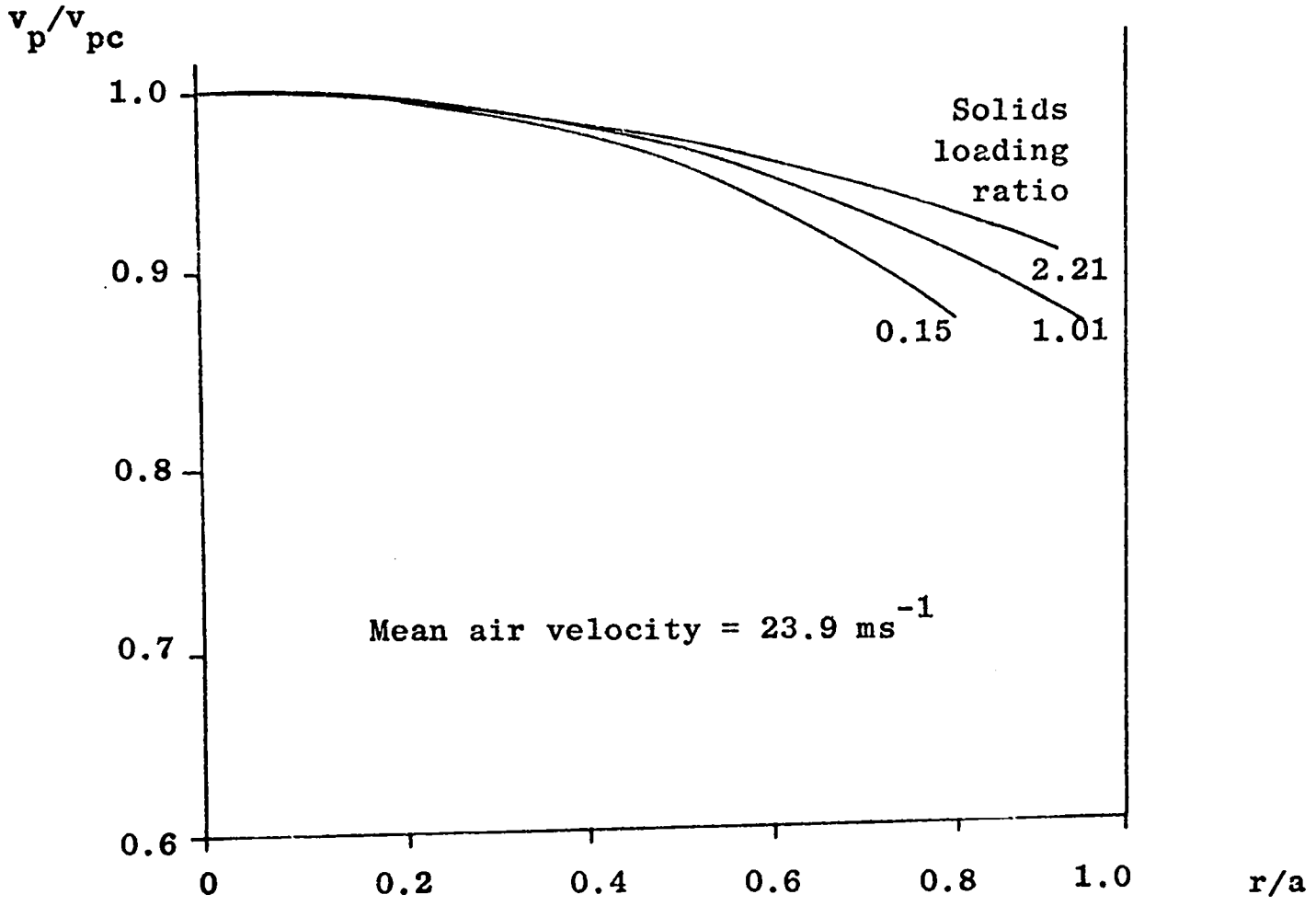

PARTICLE VELOCITY PROFILES AT CONSTANT AIR VELOCITY

Figure (8.8)

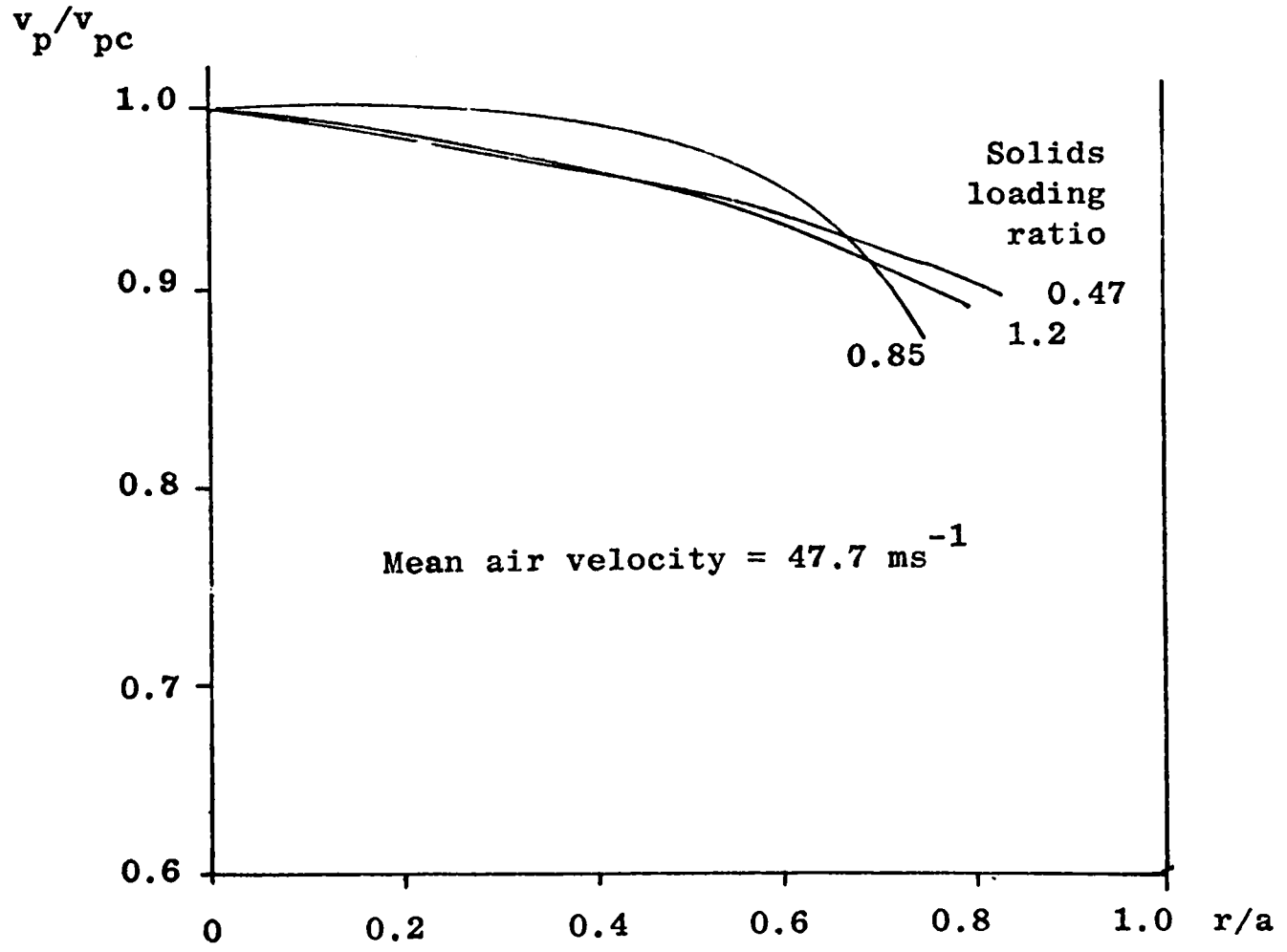

PARTICLE VELOCITY PROFILES AT CONSTANT AIR VELOCITY

Figure (8.9)

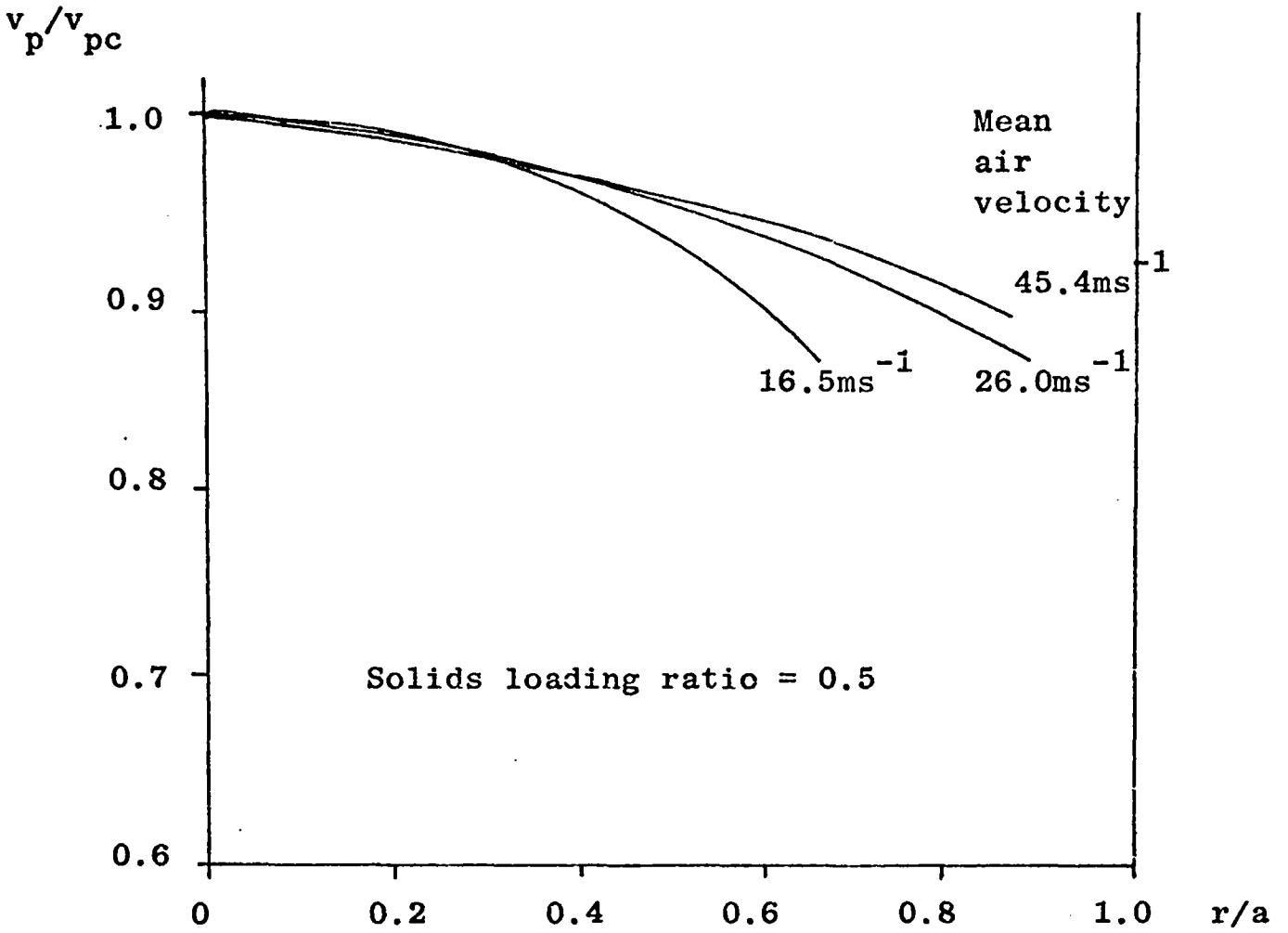

VELOCITY PROFILES AT A CONSTANT SOLIDS LOADING RATIO

Figure (8.10)

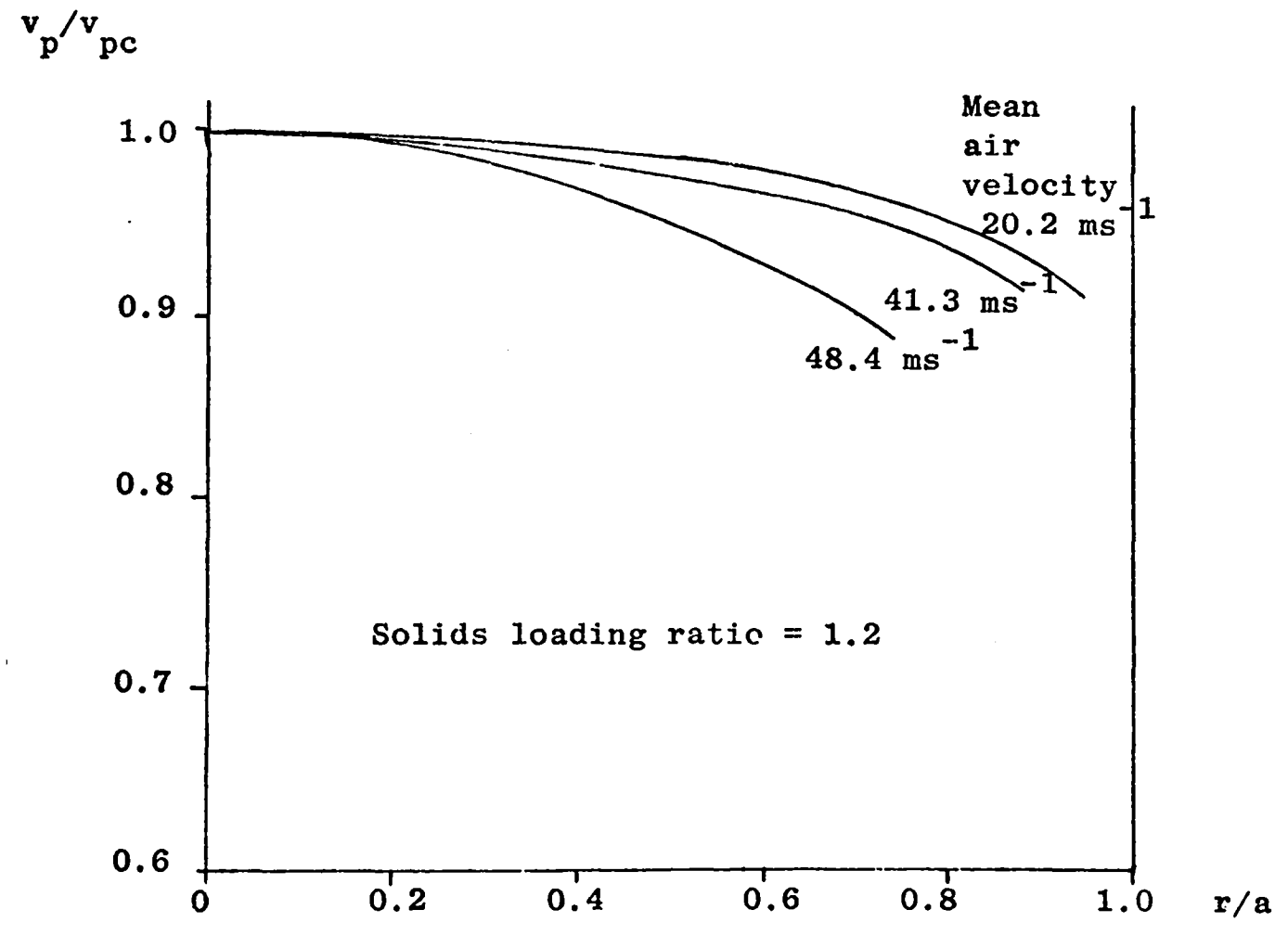

VELOCITY PROFILES AT A CONSTANT SOLIDS LOADING RATIO

Figure (8.11)

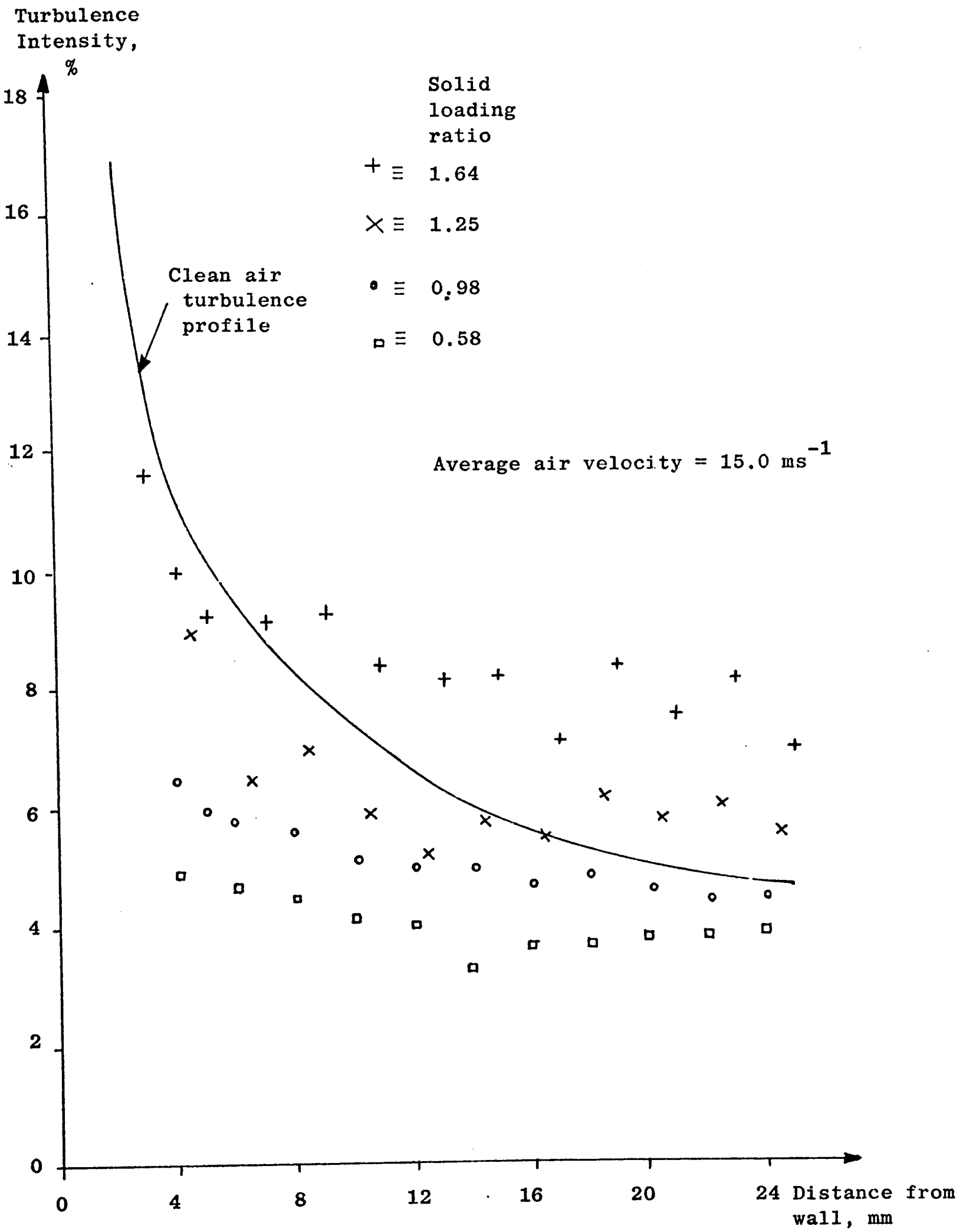

TURBULENCE PROFILES

Figure (8.12)

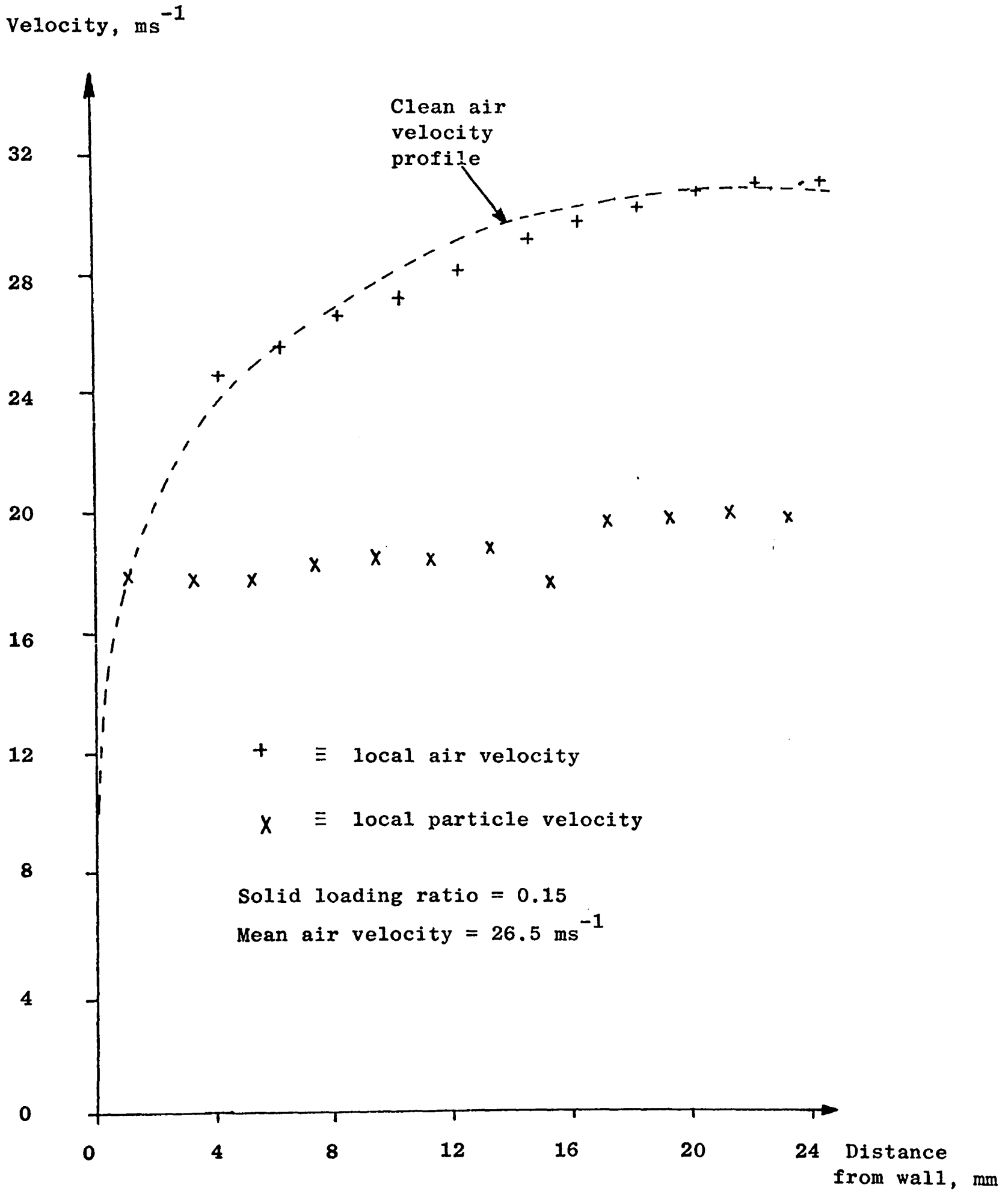

AIR AND PARTICLE VELOCITY PROFILES

Figure (8.13)

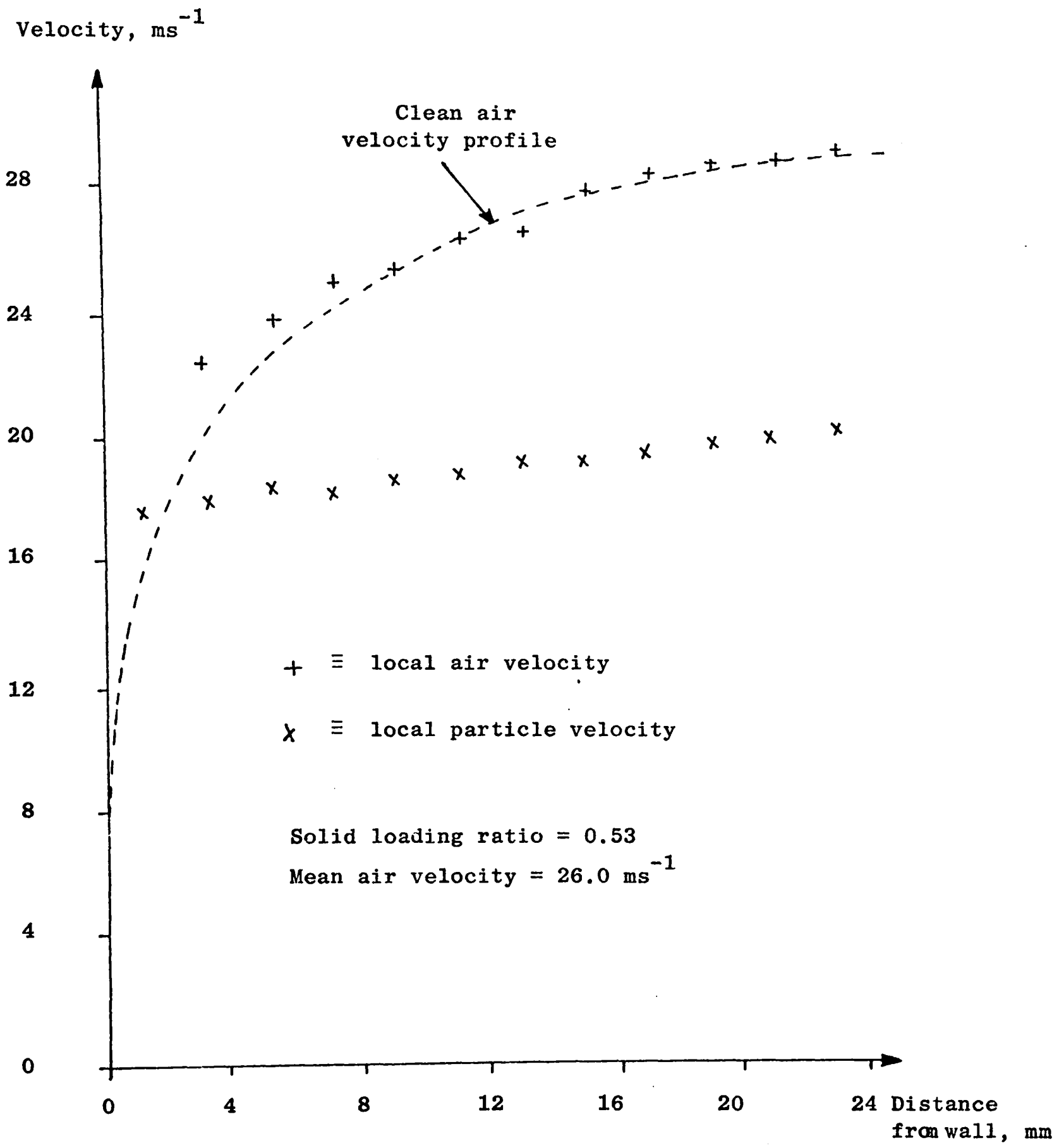

AIR AND PARTICLE VELOCITY PROFILES

Figure (8.14)

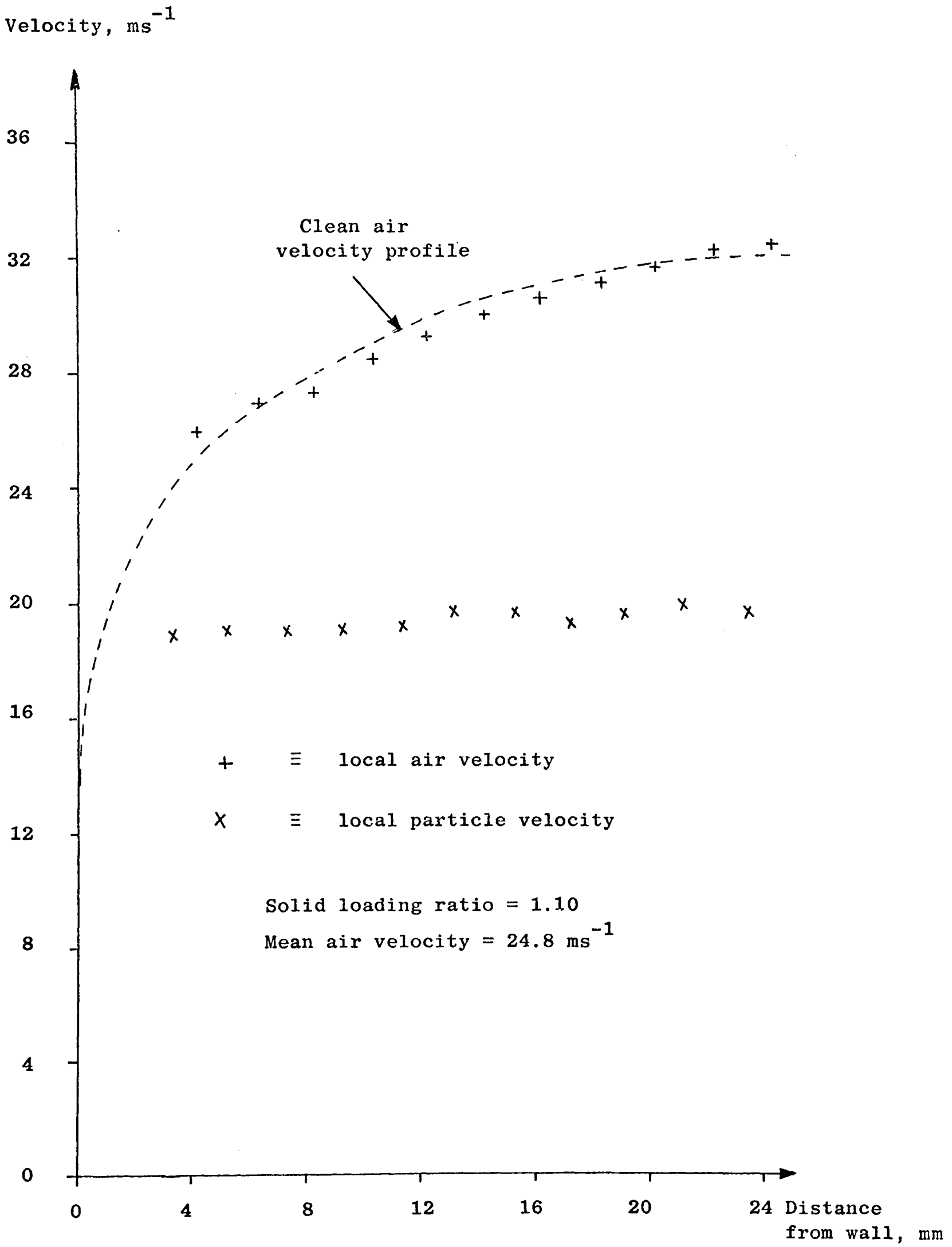

AIR AND PARTICLE VELOCITY PROFILES

Figure (8.15)

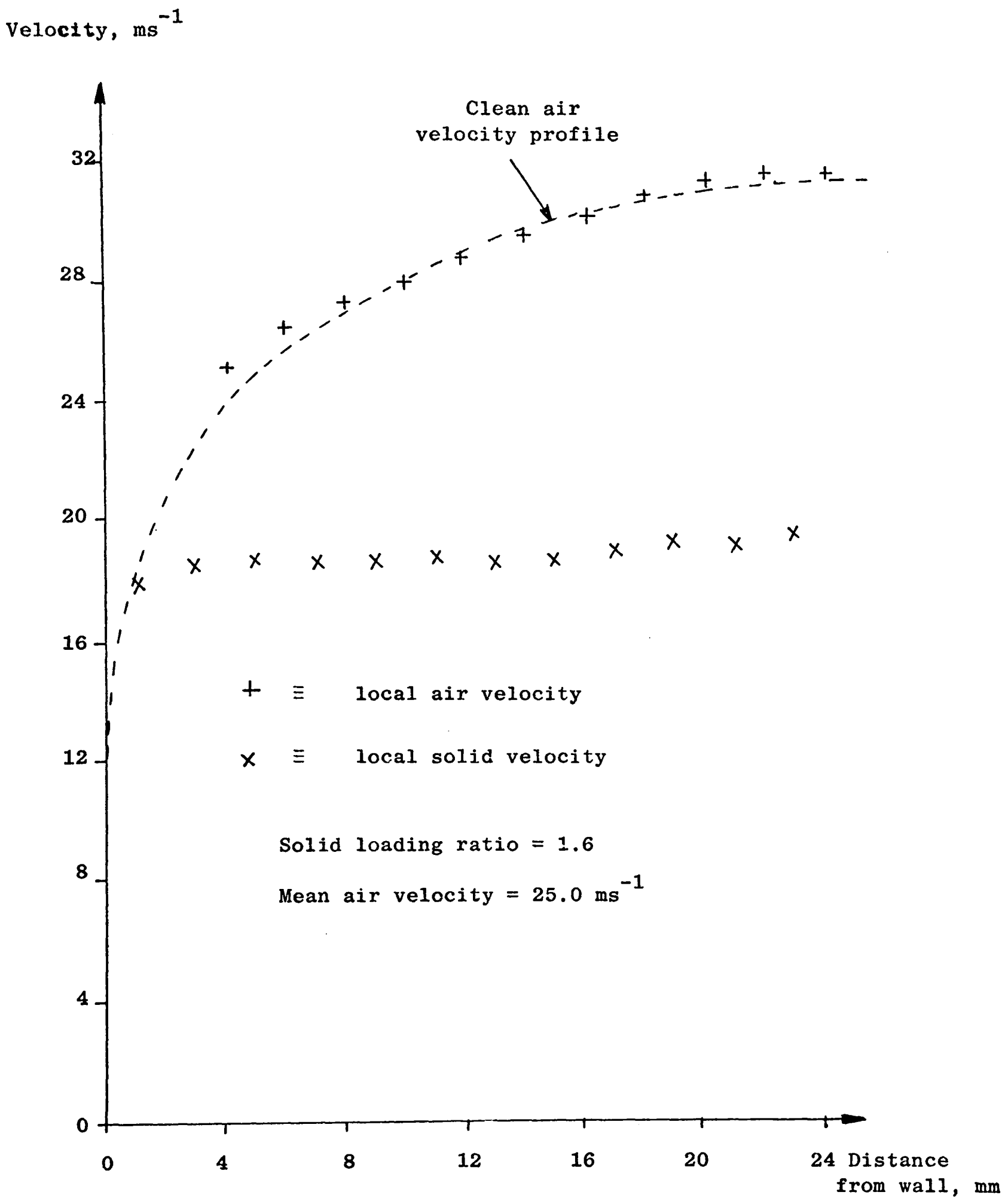

AIR AND SOLID VELOCITY PROFILES

Figure (8.16)

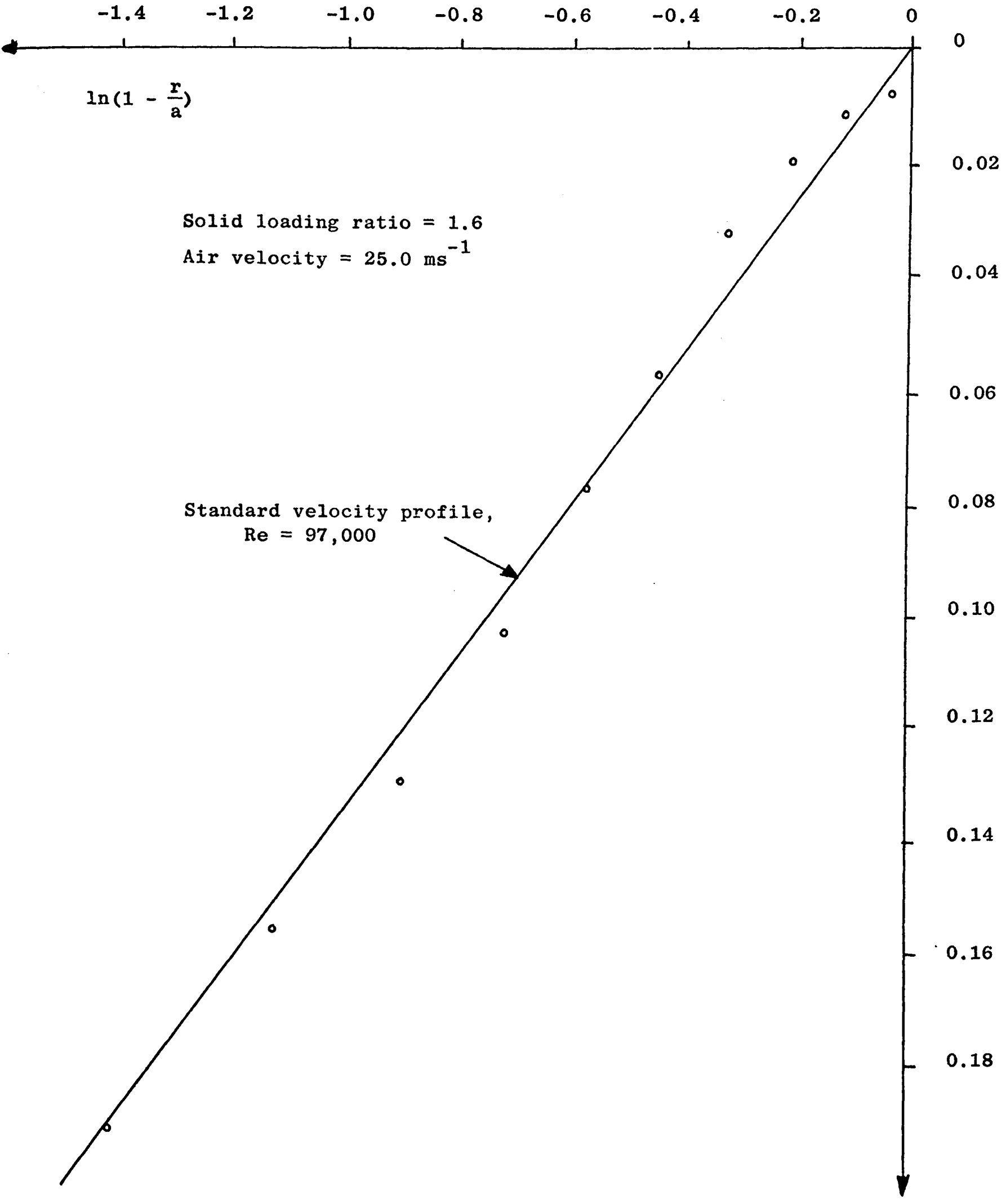

LOGARITHMIC PLOT OF AIR VELOCITY PROFILE

Figure (8.17)

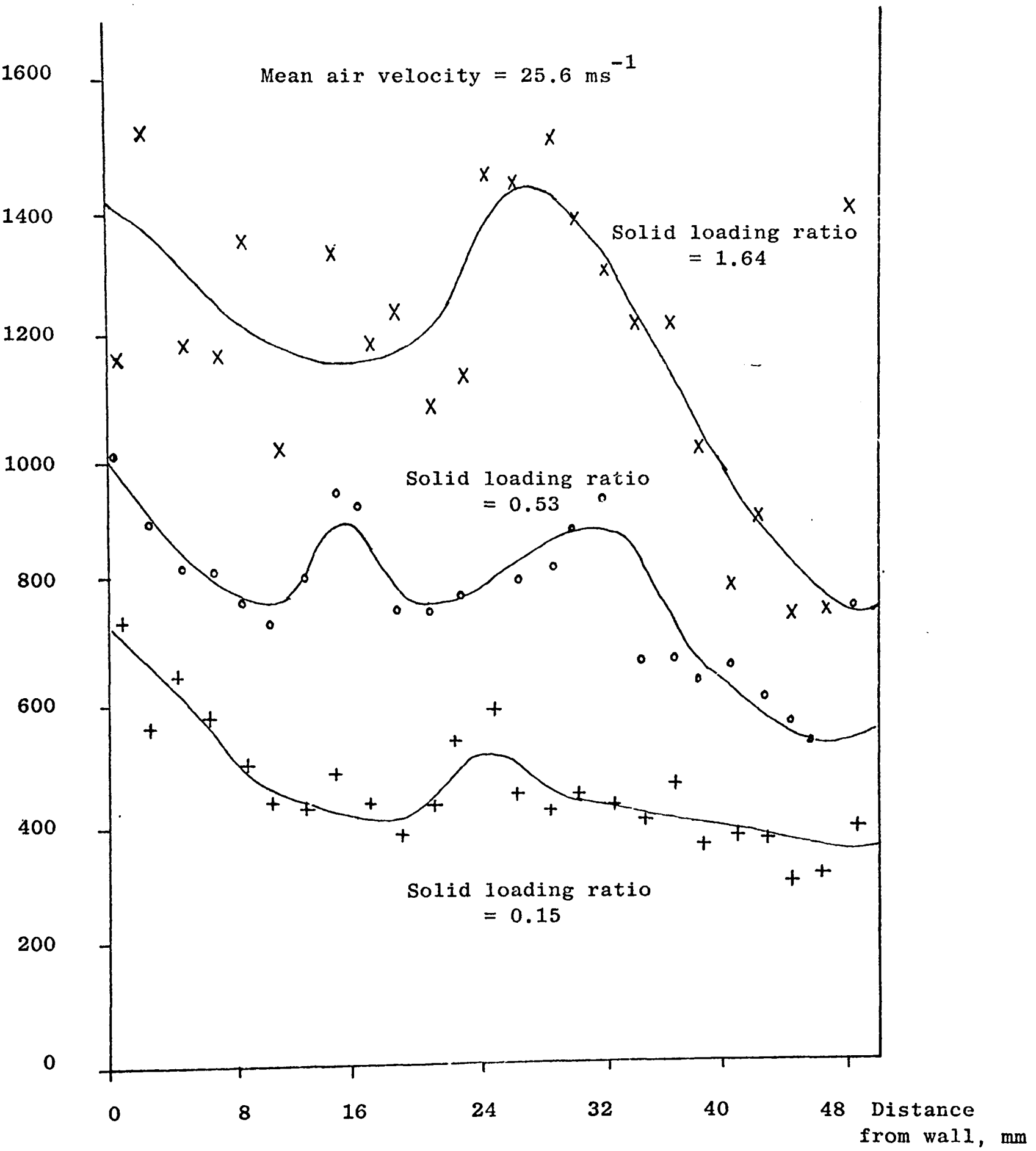

UNCORRECTED PARTICLE NUMBER DENSITY PROFILES

Figure (8.18)

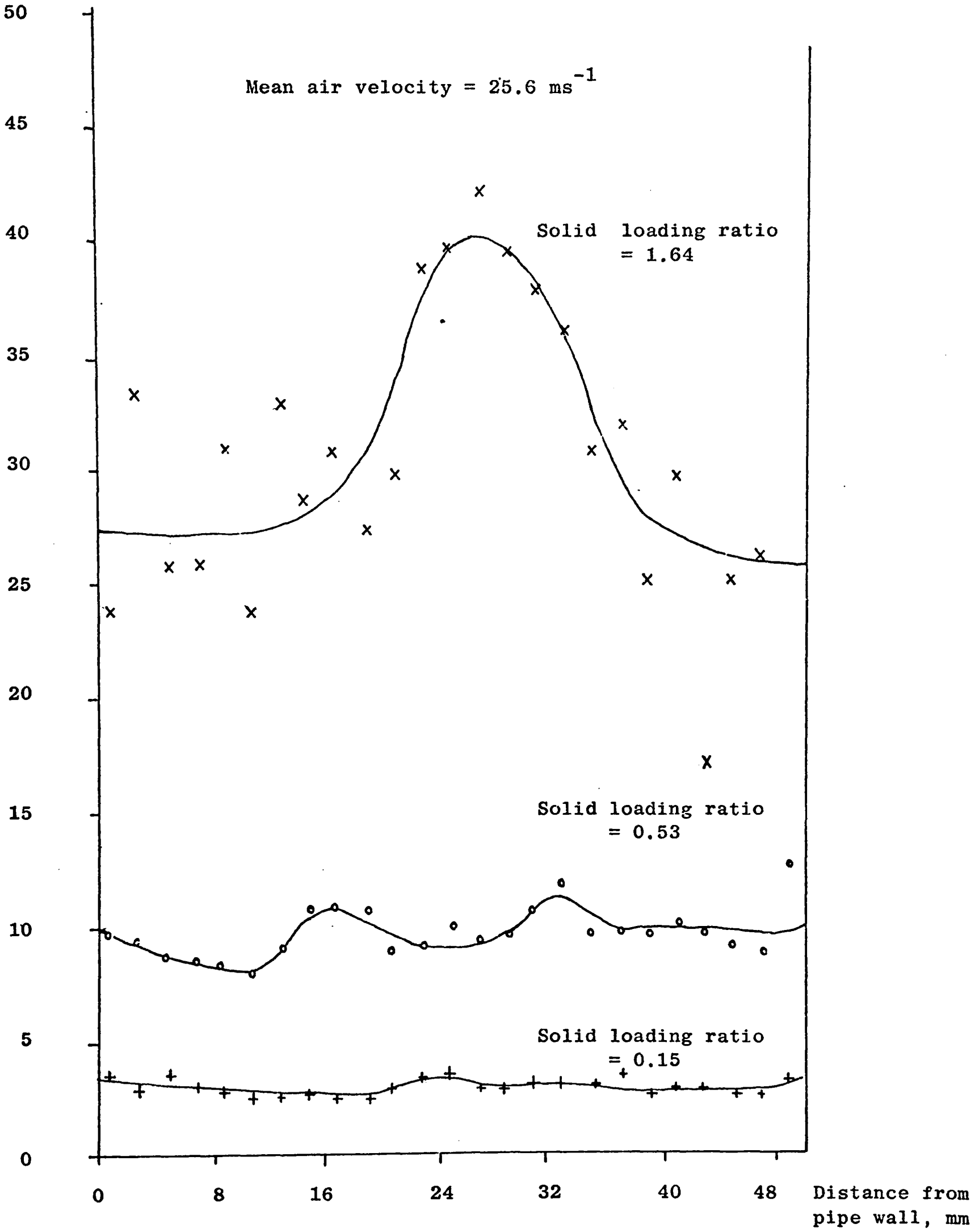

PARTICLE NUMBER DENSITY PROFILES

Figure (8.19)

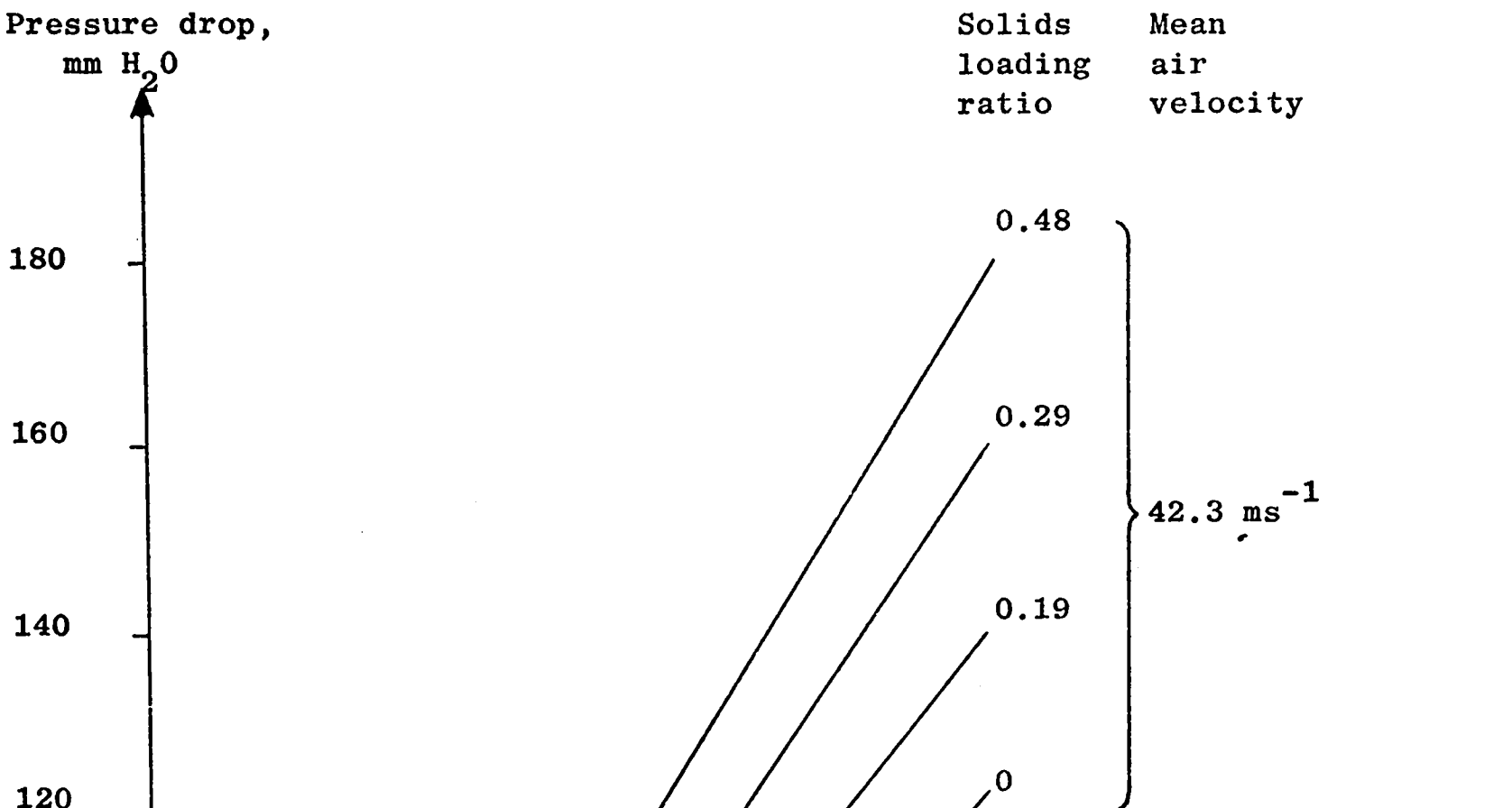

PRESSURE DROP MEASUREMENTS

Figure (8.20)

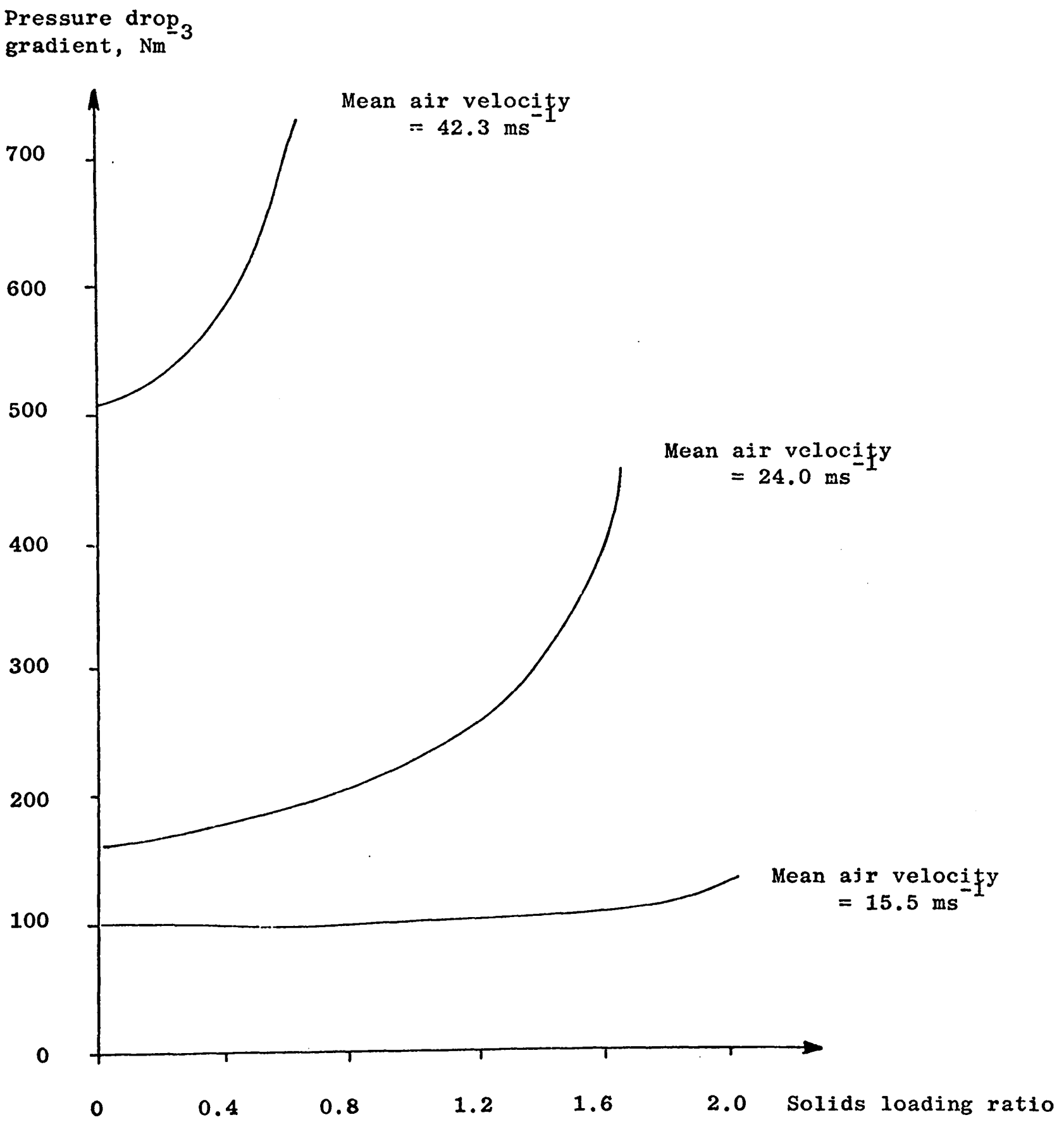

VARIATION OF PRESSURE GRADIENT WITH SOLIDS LOADING RATIO

Figure (8.21)

CHAPTER 9

MEASUREMENTS IN AN AIR-SAND FLOW

9.1 Introduction

The work described here is similar to that in the last chapter, but with sand suspended in the air flow. The sand, type 52/100, was used both unsieved and sieved between 300 μm and 355 μm in order to reduce the size range. The size analysis of both these solids is given in chapter 4. The flows were investigated with solids to air mass flow rate ratios, or solids loading ratios, of up to 2.5 and with velocities of 40 ms^{-1} in the vertical test section. The air mass flow rate was again measured with the orifice plate meter and the solid mass flow rate was determined by the setting on the screw feeder.

The properties measured in the flowing air-sand suspension are the particle velocity and turbulence profiles and the pressure drop. The air velocity profile was not measured since the method explained in section (8.4) involving the use of a Pitot-static probe in the flow could not be used. The sand flow was found to be much more abrasive than the ballotini flow, since the grains were angular and there were a large number of fines in the flow. The number density profile was not measured since the measurement technique employed in the air-ballotini flow [see section (8.6)] was found to be inaccurate.

9.2 Particle Velocity Measurement

9.2.1 Introduction The arrangement of the LDV employed for particle velocity measurement in the sand suspension was the same as that used in the ballotini suspension [see section (8.2)]. However, an additional

difficulty was encountered in the experiments due to the very abrasive nature of the sand flow. The glass test pipe became 'frosted' after being subjected to the sand flow for a very short time. This is demonstrated in figure (9.1) which shows the surface profile of a piece of the pipe, measured with a Tallysurf, before and after being exposed to the sand flow. The roughness of the surface scattered light passing through it and reduced the light intensity in the measuring volume, and the signals were very weak.

Even with this problem, however, it was possible to use the Cambridge Consultants tracking filter for all measurements, which was not the case for ballotini flow. Even so, great care had to be taken to ensure that the instrument was tracking on the Doppler frequency and not on spurious noise produced both by extraneous light falling on the photomultiplier, and by the photomultiplier and tracker themselves.

9.2.2 Results and Discussion The particle velocity profiles of the unsieved sand are shown in figures (9.2) to (9.5), and those of sand sieved between 300 μm and 355 μm are shown in figures (9.6) and (9.7). Again the mean air velocity varied between measurements at nominally constant air velocity, although in this case the variation was kept below 7%.

As with the measurements on the ballotini, the large degree of scatter in the points obscures any trends in the results. The smoothed curves are shown in figures(9.8) to (9.15) in which the non-dimensional velocity is plotted against the non-dimensional radius. Since the velocity gradient was expected to increase smoothly towards the edge of the pipe with no 'bumps' which might be caused by changing flow conditions, the smoothing was done by 'eye' rather than by fitting the curve to a polynomial using the least squares method. The particle

velocity profiles of the unsieved sand became less flat with increasing solids loading ratio, but those of the sieved sand showed no obvious trends. Figures (9.12) and (9.15) show the variation of the particle velocity profiles with overall average air velocity at a constant loading ratio. In both cases the curvature decreases with increasing air velocity. These effects will be discussed more fully in chapter 10.

Since no one trend in the velocity profiles was found which was followed by each type of solid, it suggests that many factors were involved. The bounce of the particles from the pipe wall is very likely to be dependent on both the particle size and shape, as well as other properties such as the electrostatic charge on the particles. This dependency is likely to influence the effect of the air velocity profile on the particle velocity profile, which would help to explain the variation in the results. For the velocity profiles to be further analysed the number of variables in the flow would have to be reduced. These results indicate the complexity of the air-solid flow.

9.3 Turbulence Intensity Measurements

9.3.1 Introduction The method of turbulence intensity measurements was described in section (8.3). Since all the Doppler frequency measurements in this chapter were made with the tracking filter, then turbulence measurements could normally be made. However, at high air velocities, above about 35 ms^{-1}, the signal drop out was too great for sensible turbulence readings to be made, even though it was still possible to track the signal. This was also true for flows with solids loading ratios above about 1 and air velocities above about 25 ms^{-1}.

9.3.2 Results and Discussion Figures (9.16) to (9.20) show some of the turbulence intensity measurements made on the particles in the air-sand flows. In the profiles for the unsieved sand, given in figures (9.16) to (9.17), the central turbulence intensity tends to increase with

solids loading ratio and decreases with the air velocity. The profiles for the sieved sand, in figures (9.19) and (9.20), also show an increase in the central turbulence intensity with increasing solids loading, but there is sufficient data for examining the variation of the turbulence with air velocity in this case. There was much less variation in the turbulence intensity found across the pipe for the sieved sand as opposed to the unsieved sand, but similar values for the central turbulence was found in each case. The decrease in the measured turbulence which was expected for the reduced size range of the sieved sand was not obvious, which indicates that the spread in sizes contributes little to the variation of the Doppler frequency.

9.4 Pressure Drop Readings

9.4.1 Introduction The same method of static pressure measurements as that used on the flow conveying the ballotini [see section (8.6)] was used on the air-sand flow. Except for the flow conveying the sieved sand, the pressure drop up the test pipe was measured during each experimental run. No particular difficulties were encountered in these measurements, but again, at high solids loading ratios violent fluctuations in the pressure occurred, decreasing the accuracy of the results.

9.4.2 Results and Discussion The results are given in figures (9.21) to (9.23). The curves are similar to those found for the ballotini flow, with the pressure drop becoming linear after the two phases had been accelerated to a fully developed state, about 1 metre from the first tapping. As the number of particles in the flow was increased, the pressure drop increases due to the additional resistance.

Figure (9.24) shows the dependence of the pressure gradient in the linear section on the solids loading ratio. The shape of each curve at constant air velocity is similar, with the pressure gradient increasing with solids loading ratio.

9.5 Conclusions

As with the air-ballotini flow described in chapter 8, a number of different properties of the air-solid flow were measured. The same properties were measured, except the local air velocity, which could not be measured due to the abrasive nature of the sand flow. Also, no suitable method for measuring the particle number density was available, since the method described in section (8.5) was found to be unsatisfactory.

The laser-Doppler velocity meter was used with more success for particle velocity measurements in the air-sand flow than in the air-ballotini flow, since it was possible to use the tracking filter as a signal processor and this greatly reduced the time needed for each measurement. The reason for this difference in behaviour of the LDV for the two types of particles was probably mainly due to the smaller size of the sand particles. This gave an increased number density for the same solids loading ratio and it also increased the signal visibility. However, some reduction in the latter was caused by the 'frosting' effect on the glass caused by the abrasion of the particles. A more powerful laser would overcome the latter difficulty and enable the laser-Doppler velocimeter to provide a very useful tool for dilute phase air-solid flow investigations.

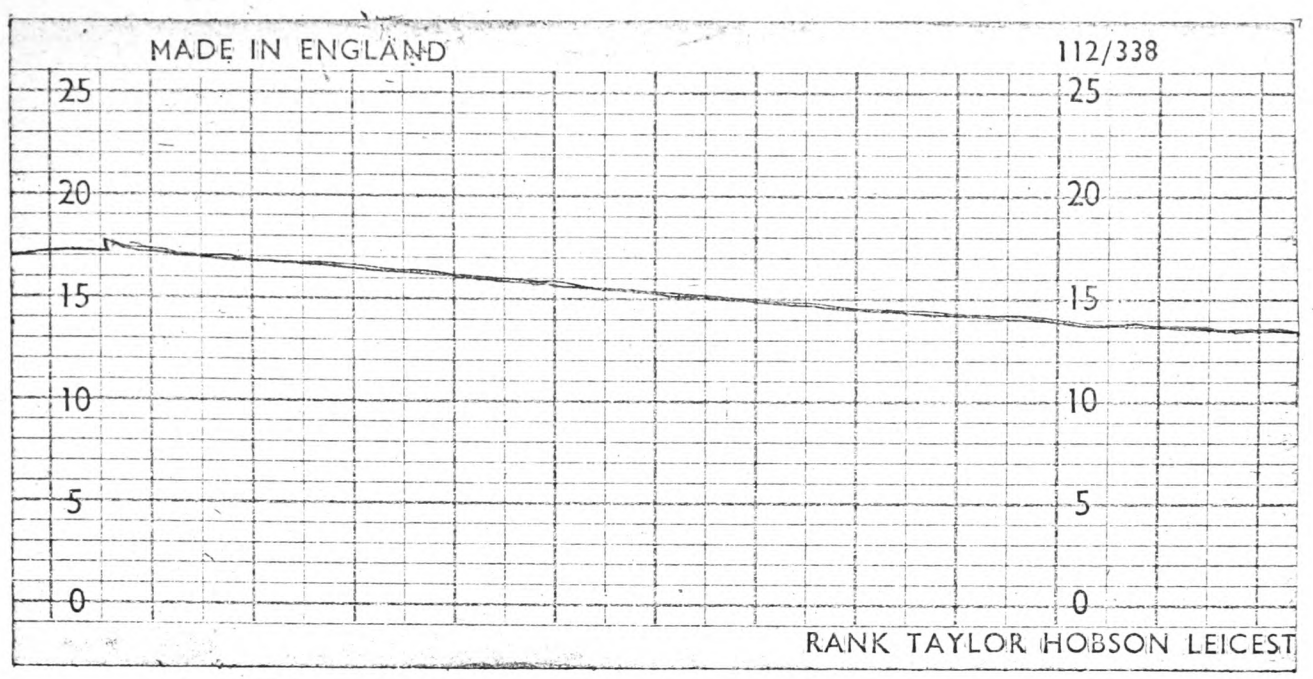

Unused Pipe

Horizontal Scale × 20

Vertical Scale × 10,000

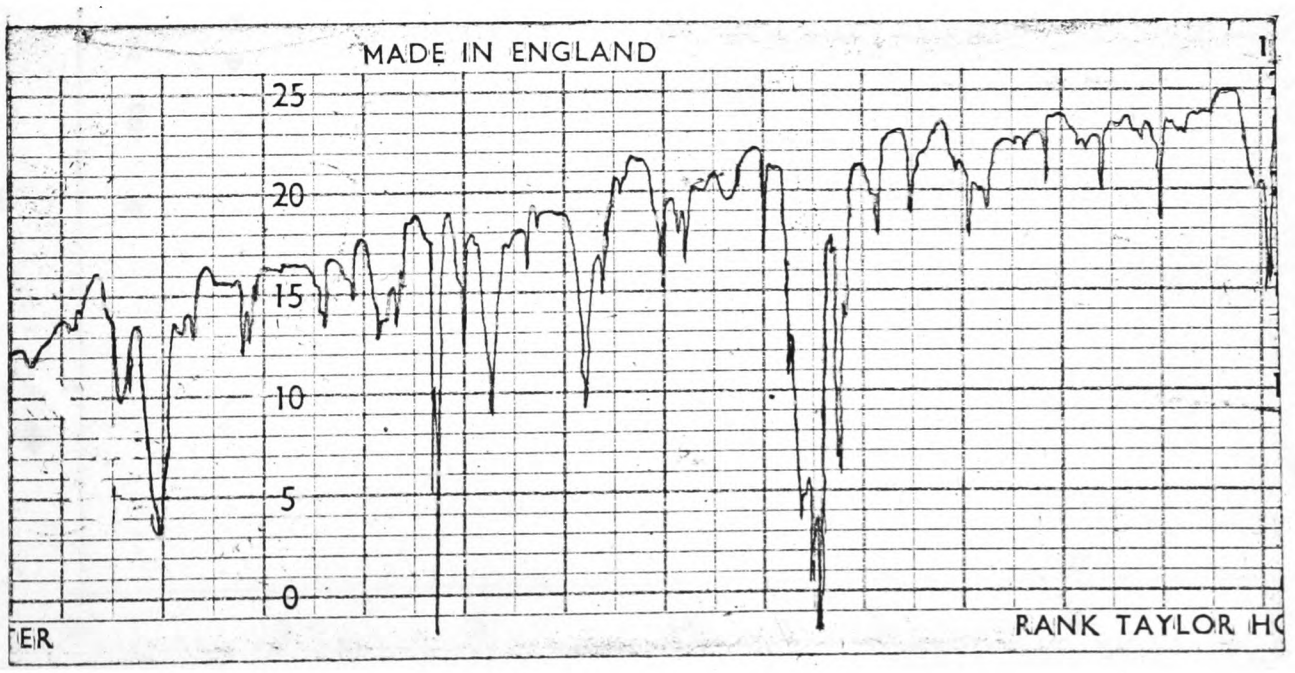

Used Pipe

SURFACE PROFILE OF TEST PIPE

Figure (9.I)

	Solids Loading Ratio	Mean Air Velocity
+	0.53	20.2 ms^{-1}
o	0.27	20.6 ms^{-1}
×	0.90	20.I ms^{-1}
□	I.3	20.0 ms^{-1}
▽	I.7	I9.2 ms^{-1}
△	2.I	I9.I ms^{-1}

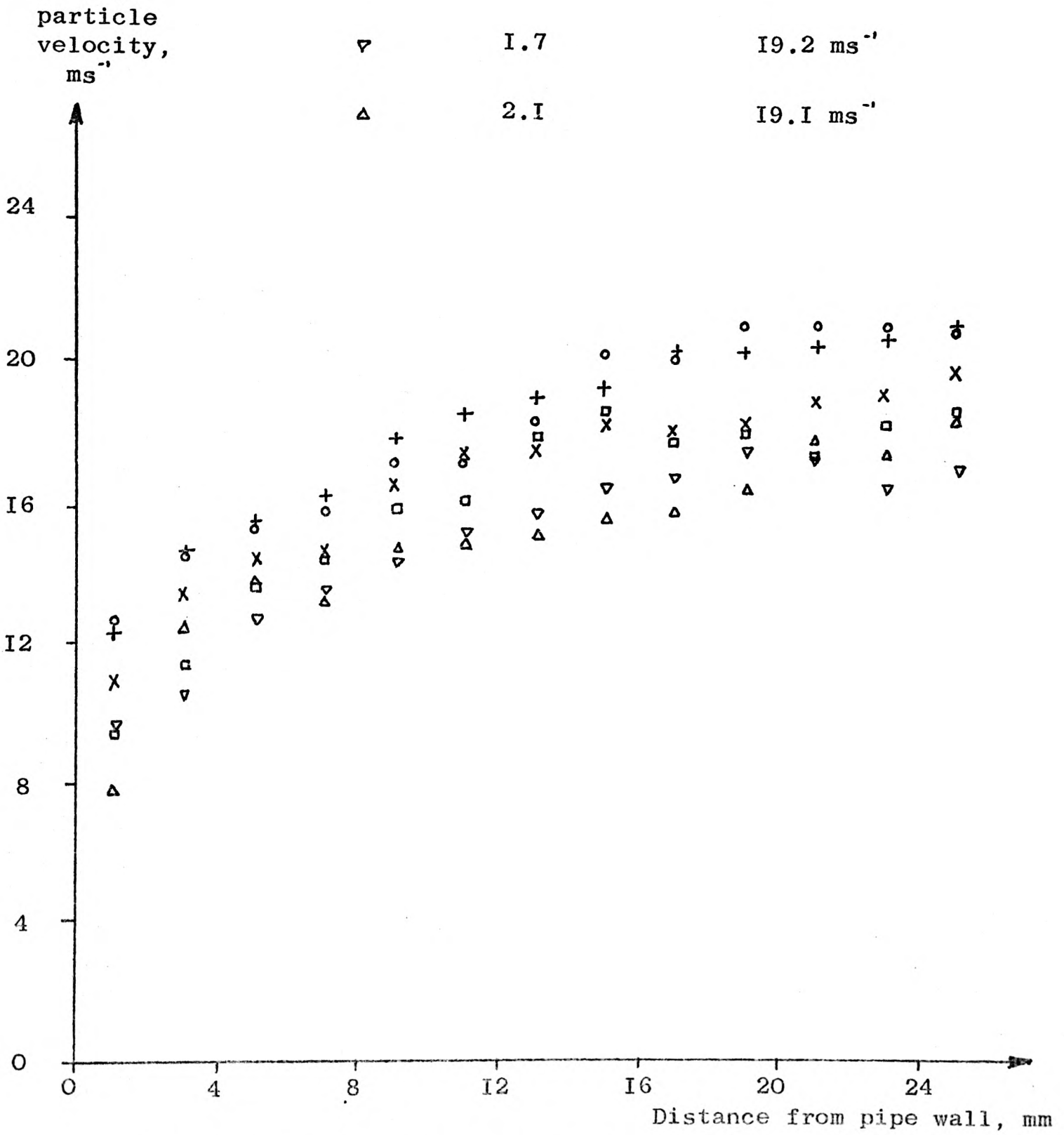

PARTICLE VELOCITY PROFILES, RUNS CI, WITH UNSIEVED SAND

Figure (9.2)

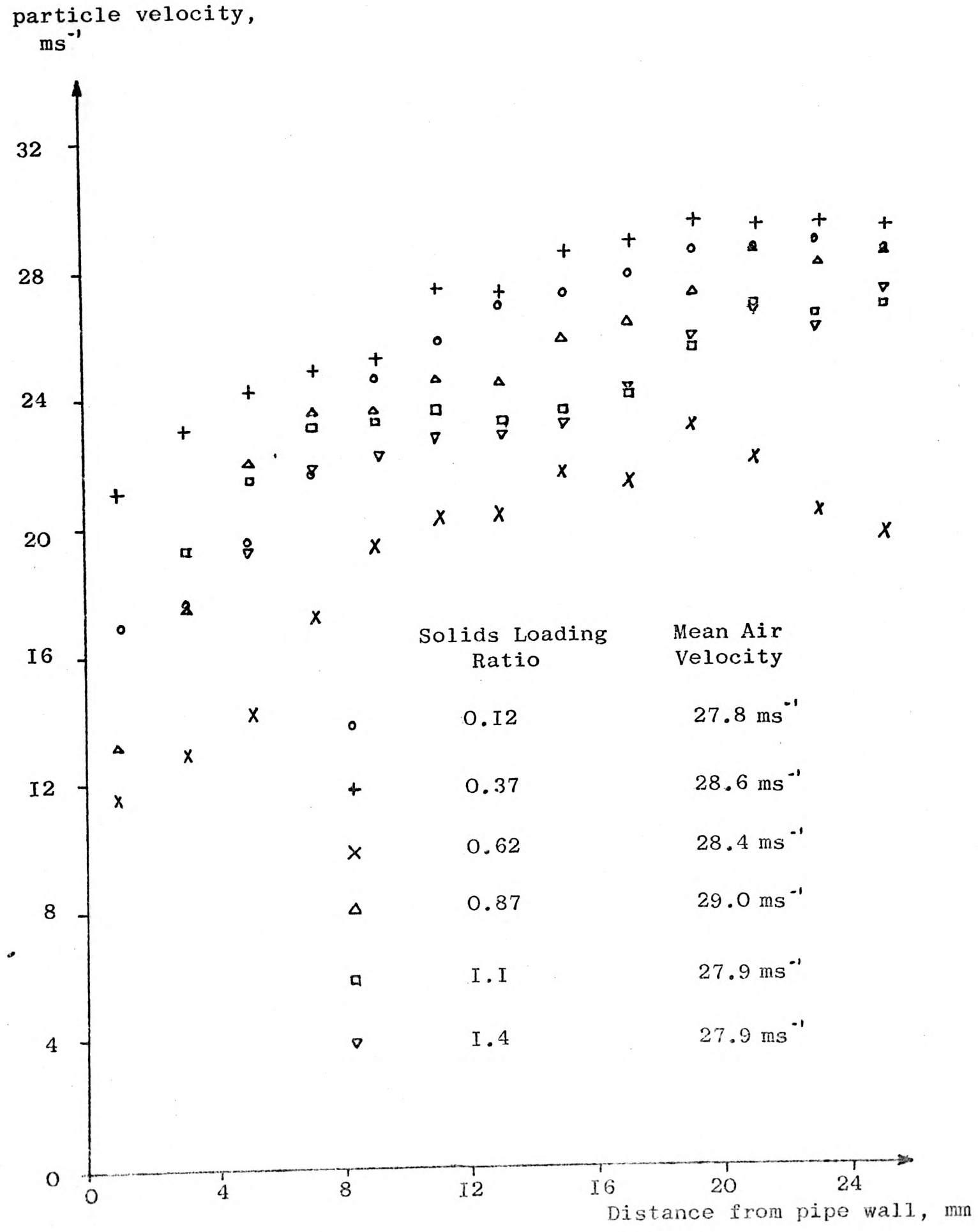

PARTICLE VELOCITY PROFILES, RUNS C2, WITH UNSIEVED SAND

Figure (9.3)

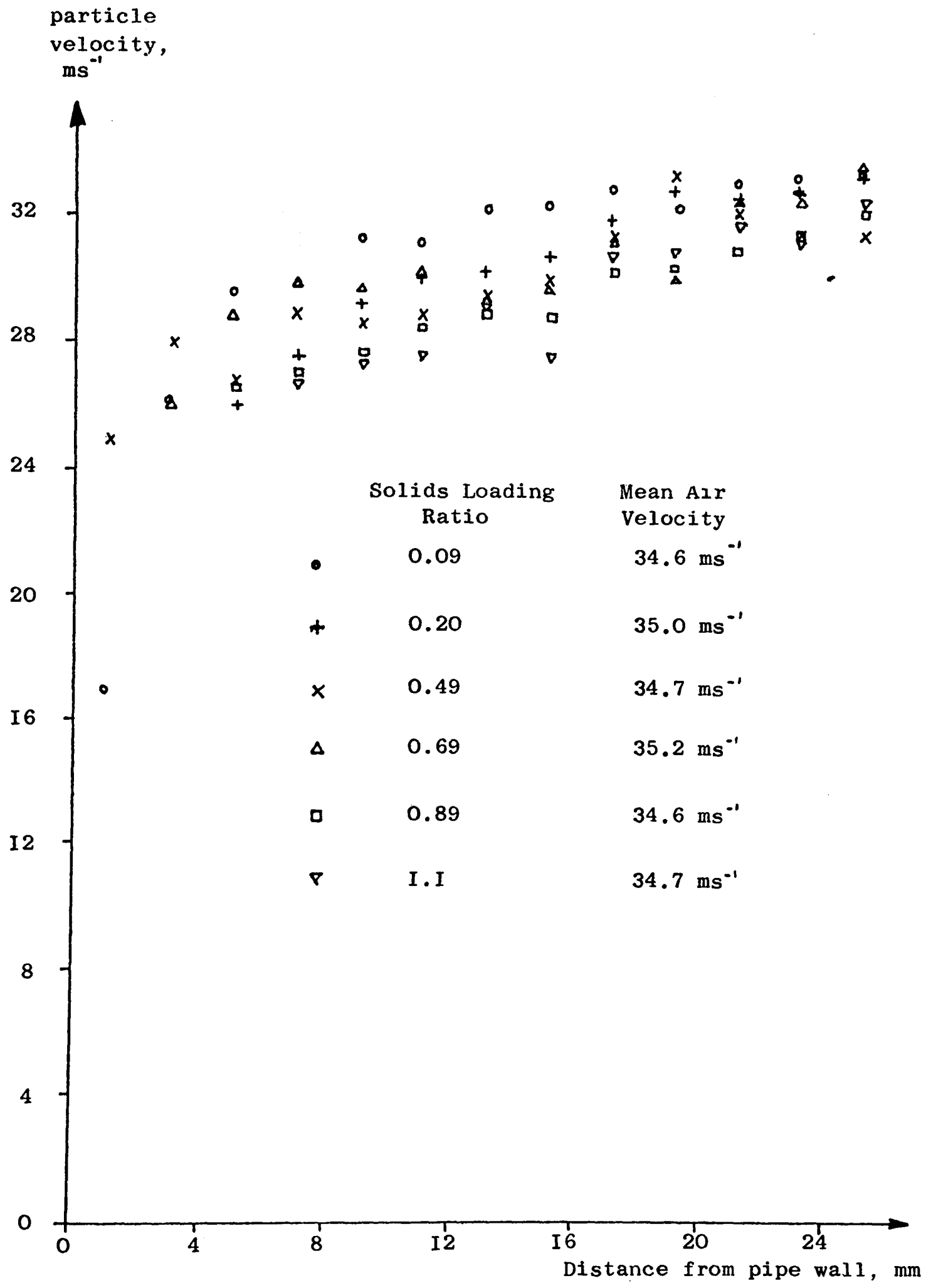

PARTICLE VELOCITY PROFILES, RUNS C3, WITH UNSIEVED SAND

Figure (9.4)

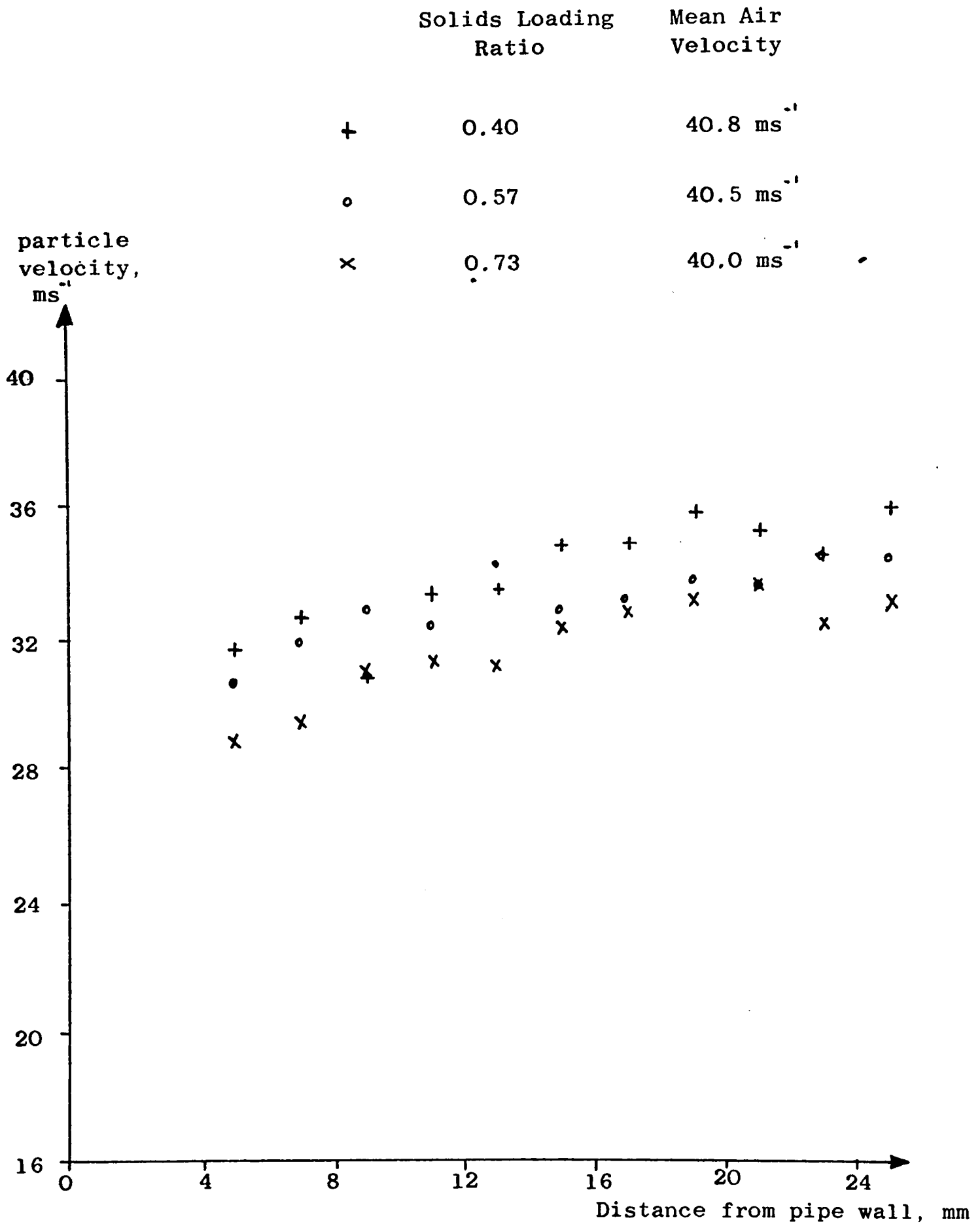

PARTICLE VELOCITY PROFILES, RUN C4, WITH UNSIEVED SAND

Figure (9.5)

	Solids Loading Ratio	Mean Air Velocity
o	0.22	15.5 ms^{-1}
×	0.66	16.7 ms^{-1}
□	1.11	16.7 ms^{-1}
+	1.56	16.7 ms^{-1}
△	2.04	16.4 ms^{-1}
▽	2.51	16.2 ms^{-1}

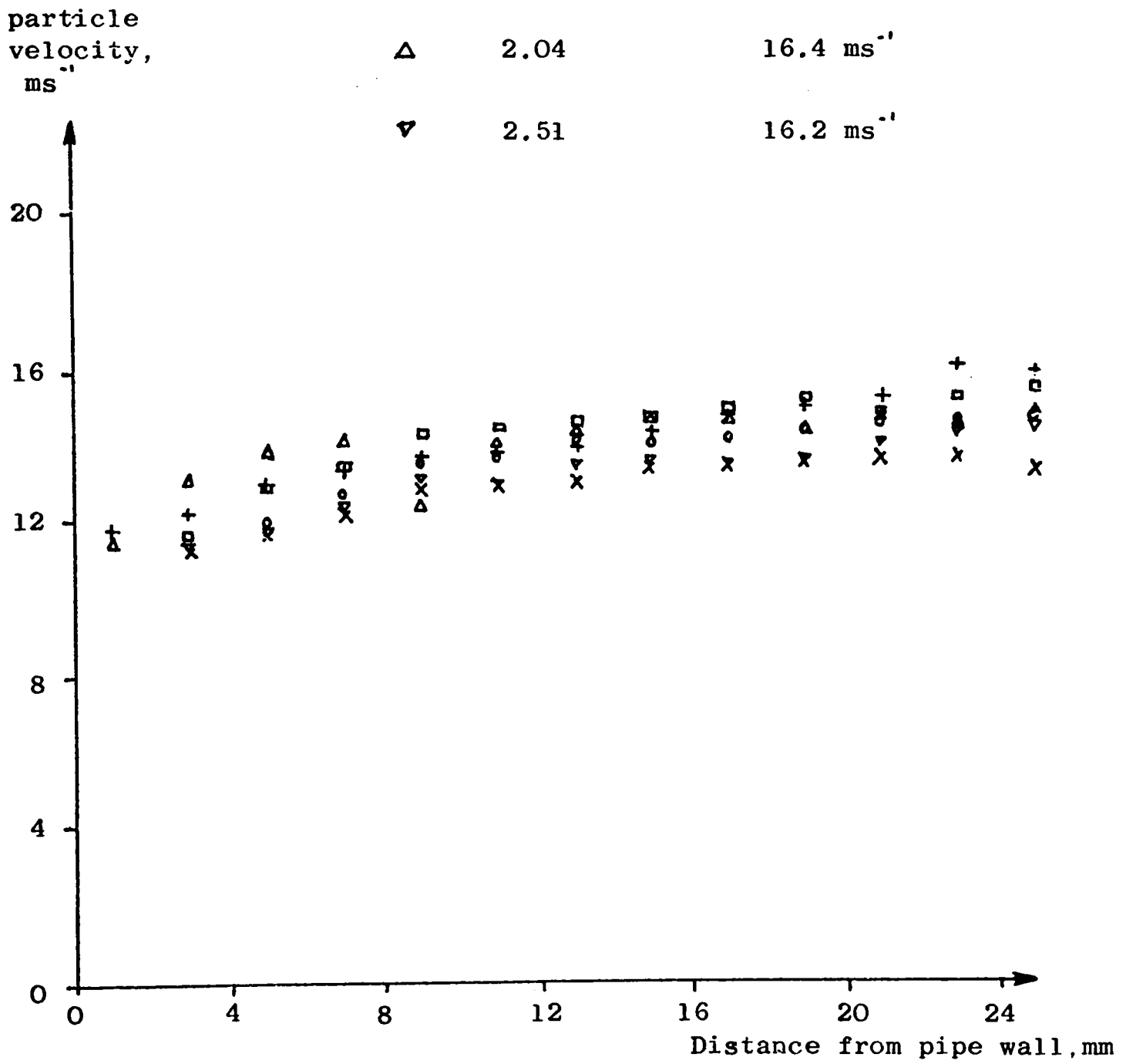

PARTICLE VELOCITY PROFILES, RUNS CA1, WITH SIEVED (300-355 μm) SAND

Figure (9.6)

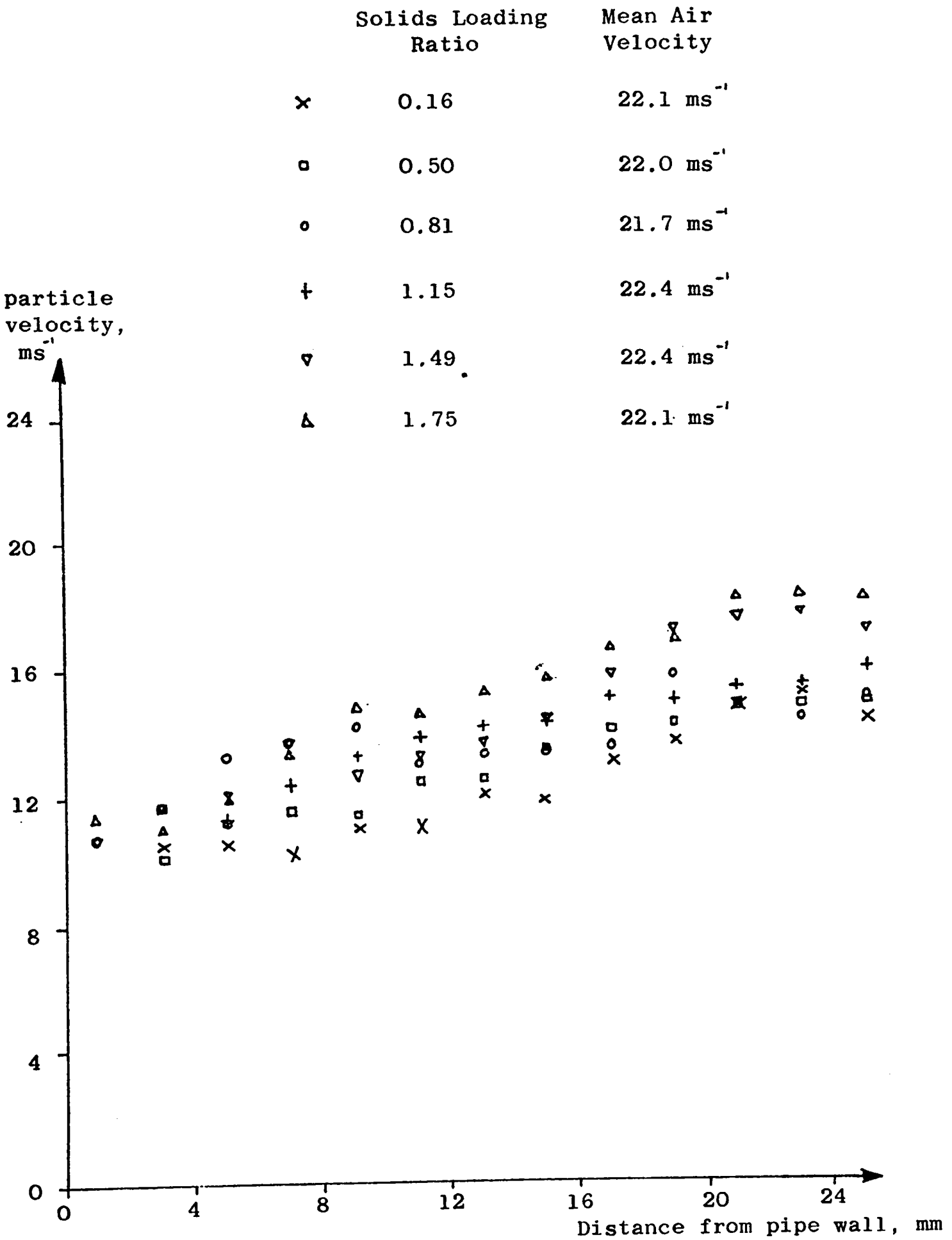

PARTICLE VELOCITY PROFILES, RUNS CA2, WITH SIEVED (300-355 μm) SAND

Figure (9.7)

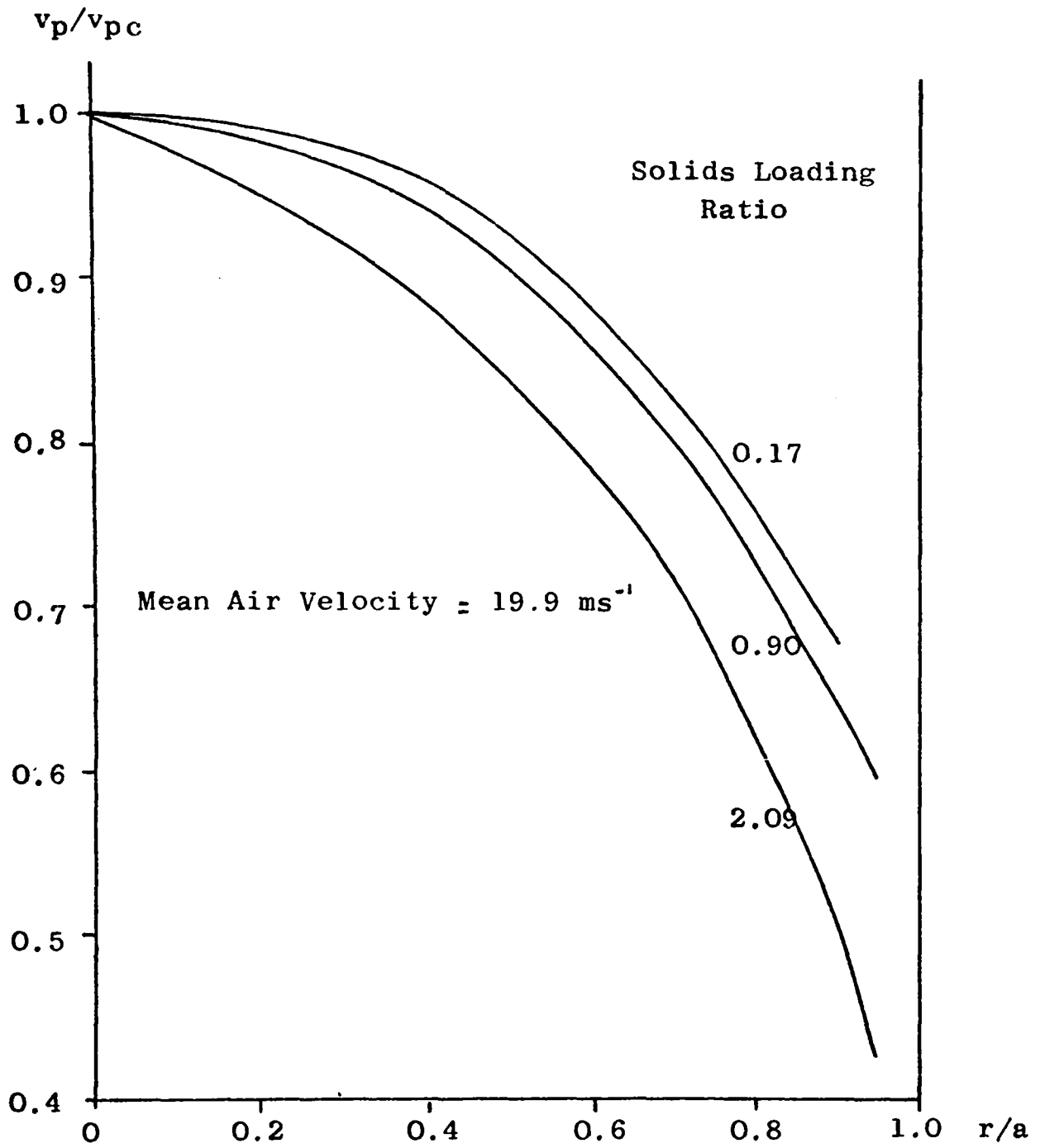

VELOCITY PROFILES FOR UNSIEVED SAND
AT CONSTANT AIR VELOCITY

Figure (9.8)

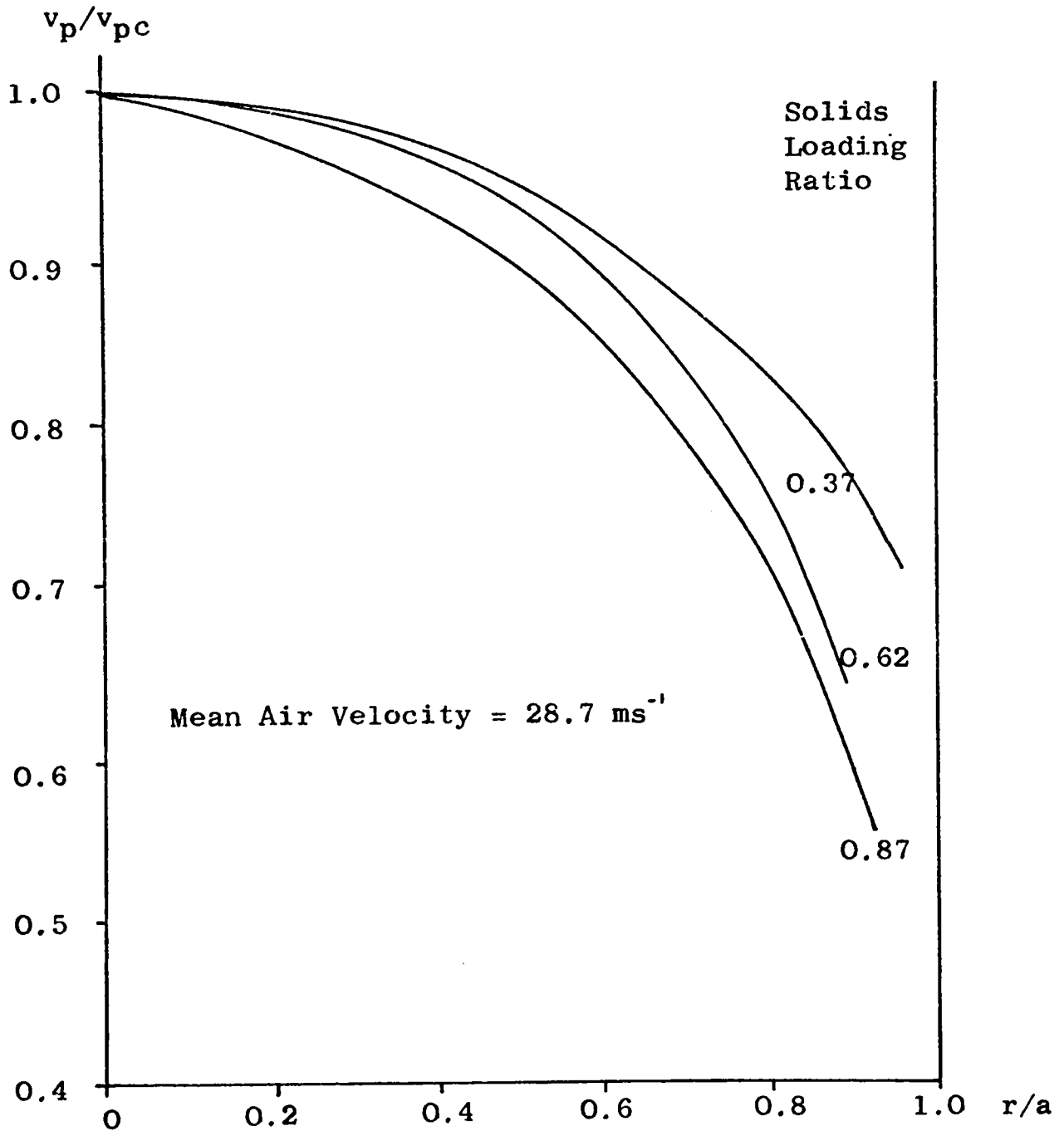

VELOCITY PROFILES FOR UNSIEVED SAND
AT CONSTANT AIR VELOCITY

Figure (9.9).

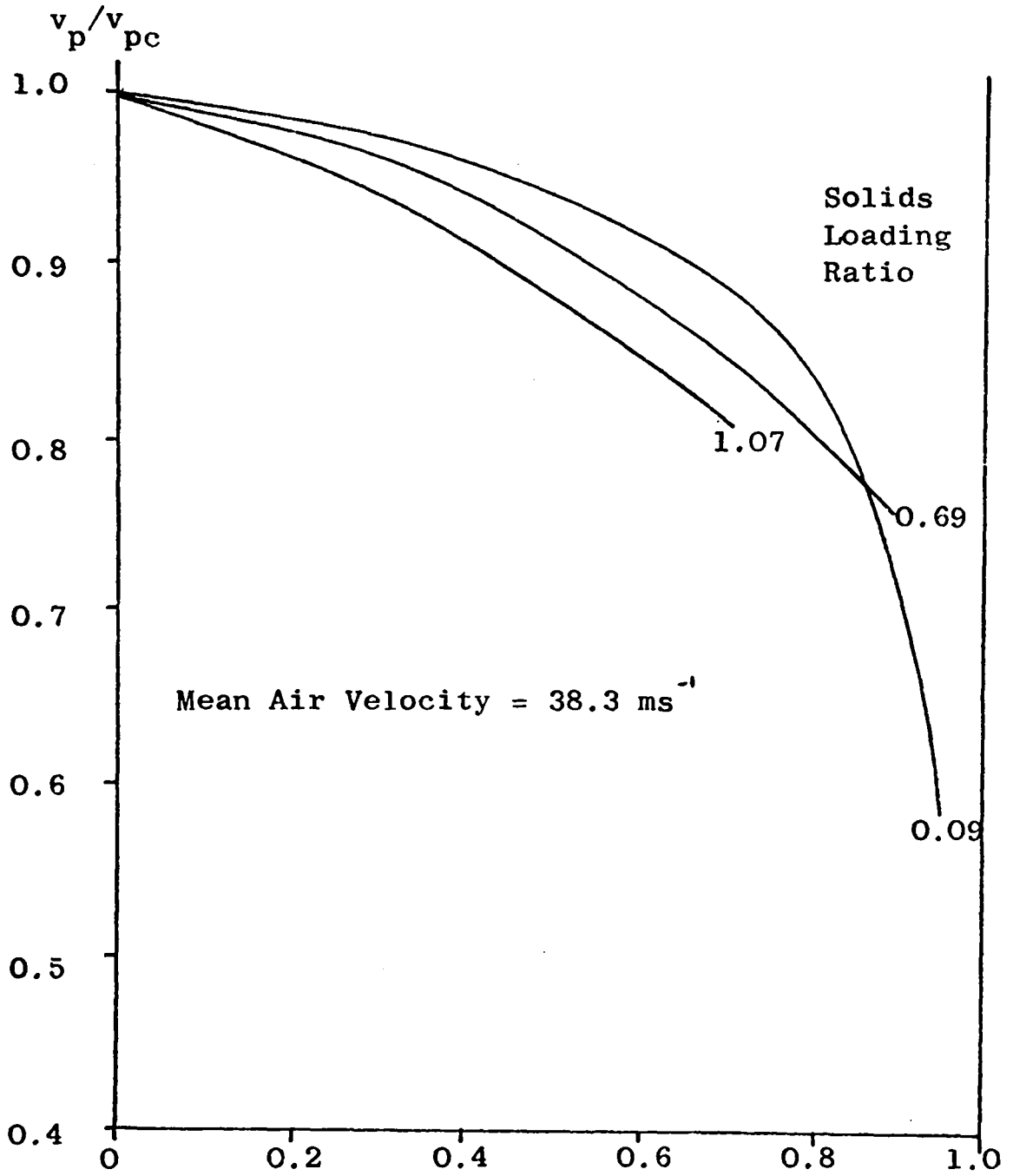

VELOCITY PROFILES FOR UNSIEVED SAND
AT CONSTANT AIR VELOCITY

Figure (9.10)

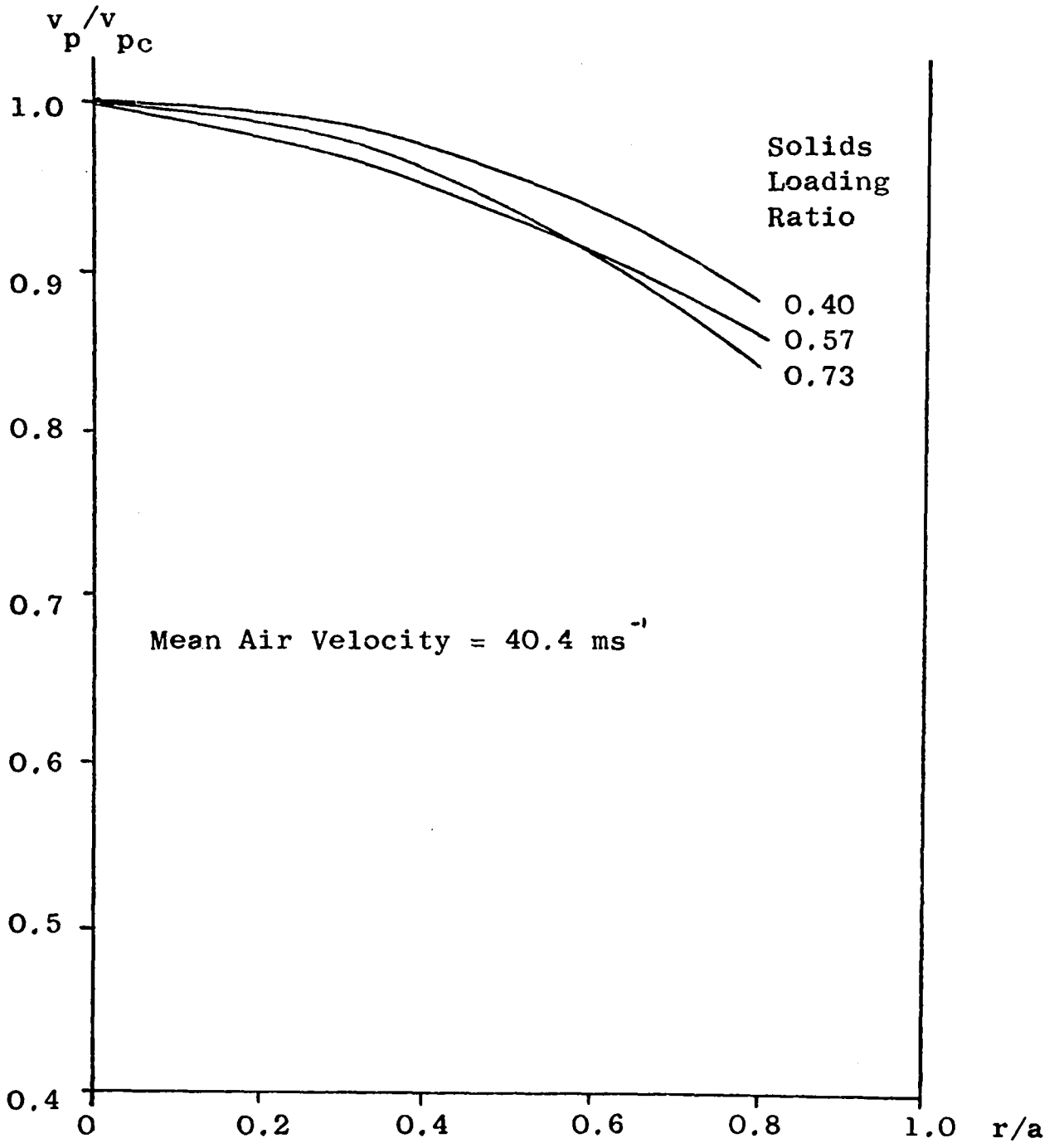

VELOCITY PROFILES FOR UNSIEVED SAND
AT CONSTANT AIR VELOCITY

Figure (9.11)

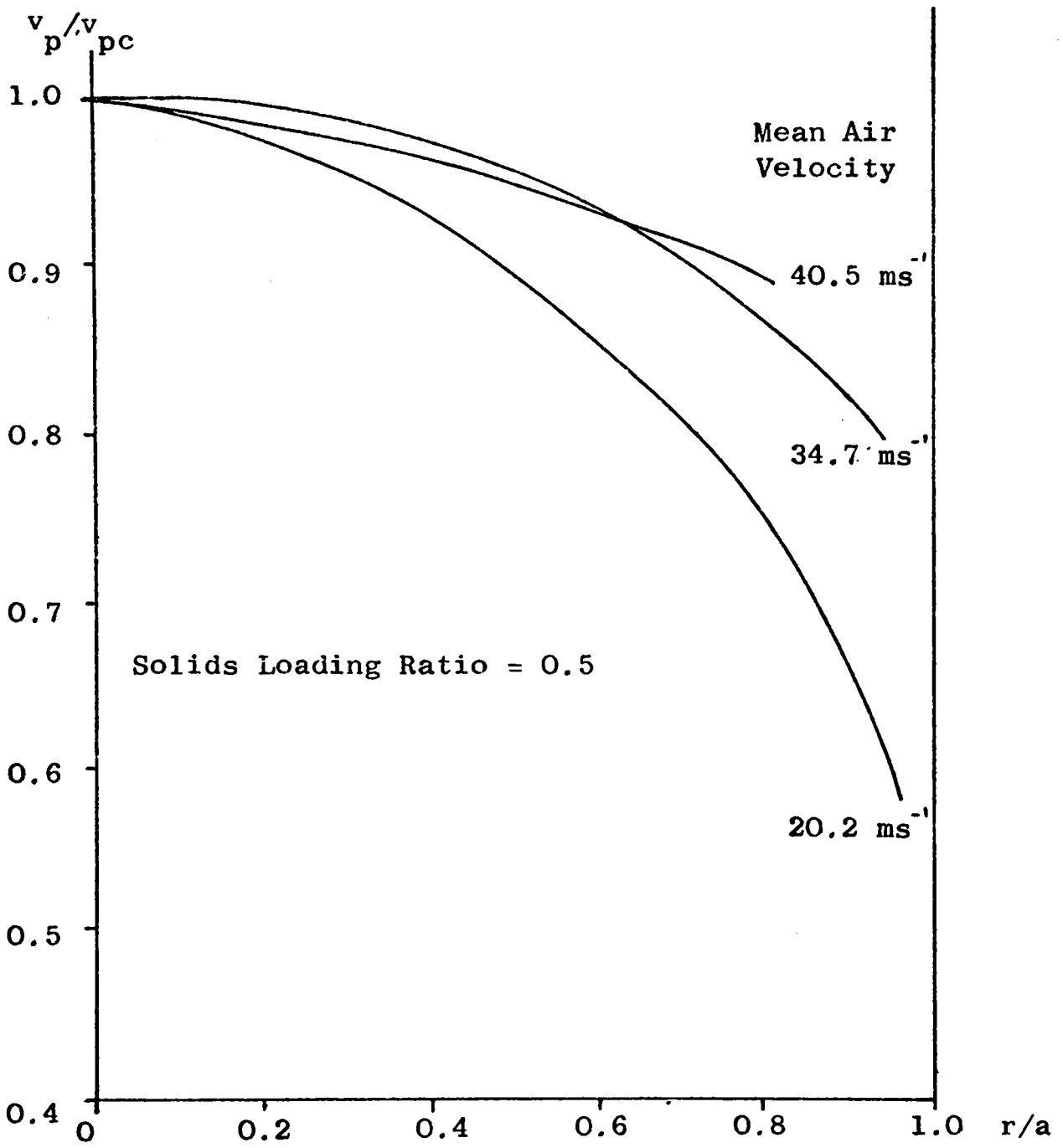

VELOCITY PROFILES FOR UNSIEVED SAND
AT CONSTANT SOLIDS LOADING RATIO

Figure (9.12)

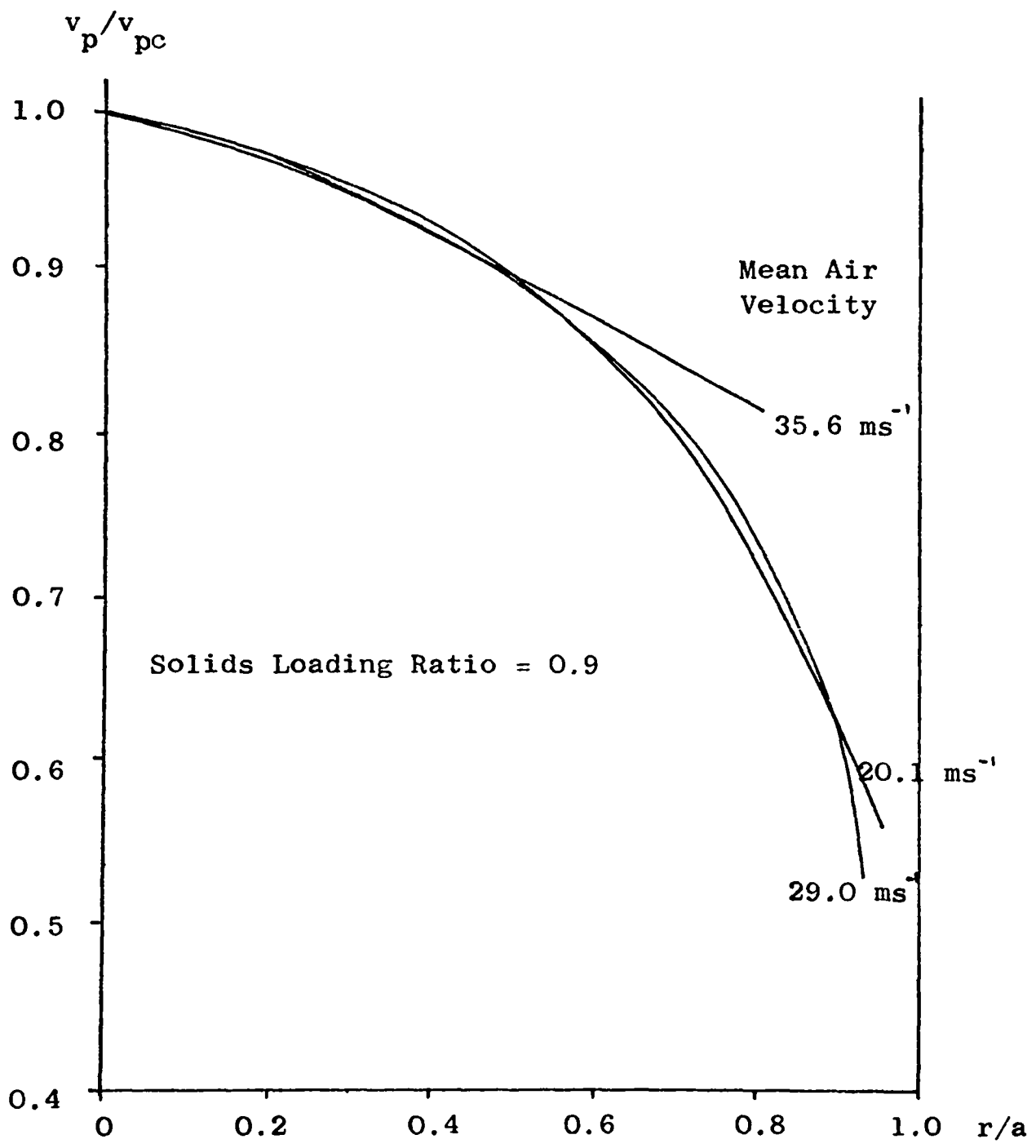

VELOCITY PROFILES FOR UNSIEVED SAND
AT CONSTANT SOLIDS LOADING RATIO

Figure (9.13)

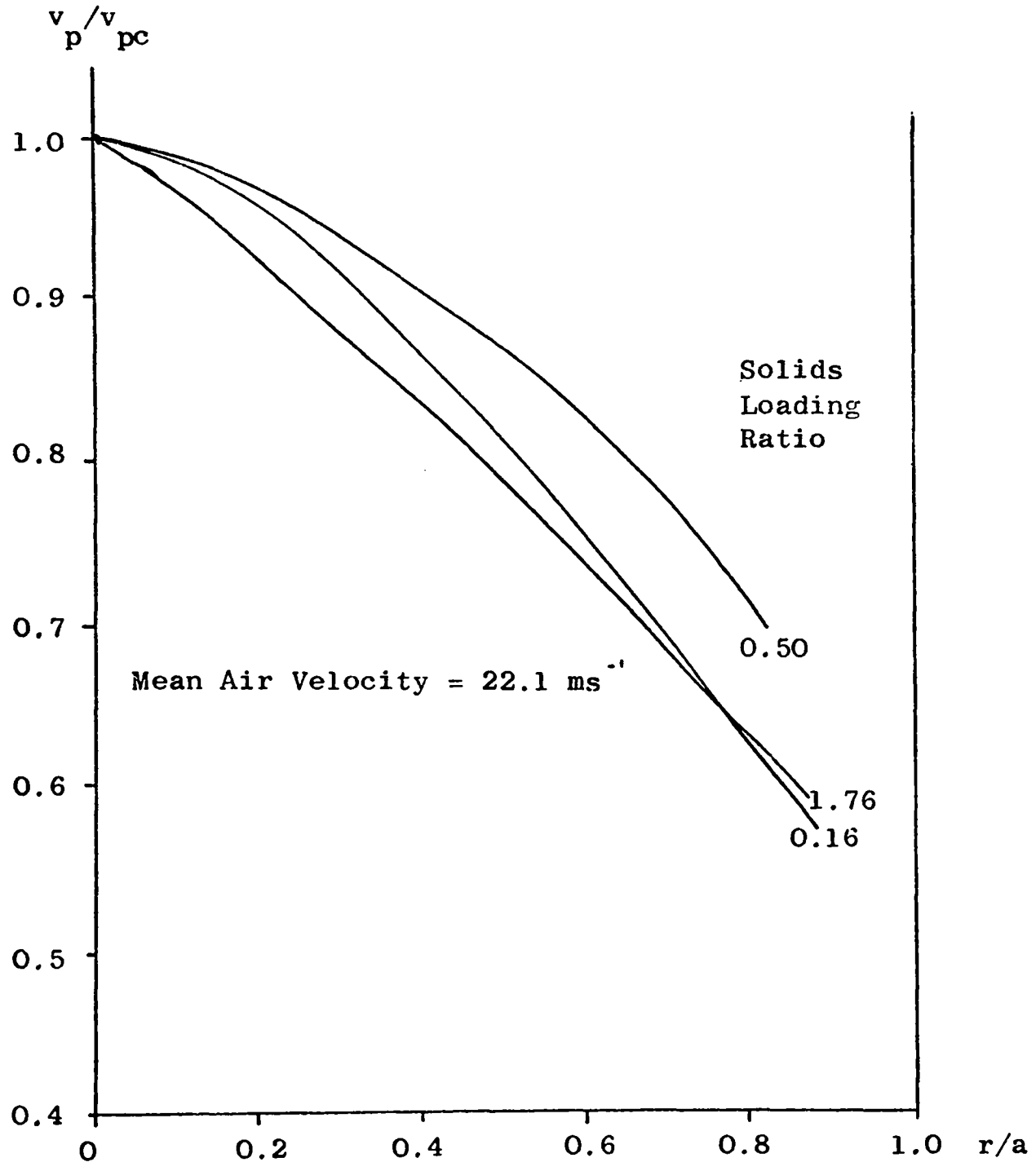

VELOCITY PROFILES FOR SIEVED (300-355 μm) SAND
AT CONSTANT AIR VELOCITY

Figure (9.14)

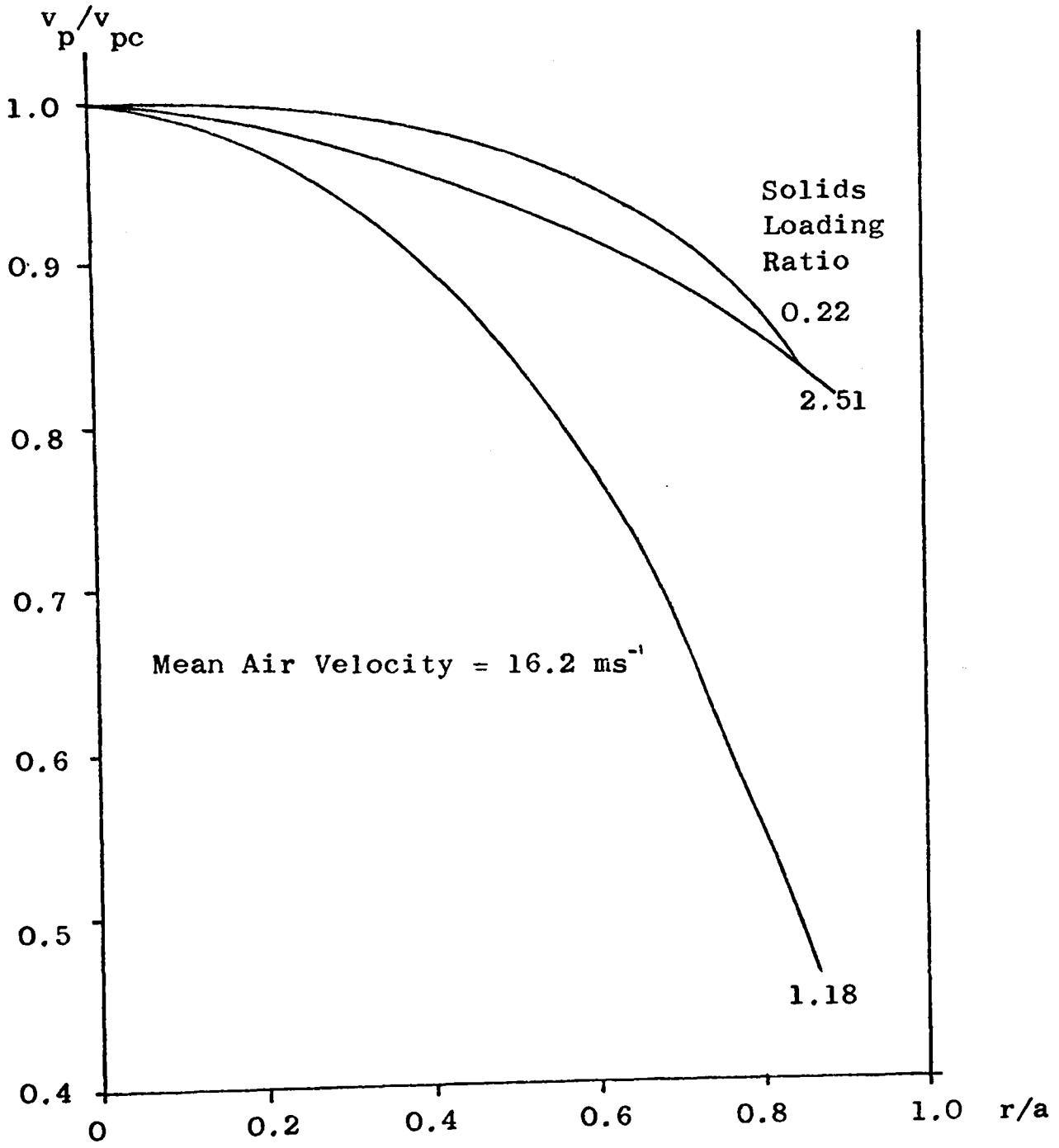

VELOCITY PROFILES FOR SIEVED (300-355 μm) SAND
AT CONSTANT AIR VELOCITY

Figure (9.15)

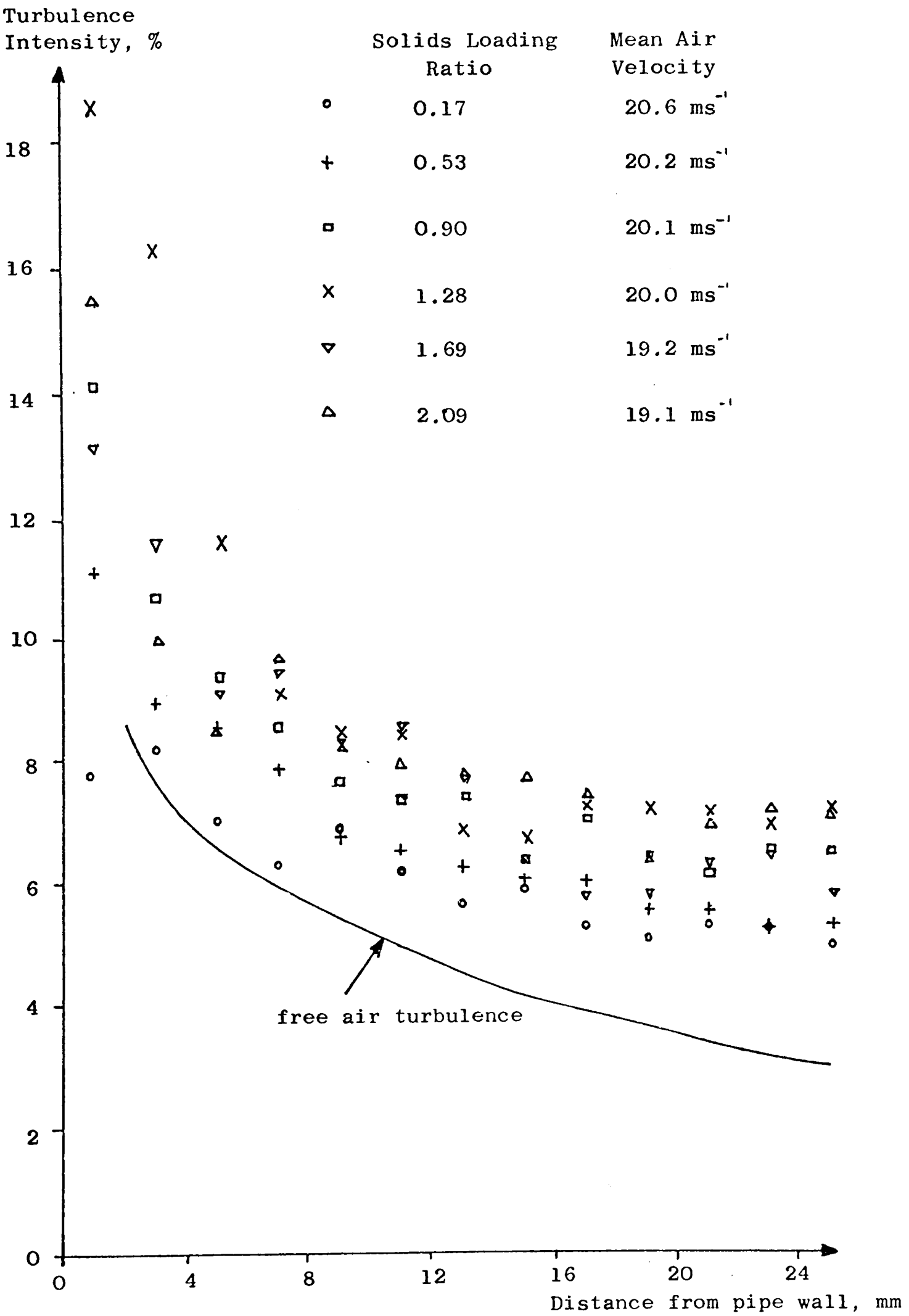

PARTICLE TURBULENCE PROFILES, RUNS C1, FOR USIEVED SAND

Figure (9.16)

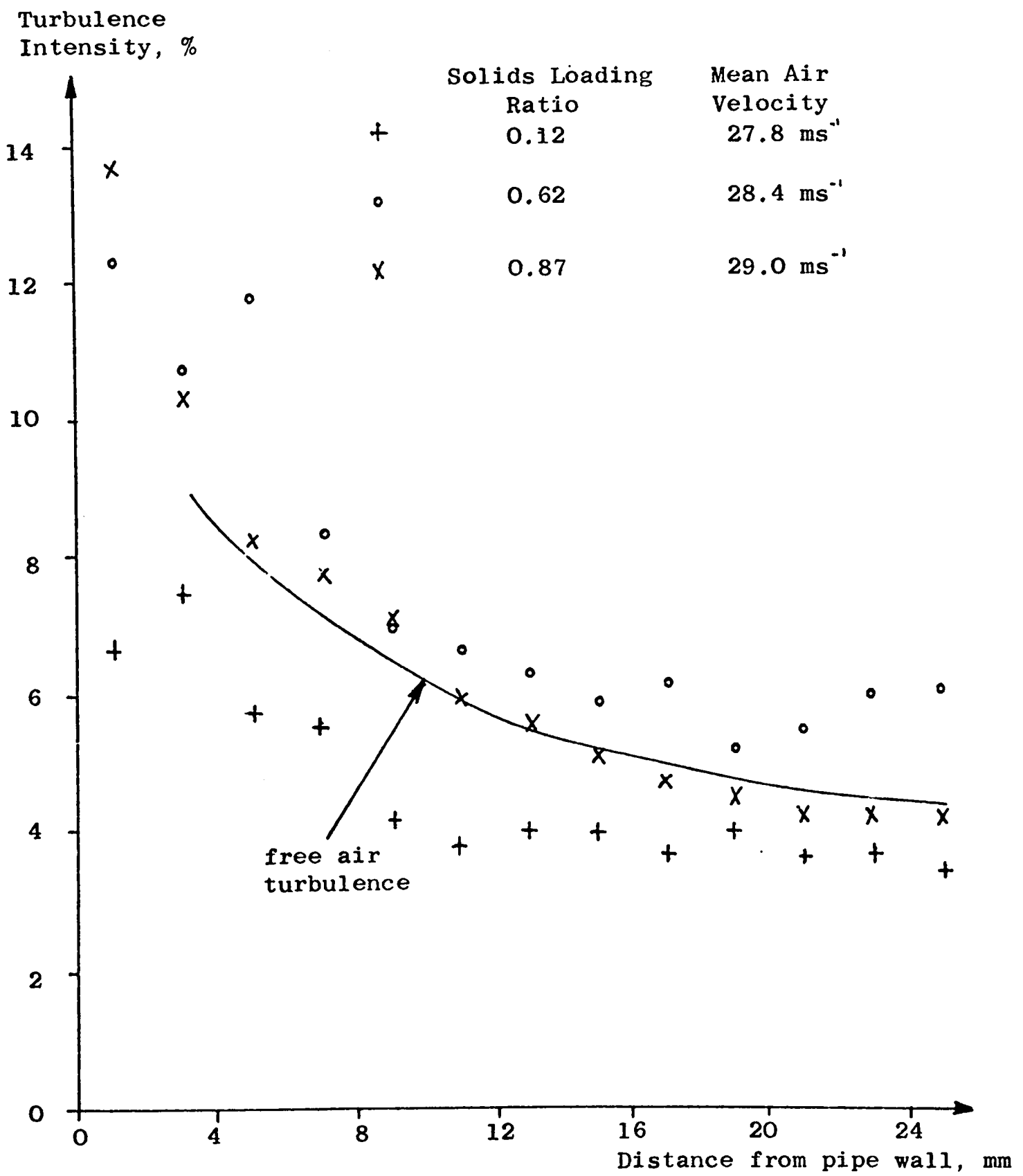

PARTICLE TURBULENCE PROFILES, RUNS C2, FOR UNSIEVED SAND

Figure (9.17)

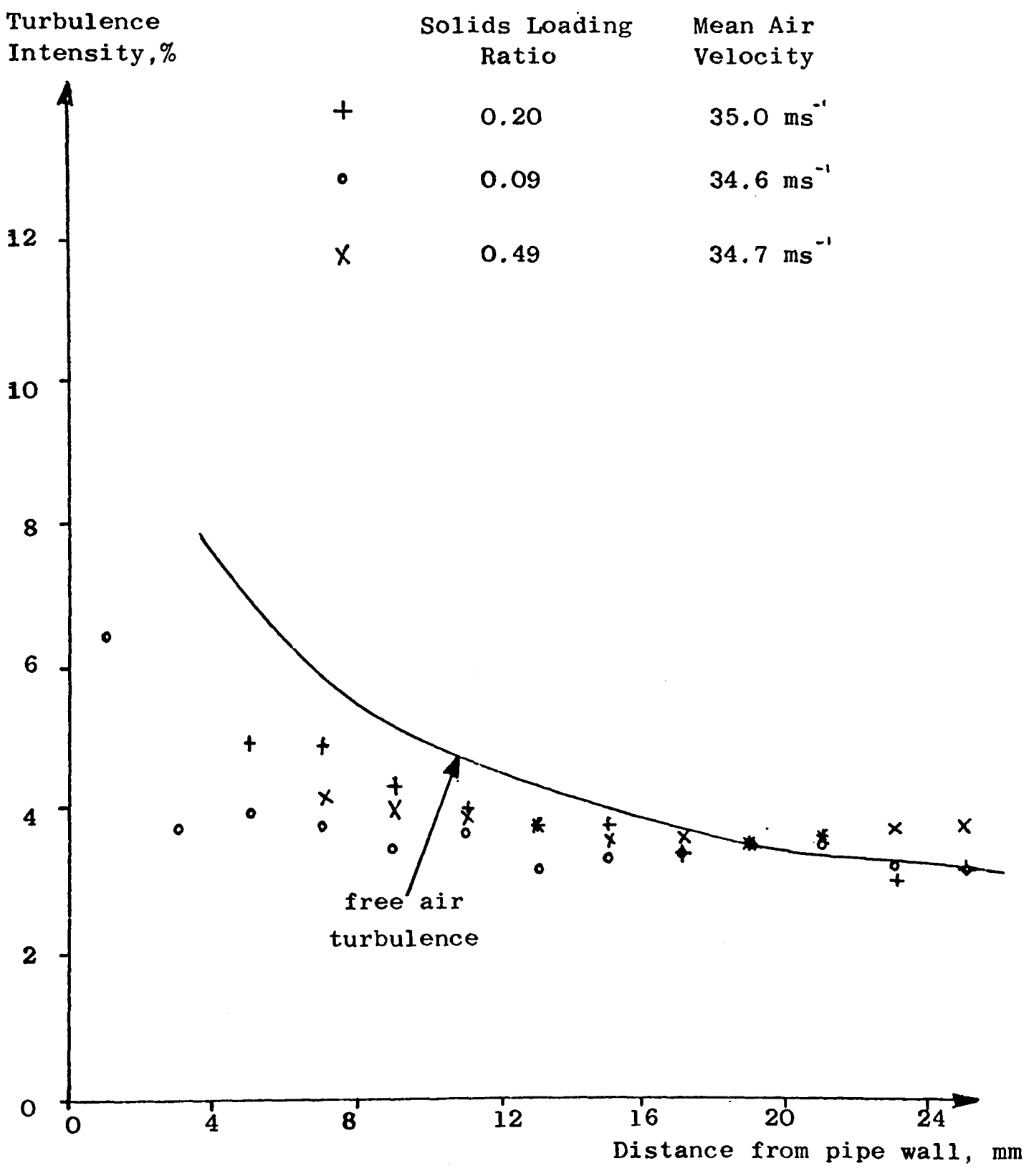

PARTICLE TURBULENCE PROFILES, RUNS C3, FOR UNSIEVED SAND

Figure (9.18)

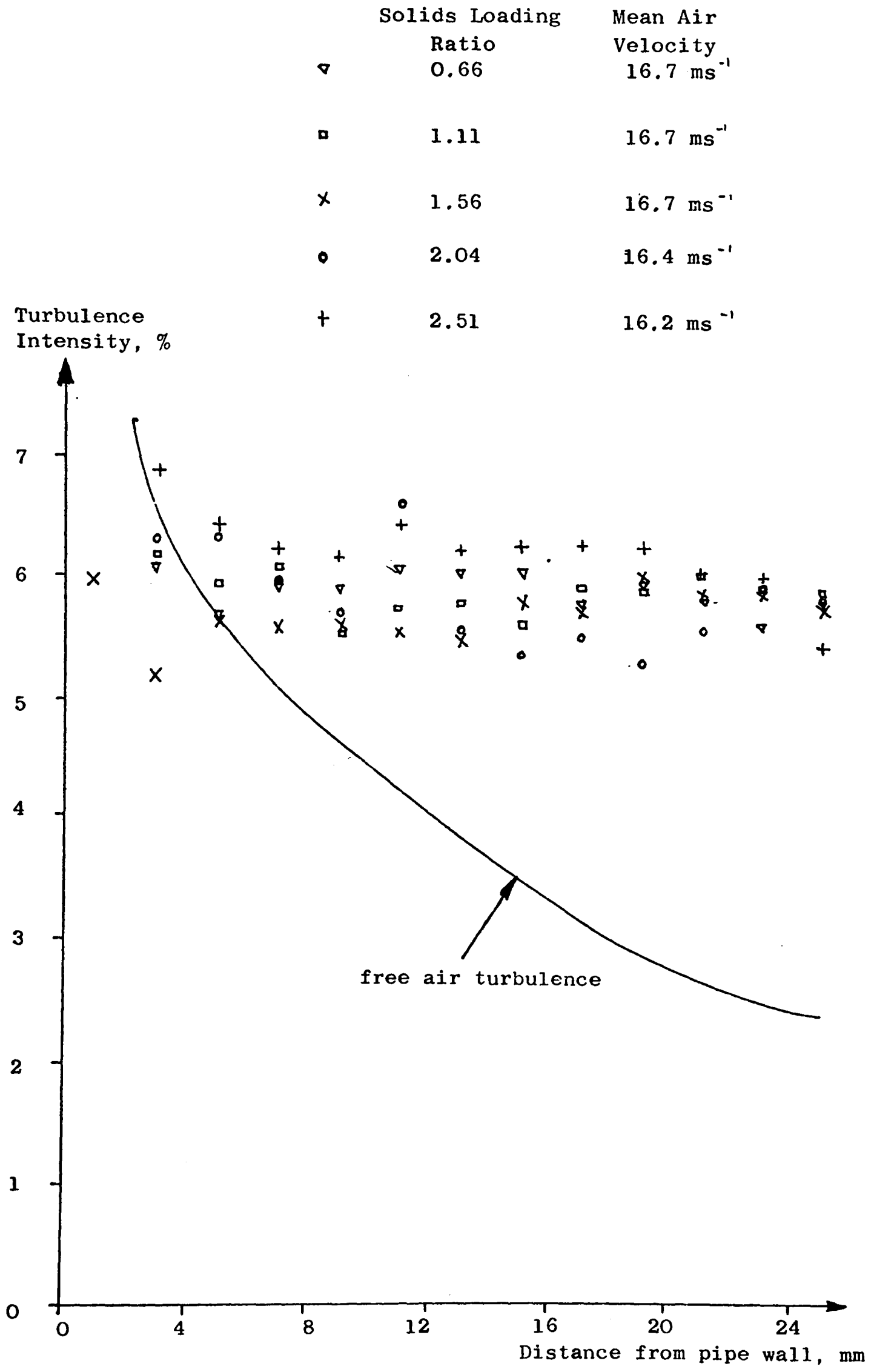

PARTICLE TURBULENCE PROFILES, RUNS CA1,
FOR SIEVED (300-355 μm) SAND

Figure (9.19)

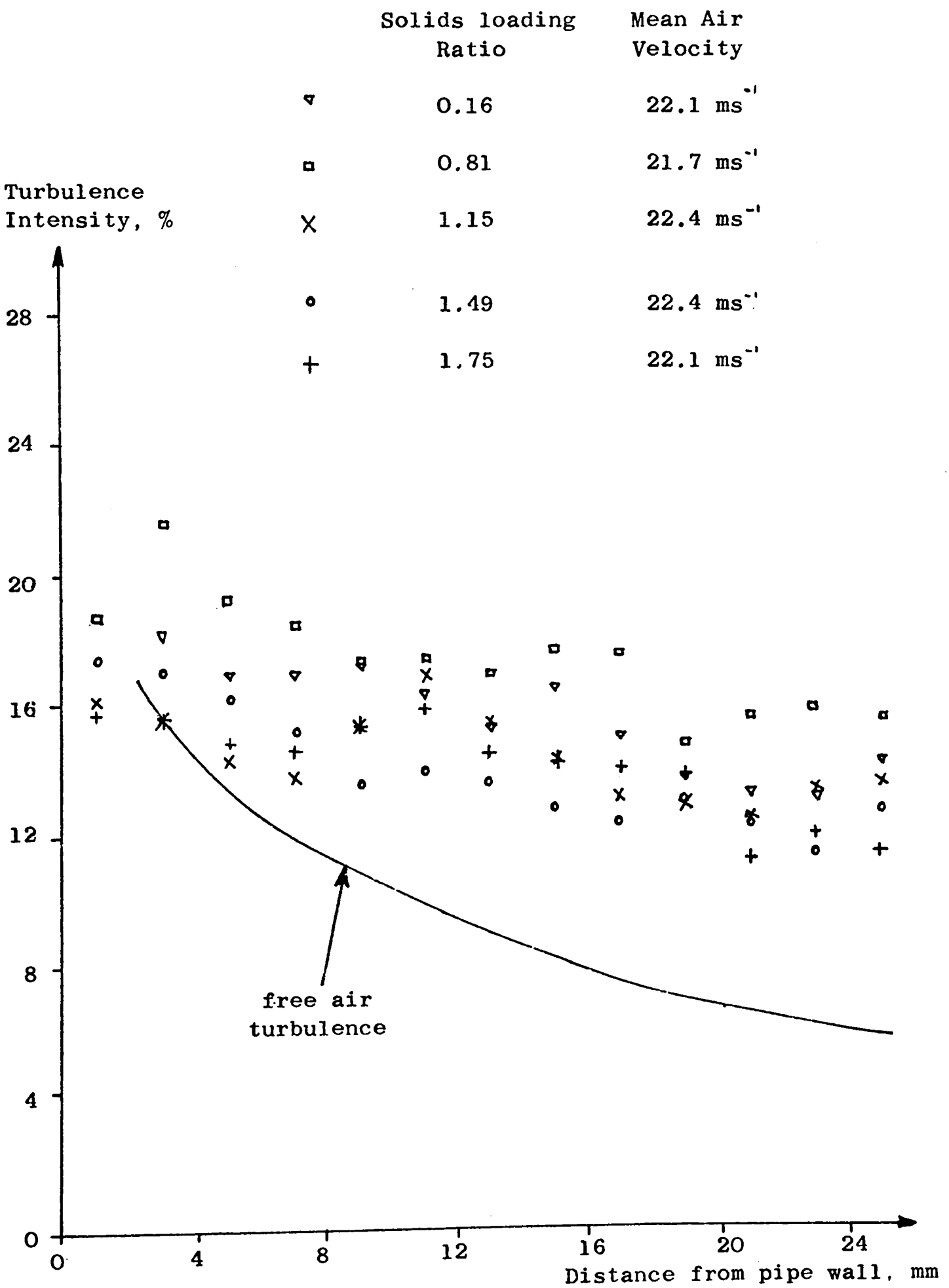

PARTICLE TURBULENCE PROFILES, RUNS CA2,
FOR SIEVED (300-355 μm) SAND

Figure (9.20)

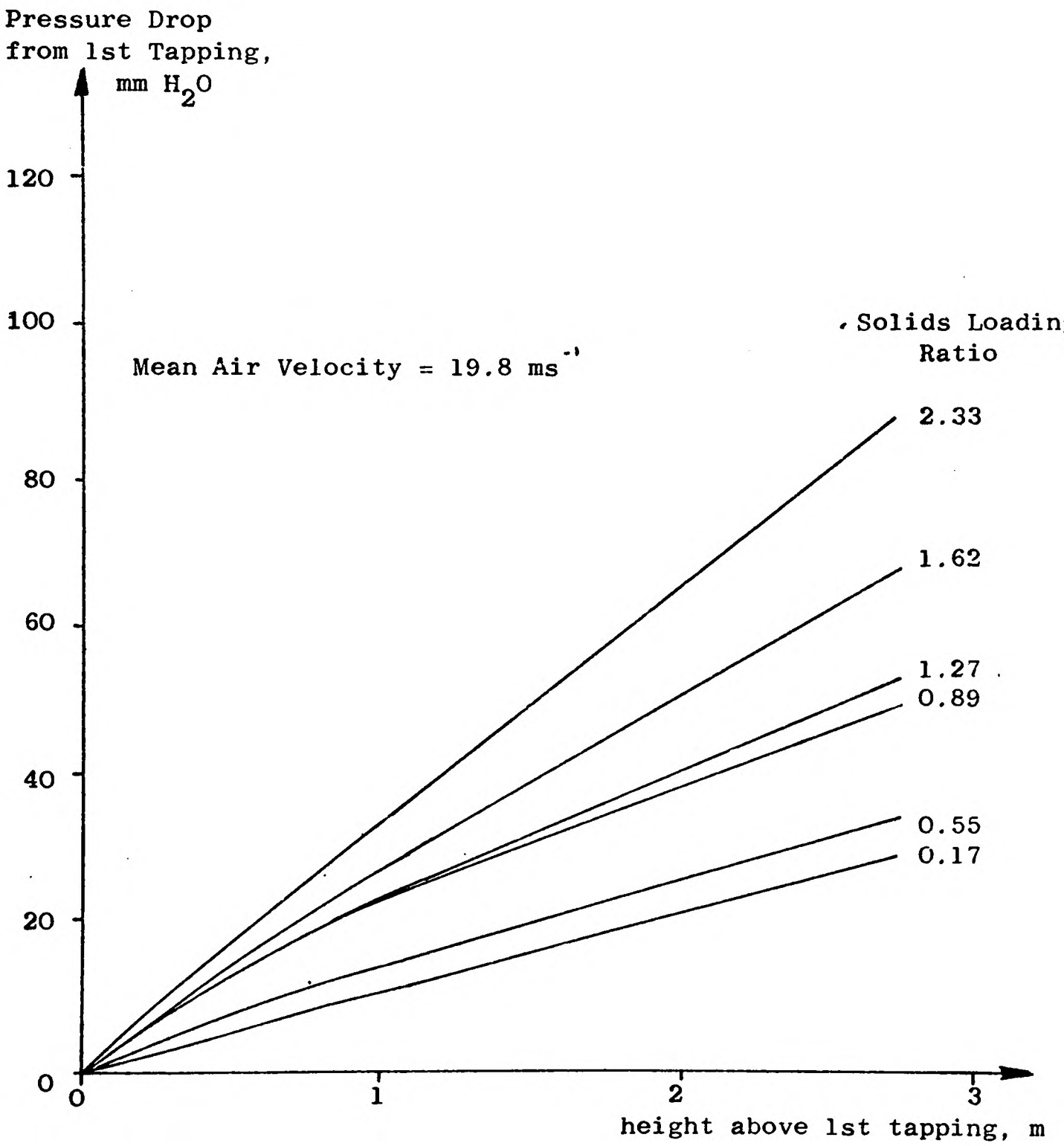

PRESSURE DROP MEASUREMENTS FOR UNSIEVED SAND

Figure (9.21)

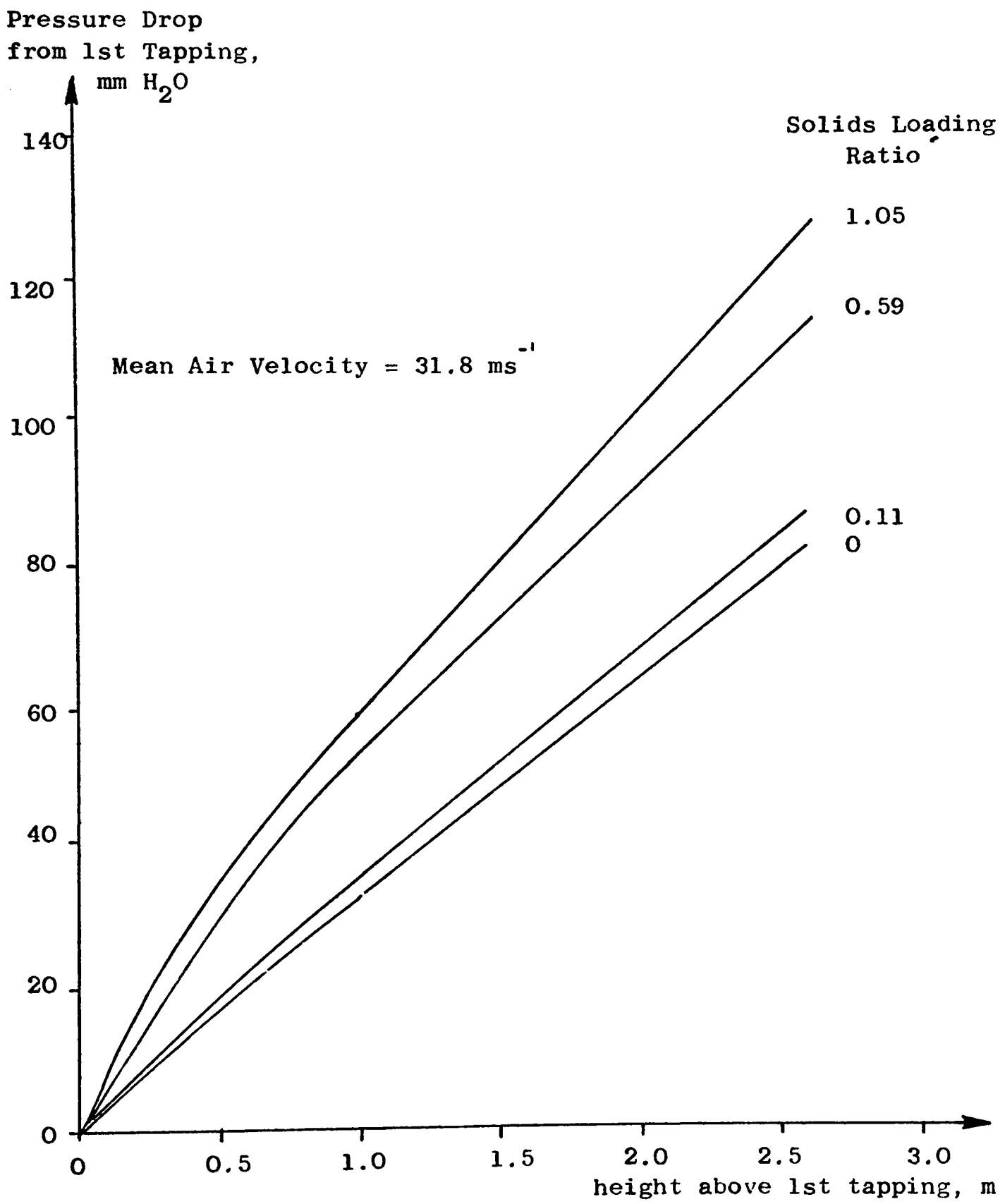

PRESSURE DROP MEASUREMENTS FOR UNSIEVED SAND

Figure (9.22)

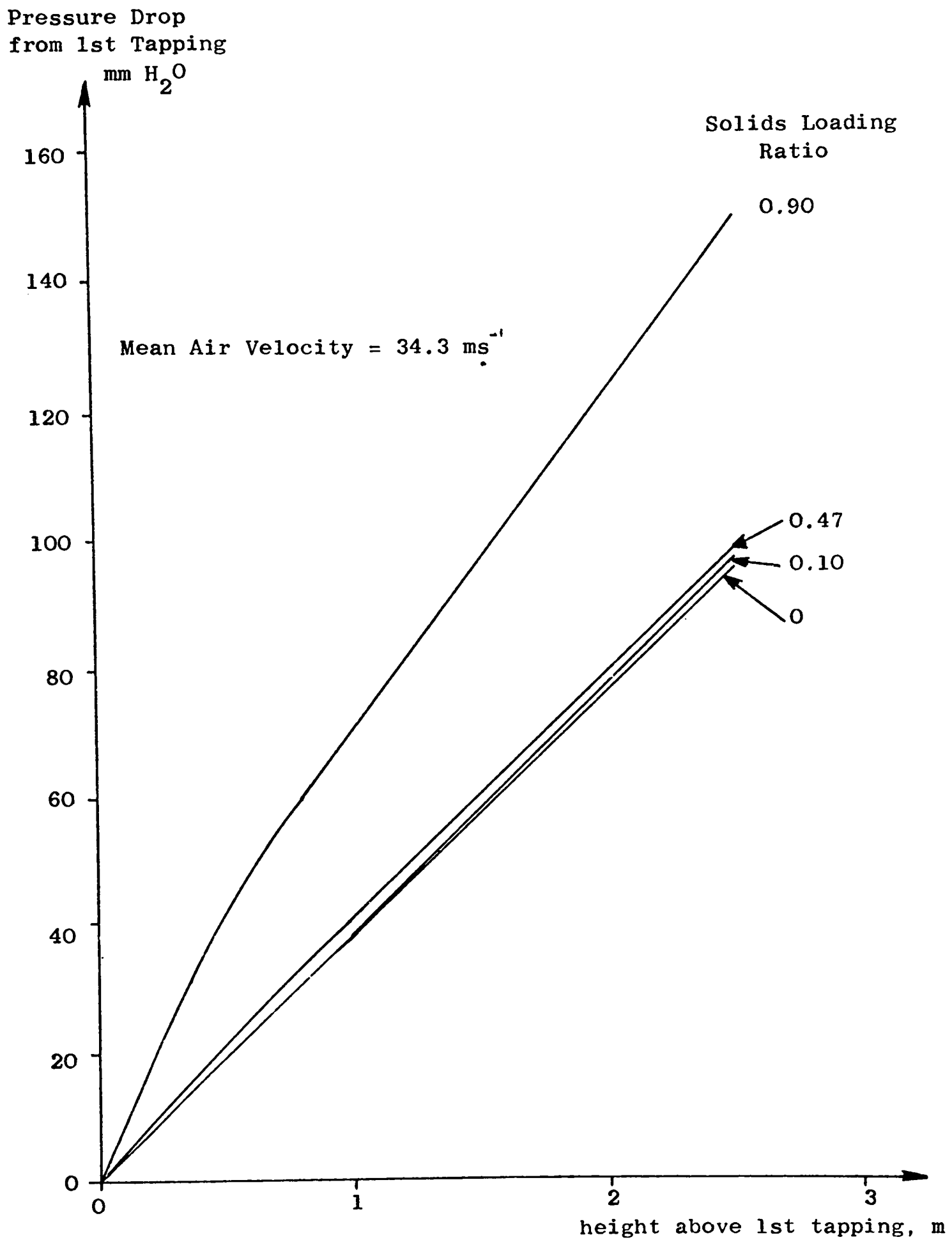

PRESSURE DROP MEASUREMENTS FOR UNSIEVED SAND

Figure (9.23)

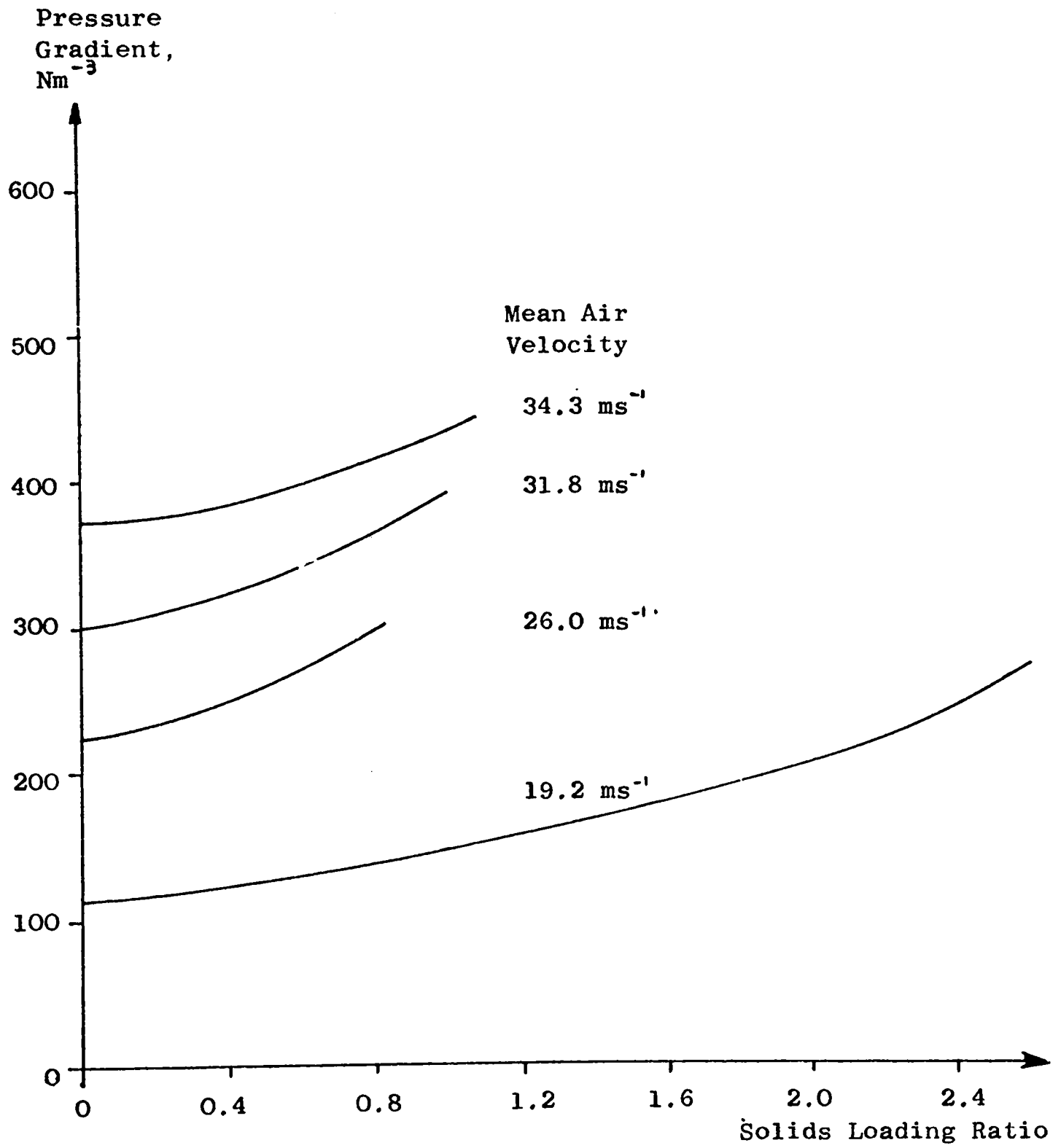

VARIATION OF PRESSURE GRADIENT WITH SOLIDS LOADING RATIO

Figure (9.24)

CHAPTER 10

THE BEHAVIOUR OF AIR-SOLID FLOWS

10.1 Introduction

Chapters 8 and 9 described the investigations undertaken in this project into the properties of dilute phase air-solid suspensions flowing upwards in a vertical glass pipe, 50 mm in diameter. This chapter collates these measurements and compares them with work in the published literature. Although there is insufficient data available to produce a model capable of accurately predicting the behaviour of an air-solid flow, it is possible to comment critically on some of the approximations made in producing a number of theoretical models.

The relationships between the various parameters of the flow are explored. Since all measurements were made under similar flow conditions, it should be possible to establish such relationships. However, care must be taken when applying the results obtained in this project to other pneumatic conveying systems, since the effect of many variables, such as the pipe diameter, was not investigated in this study.

10.2 Particle Velocity

10.2.1 Particle Velocity Profiles The ballotini velocity profiles shown in figures (8.6) to (8.11) are flatter than those of the free air, given in figure (10.1), whereas the sand velocity profiles in figures (9.8) to (9.15) are similar in shape to the air profiles. As the solids loading ratio was increased, the particle velocity profiles in the ballotini flow became flatter, whilst those in the sand flow became less flat. Because there was a large scatter in the results it was

difficult to differentiate between real trends and inaccuracies in the measurements. It is likely that the ballotini would follow the air flow less faithfully than the sand because of the greater momentum of the larger particles. Also the size distribution of the used ballotini shown in figure (4.13) reveals that the solid was composed of relatively unbroken particles together with fines from completely broken particles, whereas the used sand [see figure (4.15)] consisted of a wide spectrum of particle sizes. The fines in the ballotini flow were too small to contribute to the measured Doppler frequency, so that only the complete particles contributed to the measured velocity, whilst in the sand flow particles with diameters considerably less than the mean diameter could contribute to the measured velocity, and these smaller particles would follow the air flow more closely than larger particles.

Soo et al (1964) suggested that the particle velocity profile could be described by the equation :-

$$\frac{v_{pr} - v_{pw}}{v_{pc} - v_{pw}} = \left(\frac{x}{a}\right)^{1/m} \qquad (10.1)$$

where the subscripts r, c and w indicate the value at radius, r, the pipe axis, and wall respectively. This expression is a modification of the standard profile for a single phase fluid given in equation (7.1), and it takes account of the non-zero particle velocity at the wall, v_{pw}. However, no allowance is made in equation (10.1) for the finite size of the particles, which means that the closest the particles get to the wall is d/2. For this reason, Reddy and Pei (1969) further modified the equation to give :

$$\frac{v_{pr} - v_{pw}}{v_{pc} - v_{pw}} = \left(\frac{x - d/2}{a - d/2}\right)^{1/m} \qquad (10.2)$$

where d is the mean diameter of the particles and m is a constant.

A comparison was made between equation (10.2) and the measured particle velocity profiles. Some of the typical comparisons are shown in figures (10.2) to (10.4) and (10.6) and (10.7). These diagrams are logarithmic plots of equation (10.2). For the profile to fit the expression the measuring points should be in a straight line. The particle velocity profiles for the ballotini see figures (10.2) to (10.4) fit equation (10.2) fairly well. The value of m, however, does not show any trends within the range of flows tested. Chandok and Pei (1971) found that m varied linearly with the particle Reynolds number, Re_p, defined by the equation :-

$$Re_p = \rho_a(\bar{v}_a - \bar{v}_s)\, d/\mu \qquad (10.3)$$

where $(\bar{v}_a - \bar{v}_s)$ is the average slip velocity between the air and the particulate phases of the flow, and ρ_a and μ are the air density and viscosity respectively. A plot of m against Re_p for the ballotini flow, given in figure (10.5), shows no linearity. However, it is unlikely that the linear equation for the dependence of m on the particle Reynolds number could be complete since this would predict a zero value for m, implying a completely flat particle velocity profile.

The particle velocity profiles for the sand did not fit equation (10.2), as shown in figures (10.6) and (10.7). The results disagree with the theoretical curve towards the edge of the pipe, where the curvature of the measured profile was greater than that predicted. This divergence from the predicted curve may have been caused by the angular shape of the sand particles, since the formula was derived for spherical particles. Both Reddy and Pei (1969) and Chandok and Pei (1972) measured particle velocity profiles that fitted equation (10.2) in flows conveying spherical glass balls, similar to the ballotini used in this investigation. However, Birchenough (1975), conveyed alumina particles and found that the measured profiles disagreed with

the predicted profile at the edge of the pipe. It seems, therefore, that equation (10.2) holds quite well for spherical particles, but not for non-spherical particles such as sand and alumina.

10.2.2 Slip Velocity The slip velocity is the difference in the velocities of the conveying fluid and the solid particles. Since the velocity profiles of the air and solid phases were found to be different in shape, the slip velocity varied across the pipe. The greatest slip was found at the centre of the pipe and decreased towards the edge of the pipe. Since no velocity measurements could be made in either phase close to the pipe wall, the slip velocity in this region was unknown, and could possibly have had a negative value. These results contrast strongly with the results of Soo et al (1964), who found zero slip velocity at the centre of the pipe in flows with similar particles and mass flow rates close to those used in the present investigation. Following this paper, Peskin and Dwyer (1964) assumed zero slip velocity at the centre of the pipe in order to calculate the velocity profile of the particles with maximum slip velocity at a radius about half that of the pipe, and their results are therefore rather suspect.

The average slip velocity was taken as the difference between the average velocity of the air and solid phases ($\bar{v}_a - \bar{v}_s$) rather than the local slip velocity averaged across the pipe. The variation of the slip velocity with the solids loading ratio is shown in figures (10.8),(10.9) and (10.10). The variation was found to be approximately linear in all cases, but while for air-ballotini flows and flows conveying unsieved sand, the average slip velocity increased slightly with increasing solids loading ratio, the opposite trend was found for the flow conveying sieved sand. It is difficult to suggest a reason for this behaviour. Birchenough (1975) found that the mean slip velocity increased slightly

with solids loading ratio in an air-alumina flow with similar solids loading ratios to the present tests, and van Zuilichen et al (1973) also found that the slip velocity increased with solids loading ratio, with values of the solids loading ratio in the range (10 to 32). Both Reddy and Pei (1969) and Chandok and Pei (1971) found that the centre slip velocity increased also, but Kramer and Depew (1972) found little variation in the average slip velocity with solids loading ratio. The centre slip velocity in the present tests were found to be roughly proportional to the average slip velocity, with a constant of proportionality of about 1.5. Uncertainty in the slope of the curves measured might have been partly caused by variations in the mean conveying air velocity, since the slip velocity was found to vary as the square of the conveying velocity. Also, since the particle velocity was not measured at the edge of the pipe, the profile at this point had to be estimated for mean velocity calculations which were made using the computer program described in appendix A-I.

The variation of the slip velocity with Froude number $Fr = v_a^2/gD$ is given in figures (10.11) and (10.12). The curves are quite linear, which indicates that the slip velocity varies as the square of the overall mean air velocity. The results of Birchenough (1975) for measurements in an air-alumina flow are also included, and they are also linear. At a solids loading ratio of 0.5, the slip velocity increases with increasing particle size, as expected, but at a solids loading ratio of 1, the slip velocity for the sand is greater than that of the ballotini above an overall mean air velocity of 28 ms^{-1}. The reason for this is unclear, but it may be related to the non-spherical shape of the sand particles.

The terminal velocity of the particles when unaffected by inter-particulate interaction was calculated as follows:-

The drag force, F_D, on a particle with a cross-section normal to the direction of motion of A, moving at velocity v in a fluid, density ρ_f, of infinite extent is :-

$$F_D = \tfrac{1}{2}\rho_f \, v^2 \times A \times C_D \qquad (10.4)$$

where C_D is the drag coefficient. If the particle is falling at its terminal velocity v_τ, the force acting on it due to gravity will exactly balance the drag force and buoyancy force acting on the particle. This gives the equation for the terminal velocity of a sphere :-

$$v_\tau = \left[\frac{4}{3} d \, \frac{(\rho_f - \rho_s)}{\rho_f \, C_D} \right]^{\frac{1}{2}} \qquad (10.5)$$

However, the drag coefficient, C_D, is dependent on the particle Reynolds number Re_p except in the region where $Re_p > 500$, when C_D is approximately constant (Newton's Law). An estimate of the terminal velocity was obtained by substituting an assumed value of the drag coefficient into equation (10.5). Using this value, an estimate of the particle Reynolds number was calculated, and a better estimate of the drag coefficient was found from the graph, giving the relation between C_D and Re_p in an infinite, non-turbulent fluid, from Boothroyd (1971) [see figure (10.15)]. This process was repeated until the value of the terminal velocity could not be improved upon.

The terminal velocities of the particles used in the project were calculated by this method, taking the diameter as the numerical mean for the unsieved solid, since this will give the maximum likely terminal velocity. The values are given in table (10.1).

Solid	Mean Particle Diameter	Terminal Velocity
Ballotini	455 μm	3.76 ms^{-1}
Sand, unsieved	176 μm	1.12 ms^{-1}
Sand, sieved	366 μm	2.79 ms^{-1}

TABLE (10.1) Terminal Velocities

Except at the lowest mean air velocities, the slip velocities measured in this project were significantly higher than the terminal velocities listed in Table (10.1). This indicates that the turbulence of the conveying fluid and interactions between the particles and the pipe wall and between the particles causes the particles to slow down. Several authors [Leung and Wiles (1976) and Konno and Saito (1969)] equate the slip velocity to the terminal velocity in theoretical derivations of the pressure drop. Peskin and Dwyer (1964) reported an average slip velocity of 1.88 ms^{-1} with an average air velocity of 31 ms^{-1} and a solids loading ratio of 2. This contrasts with a terminal velocity of the particles of 0.391 ms^{-1}, calculated from the physical data given for the spherical particles used. However, although this result agrees with those obtained in the present project, the assumptions made in the particle velocity measurement technique used in this paper make the magnitude of the slip velocity suspect. However, the results of Birchenough (1975), in which more confidence can be placed, also found that in all but the lowest air velocities the measured slip velocities were greater than the calculated terminal velocity of 0.323 ms^{-1} [see figure (10.11)].

10.3 Particle Turbulence Intensity

The particle turbulence intensities shown in figure (8.12) and figure (9.17) to (9.20) all indicate much less variation across the pipe than the free air, with fairly constant turbulence in the core of the flow. There is a tendency for the particle turbulence to increase with solids loading ratio, often to a value at the centre of the pipe greater than that for the free air. This indicates that the increased number density of the particles causes the turbulence intensity to increase, probably because the interparticulate interactions increase. This trend is confirmed by the results of Birchenough (1975) and

Carlson and Peskin (1975). Durst (1978) used an LDV to measure the turbulence intensity of both phases and found the turbulence intensity of the particles in the core of the flow higher than the air turbulence, but the conveying air turbulence in the core of the flow was increased to an even higher value. There is little other work published on particle turbulence measurements. Reddy and Pei (1969) found a constant, unspecified, turbulence intensity across the pipe, as did Eichhorn et al (1964) who gave a value of 30%, which seems very high, but some additional turbulence may have been caused by the large measuring probe.

The range of Reynolds numbers of the flows in which the turbulence intensities could be measured was not sufficiently great for the variation of the turbulence intensity with the air velocity to be ascertained. The turbulence measured in the air-ballotini and air-sand flows are compared in section (9.3).

Soo et al (1956) suggested that the drag coefficient, C_D, could be calculated from the difference between the mean velocity variations of the air and solid phases, but since the air turbulence was not measured whilst conveying solids, it was not possible to test this.

10.4 Pressure Drop Readings

10.4.1 Friction Factor The friction factor in single phase flows in round pipes, diameter D, and full of fluid is defined by the equation:-

$$F_a = \frac{\Delta p_{Fa}}{L} \times \frac{D}{2\bar{v}_a^2 \rho_a} \qquad (10.6)$$

and using this equation the friction factor, F_a, for the free air in the test pipe was calculated. The pressure drop due to the air friction, Δp_{Fa}, was found by subtracting the static head of air, Δp_{ha}, from the measured pressure gradient in fully developed free air flow. The static head pressure gradient was found from the equation :-

$$\Delta p_{ha} = \rho_a g \qquad (10.7)$$

The value of the mean air velocity, $\bar{v}_a$, used in equation (10.6) was that at the measuring point. The friction factors calculated in this manner were higher than those for a smooth pipe given in a Moody diagram [Massey (1968)] for the Reynolds number calculated at the measuring point. Using the Moody diagram the results showed that the relative pipe roughness was 0.008, which is slightly large for a glass pipe, but was probably due to abrasion by the particles.

Many authors [see chapter 2] have suggested that the total pressure drop in a flow conveying a solid can be split up into the pressure drop due to each phase, as :-

$$\Delta p_T = \Delta p_a + \Delta p_s \qquad (10.8)$$

This equation assumes that the pressure drop due to the air is unaffected by the presence of solids, which seems unlikely since the results of Durst (1978) show a large increase in the turbulence intensity of the conveying air. However, for simplicity this assumption is used in the calculations.

As with the single phase fluid, the pressure drop due to the solids in fully developed flow can be split up into the pressure drop due to the static head of solids, and that due to the solids friction. It has been postulated that the latter can be related to a solids friction factor, F_s, defined by the equation :-

$$\frac{\Delta p_{sf}}{L} = \frac{2F_s \rho_m \bar{v}_s^2}{D} \qquad (10.9)$$

where ρ_m is the average dispersed density of the solid in the flow. The pressure drop due to the solids static head is given by the equation :-

$$\frac{\Delta p_{sh}}{L} = \rho_m g \qquad (10.10)$$

Since the particle velocity was measured with reasonable accuracy, it was possible to investigate the dependence of the solids friction factor, F_s, on other variables in the flow. The solids friction factor is plotted against the solids loading ratio in figures (10.13) and (10.14). The friction factor was found to increase with solids loading ratio, but little variation with Reynolds number was found, although this might have been disguised by the scatter of the points. The equation of these curves was found to be :-

$$F_s = \alpha L_s^{\beta} \qquad (10.11)$$

where L_s is the solids loading ratio, and α and β are constants. For the ballotini the values of α and β are respectively 3.95×10^{-3} and 0.683, and for the sand 2.21×10^{-3} and 0.636 respectively.

Some authors have reported similar trends of the solids friction factor with the solids loading ratio, such as Farber (1949), Birchenough (1975), Muralidhara et al (1979), whilst others [Hariu and Molstad (1949), Clark et al (1952)] found little variation with solids loading ratio. However, it is difficult to compare the friction factor measured here with those given in many papers since there are a large number of definitions of the solids friction factor. In many cases, the mean velocity of the air rather than the solid was used in equation (10.9) and often the static head due to the air was included in the pressure gradient in this equation. However, the results found in this investigation are of the same order of magnitude as those given by other authors.

Jokati and Tomita (1971) found significant variation of the friction factor with Froude number ($Fr' = \bar{v}_a/\sqrt{gD}$), which is not evident in the results described here.

The solids friction factor is important in calculating the pressure drop in an air solids conveying line. The large variation in the definition of the solids friction factor and in the experimental results make it difficult to discover a correlation between the solids friction factor and other parameters of the flow. There is a need for collating the reliable results in the literature in order to produce a consistent model. Modi et al (1978), Leung and Wiles (1976), and Muralinhara et al (1979), attempted to produce such a correlation, but the widely differing results meant that no one correlation fitted all the results.

10.4.2 Drag Coefficient The average drag force, F_D, acting on each particle in the flow is given by the equation :-

$$F_D = \tfrac{1}{2}\rho_a(\bar{v}_a - \bar{v}_s)\ \frac{\pi d^2}{4} C_D' \qquad (10.12)$$

where C_D' is the average drag coefficient of each particle in the flow. The extra pressure drop caused by the drag of the particles is :-

$$\frac{\Delta p_s}{L} = \frac{4n \times F_D}{\pi D^2} \qquad (10.13)$$

where n is the average number of particles in unit length of pipe, which can be found from the solids mass flow rate, $\dot{M}_s$, using the expression :-

$$n = \frac{6\ \dot{M}_s}{\rho_s\ \pi d^3 \bar{v}_s} \qquad (10.14)$$

Substituting equations (10.12) and (10.14) into equation (10.13) gives:-

$$\frac{\Delta p_s}{L} = \frac{3\dot{M}_s}{\pi d D^2} \times \frac{\rho_a}{\rho_s} \times \frac{(\bar{v}_a - \bar{v}_s)^2}{\bar{v}_s} C_D' \qquad (10.15)$$

Using this equation the average drag coefficient, C_D', of each particle can be calculated if the pressure drop due to the air is assumed to be unchanged by the solids, and equation (10.8) is used. The results are shown in figures (10.15) and (10.16), and compared with the standard drag coefficient, C_D, for a single particle moving in still unbounded air. In both cases the resulting drag coefficients

are widely dispersed, more so in the case of the ballotini than the sand, but a wider range of flow conditions are represented in the results for the ballotini. The values for the sand were all below the standard drag coefficient, as were the majority of values for the ballotini. As the air Reynolds number increased and the solids loading ratio increased, the drag coefficient increased. However, the scatter in the results was such that no correlation was possible. Reddy and Pei (1969) found that the drag coefficient of glass spheres in an air-solid flow was greater than C_D, and also found that the drag coefficient decreased as the solids loading ratio increased. However, the slip velocity of the particles was much less than those used here and the particle Reynolds number was in the range 4 - 40, which may explain the disagreement of their results with the present investigation.

10.5 Conclusions

In section (10.2.1) the measured particle velocity profiles were compared with a theoretical equation for the velocity profiles. It was found that the ballotini profiles fitted the equation fairly well, but the sand profiles did not. This may have been due to the deviation of the sand flow from the simplest problem of a monodispersed flow of spheres. In order to produce an equation for the particle velocity profile of a polydispersed flow conveying angular particles, such as the air-sand flow, greater knowledge of the air-particle interactions must be obtained. The results described in the previous two chapters show the variation of particle velocity across the diameter of the pipe, and indicate that the assumption of zero velocity at the centre of the pipe is unfounded.

The average slip velocity of the particles was found to increase both with solids loading ratio and the average air velocity. The variation with the solids loading ratio was found to be approximately

linear over the range tested, and was probably caused by increased drag due to greater air turbulence and increased interparticulate interactions. The slip velocity varied as the square of the mean conveying air velocity. The cause of this increase is more difficult to explain, but is possibly also caused by increasing air turbulence. The average slip velocity was greater than the terminal velocity of a single particle in all flows except those with the lowest Reynolds numbers.

The axial particulate turbulence intensity profiles, described in section (10.3), were fairly flat, varying less across the pipe than the turbulence of single phase air. The central particulate turbulence was found to increase with solids loading ratio to a value greater than that of single phase air. It was not possible to measure the turbulence of the conveying air, but work published by Durst (1978) indicates that this too is increased, so that the air phase turbulence is always greater than the solid phase turbulence. This suggests that the air phase is considerably affected by the particles, and it is doubtful if assumptions that the properties of the air, such as the pressure gradient are unchanged by the particles, are valid.

Using this last dubious assumption, the solids friction factor was calculated from the pressure gradient results and the mean slip velocity. Again this was found to increase with the solids loading ratio, and the exponent to which the solids loading ratio was raised in the relation to the solids friction factor was nearly equal for both solids. The variation with Reynolds number was too small to measure, although other authors have found significant variation. Difficulties were caused in comparisons with work by other authors due to the diversity in the definition of the solids friction factor.

The drag coefficient was also calculated from the pressure gradient due to the solids and the slip velocity, but there was too much scatter in the results for any definite conclusions to be made.

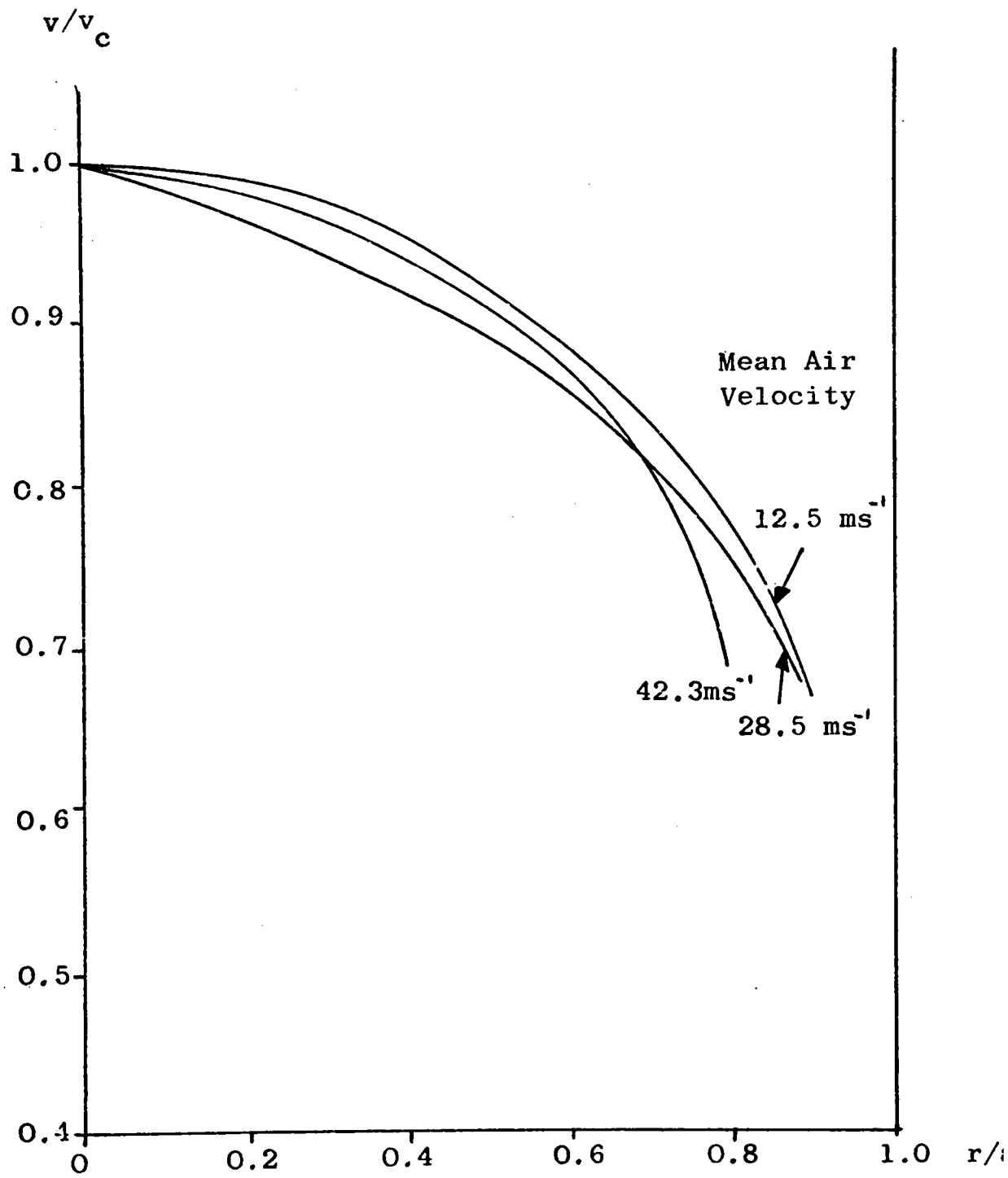

AIR VELOCITY PROFILES

Figure (10.1)

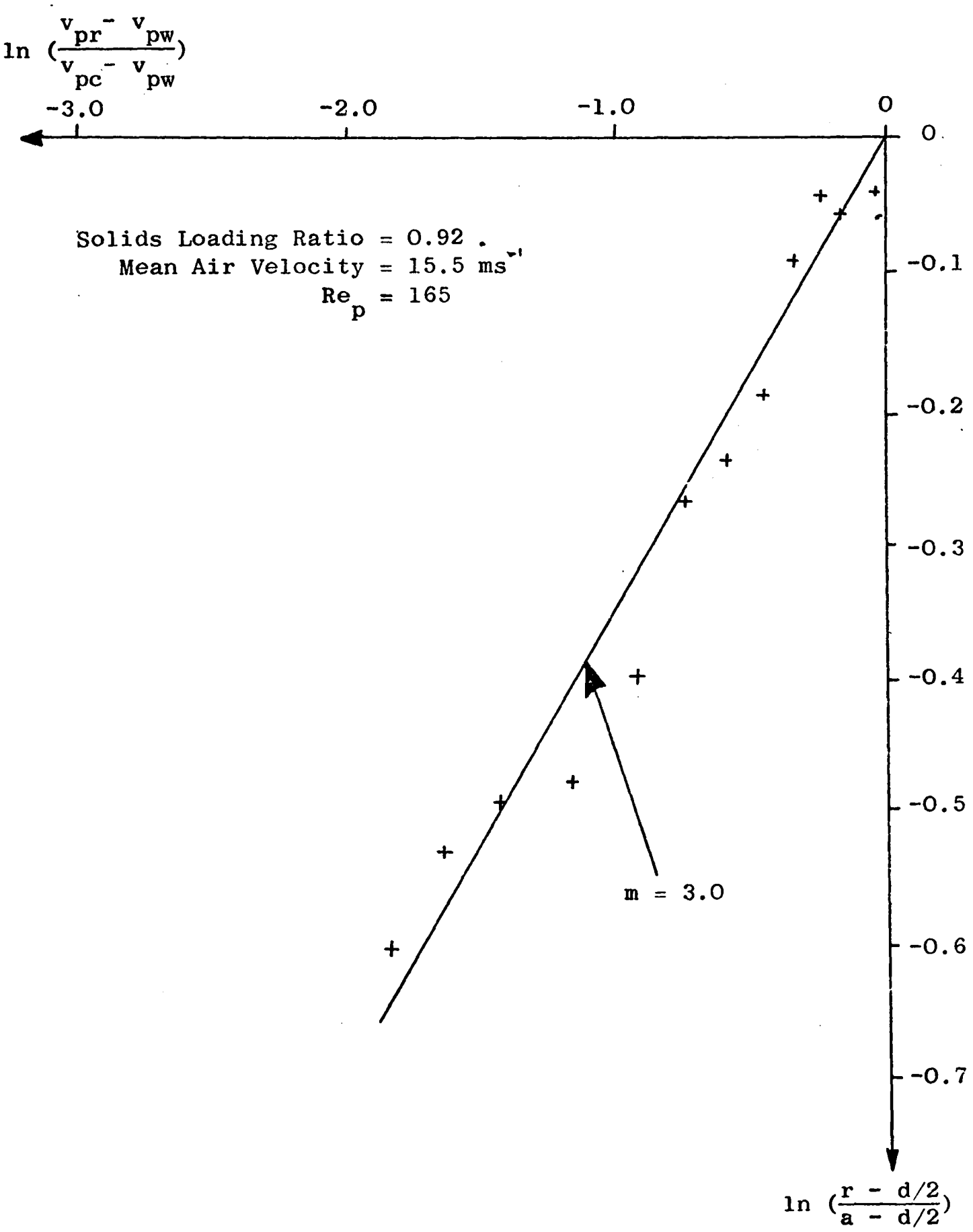

PLOT OF EQUATION (10.2) FOR BALLOTINI

Figure (10.2)

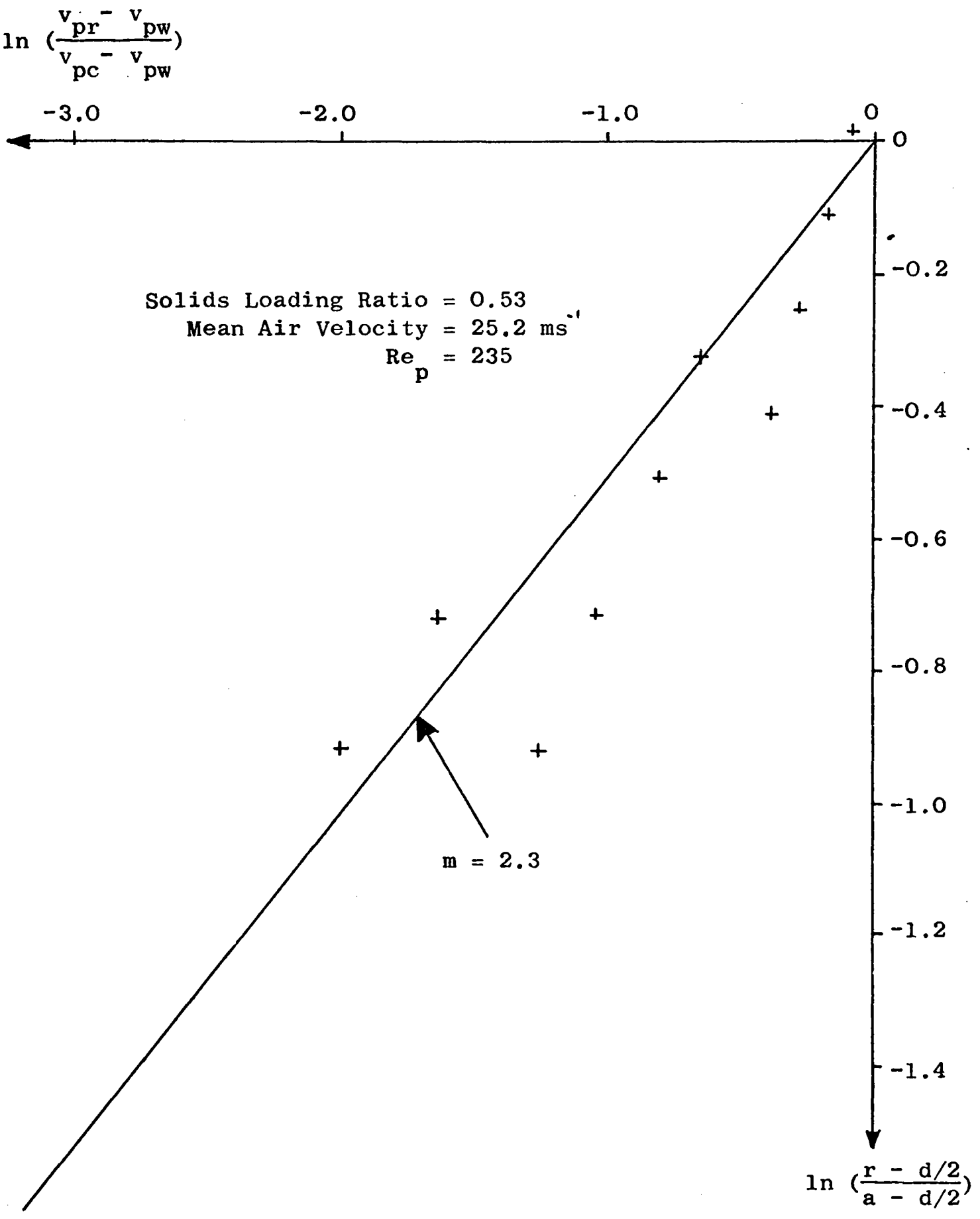

PLOT OF EQUATION (10.2) FOR BALLOTINI

Figure (10.3)

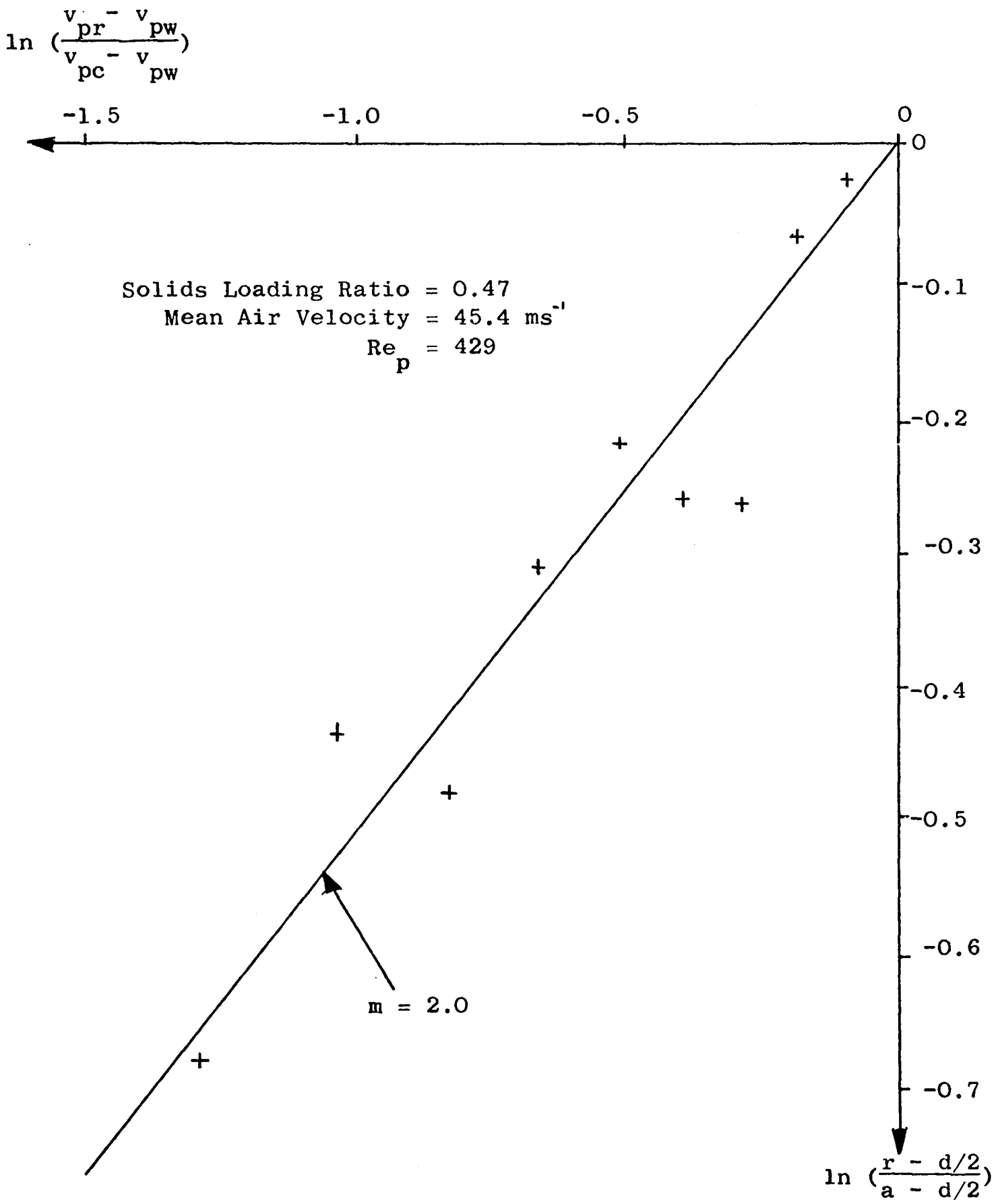

PLOT OF EQUATION (10.2) FOR BALLOTINI

Figure (10.4)

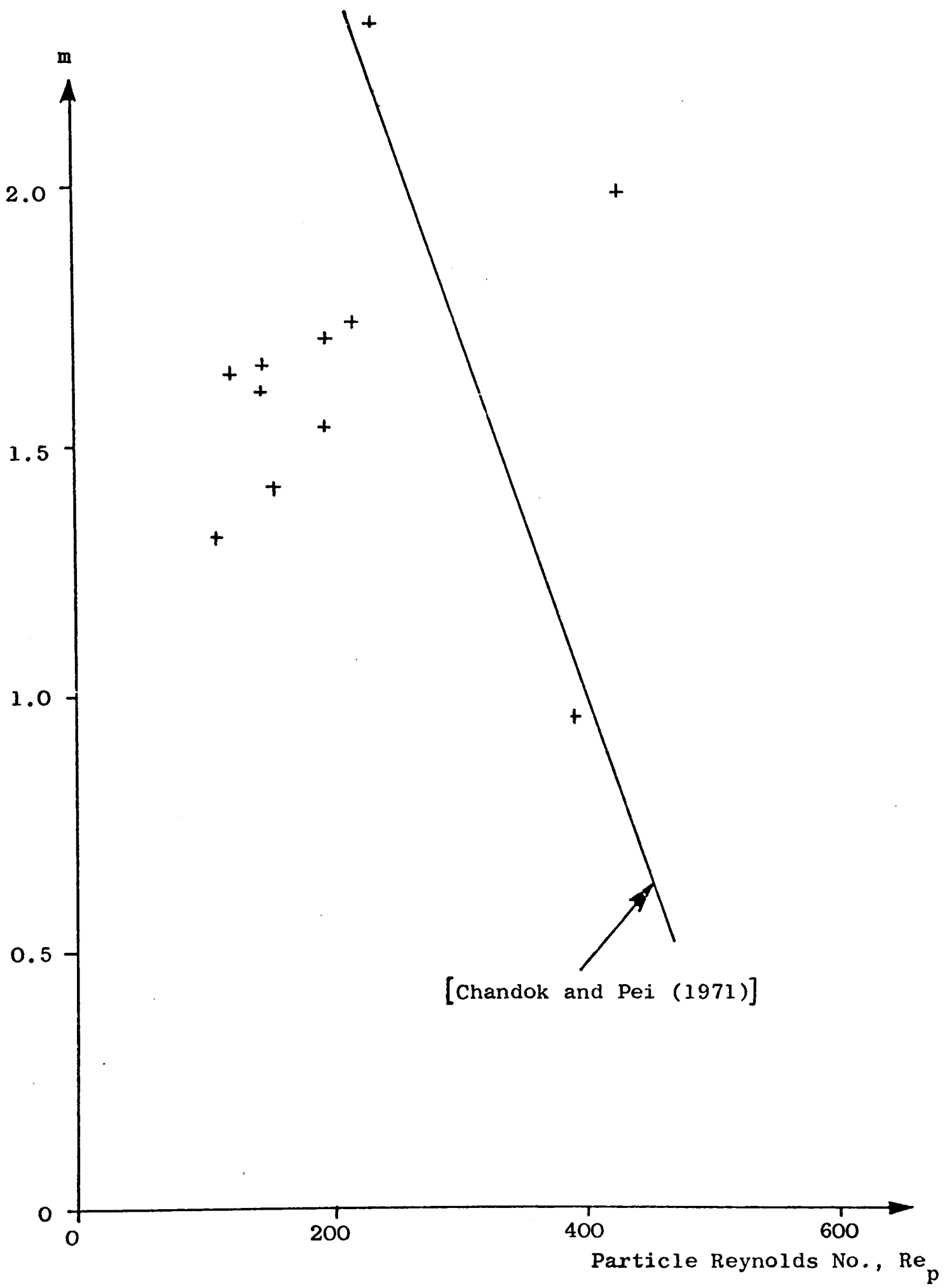

VARIATION OF CONSTANT IN EQUATION (10.2)
WITH PARTICLE REYNOLDS NUMBER

Figure (10.5)

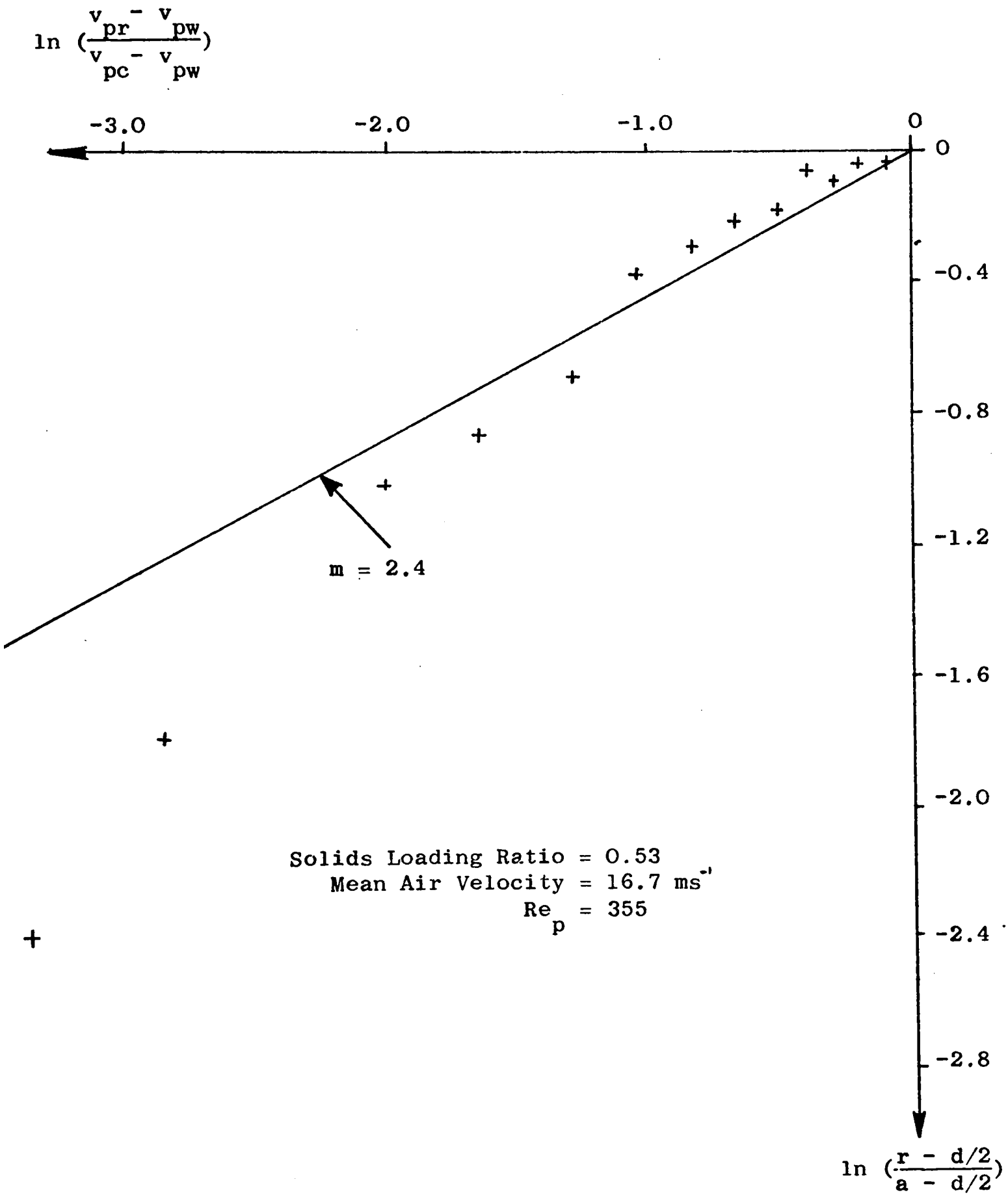

PLOT OF EQUATION (10.2) FOR UNSIEVED SAND

Figure (10.6)

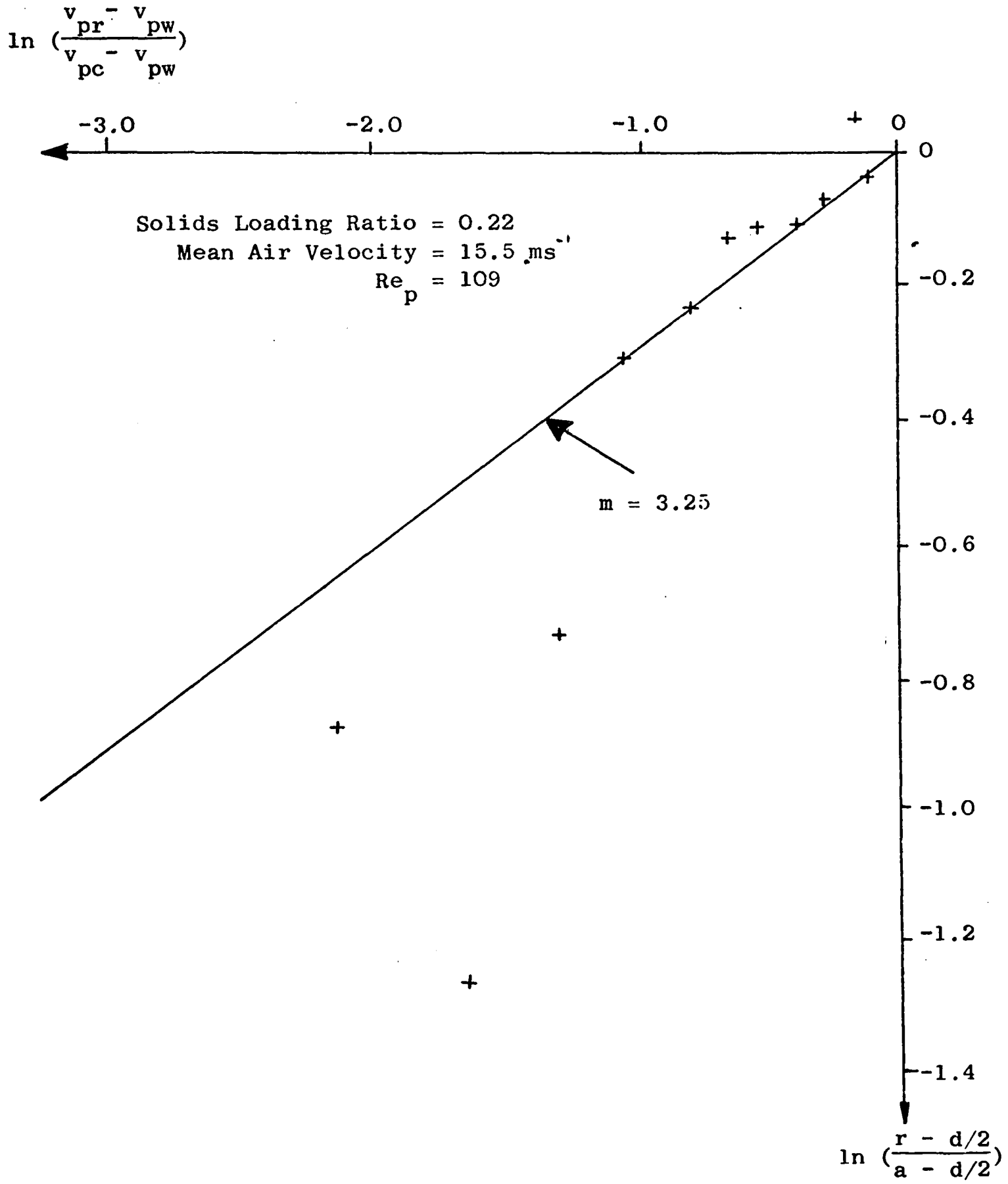

PLOT OF EQUATION (10.2) FOR SIEVED SAND

Figure (10.7)

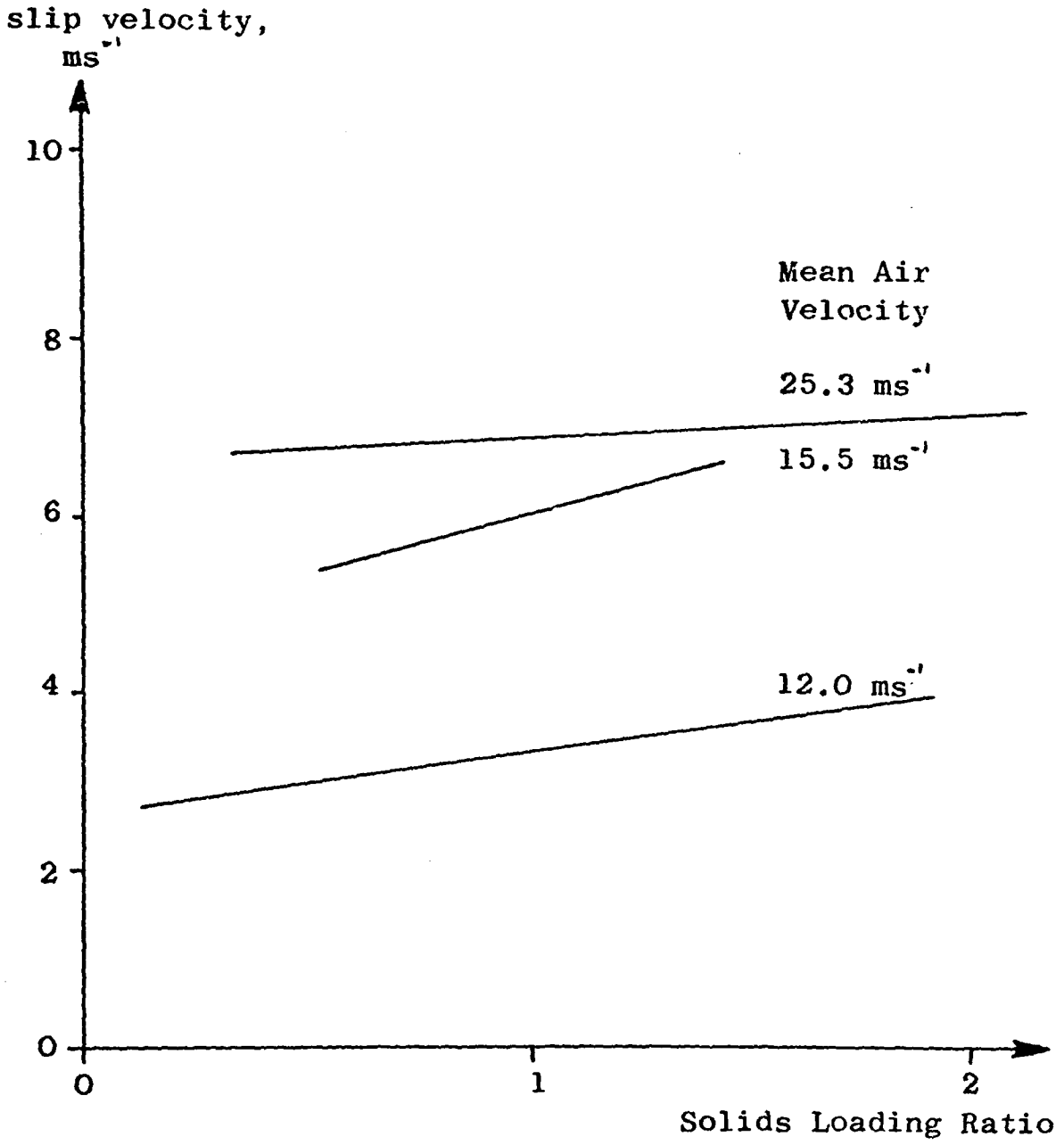

VARIATION OF SLIP VELOCITY WITH SOLIDS LOADING RATIO, BALLOTINI

Figure (10.8)

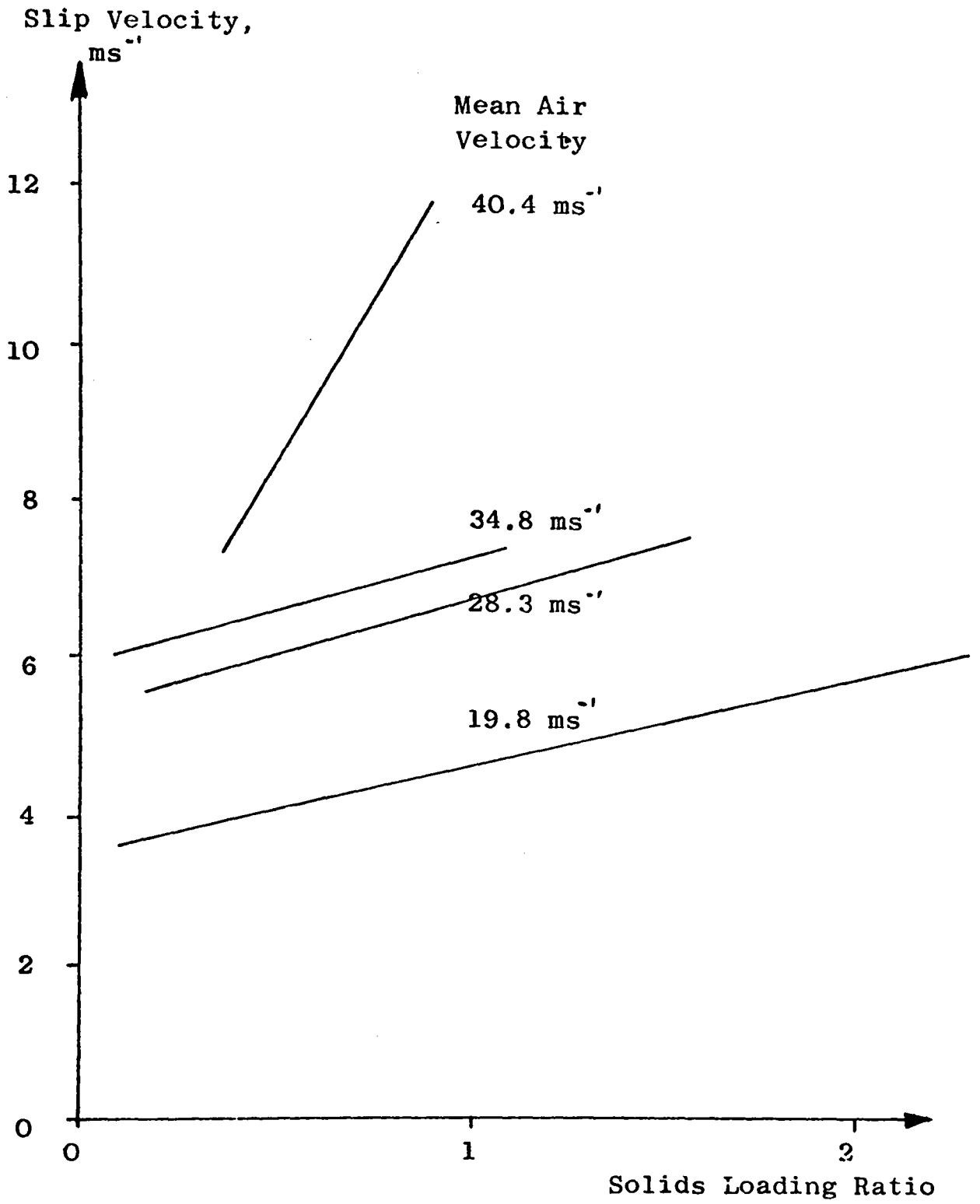

VARIATION OF SLIP VELOCITY WITH SOLIDS LOADING RATIO, UNSIEVED SAND

Figure (10.9)

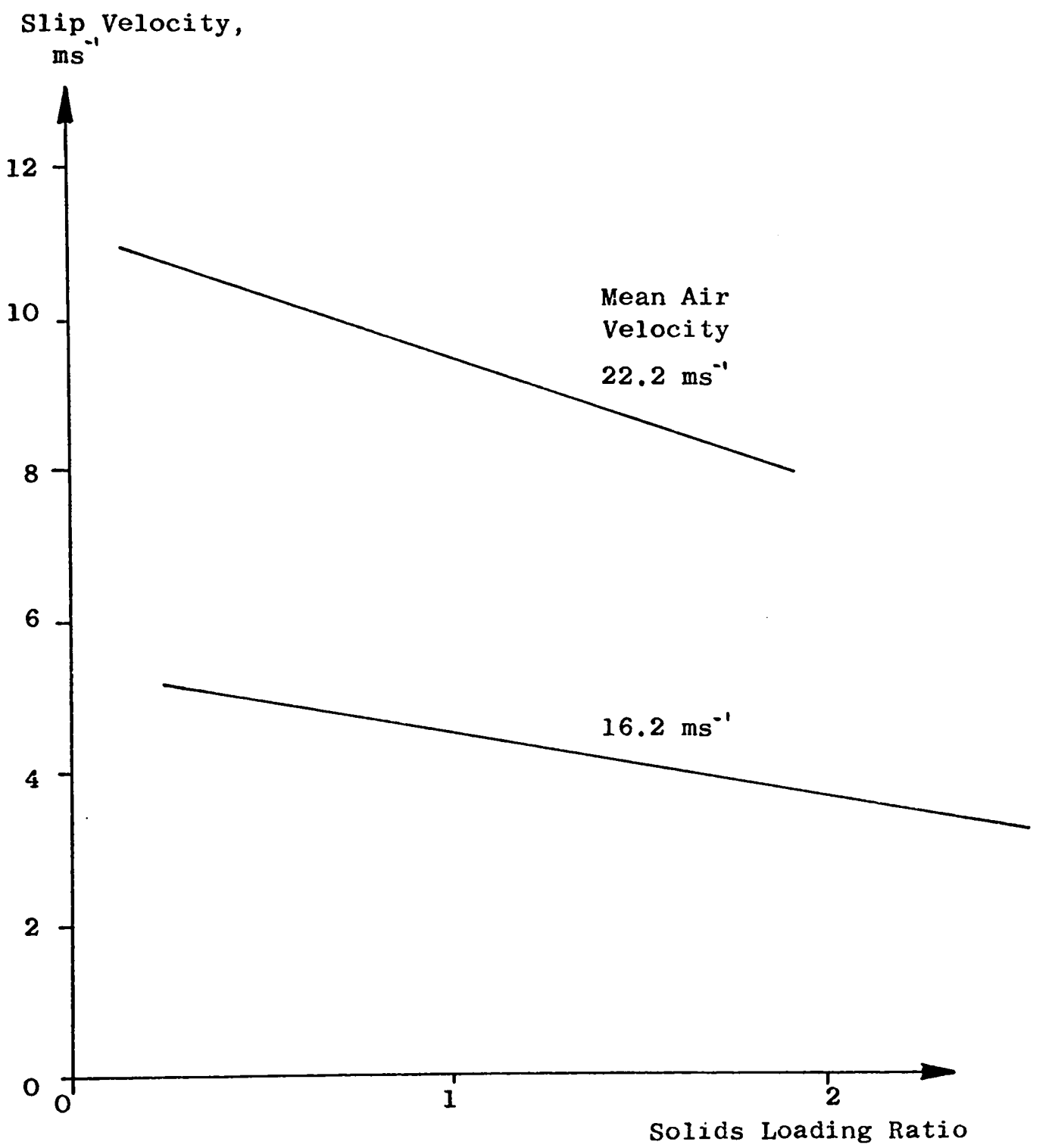

VARIATION OF SLIP VELOCITY WITH SOLIDS LOADING RATIO, SIEVED SAND

Figure (10.10)

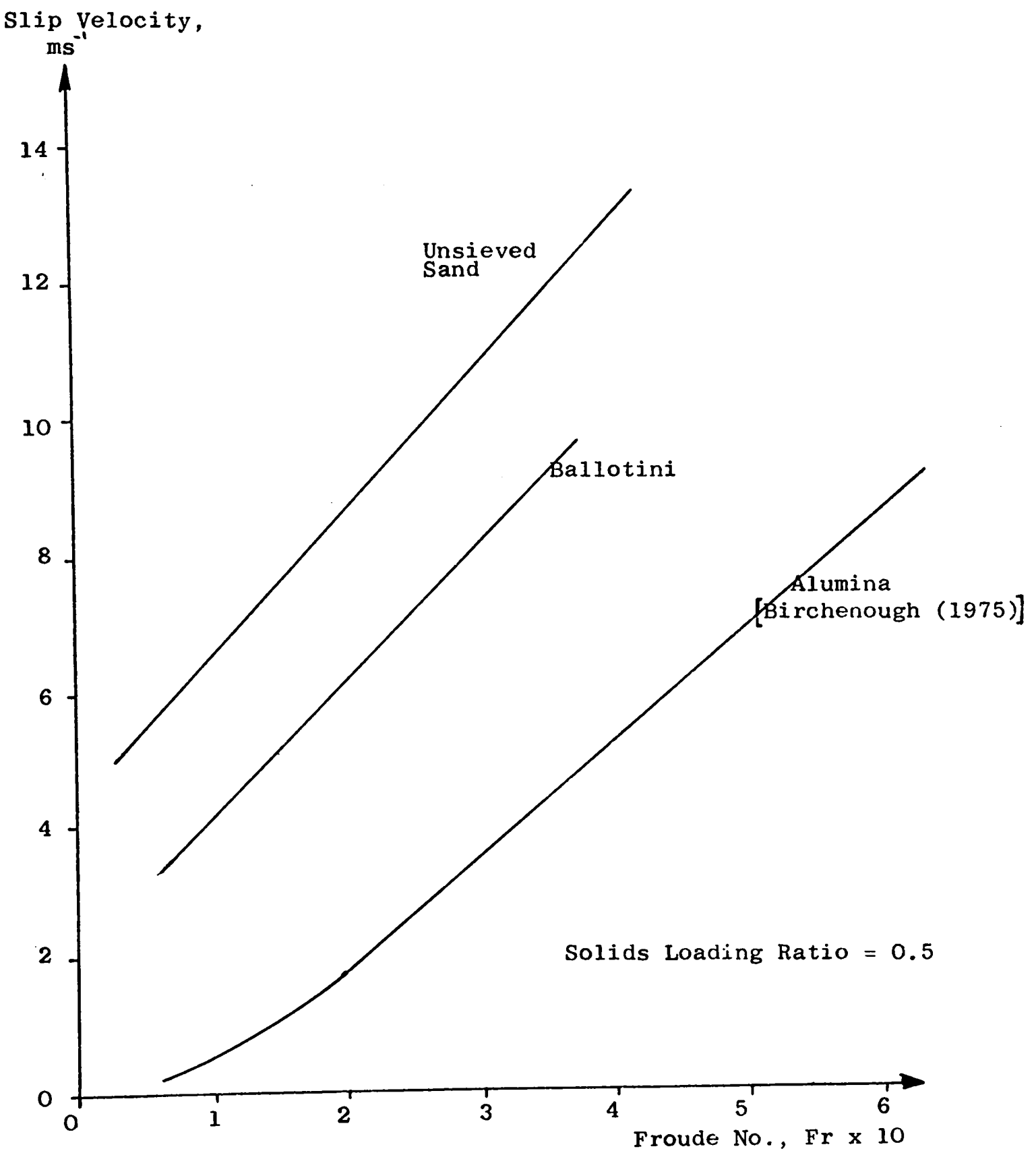

VARIATION OF SLIP VELOCITY WITH FROUDE NUMBER

Figure (10.11)

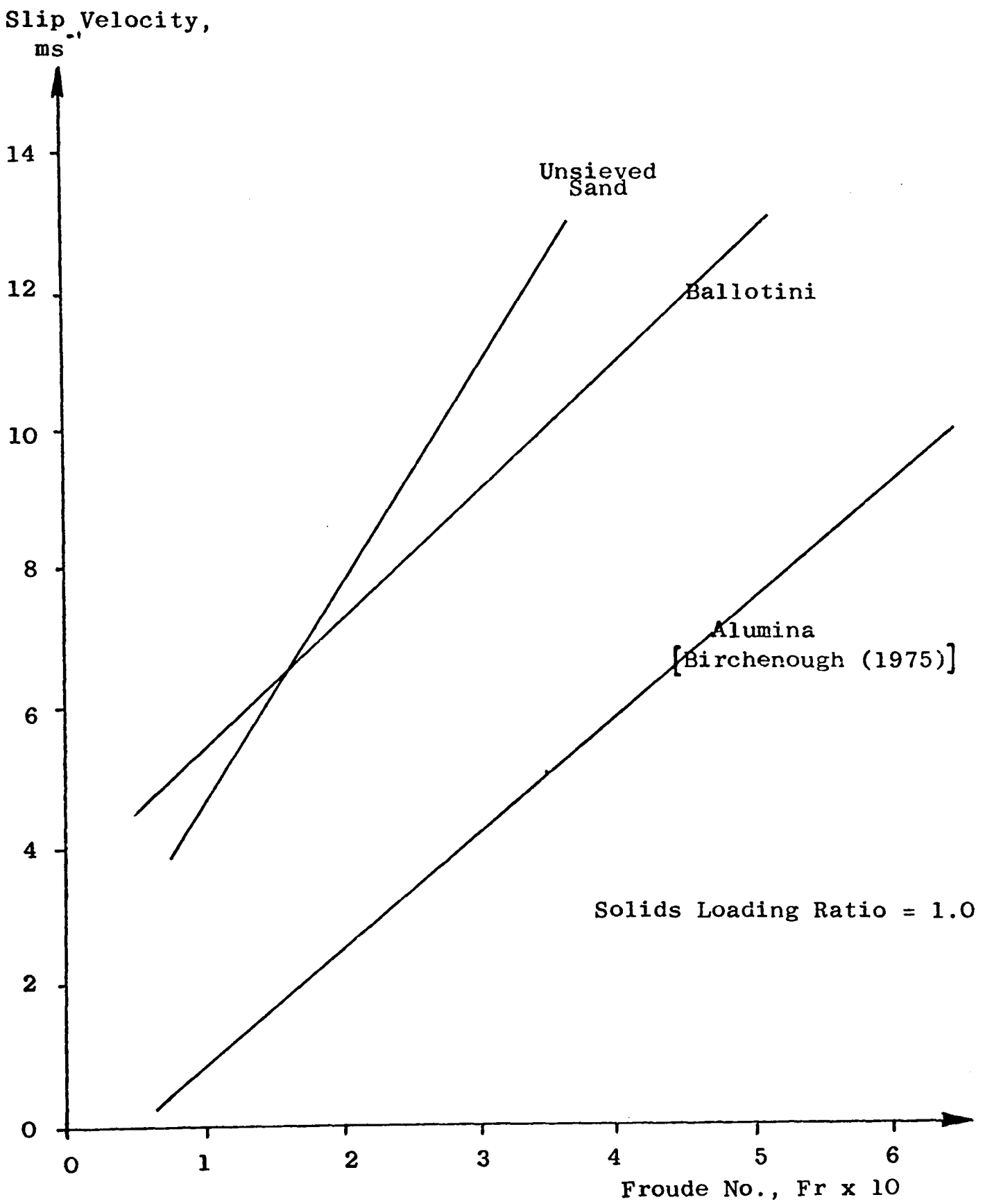

VARIATION OF SLIP VELOCITY WITH FROUDE NUMBER

Figure (10.12)

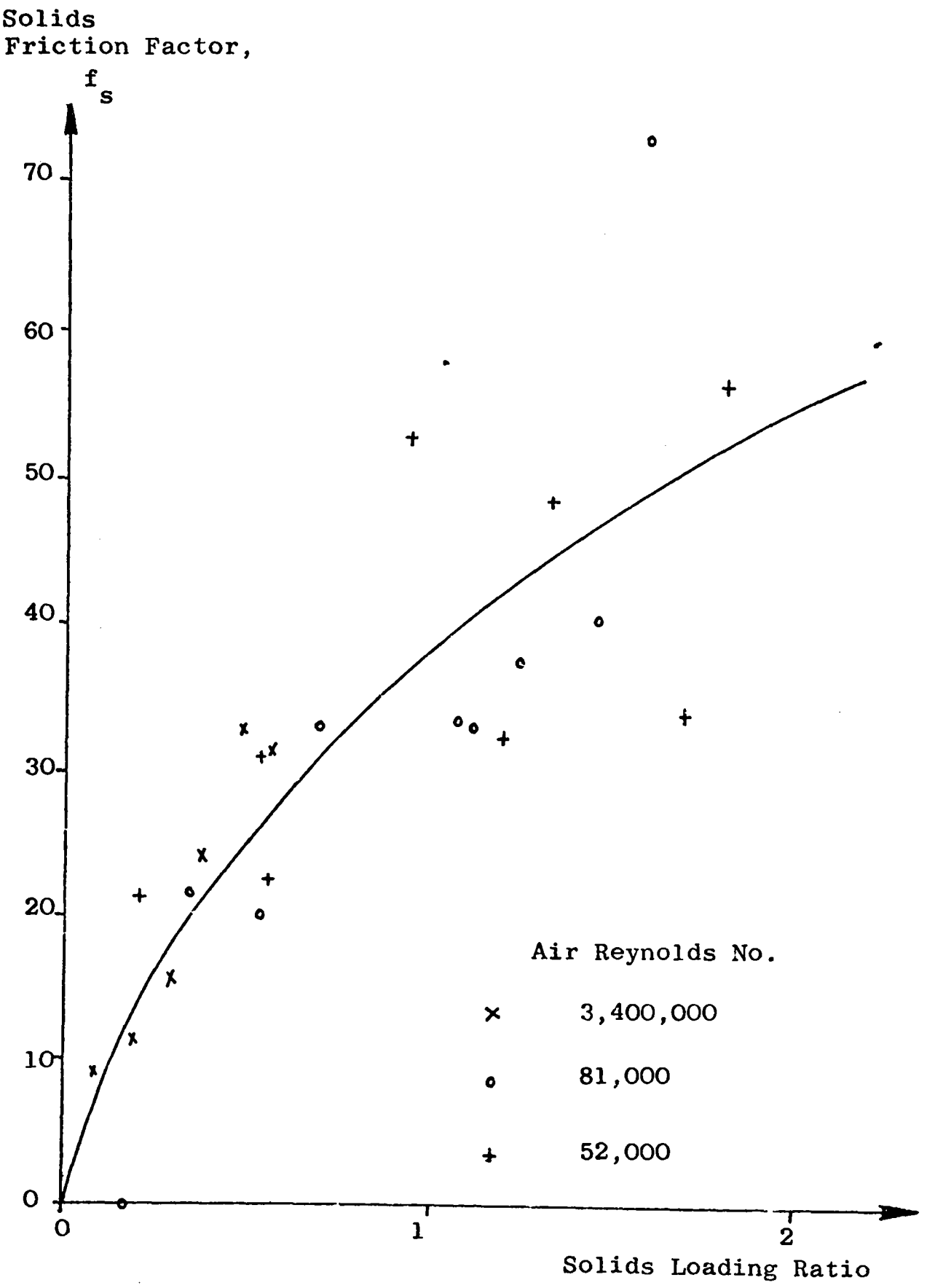

VARIATION OF SOLIDS FRICTION FACTOR
WITH SOLIDS LOADING RATIO FOR BALLOTINI

Figure (10.13)

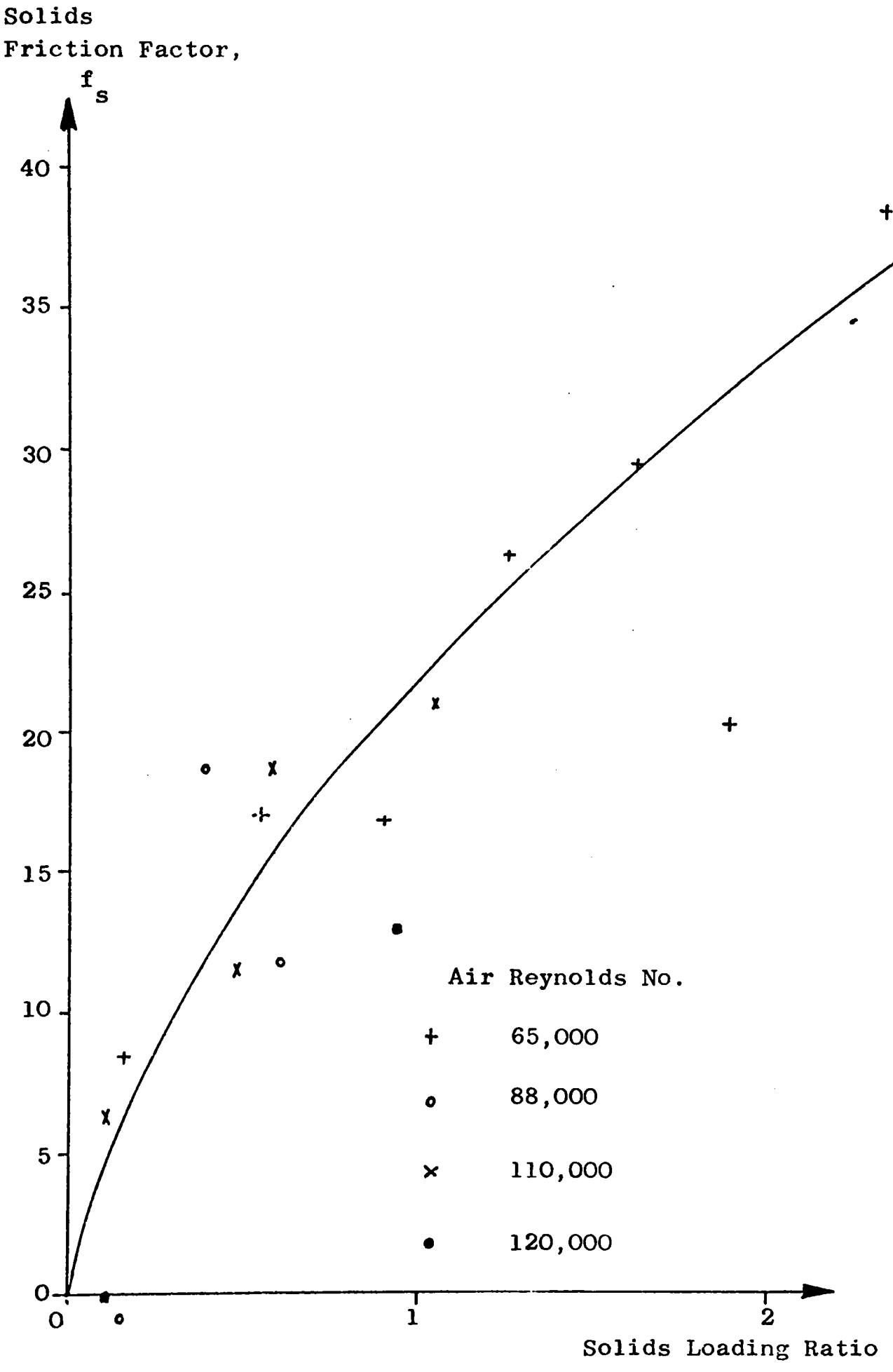

VARIATION OF SOLIDS FRICTION FACTOR
WITH SOLIDS LOADING RATIO FOR SAND

Figure (10.14)

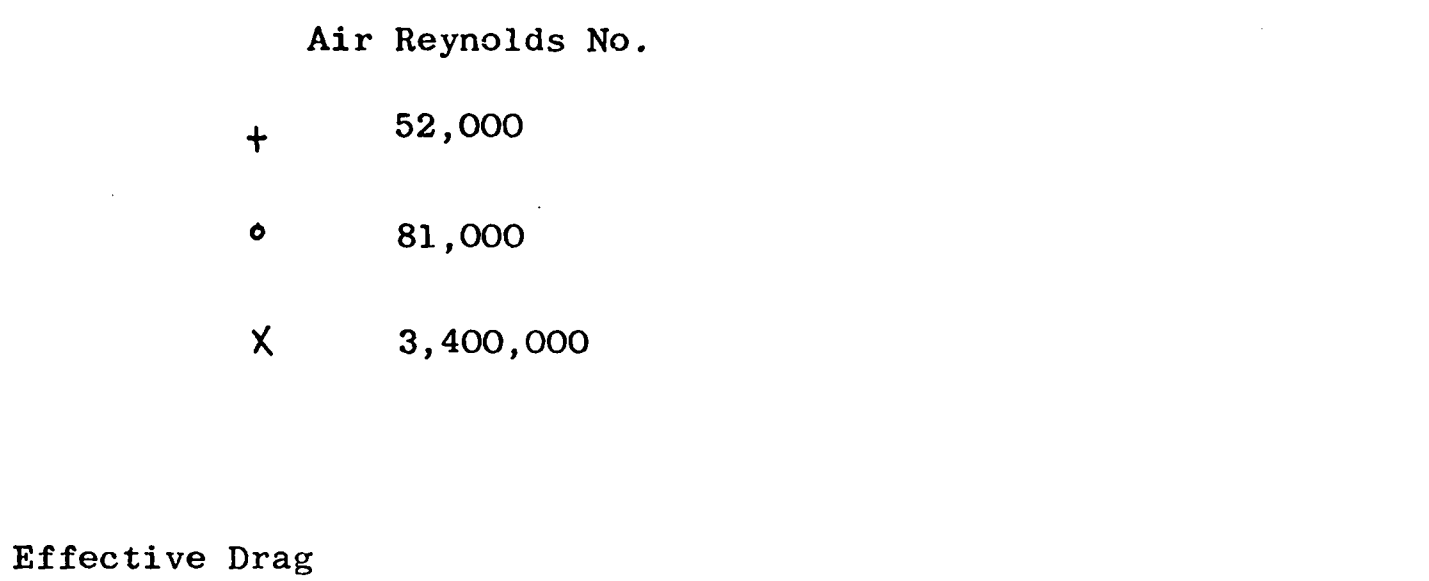

EFFECTIVE DRAG COEFFICIENT OF BALLOTINI

Figure (10.15)

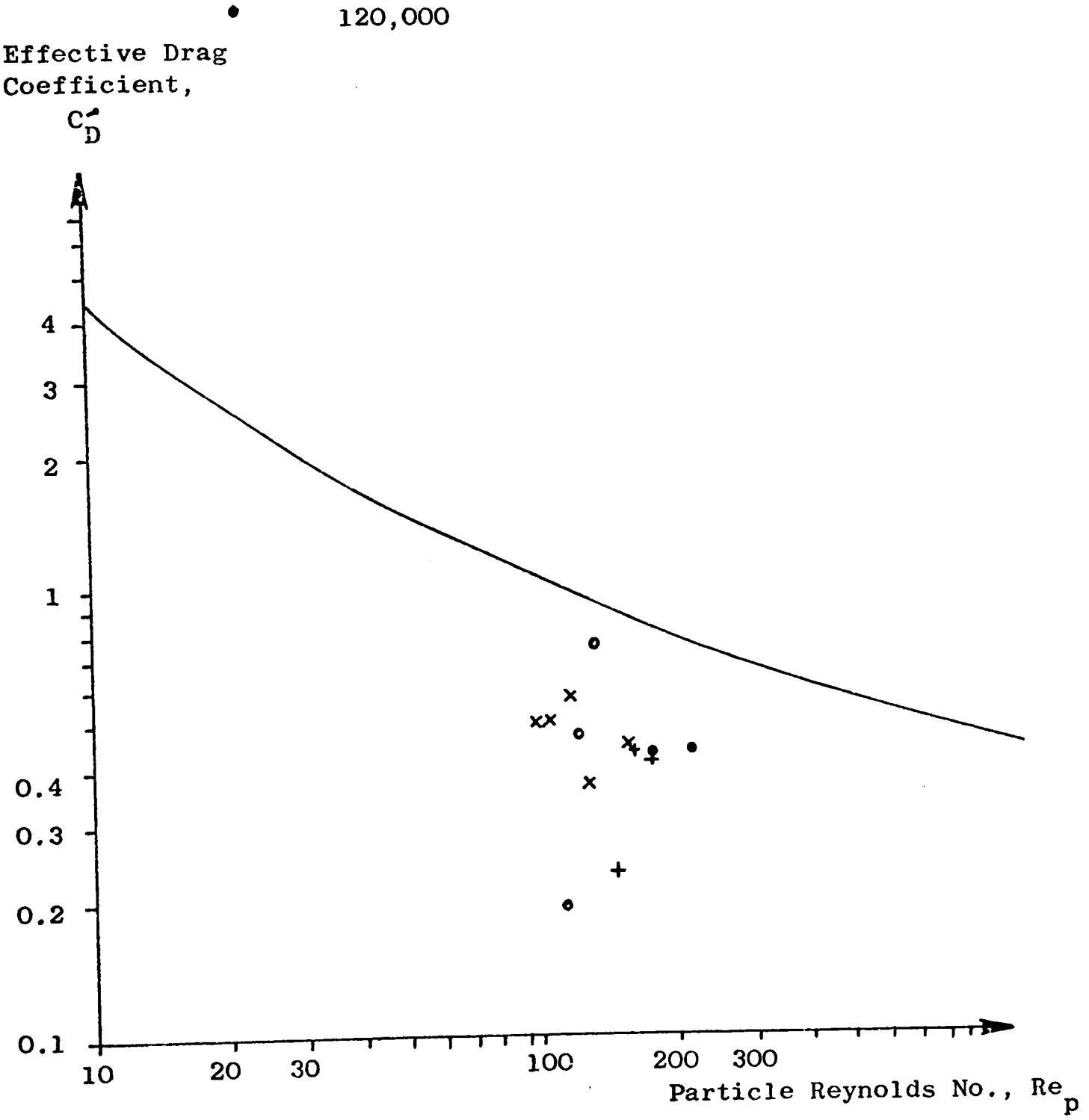

EFFECTIVE DRAG COEFFICIENT OF SAND

Figure (10.16)

CHAPTER 11

VELOCITY MEASUREMENTS ON LARGER PARTICLES

11.1 Introduction

In this chapter velocity measurements on plastic particles several millimetres in diameter using the laser Doppler velocity meter are discussed. Most of the measurements were carried out on the small conveying plant described in section (3.4). Measurements on the visibility of the signal from such particles were made. Since the visibility of the signal was large enough for the velocity to be found, the velocity profile of the solids in the vertical section of the square pipe was measured. Air velocity profiles were also taken for comparison. These were found by introducing sub-micron titanium oxide tracer particles into the flow, and then measuring the frequency output of the laser Doppler velocity meter.

The main aim in the experiments described here was to study the suitability of the laser Doppler velocimeter, LDV, for measuring the velocity of particles which were much larger than those previously used in air-solid flows. Most of the published work on particle velocity measurements by LDV in air-solid flows concerns particles with diameters very much smaller than 1 mm, although Durst and Zaré (1975) successfully measured the velocity of a large swinging ball bearing of unrecorded diameter.

The particles chosen for these experiments were long plastic chips whose physical poperties were reported in Chapter 4. The particles were of the same order of magnitude as the length of the measuring volume and were much larger than the other dimensions of the measuring volume of the

LDV. Also the numerical concentration of the particles in the flow was of necessity very low to allow the laser beam to pass through it. For these reasons the problems of the particle velocity measurements were greater than those encountered with smaller particles. However, the experiments proved that the LDV could be used successfully for particle velocity measurement in flows with large particles.

11.2 LDV Optical Arrangement

The distribution of the light intensity scattered by particles passing through the laser beams is greatly affected by the particles (see Chapter 6). The particles used in these experiments had dimensions much greater than the diameter of the laser beam and, for particles of this size, conventional scattering rather than Mié scattering applies. Although one type of particle was translucent, neither type of particle allowed a significant light intensity to be transmitted across the pipe and experimental trials showed that the LDV did not produce useful signals from these particles in the forward scatter mode. In the back scatter mode a high light intensity was received by the photomultiplier, even though the particles were not particularly reflective. The direction in which the light was reflected was determined by the angle of inclination of the reflecting surface to the laser beams, but since the particle surfaces were not completely smooth, sufficient light was reflected towards the photomultiplier for many particles to produce a signal. Therefore, for all the experiments described in this chapter, the LDV was used in the backscatter mode.

The transmitting optics employed for these tests utilised the rotating diffraction grating described in chapter 6 for splitting the laser beams and producing a frequency difference between the resulting two beams. The optical arrangement is shown in plan view in figure (11.1). It was hoped to be able to measure the velocities of both phases

simultaneously using this arrangement, since the small particles scatter most light in the direction of the forward scatter mode photomultiplier, and the large particles scatter most light towards the back scatter mode photomultiplier. However, it was found that insufficient light reached the forward scatter mode photomultiplier when there were particles in the flow for air velocity measurements to be made. For this reason, the air velocity could only be measured in single phase flows. When frequency shifting was used, the frequency difference, ν_s, (see chapter 5), was found by placing a reflecting surface in the measuring volume, and finding the resulting output frequency from the photomultiplier by means of the Cambridge Consultants tracking filter.

11.3 Particle Visibility

Some measurements were made on the visibility of the signal produced by the plastic pellets conveyed in the small plant. The measurement technique involved freezing the signal from a particle on a storage oscilloscope and measuring the ratio of the maximum of the signal to the next minimum, as shown in figure (11.2), which was produced by a black plastic pellet. Since the particles were irregular in shape, the resulting pedestal signal was also irregular in shape, and choosing the maximum point of the signal was difficult. The maximum velocity of particles whose visibility and velocity could be measured in this way was limited by the writing speed of the oscilloscope. Particles moving faster than about 4 ms^{-1} produced a trace whose properties could not be distinguished. The variation of the visibility with collecting angle was difficult to test due to the physical arrangement of the optics, and so the collecting optics were kept at 30^{o} to the direct backwards line of collection.

The spread in the visibility of the signal from the black plastic pellets is shown in figure (11.4). There was little variation in the

visibility and the velocity of the particles, which was in the range of 0.5 to 3.6 ms^{-1}, had no measurable effect on the visibility. The mean visibility was 0.48 and in all cases it was large enough for frequency measurements to be made easily from the oscilloscope screen. The visibility was also adequate for an electronic method of frequency analysis to be used, but unfortunately the signal was too intermittant for the available frequency trackers, and another form of analyser for which such intermittancy was not a problem would have resolved this problem.

A typical example of the signal obtained from the clear plastic pellets is shown in figure (11.3). In all cases it was found that the signal visibility for these particles was very poor, and the Doppler signal was too small for frequency measurements to be made with any accuracy. The average visibility measured was about 0.08, but it was difficult to measure the visibility accurately. The reason that the signal visibility for the transparent particles was much less than that for the black particles, despite the similarity in particle size, is unknown. Possibly the light in the probe volume was distorted by the transparent particles, whereas the light was scattered by the surface of the black particles. Further measurements using these particles were abandoned because of this difficulty, although it might have been possible to obtain the Doppler frequency from this signal by using appropriate filtering and signal analysis.

In an attempt to improve the signal a laser line filter, bandwidth 10 nm, was fitted onto the collecting optics. However, it had little effect on the noise characterisation of the signal and slightly reduced the signal intensity.

11.4 Particle Velocity Measurements

11.4.1 Introduction In order to test the practicality of using the LDV for measurements on large particles it was decided to attempt the measurement of the velocity profile of the black pellets in the square pipe. Initially, air velocity measurements were made in the pipe to find the shape of the air velocity distribution. The particle velocity distribution was then measured and compared with the air velocity distribution.

The black pellets were found to shatter easily and the glass windows rapidly became coated with plastic fragments and they had to be removed and cleaned frequently. This demonstrated the usefulness of the removable windows, but since the plant had to be shut down before removing the windows, it was difficult to keep the flow conditions constant whilst a complete velocity distribution was measured.

The frequency measurements on the signal from the black particles were made on the storage oscilloscope since the tracking filter was not capable of analysing the signal. It was found that the Cambridge Consultants tracker could track the signal from a single particle attached to a rotating disc, which gave a Doppler signal for only about 1% of the time. This showed that the failure to track the particles in the flow was not solely caused by the large drop out in the signal, but was due to a combination of the high turbulence intensity and the high drop out in the signal.

In order to ensure that the measured signal originated from the large particles, as opposed to the smaller particle fragments, the gate shown in figure (6.11) was used to remove those signals with pedestals less than a threshold voltage.

11.4.2 Air Velocity Measurements The air was seeded using the fluidiser described in chapter 7. Air was bled from the pipe immediately after the compressor on the small conveying rig, and the air plus trace

particles was fed into the venturi section via a pressure tapping. This method had the disadvantage of allowing the air through the fluidiser to bypass the point where the total air mass flow rate was measured by Pitot-static traverse. However, it was necessary in order to develop sufficient pressure difference across the fluidiser, and the accuracy required for the air mass flow rate measurement was not high.

The forward scatter mode shown in figure (11.1) was used and the Doppler frequency from the photomultiplier was analysed with the Cambridge Consultants tracker. An adequate signal was obtained, but the windows had to be removed and cleaned frequently since the sub-micron titanium oxide particles stuck to the glass and reduced the signal intensity.

Air velocity profiles were measured across the pipe in a series of points across the window. These profiles are shown in figure (11.5) and a contour diagram of the flow velocity is given in figure (11.6). The air velocity gradient increased towards the centre of the duct. The profiles obtained are very similar to those measured in a turbulent horizontal water flow in a square duct by Melling and Whitelaw (1973). The air mass flow rate was calculated from the air velocity profile and the pressure at the measuring point, and was found to be greater than that calculated from the results of the Pitot-static traverse.

11.4.3 Results and Discussion The particle velocity measurements are displayed in figure (11.7) and a contour diagram of the velocity distribution in the pipe is given in figure (11.8). The mean velocity during these measurements was less than that during the air velocity measurements. The curves in figure (11.7) are those of polynomials fitted to the results using the method of least squares, since there was a large degree of scatter in the results. The profiles show an increase in curvature towards the centre of the pipe, which is the same

trend as that displayed by the air velocity profiles in figure (11.5), but the scatter in the results means that the trend is not so smooth. The scatter is probably due to the high degree of particle turbulence and the small sample of signals measured at each point. The contour diagram in figure (11.8) was obtained from figure (11.7), and is only approximate. The mean particle velocity was calculated to be 2.5 ms^{-1} from this contour diagram, which gives a mean slip velocity of 7.6 ms^{-1} with a solids loading ratio of 0.05. This is very much greater, even allowing for inaccuracies, than the terminal velocity of an average sized particle in still air of 2.61 ms^{-1}, calculated by means of the method described in section (10.2). This shows that the air turbulence and other interactions have a large effect on the slip of these particles, even at very low solids loading ratios.

As was found in the work on the particle velocity profiles of ballotini and sand in the round test pipe, described in chapters 8, 9 and 10, the particle velocity profile was flatter than the air velocity profile. This is especially shown by the wide spacing of the contour lines in figure (11.8), as compared to those for air in figure (11.6). However, many more measurements are needed for reliable knowledge of the flow properties of such a system.

11.5 Conclusions

In this chapter the investigation into the suitability of the laser Doppler velocity meter for measuring the velocity of large particles was described. Particles with dimensions of over 3 mm were used, and they produced Doppler signals with the LDV. However, it was found that the visibility was small and, in the case of the transparent plastic particles, the visibility was too small for the Doppler frequency to be measured by conventional methods.

Both air and particle velocity measurements were taken in the square, vertical duct. This showed that such measurements were possible, but also revealed some of the problems in such a measuring system which need to be overcome. The windows were obscured very rapidly due to the break up of the particles, and some method of keeping the windows clear is required, such as an internal scraper. The main problem encountered, however, was signal analysis. The tracking filters could not follow the signal, and because of the high particle turbulence, the technique of measuring the frequency from a storage oscilloscope required too large a sample of signals to be practical, since the time for a traverse was large. A period counter would probably be able to measure the Doppler frequency, but the large degree of filtering needed for such an instrument might reduce the measured frequency spread. Possibly the most suitable frequency analyser would be a filter bank.

With appropriate signal analysis, the laser Doppler velocity meter seems to be a useful instrument for measuring the velocity of any size of particle which has suitable optical characteristics, in an air-solid flow.

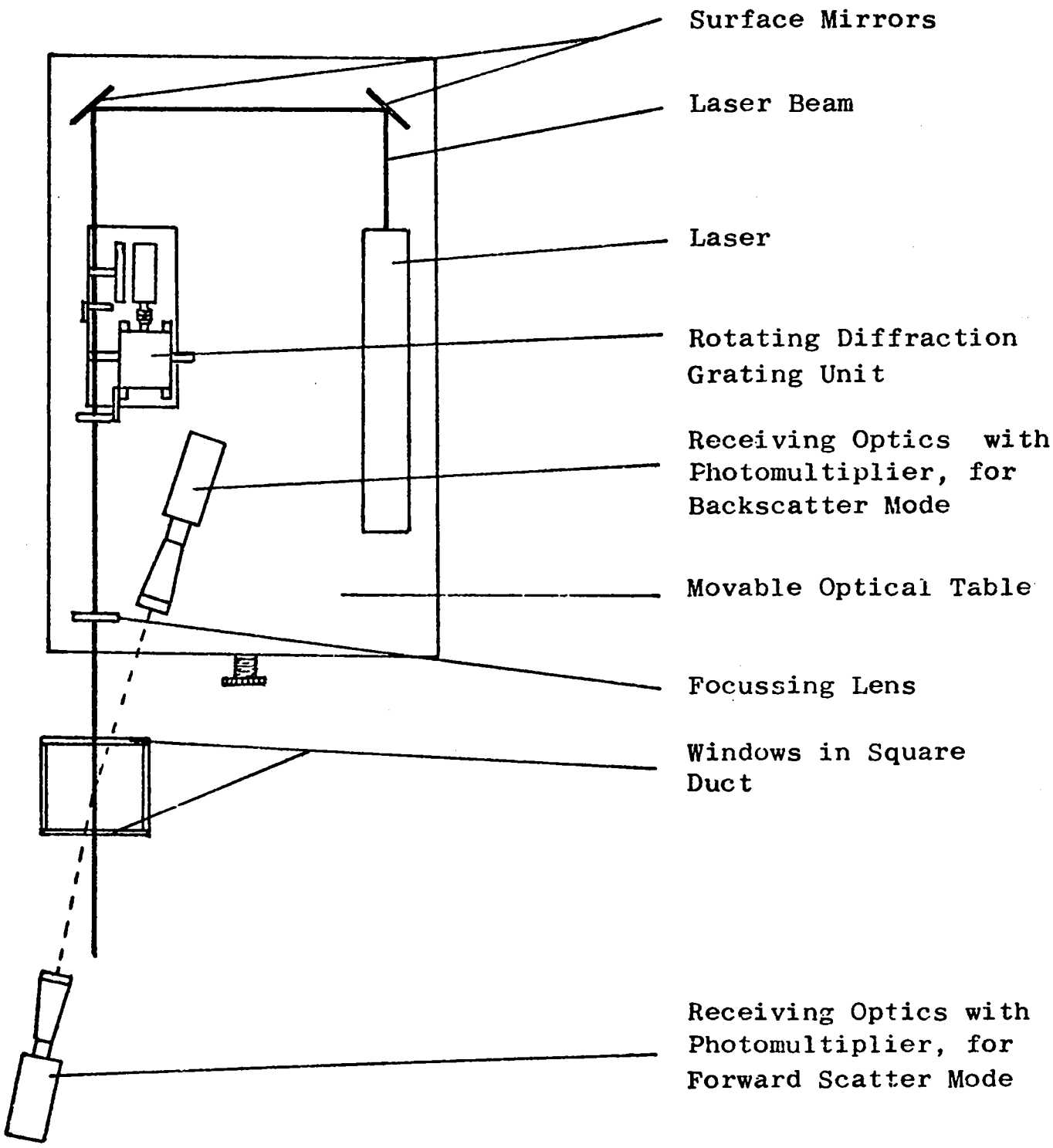

LDV FOR MEASURING AIR AND PARTICLE VELOCITIES IN SQUARE DUCT

Figure (11.1)

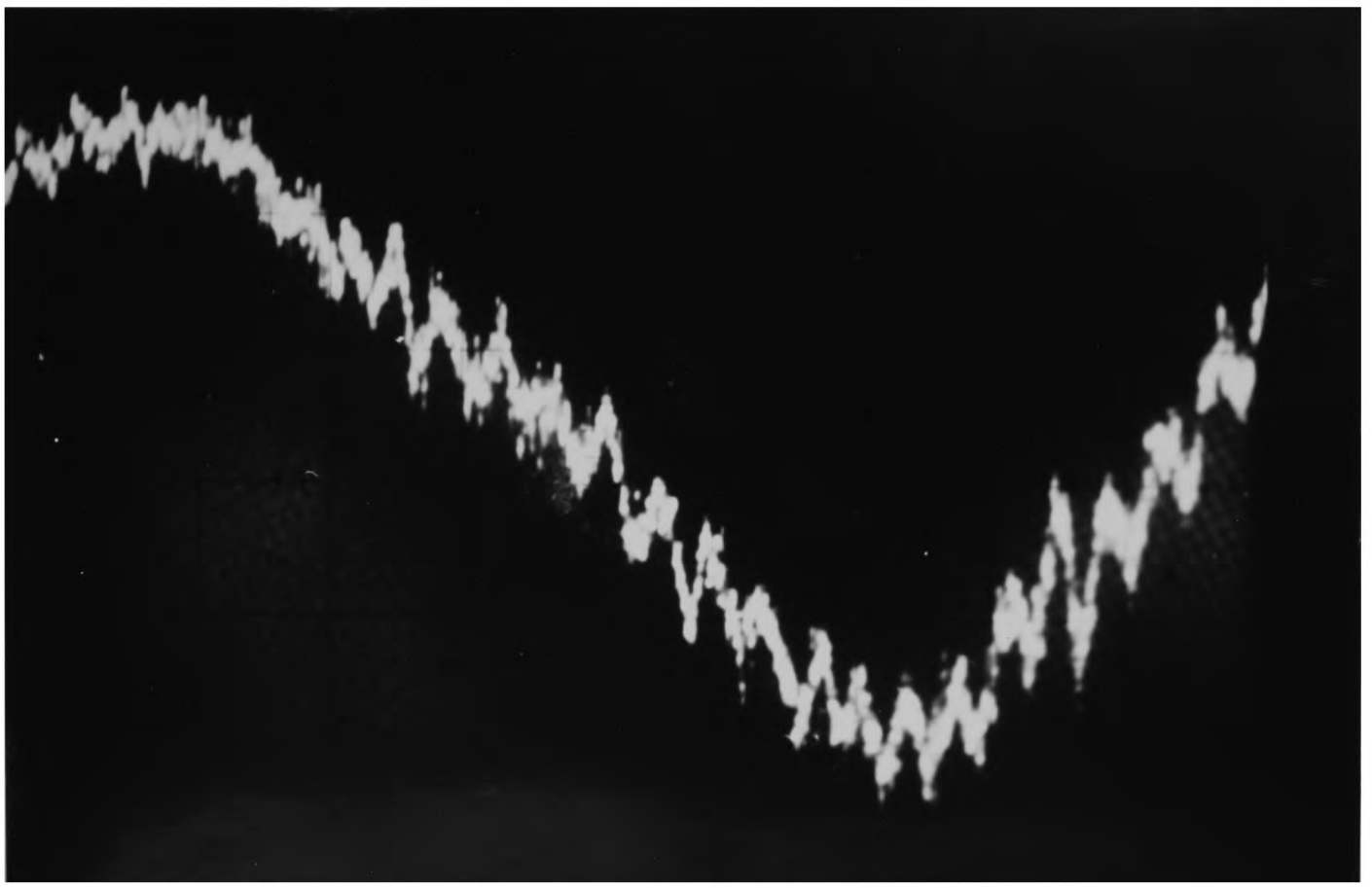

TYPICAL SIGNAL FROM BLACK PLASTIC PELLET

Figure (11.2)

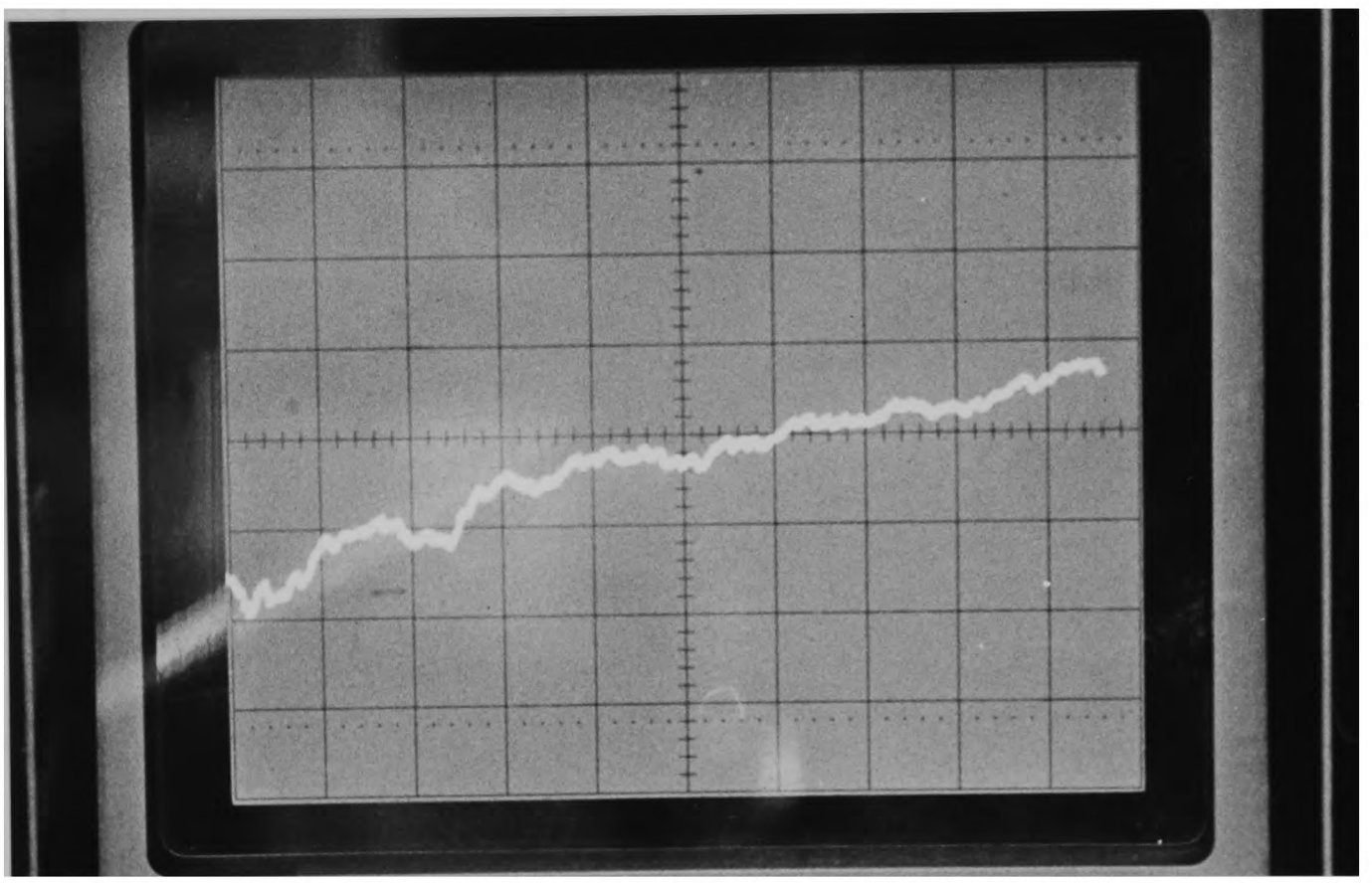

TYPICAL SIGNAL FROM TRANSPARENT PLATIC PELLET

Figure (11.3)

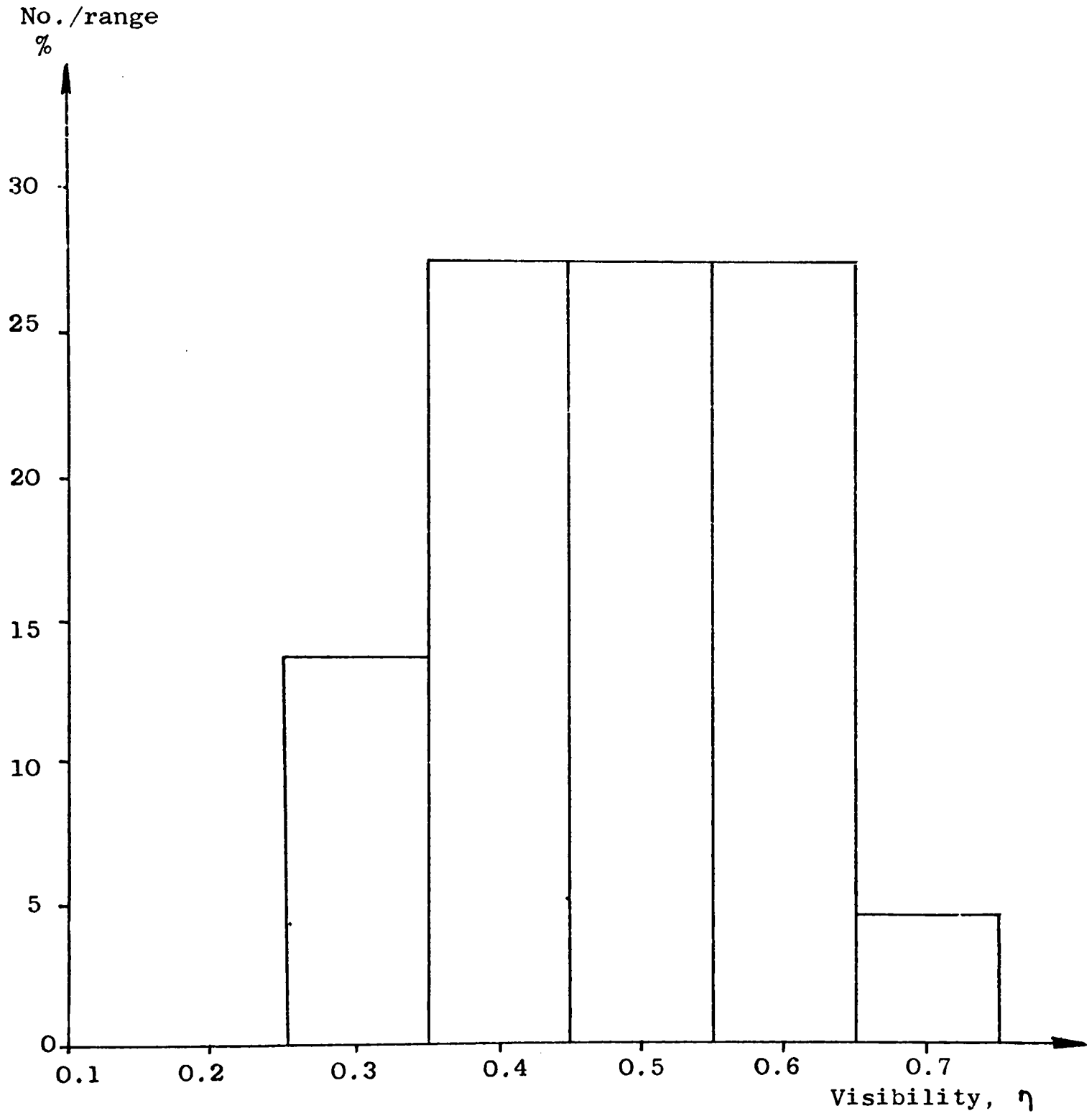

VISIBILITY OF SIGNAL FROM BLACK PLASTIC PELLETS

Figure (11.4)

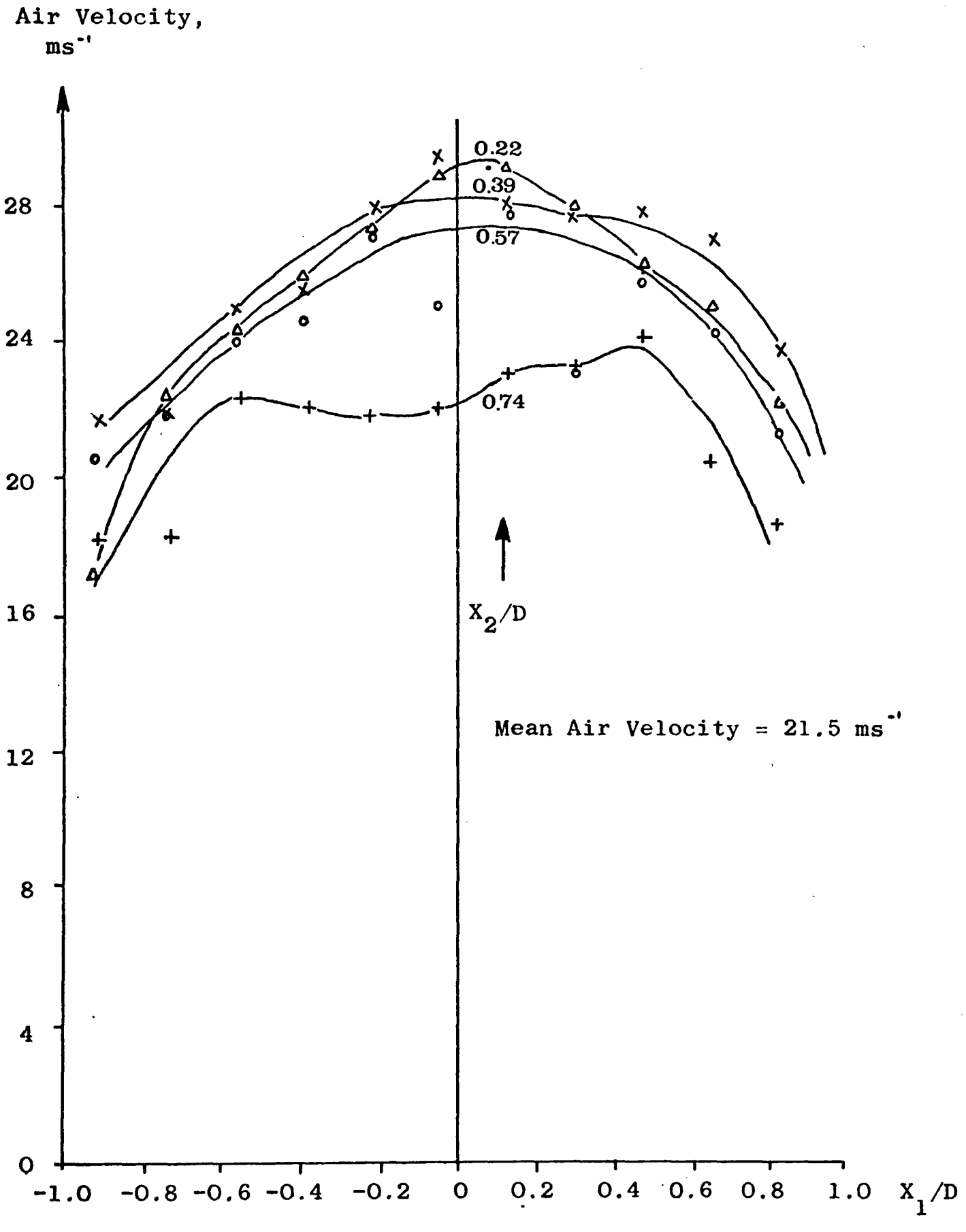

AIR VELOCITY PROFILES, SQUARE PIPE

Figure (11.5)

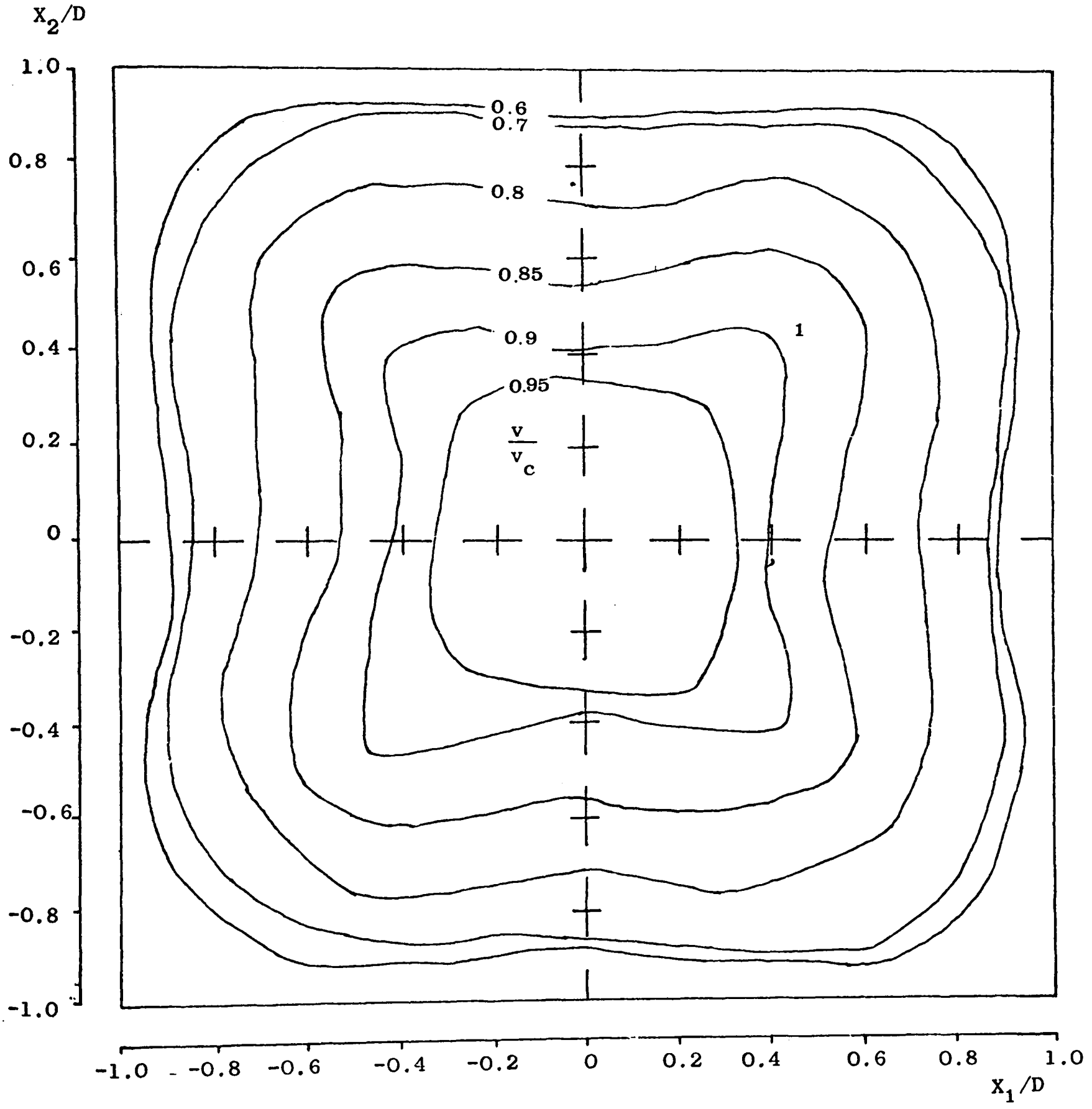

Mean Air Velocity = 21.5 ms^{-1}

AIR VELOCITY DISTRIBUTION IN SQUARE PIPE

Figure (11.6)

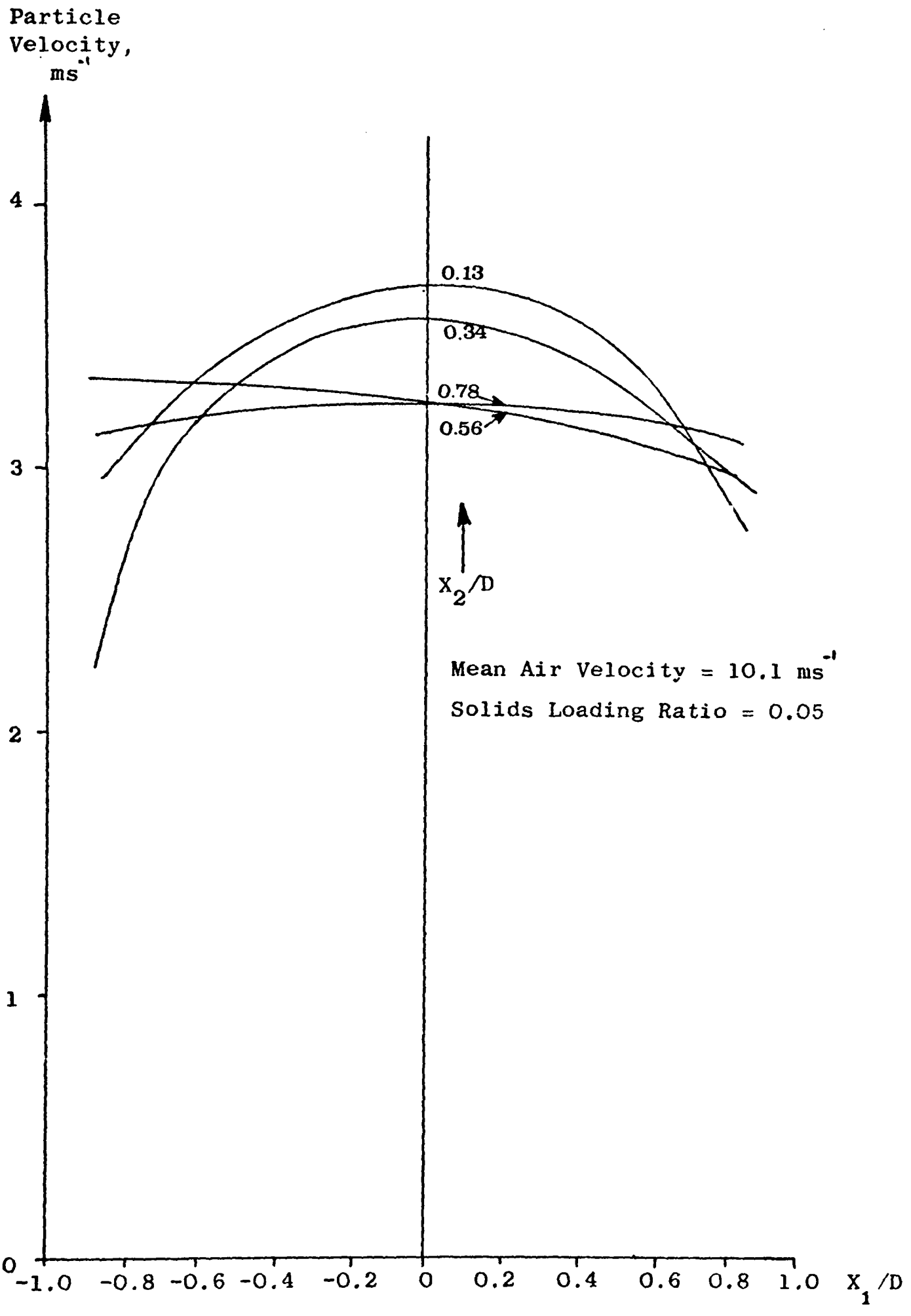

PARTICLE VELOCITY PROFILES, SQUARE PIPE

Figure (11.7)

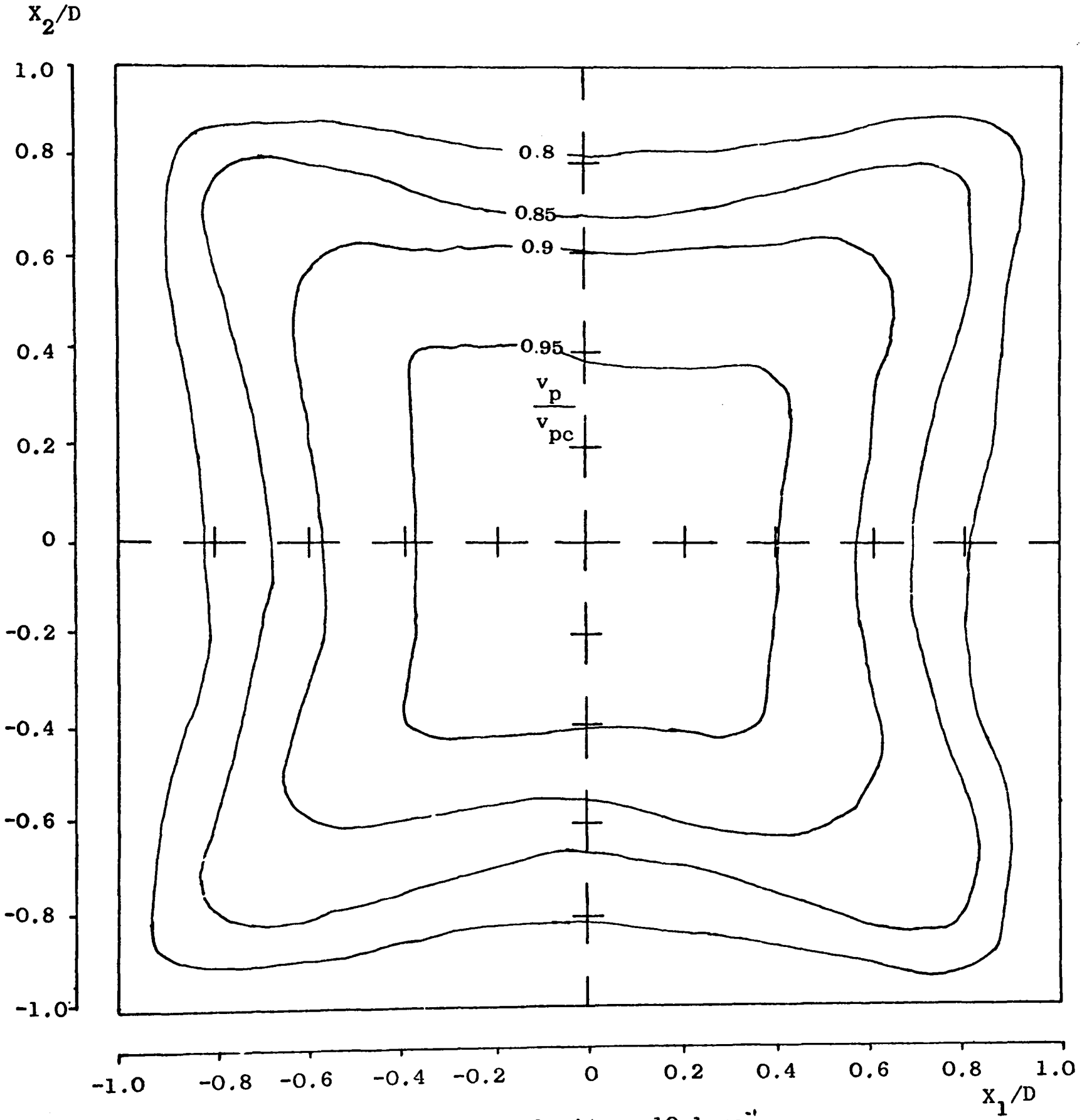

Mean Air Velocity = 10.1 ms^{-1}
Mean Particle Velocity = 2.5 ms^{-1}
Solids Loading Ratio = 0.05

PARTICLE VELOCITY DISTRIBUTION IN SQUARE PIPE

Figure (11.8)

CHAPTER 12

DISCUSSION AND CONCLUSIONS

12.1 Discussion

The work described in this thesis was based on two main aims. Firstly, it was intended to investigate the suitability of the laser Doppler velocity meter, LDV, for particle velocity measurements in ducted air-solid flows and also to find problems involved with these measurements. Secondly, it was intended to make velocity measurements in specific flows and to seek any correlations between the properties of the flow that can be measured.

This research program was initiated because pneumatic conveying is very important in industry and relatively little is known about the behaviour of air-solid flows. Particle velocity is an important factor in such flows, but since there is currently no satisfactory model for two-phase flows, it is impossible to predict the velocity from other measurements. For this reason there is a need for the accurate measurement of particle velocities. A comparison of the available methods of particle measurement showed that the laser Doppler velocity meter appeared to offer the most advantages, but it was only applicable in dilute-phase flows. The research was designed to establish the range of flows for which this instrument was suitable.

12.2 Conclusions

Chapter 2 A survey of the literature published on air-solid flows showed that there were many differences, both in the theoretical and in the experimental work. This indicated a need for more accurate

experimental work, especially on particle velocities. The laser Doppler velocity meter seemed to be one of the most suitable instruments for taking such measurements.

Chapter 4 The air mass flow rate calculated from the orifice plate meter reading using British Standard B.S. 1042 agreed well with the air mass flow rate calculated from the air velocity profiles measured with a Pitot-static tube. Pressure pulsations caused by the solids in the flow did not affect the calibration of the orifice plate. The air velocity profiles measured with the Pitot-static tube above the glass test section differed little from the standard air profiles.

The solid mass flow rate was found to be a function of the pressure drop across the orifice plate and the setting of the screw feeder.

Chapter 6 The literature published on the use of the laser Doppler velocity meter in two-phase flows revealed many problems. The visibility and signal to noise ratio are those for large particles, although the visibility for these particles is much greater than that predicted by the fringe theory. The signal was found to be very intermittent from two-phase flows, and ideally a signal processor was required which was not affected by this intermittency. For most particles forward scatter-dual Doppler mode was found to be best suited.

Chapter 7 The air velocity profiles, when measured with the laser Doppler velocity meter, agreed well with the standard profiles at low velocities, but at higher velocities some deviation from the standard profiles appeared. This was considered to be due to agglomeration of the titanium oxide particles, and the air profiles were taken as standard. The turbulence intensity variation across the pipe was nearly identical to that found by other authors.

Chapter 8 The laser Doppler velocity meter was successfully used in measuring the particle velocity profiles in a flow conveying ballotini. The solids velocity could be measured in flows with solids loading ratios up to 2.5 with the present equipment, but with a more powerful laser this figure could probably have been increased. The frequency tracker was able to follow the signal in flows with air velocities below about 25 ms^{-1}, but with higher air velocities the frequency of each signal had to be read from a storage oscilloscope screen. The velocity of air could be measured with a Pitot-static tube with the ballotini in the flow. The measurement of the particle number density using a pulse counter was found to be impractical.

The curvature of the particle velocity profiles of the ballotini in the air-solid flow was found to decrease with increasing solids loading ratio and with decreasing air velocity. The turbulence intensity of the particles varied less across the pipe than that of free air, and the turbulence in the core of the flow increased with solids loading ratio to a level greater than that of free air. The air velocity profile was unchanged by the particles except for a very slight flattening at the edge of the flow. The pressure drop was found to increase both with solids loading ratio and with the air velocity.

Chapter 9 Equal success was achieved in measuring the particle velocity of the sand in an air-solid flow, using a laser Doppler velocity meter. With the present system the maximum solids loading ratio in which the velocity of the sand particles could be measured was 2.5. Frosting of the pipe wall due to abrasion by the particles was found to be a problem. The frequency tracker could follow the signal of all the flows tested, but the turbulence could not be measured at high velocities and solids loading ratios due to the very intermittent signal.

Air velocity measurements could not be made with the Pitot-static tube due to the excessive degree of abrasion caused by the flow.

The curvature of the velocity profiles was found to increase with the solids loading ratio, which is the opposite trend to that found for the ballotini flow. The turbulence intensity of the sand varied less across the pipe than for the single phase air, and the turbulence intensity at the core of the flow increased with the solid loading ratio. Both of these effects are the same as for the ballotini flow. The pressure drop graphs were also found to be similar to those for the ballotini. Little difference was found between the results for the sieved and unsieved sand.

Chapter 10 The velocity profiles of the sand particles were similar to those for the air, whereas those for the ballotini were flatter than those for the air. The ballotini profiles were found to fit the equation (10.2) of Reddy and Pei (1969), but the sand profiles did not.

The slip velocity was found to increase with the solids loading ratio and as the square of the mean air velocity. The slip was greater than the terminal velocity of individual particles except in flows with the lowest air velocities.

The solids friction factor was found to increase with the solids loading ratio, but comparisons with other authors was difficult due to variations in the definitions of the solids friction factor. No conclusions could be drawn from the calculated drag coefficients of the solids in the flow since no trends were obvious.

Chapter 11 The laser Doppler velocity meter was found to be capable of measuring the velocity of particles several millimetres in diameter. The visibility from opaque particles was much greater than the visibility from transparent particles. The latter visibility was found to be too small to be analysed. Backscatter mode was found to be suitable for velocity measurements on particles of this size.

CHAPTER 13

SOME SUGGESTIONS FOR FURTHER WORK

13.1 Development of the LDV

The work described in this thesis has shown that the laser Doppler velocity meter is suitable for measuring the velocities of particles in dilute air-solid flows. However, it was found that the apparatus available for this work was not ideally appropriate. There is, therefore, a need for developing a laser Doppler velocity meter specifically for this purpose. The main area in which the LDV could be improved is in the processing of the Doppler signal received by the photomultiplier. The present investigation has shown that for particles several hundred microns in diameter, the tracking filter is inappropriate for air-solid flow measurements, though for smaller particles it has been used with some success [Birchenough (1975)]. For particles 500 μm in diameter, Riethmuller and Ginoux (1973) used a period counter for signal analysis, and this method has the advantage that it is not affected by intermittent signals. However, although the period counter has obvious advantages over the frequency tracker, the high degree of filtering necessary for it to work may remove some of the useful signal in highly turbulent flows. Recently, [Baker and Wigley (1975)] filter banks have been developed which may prove useful in two phase flow measurements.

The maximum solids to air mass flow rate ratio of the flow in which particle velocities can be measured is dependent both on the laser power and on the size of the particles. This dependence on the size of the particles needs to be further investigated. Large particles have a smaller number density than small particles in a flow with the same

solids loading ratio, but the larger particles obscure more of the light beam. Increasing the power of the laser will increase the light in the measuring volume. This should enable velocity measurements to be made in flows with higher solids loading ratios, since even if a high proportion of the light is scattered, sufficient light will reach the probe volume.

In chapter 11 it was found that the LDV could be used successfully in measuring the velocities of quite large particles. Difficulties were found in the poor quality of the signal from the transparent particles, though the reasons for this were not clear. In order to obtain a better knowledge of the limitations of the instrument, and the reasons for these limitations, research into the behaviour of the LDV with a larger variety of particles should be undertaken. This would indicate the types of solids which are suitable for measurements with the LDV.

Development of an industrial LDV for use in air-solid flows is a possibility, but the instrument is very expensive, which would restrict the applications. Such an instrument would be useful during the commissioning of a pneumatic conveying plant, for instance in optimising the solids mass flow rate. This optimisation could be continued when the plant was in use by applying a technique suggested by Birchenough and Mason (1976) in which the particle velocity at the wall is measured using the backscatter mode. Measurements can be carried out in very dense flows and a reverse flow of particles at the wall indicates that choking is about to occur. Another industrial use for the LDV is in chemical plants, where the reaction times can be critical and particles have to remain in the flow for a fixed time. A feedback loop using the LDV could control the velocities of the particles accurately.

The laser Doppler velocity meter could be developed to measure several properties of an air solid flow in addition to the particle velocity. As described in section (8.4), it is possible to measure simultaneously the velocity and turbulence, both axial and radial, of both the air and the particles using the LDV, with appropriate electronics to separate the signals from the large and small particles. Also the technique of measuring the local particle number density with the LDV could be improved. The distribution of particle sizes in the flow could also be measured by measuring the length of each pulse, provided that the diameter of the measuring volume was known as well as the particle velocity. All these techniques should preferably be performed with the aid of electronic processing in order that a statistically significant sample can be obtained.

Another measurement on the flow that could possibly be made is the electrostatic charge on the particles. If a strong transverse electric field was switched on whilst both the axial and transverse particle velocities were being observed by means of a two-dimensional laser Doppler velocity meter, the mean change in the transverse particle velocity would give the local mean electrostatic charge per particle. Unfortunately the mean particle charge is likely to be very small, so that for heavy particles very strong electric fields would be required in order to produce significant transverse velocities. If this method did work it would provide a means of finding the charge on each particle without greatly disturbing the flow. The particle charge has not so far been measured without ambiguity.

13.2 Air-Solid Flows

It was suggested in chapter 2 that there is a great need for accurate experimental work to be carried out on a variety of flows, in order that some progress can be made towards establishing a useful

model of air-solid flows. If the properties of enough flows were reliably investigated, then correlations between the properties and parameters of the flow could be obtained.

The LDV could be usefully employed in measuring the properties of flows such as those investigated in the present work, but with different solids, so that the effects of particle shape, size, density, et cetera could be tested. Also the diameter of the pipe could be varied and the inclination of the pipe to the horizontal could be changed to find how the flow behaviour is determined by these factors.

Another area of interest which needs to be investigated is flows which are not fully developed, such as in pipe bends and acceleration regions. The flow in pipe bends would be particularly difficult to determine using the LDV since large pipe bends are difficult to obtain. Also, the laser beams would be refracted by the curvature of the pipe in more than one direction, making it difficult to get the two beams to cross in one plane. The measurement of the properties on a linear acceleration region should be fairly straightforward and would be very useful. A comparison of the velocity profile of the air and the solids in such a region with the pressure drop in the pipe would be valuable and indicate how long the flow takes to develop.

CALCULATION OF AIR MASS FLOW RATE

The computer program "Pitot" was written to calculate the air mass flow rate from the Pitot-static traverse measurements. The principle of the programe was as follows :-

The air velocity, v(r), from equation (4.3) and the radial position, r, at the measuring point and a polynomial was fitted to the curve of v(r).r against r using the method of least squares. This polynomial was integrated across the pipe and, using equation (4.5), the air mass flow rate was calculated. The volumetric flow rate and average air velocity were calculated using equations (4.6) and (4.7) respectively. The air velocity profile was compared with the standard air profile given by Ower and Pankhurst (1977).

Errors were caused by the use of a polynomial fit to the curve, especially near the edge of the pipe. However, these errors were small, and excellent agreement was found when in a few cases the air madd flow rate calculated using this computer program was compared with the results of a graphical model. The latter method took account of the zero air velocity at the pipe wall, which the computer program did not.

On the following pages a block diagram of the computer program is given, together with the program itself and an example of the print-out.

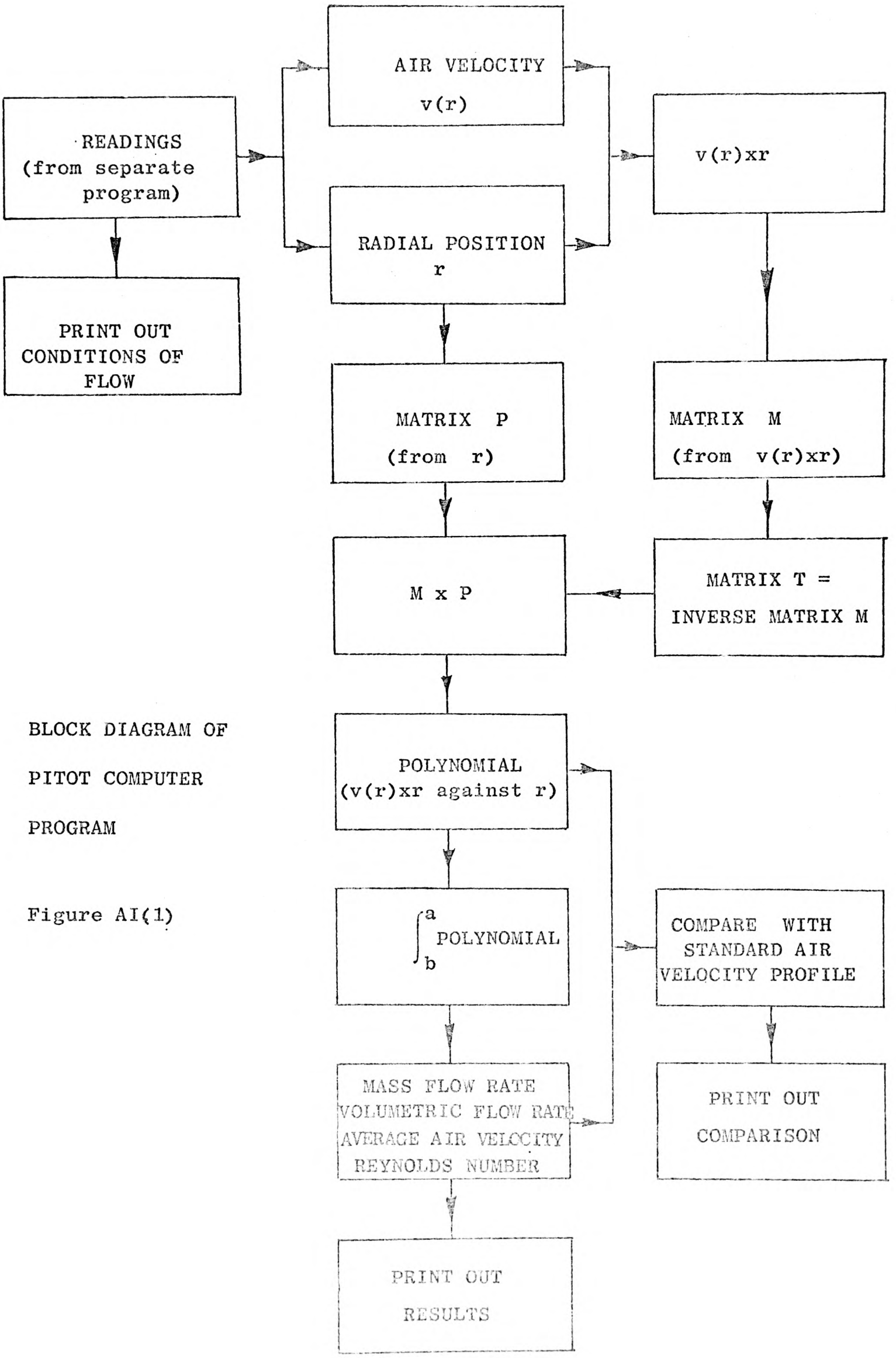

BLOCK DIAGRAM OF

PITOT COMPUTER

PROGRAM

Figure AI(1)

```
4 FILES FGAS33
5 DIM A(50),B(50),C(50),D(50,50),P1(10,50),Y1(50),U1(50)
6 DIMU(50),X(50),Y(50),A1(50),B1(50)
7 DIM M(5,5),P2(5,1)
10 READ #1,N1,A1,T1,N,P5,P6,T5,T6,P7,Z1,K5
12 READQ,W,Z,M1,M2
80 LET R=((T1+273)*58.512)/((P7*M1)+(A1*.136))
85 PRINT
90 PRINT "RUN NO:" N1
100 PRINT "ATMOSPHERIC PRESSURE"A1"CM OF HG"
110 PRINT "TEMPERATURE"T1"CELSIUS."
112 PRINT "PRESSURE DROP ACROSS ORIFICE"P5"CM OF H20"
114 PRINT "UPSTREAM PRESSURE"P6"CM OF HG"
116 PRINT "TEMPERATURE,WET"T5",DRY"T6"CELSIUS"
118 PRINT "STATIC  PRESSURE"P7*M1"M OF H20"
119 PRINT "LOADING" K5
120 PRINT
125 PRINT "DISP","PRESS.DIFF"
130 FOR A=1 TO N
140 READ #1,A(A),B(A)
150 PRINT A(A),B(A)
160 LET A1(A)=Z1-A(A)
170 LET X(A)=SGN(A1(A))*A1(A)*.01
180LET U(A)=SQRT(R*B(A)*M2*9.81)
190 LET Y(A)=X(A)*U(A)
200 NEXT A
230
642 LET N2=N2-(62.5*(R1↑4))
1060 FOR B=1 TO N
1070 LET D(0,B)=1
1080 FOR C=1 TO 2*(Q+1)
1090 LET D(C,B)=D(C-1,B)*X(B)
1100 NEXT C
1110 NEXT B
1120 FOR E=1 TO 2*(Q+1)
1130 FOR D=1 TO N
1140 LET S(E)=S(E)+D(E,D)
1150 NEXT D
1160 NEXT E
1170 LET S(0)=N
1180 LET F=0
1190 FOR G=1 TO Q+1
1200 FOR H=1 TO Q+1
1205 LET M(G,H)=S(F)
```

```
1210 LET F=F+1
1220 NEXT H
1230 LET F=F-Q
1240 NEXT G
1260 MAT T=INV(M)
1270 FOR I=1 TO N
1280 LET P3=1
1290 FOR J=1 TO Q+1
1300 LET P1(J,I)=P3*Y(I)
1310 LET P3=X(I)*P3
1320 NEXT J
1330 NEXT I
1340 FOR K=1 TO Q+1
1350 FOR L=1 TO N
1360 LET P2(K,1)=P1(K,L)+P2(K,1)
1370 NEXT L
1380 NEXT K
1384 PRINT
1385 MAT O=T*P2
1450 FOR Q1=1 TO N
1460 FOR N1=1 TO Q+1
1470 LET Y1(Q1)=O(N1,1)*X(Q1)↑(N1-1)+Y1(Q1)
1480 NEXT N1
1490 LET U1(Q1)=Y(Q1)-Y1(Q1)
1510 LET S2=S2+U1(Q1)*U1(Q1)
1520 NEXT Q1
1530 LET S3=S2/(N-Q)
1540 PRINT "STANDARD ERROR OF POLY-FIT:"SQRT(S3)
1545 IFA3>0 THEN 3000
1546 LET A3=1
2000 FOR O1=1 TO Q+1
2020 LET A2=O(O1,1)*(Z↑(O1)-W↑(O1))/O1+A2
2040 NEXT O1
2045 PRINT
2055 LET A3=A2*6.2832
2060 PRINT "VOLUMETRIC FLOW RATE"A3"M"
2065 PRINT "MASS FLOW RATE" A3*2000/R"KG/S"
2100 DATA 4
2105 DATA 0,.02586
2110DATA .01,.01
2595 DIM V1(50),C1(50)
2600 LET U2=2*A2/Z↑2
2605 PRINT "AVERAGE VELOCITY"U2"M/S"
2610 LET R1=2*Z*2000*U2/((1.75E-5)*R)
2620 PRINT "REYNOLD'S NO:"R1
2625 PRINT
2626 PRINT
2630 PRINT " X,M"," Y,M↑2/S"," V,M/S"," V',M/S","V-V'"
2635  LET R1=R1/1E+6
2640 LET N2=6.61255+(17.609*R1)-(58.875*(R1↑2))+(98.75*(R1↑3))
```

```
2644 LET M2=1/N2
2646 LET S2=0
2648 LET O(1,1)=(N2+1)*((N2*2)+1)*U2/(N2*N2*2)
2650 FOR F1=1 TO N
2660 LET V1(F1)=O(1,1)*(1-X(F1)/Z)^M2
2670 LET C1(F1)=U(F1)-V1(F1)
2680 PRINT X(F1),Y(F1),U(F1),V1(F1),C1(F1)
2685 LET S2=S2+C1(F1)*C1(F1)
2690 NEXT F1
2700 LET S3=S2/(N-Q)
2710 PRINT
2720 PRINT
2730 PRINT "STANDARD ERROR OF POLYFIT:"SQRT (S3)
3000 END
```

```
FGAS33          11:47          09-OCT-79


10 33
20 75.555,16
30 24
40 11.85,12.3,13,18,6.22
45 6.5,0
50 4,1.78,4.2,2.16,4.4,2.28,4.6,2.72,4.8,2.94,5,3.18,5.2,3.4
60 5.4,3.58,5.6,3.84,5.8,4,6,4.18,6.2,4.3,6.4,4.4,6.6,4.44,
70 6.8,4.44,7,4.4,7.2,4.3,7.4,4.16,7.6,4,7.8,3.82
80 8,3.58,8.2,3.4,3.4,3.4,3.18,8.5,3.04
```

RUN

PITOT 12:06 09-OCT-79

RUN NO: 33
ATMOSPHERIC PRESSURE 75.555 CM OF HG
TEMPERATURE 16 CELSIUS.
PRESSURE DROP ACROSS ORIFICE 11.85 CM OF H20
UPSTREAM PRESSURE 12.3 CM OF HG
TEMPERATURE, WET 13 , DRY 18 CELSIUS
STATIC PRESSURE 0.0622 M OF H20
LOADING 0

DISP	PRESS. DIFF
4	1.78
4.2	2.16
4.4	2.28
4.6	2.72
4.8	2.94
5	3.18
5.2	3.4
5.4	3.58
5.6	3.84
5.8	4
6	4.18
6.2	4.3
6.4	4.4
6.6	4.44
6.8	4.44
7	4.4
7.2	4.3
7.4	4.16
7.6	4
7.8	3.82
8	3.58
8.2	3.4
8.4	3.18
8.5	3.04

STANDARD ERROR OF POLY-FIT: 1.14488E-2

VOLUMETRIC FLOW RATE 4.54783E-2 M
MASS FLOW RATE 5.56051E-2 KG/S
AVERAGE VELOCITY 21.647 M/S
REYNOLD'S NO: 78221.8

X,M	Y,M↑2/S	V,M/S	V',M/S	V-V'
0.025	0.422517	16.9007	16.7277	0.172959
2.30000E-2	0.428202	18.6175	19.5621	-0.944592
2.10000E-2	0.401681	19.1277	20.9609	-1.83325
1.90000E-2	0.396947	20.8919	21.9234	-1.03148
0.017	0.369247	21.7204	22.6663	-0.94593
0.015	0.338844	22.5896	23.2753	-0.685762
1.30000E-2	0.303653	23.3579	23.7935	-0.435599
1.10000E-2	0.26365	23.9682	24.2453	-0.277532
9.00000E-3	0.22341	24.8233	24.6478	0.175478
7.00000E-3	0.177346	25.3352	25.0104	0.324804
0.005	0.129495	25.899	25.3409	0.55305
3.00000E-3	7.88043E-2	26.2681	25.6449	0.623152
0.001	2.65718E-2	26.5718	25.9267	0.645131
1.00000E-3	2.66923E-2	26.6923	25.9267	0.765639
3.00000E-3	8.00769E-2	26.6923	25.6449	1.04735
0.005	0.132859	26.5718	25.3409	1.23086
7.00000E-3	0.183877	26.2681	25.0104	1.2577
9.00000E-3	0.232532	25.8369	24.6478	1.18909
1.10000E-2	0.273687	25.3352	24.2458	1.08944
1.30000E-2	0.321862	24.7586	23.7935	0.965097
0.015	0.359523	23.9682	23.2753	0.692395
1.70000E-2	0.397034	23.3579	22.6663	0.69156
0.019	0.429202	22.5896	21.9234	0.666146
0.02	0.441734	22.0867	21.4731	0.608652

STANDARD ERROR OF POLYFIT: 0.956967

TIME: 3.04 SECS.

The program was modified slightly in order to process the results of the air velocity measurements made using the LDV, which are described in chapter 7. As before, the air mass flow rate was calculated but, in addition, corrections on the turbulence intensity measurements described in chapter 6 were calculated. A similarly modified program was used to calculate the average solids velocity from the particle velocity profiles, which were measured as described in chapters 8 to 10. An example of the print out from each of these modified programs is given in the following pages.

TRAVERSE NO. 15
DATE 27 JUNE 1977
ATMOSPHERIC PRESSURE 76.665 CM OF HG
AIR TEMPERATURE 26 CELSIUS
PRESSURE DROP ACROSS ORIFICE 28.1 CM OF H2O
UPSTREAM PRESSURE 43 CM OF HG
TEMPERATURE, WET 15 ; DRY 20 CELSIUS

EXTRA AIR, VOLUME 1.07500E-3 M**3/S
EXTRA AIR, MASS 1.28132E-3 KG/S

FOCAL LENGTH 0.3 M
SINE ANGLE 5.08900E-2

DISP	DC-VOLTS	RMS-VOLTS
74	4.51	0.26
74.2	4.78	0.3
74.4	5.27	0.27
74.6	5.4	0.27
74.8	5.4	0.26
75	5.54	0.26
75.2	5.68	0.25
75.4	5.68	0.23
75.6	5.75	0.23
75.8	5.82	0.22
76	5.88	0.2
76.2	5.92	0.2
76.4	5.83	0.18
76.6	5.74	0.22
76.8	5.62	0.22
77	5.45	0.26
77.2	5.4	0.28
77.4	5.22	0.31
77.6	4.96	0.34
77.8	4.71	0.32
78	4.4	0.35

STATIC PRESSURE 0.379 M OF H2O
VOLUMETRIC FLOW RATE 9.25228E-2 M^3/S
MASS FLOW RATE 0.114289 KG/S

AVERAGE VELOCITY 46.8212 M/S
REYNOLDS NO: 108644.

RAD,M	VEL,M/S	STD.VEL,M/S	TURB.INT,%	CORRECTED,%
2.14800E-2	42.0602	43.903	5.76497	5.61728
1.94800E-2	44.5783	46.4002	6.27615	6.03761
1.74800E-2	49.148	48.2086	5.12334	4.9623
1.54800E-2	50.3604	49.6396	5	4.98981
1.34800E-2	50.3604	50.8298	4.81481	4.80312
1.14800E-2	51.666	51.8522	4.69314	4.65801
9.48001E-3	52.9717	52.7507	4.40141	4.38946
7.48001E-3	52.9717	53.5534	4.0493	4.04278
5.48001E-3	53.6245	54.28	4	3.98706
3.48000E-3	54.2773	54.9443	3.78007	3.7678
0.00148	54.8369	55.5569	3.40136	3.39127
5.19995E-4	55.2099	55.835	3.37838	3.37193
2.51999E-3	54.3706	55.2443	3.08748	3.06395
4.51999E-3	53.5312	54.6059	3.83275	3.80802
6.52000E-3	52.4121	53.9107	3.91459	3.87079
8.52000E-3	50.8267	53.1466	4.77064	4.74728
1.05200E-2	50.3604	52.2969	5.18519	5.16164
1.25200E-2	48.6817	51.3383	5.9387	5.86662
1.45200E-2	46.2569	50.2355	6.85484	6.76312
0.01652	43.9254	48.932	6.79406	6.67091
0.01852	41.0344	47.3285	7.95455	7.8077

READY
RUNNH

RUN NO:C1-1
ATMOSPHERIC PRESSURE 76.54 CM OF HG
TEMPERATURE 16 CELSIUS.
PRESSURE DROP ACROSS ORIFICE 10.8 CM OF H20
UPSTREAM PRESSURE 4 CM OF HG
STATIC PRESSURE 0.052 M OF H20
LOADING-1

RAD	VEL	TURB
0.024	12.34	11.0762
2.20000E-2	14.62	8.9843
0.02	15.46	8.59411
0.018	16.25	7.94221
0.016	17.92	6.77735
0.014	18.61	6.72996
0.012	19.14	6.34485
0.01	19.33	6.0858
0.008	20.28	5.9877
0.006	20.16	5.64636
0.004	20.51	5.54985
0.002	20.54	5.34035
0	20.96	5.32563

STANDARD ERROR OF POLY-FIT: 5.00836E-3

AVERAGE VELOCITY 16.6666 M/S

TIME: 1.20 SECS.

NOMENCLATURE

Chapter 2

A	Function in equation (2.3)
C_D	Drag coefficient of particle
D	Pipe diameter
d	Particle diameter
f	Friction factor
G	Mass flux or velocity ($\dot{m}/2\pi R$)
g	Acceleration due to gravity
k	Function in equation (2.3)
L	Length
L_s	Ratio of mass flow rate of solid to mass flow rate of air ($\dot{m}_s/\dot{m}_a$)
m	Constant in equation (2.10)
$\dot{m}$	Mass flux rate
Δp	Pressure drop
R	Radius of pipe (D/2)
Re	Reynolds Number
v	Velocity
$\bar{v}$	Average velocity
x	Perpendicular distance from pipe wall
α	Acceleration
θ	Angle of inclination to the horizontal
ρ	Density
τ	Shear stress
Subscripts:	a = air, c = pipe axis, f = friction, h = static head
	m = air-solid suspension, p = particle, s = solid,
	T = total, w = pipe wall, α = acceleration, τ = terminal

Chapter 4

h_t, h_s	Defined in section (4.6)
k	Constant in equation (4.8)
M	Mach number
$\dot{m}_a$	Mass flow rate of air
$\dot{m}_s$	Mass flow rate of solid
p	Static pressure
p_o	Pitot pressure
r	Radius of pipe
$\dot{V}_a$	Volumetric flow rate of air
$v(r)$	Air velocity at radius r
γ	Ratio of specific heats
ℓ	Setting on screw feeder

Chapter 5

A, A', A_1, A_2	Real amplitudes in equations (5.1),(5.2),(5.15), (5.16)
B_o	Real amplitude in equations (5.41) and (5.42)
C	Velocity of light
d_{ph}	Diameter of pinhole
d_v	Diameter of measuring volume
e'	Electronic charge
f_1, f_2	Focal lengths of transmitting and receiving lenses
Δf	Bandwidth of detector circuitry
G	Photomultiplier gain
h	Plank's constant
I	Light intensity
i	Imaginary number ($\sqrt{-1}$)
i_D	Photocathode dark current
K	Average gain per dynode of photomultiplier

k	Boltzman's constant
N	Integer
N_F	Number of fringes
P_1, P_2	Light power of incident beams
P_B	Light power from background
r, r'	Distance from origin in systems Σ and Σ'
r_1, r_2	Distance from origin in systems in figure (5.11)
r_o	Beam waist radius
T	Time
T'	Absolute temperature
t, t'	Time co-ordinate in systems Σ and Σ'
V	Velocity
v_x, v_y, v_z	Particle velocity components
x,y,z; x',y',z'	Linear co-ordinate in systems Σ and Σ'
$x_1,y_1,z_1;x_2,y_2,z_2$	Linear co-ordinates in systems in figure (5.11)
ΔX, ΔY, ΔZ	Dimensions of measuring volume
β	Relativistic dilation $(1-V^2/C^2)^{\frac{1}{2}}$
δ	Fringe separation normal to fringes
δ_x, δ_y	Finge separation in x- and z- directions
ε^2	Heterodyning efficiency
η	Quantum efficiency of detector
θ	Half angle of separation between beams
θ_1, θ_1'	Angles to x-axis in systems Σ and Σ'
θ_2, θ_3	Defined in figure (5.4)
θ'	Angle between receiver and x-axis
λ	Wavelength of light
λ_1, λ_2	Wavelengths
ν, ν'	Light frequency in systems Σ and Σ'
ν_r, ν_{r_1}, ν_{r_2}	Reflected light frequency in equations (5.5),(5.10),(5.11)

ν_1, ν_2	Frequency of incident light beams
ν_m	Beat frequency ($\nu_{r_1} - \nu_{r_2}$)
ν_s	Frequency difference between incident light beams ($\nu_1 - \nu_2$)
ν_D	Doppler frequency
ν_F	Frequency from fringe model
$d\nu$, $d\nu_D$, $d\nu_T$, $d\nu_G$	Bandwidth of signal:- total, Doppler, from finite transit time broadening, from velocity gradient broadening,
$d\nu_I$	from instrument broadening
ξ_1, ξ_2	Complex amplitudes in equations (5.15) and (5.16)
ξ_1^*, ξ_2^*	Complex conjugates of ξ_1 and ξ_2
Σ, Σ'	Co-ordinate systems
σ	Unfocussed beam radius
$\sigma_x, \sigma_y, \sigma_z$	Dimensions of probe volume at e^{-2} of centre intensity
ϕ	Angle between velocity vector V and x-axis
ϕ_1, ϕ_2	Phase angles in equations (5.15) and (5.16)
ψ, ψ'	Wavefunction in systems Σ and Σ'
Ω	Angle of fringes to x-axis

Chapter 6

d_s	Particle diameter
I_1	Signal intensity at maximum
I_2	Signal intensity at following minimum
L	Solids to air mass flow rate ratio
P_1, P_2, P_3	Light power defined as in chapter 5
η	Signal visibility
ρ_a	Density of air
ρ_s	Density of solid

Chapter 7

a	Pipe radius
m	Constant in equation (7.2)
r	Radius in pipe

Re	Reynolds Number
v_c	Air velocity at pipe axis
v_r	Air velocity at radius r
δ_v	Air velocity bandwidth
$\bar{\xi}$	Mean output voltage of tracker
$\xi_{r.m.s.}$	Root mean square of output voltage of tracker

Chapter 8

a	Pipe radius
f	Decay constant of light intensity
m	Constant in equation (8.1)
r	Radiusin pipe
v_c	Air velocity at pipe axis
v_r	Air velocity at radius r
v_p	Particle velocity at radius r
v_{pc}	Particle velocity at pipe axis
x	Distance from pipe wall nearest laser

Chapter 9 As chapter 8

Chapter 10

A	Cross-sectional area of particle normal to direction of motion
C_D	Drag coefficient
C_D	Effective drag coefficient
D	Pipe diameter
d	Mean particle diameter
F	Friction factor
F_D	Drag force
Fr	Froude number $(\bar{v}_a^2/gD)$
Fr	Froude number $(\bar{v}_a/\sqrt{gD})$
g	Acceleration due to gravity

L	Length
L_s	Solid to air mass flow rate ratio
m	Constant in equations (10.1) and (10.2)
n	Number of particles per unit length of pipe
Δp	Pressure drop
Re_p	Particle Reynolds Number (defined in equation (10.3))
v	Velocity
x	Distance from pipe wall
α, β	Constants in equation (10.11)

Subscripts:

a = air, c = pipe axis, f = fluid, F = friction, h = static head,

m = gas-solid suspension, p = particle, r = pipe radius, s = solid,

T = total, w = pipe wall, τ= terminal

Chapter 11

D	Length of pipe side
v_p	Particle velocity
v_{pc}	Centre particle velocity
v	Air velocity
v_c	Centre air velocity
X_1, X_2	Directions parallel to pipe sides

APPENDIX IV

PUBLICATION

Andrews,D.G.H. and Birchenough, A. (1979) "Measurement and Comparison of the Velocities of Particles in an Air-Solid Flow", paper presented at 2nd European Symposium on Particle Characterisation, 24-26 September, Nurenburg.

APPENDIX AIII

BIBLIOGRAPHY

Adrian, R.J. and Orloff, K.L. (1977) "Laser Anemometer: Visibility Characteristics and Applications to Particle Sizing" Applied Optics, Vol.16, no.3, pp 677-664.

Baker,R.J. and Wigley, C. (1975) "Design, Evaluation and Application of a Filter Bank Signal Processor" Proc. LDA-Symp.,Copenhagen, pp 350-363.

Barker, R.H. Riethmuller, M.L. and Ginoux, J.J. (1972) "The Development of a Laser Velocity Meter for Measurement of Solid Particle Velocity in a Two-Phase Flow", Von Karman Inst., Technical Note 81.

Birchenough, A. (1975) "The Application of Laser Measurement Techniques to the Pneumatic Transport of Fine Particles", PhD Thesis, Thames Polytechnic, London.

Birchenough, A. and Mason, J.S. (1976) "Particle Wall Velocity Measurements in a Densely Flowing Gas-Solid Suspension", paper B2, Pneumotransport 3, Bath, England.

Boothroyd, R.G. (1966) "Pressure Drop in Duct Flow of Gaseous Suspensions of Fine Particles", Trans. Instn. Chem.Engrs., Vol. 44 pp T306-T313.

Boothroyd, R.G. (1971) "Flowing Gas-Solid Suspension, Pub. Chapman and Hall, London.

Born, M. and Wolfe, E. (1964) "Principles of Optics" pub. Pergamon Press, Oxford.

Boutier, A. and Philbert, M. (1972)	"Velocity Measurement in Gas and Liquid Flows in an Interference Velocimeter", Project Sqid, Proc. Workshop "The use of the LDV for Flow Measurement", Purdue University, pp 33-40.
Brayton, D.B. and Goethert, W.H. (1972)	"A New Dual-Scatter Laser-Doppler-Shift Velocity Measuring Technique", ISA Trans., Vol. 10, No.1, pp 40-50.
Brayton, B.D., Kalb, H.T. and Crosswy, F.L. (1973)	"Two Component Dual-Scatter Laser Doppler Velocimeter with Frequency Burst Signal Readout", Applied Optics, Vol. 12, No.6, pp 1145-1156.
BS 1042	"Methods for the Measurement of Fluid Flow in Pipes", British Standards Institution.
Buchave, P. (1973)	"Light Collecting System and Detector in a Laser Doppler Anemometer", DISA Information, No.15, pp 15-20.
Carlson, C.R. (1973)	"Turbulent Gas-Solid Flow Measurements Utilizing a Laser Doppler Velocimeter", Thesis, Rutgers University, New Jersey.
Carlson, C.R. and Peskin, R.L. (1975)	"One Dimensional Particle Velocity Probability Densities in Turbulent Gas-Particle Duct Flow", Int.J. Multi-phase Flow, Vol. 2, pp 67-76.
Chan, V.K. (1976)	"Characteristics of Dilute Gas-Solid Suspension Flows", PhD Thesis, City University, London.

Chandok, S.S. and Pei, D.C.T. (1971) "Particle Dynamics in Solid-Gas Flows in a Vertical Pipe", paper B5, Pneumotransport 1, Cambridge, England.

Clark, R.H., Charles, D.E., Richardson, J.F. and Newitt, D.M. (1952) "Pneumatic Conveying, Part I: The Pressure Drop During Horizontal Conveyance", Trans. Instn. Chem. Engrs., Vol. 30, pp 209-224.

Cramp, W. and Priestley, A. (1924) "Pneumatic Grain Elevators", The Engineer, pp 34, 64, 89 and 112.

Cramp, W. (1925) "Pneumatic Transport Plants", J.Soc. Chem.Insdust., Vol. XLIV, No.18, pp 207T-210T, and No.19, pp 211T-213T.

Davies, W.E.R. (1973) "Velocity Measurements in Bubbly Two-Phase Flows using Laser Doppler Anemometry, Part 1", UTIAS Tech. Note No. 184, Inst.for Aerospace Studies, University of Toronto.

Deighton, M.D. and Saylel, E.A. (1971) "An Electronic Tracker for the Continuous Measurement of Doppler Frequency from a Laser Anemometer", DISA Information, No.12, pp 5 -10.

Doig, I.A. and Roper, G.H. (1967) "Air Velocity Profiles in the Presence of Concurrently Transported Particles", Indust.Eng.Chem.Fundamentals, Vol. 6, No.2, pp 247-256.

Drain, L.E. and Moss, B.C. (1972) "The Frequency Shifting of Laser Light by Electro-Optic Techniques", Proc. Conf. "Electro-Optic Systems in Flow Measurement", Southampton, England

Duckworth, R.A. and Chan, V.K. (1972) "Report on a Diaphragm Type Pressure Transducer", Research Memorandum ML.45, Dept. Mech.Eng., City University, London.

Durão, D.F.G. and Whitelaw, J.H. (1975)	"The Performance of Acousto-Optic Cells for Laser Anemometry", J.Phys.E: Sci.Instrum., Vol.8, pp 776-780
Durão, D.F.G and Whitelaw, J.H. (1979)	"Relationship between Velocity and Signal Quality in Laser Doppler Anemometry", J.Phys.E:Sci.Instrum., Vol. 12, pp 47-50.
Durrani, T.S. and Greated, G.A. (1977)	"Laser Systems in Flow Measurement", Plenum Press, New York.
Durst, F. and Whitelaw, J.H. (1971)	"Integrated Optical Units for Laser Anemometry", J.Phys.E: Sci.Instrum., Vol.4, pp 804-808.
Durst, F. and Venkatesh, P. (1975)	"Electronic Processing of Laser Doppler Signals", Rep. SFB 80/ET/54, University of Karlsruhe, Sonderforschungsberiech 80.
Durst, F. and Zaré, M. (1975)	"Laser Doppler Measurements in Two-Phase Flows", Proc.LDA-Symp.,Copenhagen, pp 403-429.
Durst, F,, Melling A.and Whitelaw, J.H. (1976)	"Principles and Practice of Laser-Doppler Anemometry", Academic Press, London.
Durst, F. (1978)	"Studies of Particle Motion by Laser-Doppler Techniques", Proc.Dynamic Flow. Conf., Marseille and Baltimore, pp 345-372.
Eichorn, R., Shanny, R. and Navon, U. (1964)	"Determination of Solid Phase Velocity in a Turbulent Gas-Solids Pipe Flow", Project Squid, Tech.Rep. PR-107-P.
Farbar, L. (1949)	"Flow Characteristics of Solids-Gas Mixtures in a Horizontal and Vertical Circular Conduit", Indust.and Eng.Chem., Vol. 41, No.6, pp 1184-1191.

Farmer, W.M. (1973) "The Interferometric Observation of Dynamic Particle Size, Velocity and Number Density", Thesis, University of Tennessee.

Farmer, W.M. (1978) "Measurement of Particle Size and Concentrations using LDV Techniques", Proc. Dynamic Flow Conf., Marseille and Baltimore, pp 373-396.

Forman, J.W., George, E.W. and Lewis, R.D. (1965) "Measurement of Localized Flow Velocities in Gases with a Laser Doppler Flow meter", Appl. Phys.Lett., Vol.7, No.4, pp 77-78.

Forman, J.W. (1967) "Optical Path-Length Difference Effects in Photomixing with Multi-mode Gas Laser Radiation", Applied Optics, Vol.6, No.5, pp 821-826.

Fridman, J.D., Huffaker, R.M. and Kinnard, R.T. (1968) "Laser Doppler System Measures Three-Dimensional Vector Velocity and Turbulence", Laser Focus,Vol.4, pp 34-38.

George, W.K. and Lumley, J.L. (1971) "The Measurement of Turbulence using a Laser Doppler Velocimeter", 1st Symp. on Flow, Its Measurement and Control in Science and Industry, Pittsburgh, pp 1037-1048.

Goldstein, R.J. and Hagen W.F. (1967) "Turbulent Flow Measurement, Shift of Scattered Laser Radiations", Phys.Fluids, Vol.10, No.6, pp 1349-1352.

Grant, G.R. and Orloff, K.L. (1973) "Two-Color Dual-Beam Backscatter Laser Doppler Velocimeter", Applied Optics, Vol.12, No.12, pp 2913-2916.

Hariu, O.H. and Molstad, M.C. (1949) "Pressure Drop in Vertical Tubes in Transport of Solids by Gases", Indust. and Eng. Chem., Vol.41, No.6, pp 1148-1160.

Hiller, W.J. and Meier, G.E.A. (1972) "The Scattered Light Beam Method", Proc.Conf. "Electro-Optic Systems in Flow Measurements",Southampton, England.

Hobson, C.A., Lalor, M.J. and Weston, W. (1973) "Digital Measurement of Laser Doppler Frequency", Digital Instrumentation-IEE Conf., pp 4 - 9.

Huffaker, R.M., Fuller, C.E. and Lawrence, T.R. (1969) "Application of Laser Doppler Velocity Instrumentation to Measurement of Jet Turbulence", Rep.690266, Soc.Automotive Engrs. Inst., Automotive Engrs. Conf., Detroit, Michigan.

Humphrey, J.A.C., Melling, A. and Whitelaw, J.H. (1975) "Laser-Doppler Anemometry for the Verification of Turbulence Models", Proc. Conf. "The Engineering Uses of Coherent Optics", University of Strathclyde, pp 459-481.

Iten, P.D. and Mastner, J. (1971) "A Laser Doppler Velocimeter Offering High Spatial and Temporal Resolution", 1st Sump. on Flow, Its Measurement and Control in Science and Industry, Pittsburgh, pp 1007-1013.

Jodlowski, C. (1976) "Study of Minimum Transport Velocities for Upward Flow in Vertical Pipes", paper D2, Pneumotransport 3, Bath, England.

Jokati, T. and Tomita, Y. (1971) "Solids Velocities and Pressure Drops in a Horizontal Pneumatic Conveying System", paper B3, Pneumotransport 1, Cambridge, England.

Jones, J.H., Braun, W.C. Daubert, T.E. and Allendorf, H.D. (1967) "Estimation of Pressure Drop for Vertical Pneumatic Transport of Solids", AIChE J., Vol.13, pp 608-611.

Kerker, M. (1969) "The Scattering of Light and Other Electromagnetic Radiation", Academic Press, New York.

Kolanski, M.S., Wienbaum, S. and Pfeffer, R. (1976) "Drag Reduction in Dilute Gas Solid Suspension Flow: Gas and Particle Velocity Profiles", paper C1, Pneumotransport 3, Bath, England.

Kramer, T.J. and Depew, C.A. (1972) "Experimentally Determined Mean Flow Characteristics of Gas-Solid Suspensions", Trans. ASME, J Basic Eng., Paper no. 72-Fe-29, pp 1-8.

Laufer, J. (1954) "The Structure of Turbulence in Fully Developed Pipe Flow", N.A.C.A.,Tech. Rep. 1174.

Lehmann, B. (1975) "Optische Methoden zur Geshwingigkeit-messung in Zweiphasen-Teilchenströmungen uter Berucksichtigung Turbulenter Einphasenströmungen", Bericht SFB-MHD Nr 21, Sonderforschungsbereich Mangeto-hydrodynamik der Technische Universität, Berlin.

Lewis, R.D., Forman,J.W., Watson, H.J. and Thornton, J.R. (1968) "Laser Doppler Velocimeter for Measuring Flow Velocity Fluctuations", Phys.Fluids, Vol.11, pp 433-435.

Leung, L.S. and Wiles, R.J. (1976) "Design of Vertical Pneumatic Conveying Systems, paper C4, Pneumotransport 3, Bath, England.

McCarthy, H.E. and Olson J.H. (1968) "Turbulent Flow of Gas-Solids Suspensions", I & EC Fundamentals, Vol.7, No.3, pp 471-483.

Mason, J.S. and Smith, B.V. (1973) "Pressure Drop and Flow Behaviour of the Pneumatic Transport of Fine Particles around 90 Degree Bends", paper A2, Pneumotransport 2, University of Surrey.

Massey, B.S. (1968) "Mechanics of Fluids", Pub. Von Nostrand, London.

Mayo, W.T. (1970) "Simplified Laser Doppler Velocimeter Optics", J.Phys.E: Sci.Instrum., Vol.3, pp 235-237.

Mazumder, M.K. and Wankum, D.L. (1969) "SNR and Spectral Broadening in Turbulence Structure Measurements using C.W.Lasers", IEEE J.Quant.Electron., pp 316-318. QE-5.

Mazumder, M.K. (1970) "Laser Doppler Velocity Measurements without Directional Ambiguity by using Frequency Shifted Incident Beams", Appl.Phys.Lett., Vol.16, No.11, pp 462-464.

Mazumder, M.K. and Kirsch, K.J. (1975) "Flow Tracing Fidelity of Scattering Aerosol in Laser Doppler Velocimetry", Applied Optics, Vol.14, No.4, pp 894-901.

Mehta, N.C., Smith, J.M. and Comings, E.W. (1957) "Pressure Drop in Air-Solid Flow Systems", Indust.and Eng.Chem., Vol.49, pp 986-992.

Melling, A. (1971) "Scattering Particles for Laser Anemometry in Air: Selection Criteria and their Realization", Rep.ET/TN/B/7, Mech.Eng. Dept.,Imperial College, London.

Melling, S.C. and Whitelaw, J.H. (1973) "Seeding of Gas Flows for Laser Anemometry", DISA Information, No.15, pp 5 -13.

Mettler, S.C. and Stevenson, W.H. (1976) "Laser Velocimeter Signal Characteristics in Two-Phase Media of Moderate Particle Size and Number Density", Proc. Minnesota Symposium on Laser Anemometry, Oct. 1975, pp 389-425.

Mills, D. (1977) "The Erosion of Pipe Bends by Pneumatically Conveyed Suspensions of Sand", PhD Thesis, Thames Polytechnic, London.

Modi, M.V.,Talwalker, A.T. and Punwani, D.V. (1978) "Pressure-Drop Correlation for Designing Vertical Dilute-Phase Gas-Solid Lift Lines for Materials in Coal Conversion Processes", paper presented at "International Powder and Bulk Solids Handling and Processing Conf.", Chicago, Illinois.

Muralidera, H.S., Rebello, W. and Krishan, R.P. (1979) "A Comparison of Pressure Drop Correlations for the Design of Long Distance Horizontal Pneumatic Coal Transport Systems", Int.Conf. on Pneumatic Conveying, Café Royal, London.

Ohtsuka, Y. (1971) "Optical Processing with Twin Ultrasonic Light Moderations", Opto-Electron., Vol.13, pp 119-125.

Oldengarm, J.,van Krieken, A.H. and Raterink, H. (1973) "Laser Doppler Velocimeter with Optical Frequency Shifting", Optics and Laser Tech., Vol.5, pp 249-251.

Oldengarm, J. (1975) "Two-Dimensional Laser Doppler Velocimetry",Proc. LDA-Symp., Copenhagen, pp 553-564.

Ottjes, J.A., Meeuse, G.C. and van Kuijk, G.T.L. (1976) "Particle Velocity and Pressure Drop in Horizontal and Vertical Pipes", paper D9, Pneumotransport 3, Bath, England.

Ower, E. and Pankhurst, R.C. (1977) "The Measurement of Air Flows", Pergamon Press, Oxford.

Peskin, R.L. and Dwyer, H.A. (1964) "A Study of the Mechanics of Turbulent Gas-Solid Shear Flows", ASME 65-WA/FE-24.

Pfeffer, R. and Kane, R.S. (1974) "A Review of Drag Reduction in Dilute Gas-Solids Suspension Flow in Tubes", paper F1, presented at Int.Conf. on Drag Reduction, Cambridge, England.

Pike, E.R., Jackson , D.A. Bourke, P.J. and Page, D.I. (1968) "Measurement of Turbulent Velocities from Doppler Shift in Scattered Laser Light", J.Sci.Instrum.(J.Phys.E), Series 2, Vol.1, pp 727-730.

Pike, E.R. (1972) "The Application of Photon Correlation Spectroscopy to Laser Doppler Measurements", J.Phys.D.: Appl.Phys., Vol.5, pp L23-L25.

Pike, E.R. (1974) "Photon Correlation Methods", Proc. 2nd Int. Workshop on Laser Velocimetry, Purdue University, pp 271-288

Pike. E.R. (1975) "Laser Doppler Anemometry, a Comparative Study of the Measurement of Motion by Light Scattering", Proc. Conf."Engineering Uses of Coherent Optics", University of Strathclyde, pp 431-459

Reddy, K.V.S. and Pei, D.C.T. (1969) "Particle Dynamics in Solids-Gas Flows in a Vertical Pipe", I & EC Fundamentals, Vol.8, No.3, pp 490-497.

Reithmuller, M.L. and Ginoux,J.J. (1973) "The Application of a Laser Doppler Velocimeter to the Velocity Measurement of Solid Particles Pneumatically Transported", paper D3, Pneumotransport 2, University of Surrey.

Richardson, J.F. and McLeman,M. (1960) "Pneumatic Conveying - Part II: Solids Velocities and Pressure Gradients in a One-Inch Horizontal Pipe", Trans. Instn.Chem.Engrs., Vol.38, pp 257-266.

Riebold, W., de Cooman, E. and Friz, G. (1970) "The Application of a Correlation Method in Two-Phase Flow Investigation", Meeting of European Two-Phase Flow Group, CISE, Milan, pp 1-22.

Riley, G.S. (1977) "In Search of an Easily Measurable Particle Shape Index", J.Powder and Bulk Solids Tech., Vol.1, No.3, pp 34-39.

Rinkevichyus, B.S. (1969) " Use of a Laser for Particle Velocity Determination in Two-Phase Flow by a Heterodyning Method", Radio Eng. and Electron.Phys., Vol.14, No.10, pp 1648-1650

Rose, H.E. and Duckworth, R.A. (1969) "Transport of Solid Particles in Liquids and Gases", The Engineer, Vol. 227, pp 392-396; 430-433; 478-483.

Rudd, M.J. (1969a) "A New Theoretical Model for the Laser Dopplermeter", J.Phys.E:Sci.Instrum., Vol.2, pp 55-58.

Rudd, M.J. (1969b) "A Self-Aligning Laser Doppler Velocimeter" ICO-8, Opt.Instrum. and Tech., Oriel Press, pp 58-166.

Segler, G. (1951) "Pneumatic Grain Conveying" National Inst. of Agricultural Eng., Siso, Beds.

Smyth, R. (1978) "Direction-Sensitive Simultaneous Multivelocity Component LDV", Applied Optics, Vol.17, No.18, pp 2855-2856.

Soo, S.L. (1956) "Statistical Properties of Momentum Transfer in Two-Phase Flow", J.Chem. Eng.Sci., Vol.5, pp 56-57.

Soo. S.L. (1962) "Fully Developed Turbulent Pipe Flow of a Gas-Solid", I & EC Fundamentals, Vol.1, No.1, pp 33-37.

Soo. S.L. Trezek, G.J., Dimick, R.C. and Hohnstreiter, G.F. (1964) "Concentration and Mass Flow Distributions in a Gas-Solid Suspension", I & EC Fundamentals, Vol.3, No.2, pp 98-106.

Soo. S.L. (1967) "Fluid Dynamics of Multiphase Systems", pub.Blaisdell, Waltham, Massachusetts.

Soo. S.L. (1969) "Pipe Flow Suspensions", Appl. Sci.Res., Vol.21, pp 68-84.

Stemerding, S. (1962) "The Pneumatic Transport of Cracking Catalyst in Vertical Risers", Chem. Eng.Soc., Vol.17, pp 599-608.

Ungut, A., Yule, A.J., Taylor,D.S. and Chigier, N.D. (1978) "Simultaneous Velocity and Particle Size Measurements in Two-Phase Flows by Laser Anemometry", AIAA, 16th Aerospace Sciences Meeting, Huntsville, Alabama, paper 78-74.

Van de Hulst, H.C. (1957) "Light Scattering by Small Particles", pub. John Wiley & Sons, London.

Venselaar, H.C.J., Scott, A.M. and Paul, D.M. (1978) "Measurement of Particle Velocity in Pneumatic Transport of Granular Solids by a Laser Time-of-Flight System", Proc.Int.Symp. "In-Stream Measurement of Particulate Solid Properties", Bergen, Norway, Paper B8.

Voigt, E.G. and White, R.R. (1948) "Friction in the Flow of Suspensions, Granular Solids in Gases through Pipes", Indust.and Eng.Chem, Vol.40, No.9, pp 1731-1738.

Webb, G. (1976) Unpublished, Thames Polytechnic, London.

Welch, N.E. and Tomme, W.J. (1967) "The Analysis of Turbulence Data Obtained with a Laser Velocimeter", AIAA, 5th Aerospace Science Meeting, New York, Paper No. 67-179.

Yang, W.C. (1977) "A Correlation for Solid Friction Factor in Vertical Pneumatic Conveying Lines", Inst.Conf. "Powder and Bulk Solids Handling and Processing", Rosemont, Illinois, pp 487-493.

Yanta, W.J. and Smith, R.A. (1973) "Measurements of Turbulence-Transport Properties with a Laser-Doppler Velocimeter", AIAA, 11th Aerospace Sciences Meeting, paper 73-169.

Yeh,Y. and Cummins, H.Z. (1964) "Localised Fluid Flow Measurements with a He-Ne Laser Spectrometer",Appl.Phys. Lett., Vol.14, No.10, pp 176-178.

van Zuitichen, D.J.,Bleuwork, G.H. and de Swart, J.G. (1973) "Slip Velocity Measurements by Radiotracer-Technique in Vertical Conveying Systems", paper D4, Pneumotransport 2, University of Surrey.